



The
University
Of
Sheffield.

K K Ampah

Elucidating the function of STX19 and SNAP29 in post-Golgi trafficking

Thesis submitted for the degree of Doctor of Philosophy

August 2016

Elucidating the function of STX19 and SNAP29 in post-Golgi trafficking

Khamal Kwesi Ampah

Thesis submitted for the degree of Doctor of Philosophy

The University of Sheffield

Department of Biomedical Science

August 2016

Abstract

There has been a significant amount of research performed to identify and characterise the molecular machinery involved in vesicle transport in eukaryotic cells. This has led to the identification of several important protein families including coat proteins, small GTPases and SNAREs. There are 38 SNAREs in the human genome and they are localised to the membranes of the biosynthetic and endocytic pathways where they play a role in membrane fusion. The aim of my thesis was to elucidate the function of two poorly characterised Q-SNAREs, SNAP29 and STX19, in post-Golgi trafficking. I have set out to determine where they are localised within the cell; how they are targeted to membranes and to identify which pathways they function on.

Using in-house generated rabbit polyclonal antibodies, I have identified a pool of STX19 and SNAP29 that colocalise with tubular recycling endosomal markers, MICAL-L1, Rab8, PACSIN-2 and EHD1. This localisation data indicates that SNAP29 and STX19 have a role in endocytic trafficking. I have shown that STX19's palmitoylation is necessary and sufficient for targeting it to tubular recycling endosomes. I have also determined that MICAL-L1 regulates the recruitment of SNAP29 on tubular recycling endosomes.

To gain an insight into the pathways on which STX19 functions I have used an RNAi-based approach. Depletion of STX19 causes the loss of MICAL-L1, RAB8 and SNAP29 from tubular recycling endosomes. This, in turn, leads to the accumulation of the TF-R, GLUT1 and internalised integrins indicating that STX19 has an important role in endocytic recycling.

To identify novel molecules which co-ordinate and regulate STX19 function I have used Bio-ID based proteomics and yeast two-hybrid screening. My data indicates that STX19 directly interacts with SNAPs 23, 25 and 29; VAMPs 3, 7 and 8; STXBPs 1, 2 and 5 which validates these approaches. I have also identified several novel interacting proteins including MACF1 and DST that suggest that STX19 may have novel links to the cytoskeleton and integrin trafficking. The Bio-ID based approach has also identified potential cargo molecules which traffic via the STX19 pathway. This list included proteins such

NDGR1, ERBB2IP, VANGL1 and SCRIB that have been shown to be involved in regulating cell migration and cell polarity. Taken together, my data suggests that a pool of STX19 is playing an important role in endocytic recycling and may be required for regulating cell motility and epithelial polarisation.

Acknowledgements

I thank the Almighty Allah for giving me the strength and knowledge to pursue this PhD degree programme.

I am very grateful to my supervisor, Dr Andrew A Peden for his continuous guidance, attention and support without whom this project would not have been successful. I express my gratitude to my two advisors Professor Kathryn R Ayscough and Dr Kai Erdmann for their constructive suggestions during several advisory meetings. This helped shaped the direction of my project.

I wish to express my heartfelt gratitude to Dr Mark Collins in helping analyse the various mass spectrometry data. I also thank Dr Luke Chamberlain for giving us the 23 palmitoyl acyltransferases constructs and Dr Jennifer Greaves for help in the palmitate labelling click chemistry.

I have also received various supports from other colleagues including Dr Charlotte Leese who assisted in the generation of the GFP-TRAP beads for the protein purification analysis. Dr Darren Robinson also provided several technical supports in our 3D SIM-OMX and wide field microscope imaging, whereas Mary Snape helped in the STORM imaging. I say big thank you all. I am very grateful to various colleagues who made their plasmids constructs and protocols available for use in this project.

Last but not least, I am ever grateful to my family especially my wife Manu Serwaah Ampah for her patience and love.

This thesis is dedicated to my mother Rashida Osman for all her efforts in putting me through education and my late mentor Osofo Ibrahim Poku for his moral support and guidance.

Abbreviations

2-BP	2-Bromopalmitate
3D-SIM	Three dimensional - structural illumination microscopy
APT1/2	protein acyl thioesterases (1 and 2)
ATP	Adenosine triphosphate
Bio-ID	proximity-dependent biotin identification
BIRA*	A mutant (R118G) of 35-kDa DNA-binding protein found in E coli that promiscuously biotinylates proteins
CAAX motif	A C-terminal motif involve in protein farnesylation. The C denotes cysteine, A represents any aliphatic amino acid, and X is a terminal amino acid.
CACO-2	Human epithelial colorectal adenocarcinoma cells
CD55	Cluster of differentiation 55 or complement decay-accelerating factor
CD59	Cluster of differentiation 59
CD63	Cluster of differentiation 63 (late endosomal marker)
CDC42	Cell division control protein 42
CDE	Clathrin-dependent endocytosis
CEDNIK	A gross neuroanatomical disorder characterised by cerebral dysgenesis, neuropathy, ichthyosis, and palmoplantar keratoderma syndrome
CIE	Clathrin-independent endocytosis
CI-MPR/CD-MPR	Cation independent/dependent mannose 6-phosphate receptor (markers for studying endosome-Golgi retrieval)
CRISPR-CAS9	CRISPR-associated protein-9 nuclease for gene editing
Cys	Cysteine
DMEM	Dulbecco's Modified Eagle Medium
DMSO	Dimethyl sulfoxide
DNA	Deoxyribonucleic acid
DST/BPAG1	Dystonin/ bullous pemphigoid autoantigen 1
DUBs	Deubiquitinases
EDTA	Ethylenediaminetetraacetic acid

EEA1	early endosomal marker
EGFP	enhanced green fluorescence protein
EGF-R	epidermal growth factor receptor
EHD1	EPS15 (epidermal growth factor receptor substrate 15) homology (EH) domain-containing proteins 1
EH-domain	EPS15 (epidermal growth factor receptor substrate 15) homology (EH) domain
ER	endoplasmic reticulum
ERC	endocytic recycling compartment
EXOC1/SEC3	exocyst complex component 1/ Subunit of the exocyst complex 3
FBS	fetal bovine serum
GFPSTX19t	denotes STX19 274-294 residue only (KKRNPCRVLCCWCCPCCSSK)
GFPTrap-IP	Green Fluorescent Protein (GFP) binding protein coupled to agarose beads immunoprecipitation
GLUT1	Glucose transporter 1
GM130/P230/TGN4 6	Golgi matrix protein/Protein 72.1/Trans-Golgi Network integral membrane protein 46 (Golgi markers)
GPI-anchored	Glycosylphosphatidylinositol-anchored proteins
HA-tagged	Human influenza hemagglutinin tag
HEK293 cells	Human embryonic kidney 293 cells
HeLa cells	Human cervical carcinoma cell line
HeLaM cells	HeLa cells subclone
HEPES	(4-(2-hydroxyethyl)-1-piperazineethanesulfonic acid
HIS-Tagged	Polyhistidine-tag
HRAS	GTPases Transforming protein p21
HRP	Horseradish peroxidase
HT29 cells	Human colorectal epithelial adenocarcinoma cell line
ZWINT	Human Zeste White 10 interacting protein
IMDM	Iscove's Modified Dulbecco's medium
IPTG	Isopropyl β -D-1-thiogalactopyranoside
kDa	Kilodalton

M1-M8	STX19 cysteine mutants (cysteines mutated to leucines)
MACF1/ACF7	Microtubule actin cross linking factor 1/actin cross linking factor 7
mCherry3	monomeric red fluorescent protein
MEM	Minimum essential media
MG132	Carbobenzoxy-Leu-Leu-leucinal, a proteasomal inhibitor
MHC1	Major histocompatibility complex class 1
MICAL3	Microtubule Associated Monooxygenase, Calponin and LIM Domain Containing 3
MICAL-L1	Molecule Interacting with Crk-Associated Substrate Related Protein-Like 1 (CasL1)
ms	Mass spectrometry
NEAA	Non-essential amino acid
NH ₂ OH	hydroxylamine used to cleave thioester bond formed between cysteines moieties and the palmitate group
NPF-motif	Asparagine-proline-phenylalanine motif that usually associates with EH-domain proteins
OMX 3-D SIM	Optical microscopy experimental Three dimensional - structural illumination microscopy
Opti-MEM	Reduced Serum Media modified from Minimum Essential Media used in mammalian cell transfection
PACSIN2	Protein kinase C and casein kinase II interacting protein 2
PATs	Palmitoyl acyltransferases
PBS	Phosphate buffered saline solution
PCR	Polymerase chain reaction
PEI	Polyethyleneimine
PFA	Paraformaldehyde
PM	Plasma membrane
PRD motif	Proline-rich membrane binding domain motif
Q-SNARE	Contributes glutamine at the "0-layer" during SNARE complex formation
RAB8A	Ras-related proteins in brain 8

RAC1	Ras-related C3 botulinum toxin substrate 1
RIPA buffer	Radioimmunoprecipitation assay, cell lysis buffer
RPE cells	Human retinal pigment epithelial cells
RPMF1/2	Roswell Park Memorial Institute medium
R-SNARE	Contributes arginine at the "0-layer" during SNARE complex formation
SFKs	Src family kinases
SH3 domain	SRC homology-3 domain
SILAC	Stable isotope labelling of amino acid in cell culture
siRNA	small interfering Ribonucleic Acid
SNAP29/GS32	Synaptosomal-Associated Protein, 29kDa/ Golgi snare protein of 32 kDa, contributes two glutamine residues during SNARE complex formation
SNARE	Soluble NSF Attachment Protein Receptor
STORM	Stochastic Optical Reconstitution Microscopy
STX19	Syntaxin 19, contributes a glutamine residue during SNARE complex formation
STX19/13 hybrid	STX19 with the 278-294 residue replaced with STX13 transmembrane domain
STXBP	Syntaxin binding protein
TCEP	Tris (2-carboxyethyl) phosphine hydrochloride
TF-R	Transferrin receptor
TGN	Trans-Golgi network
TIFF cells	Human telomerase-immortalised foreskin fibroblasts cells
Tr	STX19 cysteine truncated mutant (278-294 residues removed)
Tr2	STX19 cysteine truncated mutant (274-294 residues removed)
TRE	tubular recycling endosomes involved protein recycling
USPs	Ubiquitin specific proteases
VAMP8/EDB	Vesicle-associated membrane protein 8/ Endobrevin, Contributes arginine at the "0-layer" during SNARE

	complex formation
ZDHHC motif	aspartate, two histidine groups and a cysteine (PAT motif)
ZDHYC motif	aspartate, histidine, tyrosine and a cysteine (PAT motif)

Table of contents

Acknowledgements	V
Abbreviations	VII
Table of contents	XII
Table of figures	XX
Table of Tables	XXIV
1 Chapter Introduction	1
1.1 Historical perspective of biosynthetic transport	1
1.2 SNAREs	2
1.3 Domain structure of SNAREs	5
1.3.1 Qa-SNAREs	5
1.3.2 Qb- and Qc- SNAREs	5
1.3.3 Qbc- SNAREs	6
1.3.4 R-SNAREs	6
1.4 SNAREs in constitutive secretion	7
1.4.1 STX9/19	7
1.4.2 SNAP29/GS32	8
1.5 The endocytic pathway	9
1.5.1 Clathrin-dependent and-independent endocytosis	10
1.6 The endocytic compartments	10
1.6.1 Endosomal maturation	10
1.6.2 Rab small GTPases	11
1.6.2.1 The structure of Rab small GTPases proteins	12
1.6.3 Endosomal maturation requires Rab5/7 switch	13
1.6.4 Recycling endosomes	13
1.6.5 Fast and slow endocytic recycling.....	14
1.7 Endocytic recycling machinery	14
1.7.1 RAB8	15
1.7.1.1 RAB8 GEFs and GAPs	15
1.7.1.2 RAB8 effector proteins	15
1.7.1.3 RAB8 function	16
1.7.2 MICAL-L1	17

1.7.2.1	MICAL-L1 function.....	17
1.7.3	EHD1	19
1.7.3.1	EHD1 function	20
1.7.3.2	EHD paralogues (EHD 2-4) function	21
1.7.4	PACSIN2/Syndapin2	21
PACSIN2	21
1.7.4.1	PACSIN2 function	22
1.8	Rab11 recycling endosomes and Rab8/MICAL-L1 tubular recycling endosomes are distinct structures	23
1.9	The physiological relevance of the endocytic pathway	24
1.10	Protein modifications	25
1.11	Palmitoylation	25
1.11.1	Definition and characteristics of palmitoylation	25
1.11.1.1	Palmitoylation is catalysed by palmitoyl acyltransferases (PATs)	26
1.11.1.2	Deacylation is catalysed by protein acyl- and palmitoyl- thioesterases	27
1.11.2	Palmitoylation and protein trafficking	28
1.11.2.1	Palmitoylation and RAS trafficking	28
1.11.2.2	Palmitoylation and SNAREs trafficking	29
1.11.3	Methods for studying palmitoylation.....	30
1.11.3.1	Mutation of key cysteine residue (s).....	30
1.11.3.2	Chemical inhibitors	30
1.11.3.3	Mutation of key hydrophobic amino acids	31
1.12	Ubiquitination	31
1.12.1	Importance of protein ubiquitination	32
1.12.1.1	Ubiquitination and protein degradation	32
1.12.1.2	Nonproteolytic functions of ubiquitination.....	33
1.12.2	Characteristics of ubiquitination	34
1.12.3	Analysing ubiquitinated proteins using mass spectrometry approach	34
1.12.4	Deubiquitination.....	35
1.13	The crosstalk between palmitoylation and ubiquitination	36
1.14	Research question	37
2 Chapter	<i>Materials and Methods</i>	46
2.1	Common Reagent and Antibodies	46
2.2	Plasmids Preparation and Analysis	46

2.2.1	Transformation	46
2.2.2	Plasmid isolation	47
2.2.2.1	Miniprep preparation	47
2.2.2.2	Maxiprep preparation	47
2.2.3	Cloning	48
2.2.3.1	DNA amplification and Gel electrophoresis	49
2.2.3.2	DNA purification from agarose gel slices	49
2.2.3.3	TOPO TA Cloning	50
2.2.3.4	Restriction digests	50
2.2.3.5	Oligo annealing	50
2.2.3.6	Klenow treatment	50
2.2.4	Multiple sequence alignment of human STX19	51
2.3	Cell Culture and transfection	52
2.3.1	Tissue culture media preparation	52
2.3.2	Cells culture	52
2.3.3	Using automatic cell counter	52
2.3.4	Cell freezing	53
2.3.5	Cell transfection	53
2.3.5.1	Preparing PEI	53
2.3.5.2	DNA transfection	53
2.3.5.3	siRNA transfections	54
2.3.6	Generating stable cell lines using viral transduction	54
2.4	Microscopy	55
2.4.1	Immunofluorescence protocol	55
2.4.2	Preparing samples for 3D-SIM OMX	56
2.4.3	Stochastic Optical Reconstitution Microscopy (STORM)	57
2.4.4	Chemical inhibitors	57
2.4.4.1	Proteasome inhibitor treatment (MG132)	57
2.4.4.2	2-bromopalmitate (2-BP) treatment	57
2.4.5	Antibody uptake Assay	57
2.5	Protein preparation and analysis	58
2.5.1	GFP-binding protein expression and purification	58
2.5.1.1	Bacteria culture cell lysis and coupling of proteins onto Nickel-NTA agarose beads	58
2.5.1.2	Protein elution and purification	59
2.5.1.3	Coupling of GFP-binding protein onto NHS-activated Sepharose 4 Fast Flow	60
2.5.2	Bio-Rad protein assay (Bradford assay)	60

2.6	Affinity capture of biotinylated proteins	61
2.6.1	Growing HA-tagged BIRA*STX19.....	61
2.6.2	Collection and lysis of cells	61
2.6.3	Incubation with streptavidin beads	62
2.6.4	Western blotting	62
2.6.4.1	Casting gels.....	63
2.6.4.2	Electrophoretic separation and transfer of samples.....	63
2.6.4.3	Protein visualisation	64
2.6.4.4	Blocking.....	64
2.6.4.5	Primary and secondary antibody incubation	64
2.6.4.6	Detection	65
2.7	Mass spectrometry	65
2.7.1	In-gel sample analysis.....	65
2.7.1.1	Alkylation and running samples	66
2.7.1.2	Staining, destaining and slicing gels	66
2.7.1.3	Trypsin digestion and peptide extraction	67
2.7.2	On-resin sample analysis.....	68
2.7.3	On-resin digest of palmitoylation sites in GFPTrap IP STX19.....	68
2.7.4	PEG Switch whole cell lysate assay	68
2.7.5	Palmitate labelling coupled to click chemistry.....	69
2.7.5.1	Metabolic labelling.....	69
2.7.5.2	Click chemistry	70
3	Chapter <i>Where is STX19 localised in mammalian cells?</i>.....	107
3.1	Introduction.....	107
3.2	Results.....	108
3.2.1	Endogenous STX19 is localised to tubules and vesicles.....	108
3.2.2	Overexpressed STX19 localises to similar cellular compartment as endogenous STX19	108
3.2.3	STX19 colocalises with the tubular recycling endosomal markers RAB8 and MICAL-L1	109
3.2.4	STX19 colocalises with GPI-anchored proteins on TRE.....	109
3.2.5	STX19 colocalises with proteins involved in cell migration	110
3.2.6	Investigating the function of STX19 using RNAi	110
3.2.7	STX19 depletion affects endosomal markers and endocytic cargoes	111
3.2.8	STX19 depletion affects the localisation of post-Golgi VAMPs	112
3.2.9	STX19 depletion alters the steady-state localisation of proteins which cycle between the Golgi and endosomes	113

3.2.10	STX19 depletion affects focal adhesion dynamics	113
3.3	Discussion.....	114
3.3.1	Summary of results	114
3.3.2	The cellular localisation pattern of STX19	114
3.3.3	Depletion of STX19 interferes with the endocytic pathway.....	115
3.3.4	STX19 may play a role in cell migration by regulating the trafficking of integrins 116	
3.3.5	Depletion of STX19 alters the morphology of the biosynthetic pathway and changes the levels of key factors which function on this pathway	117
3.3.6	Future experiments	118
4	Chapter <i>How is STX19 targeted to post-Golgi membranes?</i>.....	138
4.1	Introduction.....	138
4.1.1	Investigating the role of palmitoylation in STX19 trafficking	138
4.2	Results.....	139
4.2.1	STX19's cysteine-rich domain is highly conserved.....	139
4.2.2	Mapping STX19 domain required for membrane association.....	140
4.2.3	A PEG (polyethylene glycol)-switch assay shows that STX19 is palmitoylated	141
4.2.4	STX19 membrane localisation is inhibited by 2-bromopalmitate	142
4.2.5	STX19 cysteine residue mutants (M4, M6, M7, and Tr) cause the protein to be degraded	143
4.2.6	The cysteine-rich region of STX19 is necessary and sufficient for STX19's membrane localisation	143
4.2.7	STX19's tryptophan-286 and Proline-289 might be required for its initial membrane targeting	144
4.2.8	STX19's cysteines 284, 285, 287, 288 and 290 are palmitoylated.....	144
4.2.9	Identifying palmitoyl acyltransferases required for STX19 palmitoylation.....	145
4.2.10	Palmitate labelling click chemistry identifies palmitoyl acyltransferases involved in STX19 palmitoylation	146
4.2.11	Mapping STX19 ubiquitination site.....	146
4.3	Discussion.....	148
4.3.1	Summary of results	148
4.3.2	Palmitoylation targets STX19 to the PM and TRE	148
4.3.3	Multiple cysteines are required for STX19 palmitoylation.....	149
4.3.4	How is STX19 initially targeted to membranes?	149
4.3.5	Palmitoyl acyltransferases (1, 2, 3, 6, 7, 11, 14, and 15) catalyse STX19 palmitoylation	150
4.3.5.1	PAT assays	150

4.3.5.2	Colocalisation studies	151
4.3.6	Palmitoylation regulates STX19's stability	152
4.3.7	FUTURE EXPERIMENTS.....	154
5	Chapter <i>Identifying STX19 protein interacting partners</i>	178
5.1	Introduction.....	178
5.2	Results.....	179
5.2.1	Identifying STX19 interacting partners using a yeast two-hybrid screen	179
5.2.2	Generating and testing BirA*STX19 for Bio-ID assay.....	183
5.2.3	Identifying STX19 interacting partners using Bio-ID approach	184
5.2.4	Bioinformatics analysis of STX19 interacting partners.....	186
5.2.5	Validating yeast two-hybrid screen and Bio-ID data using GFPTRAP IP approach	189
5.2.5.1	ZWINT1	190
5.2.5.2	MACF1 and DST	190
5.2.6	STX19 depletion affects the organisation of actin cytoskeleton	191
5.3	Discussion.....	192
5.3.1	Summary of results	192
5.3.2	The role of SNAREs in cell migration and cell polarity.....	192
5.3.3	NDRG1.....	193
5.3.4	ERBB2IP/LAP2/ERBIN	193
5.3.5	VANGL1 (Van Gogh-like protein 1)/STB2/KITENIN	194
5.3.6	ZW10-interacting protein 1/ZWINT	195
5.3.7	Spectraplakins.....	196
5.3.8	Microtubule actin cross linking factor 1/ actin cross linking factor 7 (MACF1/ACF7).....	197
5.3.9	Dystonin/DST/BPAG1	198
5.3.10	Future direction and experiments.....	199
6	Chapter <i>Characterisation of SNAP29 membrane targeting</i>	222
6.1	Introduction.....	222
6.2	Chapter aims	222
6.3	Results.....	223
6.3.1	A pool of SNAP29, EHD1, MICAL-L1, PASCIN2 and RAB8 are localised to endocytic recycling tubules	223
6.3.2	A pool of SNAP29 colocalises with endogenous MICAL-L1 on tubular recycling endosomes.....	224

6.3.3	Overexpression of MICAL-L1 recruits SNAP29, EHD1, PASCIN2 and RAB8 on to tubular recycling endosomes	224
6.3.4	Overexpression of MICAL-L1 does not recruit SNAPs 23-47 or other SNAREs on to tubular recycling endosomes	224
6.3.5	Overexpression of PASCIN2, RAB11, RAB8 and EHD1 does not contribute to SNAP29 recruitment to tubular recycling endosomes	225
6.3.6	Mapping MICAL-L1 domain required for SNAP29 recruitment onto tubular recycling endosomes	226
6.3.7	Developing a biochemical assay to investigate the role of MICAL-L1 in SNAP29 recruitment	226
6.3.8	Depletion of EHD1 impairs endogenous SNAP29 association with the tubular recycling endosomes	227
6.4	Discussion.....	228
6.4.1	Summary of results	228
6.4.2	SNAP29 recruitment onto membranes requires a network of interactions between MICAL-L1, EHD1 and PASCIN2	228
6.4.3	Predicted model of SNAP29 membrane recruitment.....	230
6.4.4	A pool of SNAP29 has a role in cell migration	230
7	Chapter Discussion and future studies.....	252
7.1	Introduction.....	252
7.2	A pool of STX19 and SNAP29 is localised to tubular recycling endosomes.....	252
7.3	How is STX19 sorted to TRE?.....	253
7.3.1	How is STX19 endocytosed?	253
7.3.2	Is STX19 trafficking between the cell surface, TRE and Golgi?	254
7.4	SNAP29 is recruited to TRE by MICAL-L1	255
7.5	STX19 may have a role in epithelial cell polarity	256
7.6	STX19 may function in several post-Golgi pathways.....	256
7.6.1	STX19-MACF1-GOLGA4-Exocyst complex may regulate the trafficking of GPI-anchored proteins	257
7.6.2	ERBB2IP-STX19-DST-MYO18A-Exocyst complex may regulate integrin-mediated cell migration.	257
7.6.3	STX19-ZWINT complex may be required for tethering vesicles during mitosis	258
	References.....	259

Table of figures

Figure 1-1 The biosynthetic pathway.	38
Figure 1-2 Model of the neuronal SNARE complex.....	38
Figure 1-3 A simplified cartoon showing the role of SNAREs in the biosynthetic and endocytic pathways.	39
Figure 1-4 A cartoon showing domains of SNARE proteins.	40
Figure 1-5 A targeted siRNA screen identifies SNAREs and SM proteins required for secretion.....	40
Figure 1-6 Rabs small GTPases outline intracellular membrane compartments.	41
Figure 1-7 The endosomal compartments.	42
Figure 1-8 Cartoon of MICAL-L1.	42
Figure 1-9 Cartoon of EHD1.	42
Figure 1-10 Cartoon of PACSIN2.	42
Figure 1-11A modified diagram of MICAL-L1 tubular- and Rab11- recycling endosomes.	43
Figure 1-12 Palmitoylation influences the trafficking of protein.....	44
Figure 1-13 Ubiquitination influences the trafficking of proteins.	44
Figure 2-1 The purification of the GFP-binding protein (GBP).....	71
Figure 2-2 Ultrapurification, coupling and validation of the efficacy of the GBP.	73
Figure 3-1 A pool of endogenousSTX19 is localised to long branched tubular structures.	119
Figure 3-2 Transfected STX19 is localised to long tubular structures and the plasma membrane.	120
Figure 3-3 STX19 is localised to punctate structures on TREs.	121
Figure 3-4 Testing tubular recycling endosomal marker antibodies in HeLaM cells.	122
Figure 3-5 STX19 colocalises with RAB8 and MICAL-L1.....	123
Figure 3-6 STX19 colocalises with internalised CD55 and CD59.....	124
Figure 3-7 Overexpressed STX19 colocalises with HRAS, RAC1 and CDC42.	125

Figure 3-8 STX19 can be depleted using RNAi.....	126
Figure 3-9 STX19 depletion affects the recruitment of RAB8 and MICAL-L1 to tubular recycling endosomes.....	128
Figure 3-10 Depletion of STX19 leads to a defect in endosomal recycling.	130
Figure 3-11 STX19 depletion affects R-SNARE localisation.....	131
Figure 3-12 STX19 depletion affects Golgi morphology and the distribution of CD- and CI-MPR.	134
Figure 3-13 STX19 depletion affects integrin trafficking and focal adhesion dynamics.	136
Figure 4-1 STX19 cysteine-rich region is conserved in different species.	155
Figure 4-2 Mapping STX19 domain required for membrane association.	157
Figure 4-3 PEG switch assay confirms the palmitoylation state of STX19.	158
Figure 4-4 STX19 membrane localisation is dependent on its palmitoylation.....	159
Figure 4-5 STX19's cysteine-rich domain is required for its correct membrane localisation.	161
Figure 4-6 Blocking palmitoylation causes STX19 to be degraded.....	163
Figure 4-7 The cysteine-rich domain of STX19 is necessary and sufficient for STX19's membrane localisation.	165
Figure 4-8 Identification of STX19 palmitoylation sites using mass-spectrometry.	166
Figure 4-9 STX19's tryptophan-286 and Proline-289 might be required for its initial membrane targeting.....	168
Figure 4-10 PATs (1-12) are distributed on different intracellular organelles.....	169
Figure 4-11 PATs (13-23) are distributed on different intracellular organelles.....	170
Figure 4-12 STX19 colocalises with zDHHCs (2, 5, 9 and 14).....	171
Figure 4-13 PATs involved in STX19 palmitoylation.....	172
Figure 4-14 PATs involved in STX19 tail palmitoylation.....	174

Figure 4-15 Prediction of STX19 ubiquitination sites.	175
Figure 4-16 Mapping STX19 ubiquitination sites.	176
Figure 5-1 Cartoon of MACF1 and DST.	197
Figure 5-2 Cartoon of BirA*STX19.	200
Figure 5-3 BirA tagged STX19 is localised to the PM and TRE.	200
Figure 5-4 BirA*STX19 is capable of biotinylating proteins.	201
Figure 5-5 Coomassie staining of streptavidin enrich proteins.	202
Figure 5-6 Biological repeats of BirA*STX19 follows a normal distribution curve.	203
Figure 5-7 Biological repeats of BirA*STX19 correlates within and among groups.	204
Figure 5-8 Protein classification using the Panther Gene ontology consortium.	205
Figure 5-9 Protein biological processes using the Panther Gene ontology consortium.	206
Figure 5-10 Protein cellular component using the Panther Gene ontology and STRING consortia.	207
Figure 5-11 Protein classification based on biochemical properties.	208
Figure 5-12 Protein classification based on palmitoylation state.	209
Figure 5-13 STRING consortium showing STX19 interacting partners.	212
Figure 5-14 STX19 forms SNARE complexes with SNAPs (23, 29) and VAMPS (3, 8).	213
Figure 5-15 STX19 interacts with ZWINT1.	214
Figure 5-16 MACF1 does not co-immunoprecipitate with GFP-tagged STX19.	215
Figure 5-17 BirA*STX19 biotinylates MACF1 and DST.	216
Figure 5-18 STX19 depletion affects the organisation of the cytoskeleton.	220
Figure 6-1 Cartoon of SNAPs 23, 25, 29 and 47.	232
Figure 6-2 Localisation of tubular recycling endosomal markers in both polarised and non-polarised cells.	233
Figure 6-3 SIM images of tubular recycling endosomal markers.	234

Figure 6-4 SNAP29 colocalises with MICAL-L1 in both polarised and non-polarised cells.	236
Figure 6-5 Overexpression of MICAL-L1 recruits tubular recycling endosomal markers.	237
Figure 6-6 Localisation of endogenous SNAPs 23, 25, 29 and 47.	238
Figure 6-7 Overexpression of MICAL-L1 does not recruit other SNAPs onto tubular recycling endosomes.	239
Figure 6-8 Overexpression of Rab8, Rab11, PACSIN2 and EHD1 does not increase the recruitment of SNAP29 on to the TREs.	241
Figure 6-9 Overexpression of PASCIN2 recruits SNAP29 on to the plasma membrane.	243
Figure 6-10 Cartoon showing the interaction between MICAL-L1 and other tubular recycling endosomal markers.	244
Figure 6-11 SNAP29 recruitment onto the tubular recycling endosomes does not require MICAL-L1 NPF-motif.	245
Figure 6-12 Overexpression of MICAL-L1 coiled-coil domain only does not recruit SNAP29 and PASCIN2 onto tubular recycling endosomes.	246
Figure 6-13 SNAP29 does not co-immunoprecipitate with MICAL-L1.	248
Figure 6-14 Knockdown of EHD1 impairs SNAP29 tubular membrane localisation.	250
Figure 6-15 Proposed model for the recruitment of SNAP29 on to tubular recycling endosomes.	251

Table of Tables

Table 2-1 Antibodies.....	74
Table 2-2 Antibiotics.....	77
Table 2-3 Plasmid media and Reagents.....	78
Table 2-4 PCR mix.....	80
Table 2-5 Oligo annealing mixture.....	80
Table 2-6 PCR program.	80
Table 2-7 PCR master mix for generating a site-directed mutation in MICALL1.	80
Table 2-8 PCR program for generating a site-directed mutation in MICALL1.	81
Table 2-9 Ligation reaction mixture.....	81
Table 2-10 Restriction digest mixture.	81
Table 2-11 Primers.....	82
Table 2-12 Common expression vectors used in this study.....	87
Table 2-13 Expression constructs generated during this study.....	87
Table 2-14 Constructs obtained commercially or gift.....	89
Table 2-15 Cells media composition.	90
Table 2-16 Cell culture media and reagents.	90
Table 2-17 Transfection mixture.....	92
Table 2-18 Transfection reagents.....	92
Table 2-19 Cell culture materials.	93
Table 2-20 Western blot buffers.....	94
Table 2-21 Immunofluorescence buffers.	99
Table 2-22 GFP-binding protein expression and purification buffers.	100
Table 2-23 Mass spectrometry analysis buffers.....	101
Table 2-24 PEG Switch buffer.	102
Table 2-25 Palmitate labelling coupled to click chemistry buffers.	104
Table 2-26 Chemical inhibitors.	105
Table 4-1 Quantification of STX19 domain tubular recycling endosome localisation.....	157

Table 4-2 Quantification of STX19 membrane localisation with or without 2 BP.....	160
Table 4-3 Quantification of STX19 paired cysteine mutants.	162
Table 4-4 Quantification of STX19 mutants Western blot.....	164
Table 4-5 localisation of PATs in different intracellular compartments... 	169
Table 5-1 Shortlisted proteins from STX19 yeast two-hybrid screen results.	181
Table 5-2 Shortlisted proteins from STX19 Bio-ID results.....	186
Table 5-3 Shortlisted proteins based on current and previous studies... 	189
Table 5-4 Protein classification based on biochemical properties and palmitoylation state.	210

1 Chapter Introduction

1.1 Historical perspective of biosynthetic transport

Newly synthesised proteins and lipids are delivered to the cell surface by a process called biosynthetic transport (Figure 1-1). The intracellular compartments involved in this process have been studied for the past century using various microscopy-based approaches. Camillo Golgi in 1897 developed a stain that identified structures that were reticular in nature and were later named the Golgi apparatus. In the early 1940s, Porter et al., 1945 used electron microscopy to examine the structural detail of cells derived from chick embryos. These pioneering studies identified and characterised organelles including mitochondrion, Golgi Bodies and the endoplasmic reticulum (Porter et al., 1945). This then created an avenue for further investigation into how these compartments interact and how materials move from one compartment to the other. In order to investigate how newly synthesised proteins are trafficked to the cell surface, Caro and Palade, 1964 injected guinea pigs with a DL-leucine radiolabelled physiological saline and removed their pancreases at different time points (Caro and Palade, 1964). Their work showed that some of the radiolabelled proteins located in the rough endoplasmic reticulum have moved into the Golgi complex after 20 min and then to the secretory granules leading to their secretion at the PM (Caro and Palade, 1964). These results provided a direct evidence for the role of the Golgi complex in secretion. Although their results could not show how those proteins were transferred from the ER to the Golgi, they did propose that small vesicles might mediate these process (Caro and Palade, 1964). This study serves as the basis of the classical secretory pathway. The use of cell fractionation, autoradiography and electron microscopy from pancreatic exocrine cell samples also contributed greatly to the understanding of the cell structural and the functional organisation providing insights into the secretory pathways (Zagury et al., 1970, Palade, 1975). They proposed that secretory proteins are transported in a vectorial fashion and that small vesicles are most likely the intermediates in this process. However, the cellular and molecular machineries underlying these processes were not known. Many researchers have shown keen interest to unravel some of these

machineries notably among them include: Randy Schekman, James Rothman, Thomas Sudhof for which they were awarded 2013 Noble Prize Award in Medicine or Physiology towards their contribution in the discoveries of how molecules are trafficked within cells (Bonifacino, 2014).

Schekman and his group are noted for using yeast-based genetic screens. Their screens have identified various large number of genes which function on the secretory pathway. The SEC genes encode proteins which function as SNARE binding and recycling proteins, signal peptidase and RabGTPases (Schekman and Novick, 2004). Rothman's group used biochemical approaches to identify machineries involved in vesicle trafficking. Their earlier work utilised an assay that measured intra-Golgi transport (Balch et al., 1984). This assay combined with biochemical reconstitution led to the identification of NSF, SNAPs (soluble NSF attachment proteins), and SNAREs as being key players in this process. The fact that the proteins were also required for synaptic vesicle fusion lead Rothman's laboratory to develop the SNARE hypothesis. This model proposes that a transport vesicle (v-SNARE) and a target membrane (t-SNARE) with the aid of NSF, SNAPs bring the v-SNARE in close proximity to the t-SNARE facilitating membrane fusion (Sollner et al., 1993). These studies paved the way to the identification of cellular machinery required for making, tethering and fusing vesicles. It is now widely accepted that SNAREs serve as the core machineries necessary for vesicle targeting and fusion but are regulated by proteins like Sec1/MUNC18 and GTPases (Rothman, 1994, Bonifacino and Glick, 2004).

1.2 SNAREs

Membrane fusion is driven by a family of proteins known as SNAREs (Figure 1-2). Membrane fusion is required for cell division, cell growth, cell migration, hormonal signalling, membrane repair and synaptic transmission. SNAREs were first identified as being core components of synaptic vesicles (Trimble et al., 1988, Bennett et al., 1992). However, their function was still unclear. Work from Jim Rothman's group showed that there were non-neuronal versions of these proteins which were required for the fusion of intra-Golgi transport vesicles. This observation leads to the SNARE hypothesis which proposed that

SNAREs are universal machinery that drives membrane fusion (Figure 1-2) (Sollner et al., 1993).

The human genome encodes 38 SNAREs localised to different intracellular compartments (Figure 1-3). They share a unique 60-70 residue motif known as the SNARE motif. SNAREs were originally classified as vesicle (V) and target (T) SNAREs based on their membrane location (Sollner et al., 1993, Rothman, 1994). However, they are now defined as R-SNAREs or Q-SNAREs based on the presence of a highly conserved arginine and glutamine residues found in the SNARE motif (Fasshauer et al., 1998). In addition, SNAREs are grouped into Qa-, Qb-, Qc- and Qbc-SNAREs because of their sequence similarity to syntaxin and SNAP25 (Bock et al., 2001, Hong, 2005). SNAREs on the vesicle and on the target membrane must come together at the right compartment for membrane fusion to occur (Figure 1-2; Figure 1-3). The precise mechanism of how this is achieved was elucidated from the crystal structure of neuronal SNARE complex (Sutton et al., 1998). This structure showed that neuronal SNAREs zipper together in a parallel fashion which would bring the target membrane and vesicle membrane in very close proximity. They also showed that the complex consists of four SNARE motifs consisting of two SNARE motifs from SNAP25, one from STX1A and the other from VAMP/synaptobrevin (Sutton et al., 1998). For fusion to occur a SNARE complex must have a Qa, b, c and R-SNARE. However, it has been shown that SNARE complexes such as Qaaaa, Qabab, Qaabc and even QbccR could drive fusion in artificial systems (Yang et al., 1999, Bethani et al., 2007, Feldmann et al., 2009). Feldmann et al., 2009 immunoprecipitation assay from oligodendroglia cells showed that STX8, VAMP4 and SNAP 23 were in the same complex, therefore, giving a QbccR type of complex. Similarly, VAMP4, STX6 and SNAP29 were also in the same complex (Feldmann et al., 2009). The authors pointed out that these non-fusogenic complexes may act to inhibit other SNARE complex formation (Feldmann et al., 2009); however, how they do so is not well understood.

SNAREs do not function alone in membrane fusion. SM (Sec1/Munc18-like) is required for SNARE-mediated membrane fusion. SM proteins used their conserved 600 amino acid residue arched-shaped structure to clasp the

SNAREs four-helix bundle that are involved in membrane fusion (Sudhof and Rothman, 2009). There are seven SM proteins grouped into four main families Munc18, VPS33, VPS45 and SLY1 (Hong and Lev, 2014). Munc18 includes Munc18-1, Munc18-2 and Munc18-3; whereas the VPS33 consists of VPS33A and VPS33B (Hong and Lev, 2014, Graham et al., 2013). The role of SM proteins involvement in membrane fusion is still far from clear. However, a new model suggests that SM proteins promote membrane fusion by binding to either closed or open conformation of the N-terminal peptide and/or Habc domain of syntaxins (Baker and Hughson, 2016, Rathore et al., 2010, Hu et al., 2011). This initial SM binding to syntaxin was assumed to inhibit SNARE complex formation via locking syntaxin in a closed conformation (Dulubova et al., 1999, Misura et al., 2000). However, studies have shown that this provides a regulatory check to prevent premature SNARE assembly (Jahn and Fasshauer, 2012, Baker and Hughson, 2016). In addition, recent studies have shown that SM proteins chaperone STXs 1 and 11 to the plasma membrane where they mediate membrane fusion (Han et al., 2011, Dieckmann et al., 2015). Therefore, SM proteins rather play a direct regulatory and not inhibitory role in membrane fusion. The next step for SM mediated SNARE membrane fusion requires the opening of the helical hairpin of the SM protein/syntaxin complex, perhaps catalysed by Munc13, which provides an additional binding site for the attachment of an R-SNARE (Baker and Hughson, 2016). During neuronal transmission, complexin and synaptotagmin add another level of regulation and specificity by grappling the SNAREs and SM proteins to activate SNAREs vesicle-mediated signalling across the synapse (Sudhof and Rothman, 2009).

After membrane fusion, the SNARE complex becomes disassemble by NSF ATPases and SNAP. SNAP, NSF ATPase adaptor protein, binds the SNARE complex and the NSF ATPase provides the needed energy to disassemble the SNARE complex (Jahn and Scheller, 2006, Sudhof and Rothman, 2009). SNARE proteins become free to start another round of membrane fusion event.

1.3 Domain structure of SNAREs

1.3.1 Qa-SNAREs

Qa-SNAREs have an antiparallel three-helix bundle at their N-terminus termed the Habc domain (Figure 1-4). This domain in some members like STX1 and STX7 is capable of folding back onto the SNARE motif to form a close conformation so potentially regulating SNARE function (Hong, 2005, Malsam et al., 2008, Dietrich et al., 2003). However, this is not always the case and STX5 and STX16 do not form a closed formation at least not in vitro. However, they may do so in vivo (Hong, 2005). The N-terminal domain may also serve as platforms for attachment of regulatory proteins such as SM proteins (Jahn and Scheller, 2006, Ungar and Hughson, 2003, Rathore et al., 2010). The N-terminal domain harbours the N-terminal peptide and the Habc domain. The N-terminal peptide initiates the binding of SM proteins to syntaxins during membrane fusion (Rathore et al., 2010). The glutamine residue of syntaxins in the ionic layer is vital for SNARE complex dissociation (Scales et al., 2001). Q226R or Q226A mutants of STX1A form a complex with the NSF and α -SNAP similar to the wild type; however, the mutants increase the half-life of dissociation by about 5 fold (Scales et al., 2001). Syntaxins 2, 3, 4, 5, 13, 16, 17, 18 and TSNARE1 have C-terminal transmembrane domains which anchor them to membranes (Figure 1-4) (Hong, 2005). However, STX19 and STX11 have a C-terminal cysteine-rich domain which is palmitoylated that enables them to attach to membranes (Jahn and Scheller, 2006, Kang et al., 2008).

1.3.2 Qb- and Qc- SNAREs

Qb- and Qc-SNAREs can have Habc domains (Figure 1-4), however, it is unclear if they form closed conformations (Jahn and Scheller, 2006, Dietrich et al., 2003). The Qb-SNAREs include GS27, GS28, SEC20, VTI1, whereas the Qc-SNAREs include BET1, GS15, STX6, STX8, STX10, and SLT1 (Hong, 2005, Jahn and Scheller, 2006, Kloepper et al., 2008). STX6 has in addition to the Habc domain a tyrosine-based motif YGRL at residues 140-143 which facilitates its retrograde transport from the PM to TGN (Watson and Pessin,

2000, Jung et al., 2012) BET1 and GS15 are unusual as they do not have an N-terminal domain (Hong and Lev, 2014)

1.3.3 Qbc- SNAREs

SNAPs 23, 25, 29, and 47 have two SNARE motifs connected by a flexible linker (Figure 1-4) (Jahn and Scheller, 2006, Holt et al., 2006). The flexible linker has a varied length with the longest being found in SNAP47 followed by SNAP29, SNAP23 and the shortest being SNAP25. SNAP47 has an unusual extended N-terminal domain compared to the other members of this family (Holt et al., 2006). Qbc-SNAREs lack transmembrane domains but some have lipid anchors for membrane attachment (Figure 1-4) (Jahn and Scheller, 2006, Brunger, 2005). SNAP23 and SNAP25 have cysteine-rich domains which are palmitoylated whereas they are absent in SNAP29 and SNAP47 (Holt et al., 2006, Steegmaier et al., 1998, Ravichandran et al., 1996).

1.3.4 R-SNAREs

R-SNAREs can be divided into two main groups, brevins (VAMPs 1-5, and 8) and longins (Sec22b, YKT6, and VAMP7) (Figure 1-4) (Jahn and Scheller, 2006, Hong, 2005, Filippini et al., 2001). It is thought the brevins have evolved from longin type R-SNAREs (Filippini et al., 2001) as longins are highly conserved in all Eukaryotes while brevins are missing from plants and protists (Rossi et al., 2004). The longin domain is 110-140 amino acids in length and consists of five beta sheets and four alpha helices reassembling profilin (Tochio et al., 2001, Gonzalez et al., 2001). The alpha A helix lies after beta I and beta II sheets, and the remaining alpha helices (B, C and D) follow the beta III, IV and V sheet (Tochio et al., 2001, Gonzalez et al., 2001). The longin domain also contains four conserved phenylalanine amino acid residue at positions (31, 39, 42 and 43) serving as hydrophobic patches (Tochio et al., 2001). In YKT6 and VAMP7 it has been shown that the longin domain can fold back onto the SNARE motif and form a closed conformation (Pryor et al., 2008, Tochio et al., 2001). However, the longin domain of Sec22b does not interact with its SNARE motif (Gonzalez et al., 2001). The majority of R-SNAREs contain a C-terminal TM domain of 18-25 amino acids in length (Figure 1-4) (Hong, 2005). YKT6

does not have a TM domain but a cysteine-rich domain that undergoes farnesylation and palmitoylation (Filippini et al., 2001). Fluorescence and electron paramagnetic resonance analyses show that in VAMP2 the transmembrane domain is required for SNARE complex formation with SNAP25 and STX1 (Kweon et al., 2003b). The study also revealed that when the two interfacial tryptophan residues (W89S and W90S) in VAMP2 were changed to serines it increases VAMP2 SNARE complex formation (Kweon et al., 2003b). VAMP4 has an N-terminal extension containing a dileucine motif enriched with acidic amino acids which are required for its trafficking from endosomes to the TGN (Peden et al., 2001).

1.4 SNAREs in constitutive secretion

The molecular understanding of the early secretory pathway is very good and all of the SNAREs which act between the ER and the Golgi have been identified (Parlati et al., 2000, Hatsuzawa et al., 2000, Xu et al., 2002, Parlati et al., 2002, Volchuk et al., 2004). However, in animal cells, it is not known which SNAREs are required for the fusion of secretory vesicles with the plasma membrane. To address this Gordon et al., 2010 performed a SNARE specific siRNA screen. Using siRNA screening approach, our lab identified two novel post-Golgi SNAREs STX19 and SNAP29 to be required for constitutive secretion (Figure 1-5) (Gordon et al., 2010). The depletion of STX19 and SNAP29 independently reduces the number of secretory vesicles fusing with the plasma membrane (Gordon et al., 2010). SNAP29 knockdown also leads to an increase in the number of secretory vesicles docked under the plasma membrane (Gordon et al., 2010). This shows that both STX19 and SNAP29 play a role in secretion. Furthermore, the study confirms previously identified ER to Golgi SNAREs STX5, GS27, YKT6 and SEC22B that are required for secretion (Figure 1-5). A recent genome-wide siRNA by (Simpson et al., 2012) also identified SNAP29 and STX19 as being required for the constitutive secretion so confirming their involvement in this process.

1.4.1 STX9/19

STX19 was first cloned and characterised by Wang et al., 2006. STX19's closest homologue is STX11 (38% identity) an immune-specific Qa-SNARE.

STX19 is predominantly expressed in epithelial cells of the stomach, skin and lung (Wang et al., 2006). STX19 does not have a transmembrane domain but has a cysteine-rich region at its C-terminus. A study on neural palmitoyl proteomics by Kang et al., 2008 showed that STX19 is palmitoylated. Thus, STX19 may associate with membranes through this modification (Kang et al., 2008). The study by Wang et al., 2006 showed that over expressed-tagged STX19 is found at the PM and on other intracellular compartments and that overexpressed STX19 interferes with EGF-R but not TF-R trafficking (Wang et al., 2006). HA-tagged STX19 interacts with SNAP29, 23 and 25; and VAMP 3, and 8 by IP supporting its proposed role in post-Golgi transport (Gordon et al., 2010).

1.4.2 SNAP29/GS32

SNAP29 was first cloned by (Stegmaier et al., 1998, Wong et al., 1999). SNAP29 is a Qbc-SNAREs so has two SNARE motifs. It has been speculated that SNAP29 might interact with membranes via its interaction with syntaxins (Hohenstein and Roche, 2001) or other unknown proteins. It has been shown that SNAP29 can bind to the endocytic protein EHD1 (Rotem-Yehudar et al., 2001, Xu et al., 2004). However, it is unclear what the functional significance of this interaction is. In Oligodendrocyte and oligodendroglial precursor cell lines, SNAP29 shows cytoplasmic and PM staining (Feldmann et al., 2009). SNAP29 appears to be a promiscuous SNARE as it has been found to interact with SNAREs which function on different pathways such as STX4, 6 and 7 (Hohenstein and Roche, 2001). Loss of SNAP29 in humans causes CEDNIK syndrome (Cerebral Dysgenesis, Neuropathy, Ichthyosis and Keratoderma) a very rare neuroanatomical genetic disorder (Sprecher et al., 2005). Cells generated from CEDNIK patients show alteration in Golgi morphology. However, the transport of proteins such as VSVG from the Golgi to the plasma membrane appears to be normal (Rapaport et al., 2010). The main defects in trafficking observed in these cells are alterations in transferrin receptor and integrin beta one trafficking (Rapaport et al., 2010). Thus SNAP29 may be involved in cell migration and spreading (Rapaport et al., 2010). Disruption of

the SNAP29 orthologue in *C. elegans* causes defects in both the biosynthetic and endocytic pathways (Kang et al., 2011).

SNAP29 has also been implicated in autophagy. SNAP29 form a SNARE complex with STX17 and VAMP8 to drive autophagosome lysosomal fusion (Itakura et al., 2012). Using autophagy flux assay, Itakura et al., 2012 shows that knockdown of SNAP29 causes LC3-II accumulation and autophagic flux impairment (Itakura et al., 2012). A recent study has shown that O-linked β -N-acetylglucosamine (O-GlcNAc) transferase (OGT) knockdown promotes STX17-SNAP29-VAMP8 complex formation both in mammalian cells and *C. elegans* which enhance autophagosome lysosomal fusion and autophagic flux (Guo et al., 2014). SNAP29 is O-GlcNAcylated at sites S2, S61, S153 and Y130 (Guo et al., 2014). The study further reveals that the enhanced SNARE complex formation in the absence of OGT or glucose starvation is as a result of the absence or reduction of O-GlcNAcylation in SNAP29 (Guo et al., 2014). In *Drosophila* cells a stx17-usnp (snap29)-VAMP7 SNARE complex has been shown to be involved in autophagy (Takats et al., 2013). Depletion of either proteins results in the accumulation of Atg8 in the perinuclear region (Takats et al., 2013). Moreover, there was impairment in the progression of the autophagosomes into autolysosomes as they are unable to fuse with the lysosomes (Takats et al., 2013).

SNAP29, therefore, is involved in several important biological processes including; autophagy, cell development, endocytosis and exocytosis.

1.5 The endocytic pathway

Proteins and lipids are continually being internalised from the cell surface in a process known as endocytosis. Endocytosis is required for nutrient uptake as well as recycling membranes delivered to the cell surface via biosynthetic transport. In addition, it is also involved in a diverse range of processes including cell migration, cytokinesis and signal transduction (Grant and Donaldson, 2009). Endocytosis has been characterised by its magnitude, rapidity, and sorting (Steinman et al., 1983).

1.5.1 Clathrin-dependent and-independent endocytosis

Coated vesicles facilitate the endocytosis of cell surface receptors such as the TF-R and LDL-R. It was identified that the major component of this coat is clathrin (Pearse, 1976). A decade later, Brown and Orci showed that endocytic vesicles of kidney intercalated cells do not have a clathrin coat suggesting that there may be more than one type of endocytic vesicle (Brown and Orci, 1986). Over the years a large number of studies have been performed and it is generally accepted that endocytosis can be broadly classified into two main types; clathrin-dependent and clathrin-independent (Steinman et al., 1983, Pearse, 1976, Brown and Orci, 1986, Grant and Donaldson, 2009). These pathways have been defined based on endocytic machinery and cargo (Grant and Donaldson, 2009). Proteins such as the TF-R and LDL-R are only internalised by CDE; MHCII and CD59 are only internalised by CIE and EGF-R can be internalised by both processes. Surprisingly, there is evidence to suggest that after internalisation these separate pathways merge and their cargo can be found in the same endocytic recycling structures (Grant and Donaldson, 2009). Recently the idea of clathrin and clathrin-independent endocytosis has been challenged and it has been proposed that clathrin-mediated endocytosis accounts for over 95% of all endocytosis occurring within the cell (Bitsikas et al., 2014).

1.6 The endocytic compartments

The compartments of the endosomal pathway were first identified and characterised using electron microscopy. It was observed that the endocytosed material was first delivered to structures just under the cell surface and over time this material moved to structures deeper inside the cell. Subsequently, these compartments have been defined by their physiological properties and the molecular machinery which is localised to them.

1.6.1 Endosomal maturation

The endosomal system broadly consists of early endosomes, recycling endosomes, late endosomes and lysosomes (Figure 1-7). The ionic content and pH of these structures are different which reflects their function (Scott and Gruenberg, 2011). The extracellular pH decreases from 7.4 to 6.2 in early

endosomes and to 5.0 in late endosome (Figure 1-7). The potassium ion concentrations increase from 0.5 mM to 60 mM, however, sodium ions decrease from 120 mM to 20 mM (Scott and Gruenberg, 2011). There are also differences in calcium and chloride ions in the different endosomal compartment (Piper and Luzio, 2004).

Early endosomes provide the first opportunity for sorting when internalised proteins enter the cell (Scott et al., 2014). At this compartment it is decided whether internalised receptors and their ligands should be degraded or recycled back to the cell surface (Scott et al., 2014). After sorting, receptors are recycled back to the cell surface via the recycling endosomes and their ligands degraded in the lysosome (Scott et al., 2014). Lipids and protein components that are destined for degradation form intraluminal vesicles and the early endosomes are then called multivesicular bodies (Scott et al., 2014). The multivesicular bodies fuse with the late endosomes or exosomes. The late endosomes fuse with the lysosomes to degrade their content. Lysosomes not only fuse with late endosomes but also fuse with autophagosomes, phagosomes and macropinosomes (Luzio et al., 2007, Huotari and Helenius, 2011). During endosomal maturation, there is a continual exchange of materials between the endosomal compartments and the TGN (Huotari and Helenius, 2011). This process plays a part in the delivery of newly synthesised hydrolases to late endosomes (Huotari and Helenius, 2011). The array of changes required for the maturation of early endosome to late endosome is very complex and cannot all be covered in this thesis. The process requires changes in Rab proteins, recruitment of new tethering and SNARE complexes for fusion, the formation of intraluminal vesicles, acquisition of new motor proteins to aid movement to the perinuclear region, changes in phosphatidylinositide present in the endosomal membranes

1.6.2 Rab small GTPases

There are about 70 characterised Rabs in humans (Figure 1-6). Rabs switch between activated GTP-bound and inactivated GDP-bound state facilitated by a guanidine nucleotide exchange factor (GEF) and GTPases activating proteins (GAPs) (Stenmark, 2009, Lee et al., 2009, Zhen and Stenmark, 2015,

Wandinger-Ness and Zerial, 2014). GEFs activate Rabs by removing GAP and then exchange GDP with GTP (Figure 1-6). The GAPs promote GTP-bound Rab to hydrolyze GTP into GDP thereby switching off the activated Rab (Figure 1-6). Rab effectors mostly associate with a GTP-bound state of Rab. Rabs serve as a regulator during vesicle trafficking as they cycle through their membrane-bound active state and cytosolic inactive state and this they do with their effectors (Bock et al., 2001, Zhen and Stenmark, 2015). Rabs spatiotemporally recruit and activate their effectors to bring about this regulatory mechanism during vesicle trafficking (Bock et al., 2001). Also, effectors may recruit Rabs to a defined intracellular compartment for it to function properly.

1.6.2.1 The structure of Rab small GTPases proteins

Rabs share a conserved guanine, phosphate and magnesium binding motif as the other members of the RAS superfamily (Pereira-Leal and Seabra, 2000). They are distinguished from the superfamily by other different conserved motifs including RabF1-F5, RabSF1-F4, double cysteines for prenylation (few with one cysteine), Rab complementarity domain region (RabCDRI-III)(Pereira-Leal and Seabra, 2000, Merithew et al., 2001). The RabF1-F5 together with the switch regions may serve to discriminate between Rab effectors and regulators in relationship to active or inactive Rab by binding to RabGDI (RAB dissociation inhibitor) and REP (Rab escort protein) (Pereira-Leal and Seabra, 2000) . The RabCDRI-III correspond to RabSF1, RabSF3 and RabSF4 respectively and they provide specificity between Rabs and their different effectors and regulators (GEFs, GAPs) (Pereira-Leal and Seabra, 2000).

Rabs like other small GTPases have a C-terminal hypervariable domain that harbours the prenylation cysteine site. Most Rabs have two cysteines (few have one cysteine) that are required for geranylgeranylation. Geranylgeranylation is a post- translation modification that promotes Rab membrane association catalysed by geranylgeranyl transferase (GGTasell) and REP. Conversely, RABGDI promotes cytosolic forms of RABs by removing GGTasell and then transport them to another membrane compartment.

1.6.3 Endosomal maturation requires Rab5/7 switch

Rab5 together with its effectors regulate the recruitment of tethering complexes for the fusion of endocytic cargoes with the early endosomes. Also, Rab5 acts with its effectors EEA1, Rabenosyn-5 and Rabaptin-5, endosomal SNAREs (STX12, STX16, VTI1, VAMP4) to promote homotypic fusion in the early endosome (Galvez et al., 2012). Rab5 effectors VPS34/p150 (p150 is for yeast) is also involved in the formation of Ptlns(3)P. This creates an opportunity for further recruitment of proteins containing FYVE, PH, PX and GRAM domains that binds to phosphoinositide (Huotari and Helenius, 2011). During the progression of early endosome to late endosome, Rab5 is exchanged for Rab7 (Huotari and Helenius, 2011, Galvez et al., 2012). Rab7GTP recruits effectors such as RILP. RILP recruits dynein onto late endosomes and aids the movement to the perinuclear region where they can fuse with lysosomes (Huotari and Helenius, 2011). The main purpose of the exchange of Rab5 for Rab7 is to enable the endosomal membranes to recruit a new set of tethering and fusion complexes such as the HOPS complex (Huotari and Helenius, 2011). This is vital for the promotion of homotypic fusion between late endosome and also a heterotypic fusion between late endosomes and lysosomes or phagosomes (Huotari and Helenius, 2011, Kummel and Ungermann, 2014).

1.6.4 Recycling endosomes

Recycling endosomes have a slightly higher pH (6.4-6.5) compared to the other endosomal compartments. There are several types of RE defined by protein and lipid composition and localisation within the cell. Recycling endosomes can emanate from the early endosome (sorting endosome) and or the ERC near the perinuclear region. Recycling endosomes are involved in both fast and slow recycling of receptors, retrograde transport of cargoes to the TGN, exocytic delivery of newly synthesised proteins and lipids to the PM, autophagosome formation and lysosomal degradation (Hsu and Prekeris, 2010, Taguchi, 2013, Longatti and Tooze, 2012). E-cadherin, VSVG, tumour necrosis factor-alpha, HRAS have all been shown to exit from the Golgi to the PM through Rab11 recycling endosomes (Taguchi, 2013). Cholera and Shiga toxins utilise

recycling endosomes retrograde transport to effect its cytotoxicity (Taguchi, 2013). Golgi resident proteins such as TGN46, CIMPR are routinely retrieved back to the Golgi from the PM via retrograde transport using recycling endosomes (Taguchi, 2013).

1.6.5 Fast and slow endocytic recycling

Cells use two distinct recycling pathways which are under the regulation of different Rab proteins (Figure 1-6). Cargoes internalised in the early endosomes are either recycled back to the cell surface through Rab4 and Rab35 mediated fast recycling or can be transported to the ERC which is close to the perinuclear region using Rab11 where it is recycled back to the cell surface (slow recycling pathway). Rab11 together with its effectors Rab11FIP2 and other proteins such as EHD1, 3, 4 (Grant and Donaldson, 2009, Naslavsky et al., 2006, Sharma et al., 2008, Grant and Caplan, 2008) and MICAL-L1 (Sharma et al., 2010, Sharma et al., 2009) have been associated with the regulation of the slow recycling pathway. Cargoes sorted are trafficked with the help of SNX4 and dynein motors to the ERC thereby protecting them from degradation in the lysosome (Grant and Donaldson, 2009). Although cargoes from both CDE and CIE merges at the early endosomes and then deliver to the ERC, after recycling they go their separate way to the PM using either Rabs 8, 10, 11, 13 or 22 (Grant and Donaldson, 2009). Under different stimulation conditions receptors can change which recycling pathway they take. For example, DRD2L (dopamine receptor D₂ long isoform) is predominantly trafficked via a Rab4 dependent pathway in the absence of dopamine but in the presence of dopamine it uses a Rab11 dependent pathway (Li et al., 2012).

1.7 Endocytic recycling machinery

Several proteins have recently been identified to be involved in the biogenesis of tubular recycling endosomes. They are EHD1, MICAL-L1, RAB8A and PACSIN2 (Caplan et al., 2002, Sharma et al., 2009, Rahajeng et al., 2012, Cai et al., 2012, Giridharan et al., 2012). These proteins have been shown to form a large complex predominantly facilitated through interactions between NPF motifs and EHD1. Depletion of EHD1, MICAL-L1, and RAB8A causes defects in

the recycling of both clathrin-dependent and -independent cargo such as the TF-R and β 1-integrin.

1.7.1 RAB8

Rab8 was first identified and cloned from an MDCK cDNA library as it shares approximately 60% sequence similarity with yeast Ypt1/Sec4 (Chavrier et al., 1990). Rab8 has two isoforms Rab8A and Rab8B sharing about 83% identity (Armstrong et al., 1996). Unlike most members of the Rab family that have CC or CXC motif, Rab8 has CaaX box motif similar to other Ras proteins (Chavrier et al., 1990). However, Rab8 is geranylated either in the presence of REP (when catalysed by GGTasell) or absence of REP (when catalysed by GGTasel) (Wilson et al., 1998).

1.7.1.1 RAB8 GEFs and GAPs

Rab8 cycles between an active GTP-bound and inactive GDP-bound state. Rabin8 and GRAB serve as RabGEFs for Rab8. They were identified through yeast two-hybrid screening and GST pull-down assays (Hattula et al., 2002, Yoshimura et al., 2010). Rabin8 specifically binds GDP-Rab8 (T22N) and not GTP-Rab8 (Q67L). Rabin8's GEF activity was confirmed by using radioactive labelled GDP-Rab8 in the presence of excess GTP. The addition of purified Rabin8 dramatically enhanced the rate at which GDP was exchanged for GTP (Hattula et al., 2002).

The crystal structure of Rab8 in complex with its GEFs Rabin8 (157-232) and GRAB (79-149) have been solved (Guo et al., 2013). The GEFs mainly interact with the switch regions which undergo conformational changes, as a result, the nucleotide binding affinity is lost (Guo et al., 2013). Phe-33 and Ile-38 both in the switch I is displaced and also there is a creation of a new α -helix affecting nucleotide binding affinity (Guo et al., 2013). TBC1D30, TBC1D1, and TBC1D4 have all been identified as Rab8 GAPs, although they may have a broad range of GAP activity towards other Rab proteins (Peranen, 2011).

1.7.1.2 RAB8 effector proteins

A number of Rab8 effector proteins have been identified including OCRL1, MICAL-3, MICAL-L1, MICAL-L2, Rabaptin5, Myosin5 (Hou et al., 2011,

Peranen, 2011). Rab8 associates with OCRL1 using the β - β zipping mode (Khan and Menetrey, 2013, Hou et al., 2011). Residues 539_901 of OCRL1 bind to Rab8 (Hou et al., 2011). The crystal structure of Rab8 (6-176) and OCRL1 (540-678) indicate that Rab8 associates with OCRL1 via Rab8 switch I (E30, I41, G42, I43) and switch II (R69, F70, Y77) in addition to α 1 helix, β 2 strand to form a complex with β 9 strand of OCRL1 (Hou et al., 2011). A point mutation in OCRL1 S564P completely abolishes the interaction between OCRL1 and Rab8 by interfering with the α 1 helix conformation (Hou et al., 2011).

1.7.1.3 RAB8 function

Rab8 and its effector proteins are thought to be involved in both biosynthetic and endocytic transport. Rab8 is localised to secretory carriers such as GLUT4 vesicles budding from the TGN (Miinea et al., 2005). Rab8 has been proposed to play a key role in docking secretory vesicles with the PM. It is thought that Rab6 recruits Rab8 onto biosynthetic vesicles that have exited from the Golgi (Grigoriev et al., 2011). MICAL3 binds Rab8 via its coiled-coil domain and links Rab8 and ELKS (A Rab6 interacting cortical factor) (Grigoriev et al., 2011). However, depletion of Rab8 using siRNA only has a very modest effect on constitutive secretion.

Rab8 also functions in primary ciliogenesis and recycling of proteins from the ERC (Grant and Donaldson, 2009) . During ciliogenesis, GTP-bound Rab11 interacts with Rabin8 which facilitates the latter's GEF activity towards Rab8 (Knodler et al., 2010). This coordinates the delivery of cargoes from the Rab 11 recycling endosomes and subsequent docking of vesicles at the PM via Rab8 providing the necessary proteins required for ciliogenesis (Knodler et al., 2010).

Rab8 is thought to play an important role in regulating cell migration and invasion. Rab8 is localised to filopodia and lamellipodia of migrating cells and is also found on endocytic tubules (Peranen, 2011). In MDA-MB-231 cells, overexpression of constitutively active Rab8 (Rab8Q67L) or wtRab8 but not membrane inactive Rab8 mutant increased transport of MT1-MMP to invadopodia causing increased degradation of collagen (Bravo-Cordero et al., 2007). During cell migration, cells form adhesive contacts both at their rear and

at their leading edge front (Hood and Cheresch, 2002). Cells protrude due to actomyosin forces acting on them (Geiger et al., 2009). Depletion of Rab8 or overexpression of a dominant negative Rab8 (T22N) strongly impairs cell protrusion by enhancing actin stress fibre formation and increased cell-cell contact (Hattula et al., 2006). Rab8 thus regulates cell migration by either directly regulating actomyosin force generation and or delivery of materials to the protruding edge of the migratory cell. In polarised epithelial cells, Rab8 interaction with its effector myosin 5b is required for lumen formation. Myosin 5b is an effector for Rabs 8, 10 and 11. Point mutations in myosin 5b (Q1300L and Y1307C) which abolishes its interaction with Rab8 impairs with the apical delivery of podocalyxin/gp135 in MDCK cells which affects de novo lumen formation (Roland et al., 2011).

1.7.2 MICAL-L1

MICAL-L1 is a Rab8 effector protein (Sharma et al., 2010). It has two unique NPF motifs (NPF1, NPF2), two coiled-coil domains and is lacking the FAD domain found in other members of the MICAL family (Figure 1-8) (Rahajeng et al., 2010). MICAL and MICAL-like family proteins possess a calponin homology (CH) and Lin1-1, Isl-1 and Mec3 (LIM) domains that have been shown to interact with phosphatidylinositol-(4,5)-bisphosphate (PIP₂) and cytoskeletal elements (Rahajeng et al., 2010).

MICAL-L1 can form a closed inactive conformation via the interaction between the C-terminal Rab binding domain (RBD) and the N-terminal calponin homology domain (Abou-Zeid et al., 2011). This closed conformation can be opened by its interaction with GTP Rab13 (Abou-Zeid et al., 2011).

1.7.2.1 MICAL-L1 function

It has been shown that MICAL-L1 directly recruits EHD1 and Rab8 to tubular recycling endosomes (Sharma et al., 2009). MICAL-L1 can be recruited to pre-existing tubular membranes generated from phosphatidic acid without the aid of Rab8 and EHD1 (Sharma et al., 2009, Giridharan et al., 2013). However, Rab8 and EHD1 recruitment to these structures require MICAL-L1 (Sharma et al., 2009). The NPF1 motif of MICAL-L1 is necessary for its interaction with EHD1

and its C-terminal coiled-coil domains facilitates its interaction with Rab8 and tubular endocytic membranes (Sharma et al., 2009). The coiled-coil regions of MICAL-L1, 672-863 are required for its correct tubular localisation (Sharma et al., 2009).

MICAL-L1 is required for the recycling of TF-R, integrin and EGFR. Depletion of MICAL-L1 using RNAi perturbs the endocytic recycling of transferrin receptor through the clathrin-dependent pathway and integrin beta one through the clathrin-independent pathway (Sharma et al., 2009). MICAL-L1 interaction with GTP Rab13 aids EGFR trafficking (Abou-Zeid et al., 2011). Silencing of MICAL-L1 negatively affects EGFR trafficking by promoting EGFR ubiquitination and subsequent degradation (Abou-Zeid et al., 2011). This phenotype was rescued by overexpression of either GFPMICAL-L1 or shRNA-resistant mcherry MICAL-L1 (Abou-Zeid et al., 2011).

MICAL-L1 is also required for focal adhesion turnover, cell spreading and cell migration (Reinecke et al., 2014b). In mouse embryonic SYF null cells (mutant cells lacking Src, Yes and Fyn), MICAL-L1 transiently colocalises with both endogenous and overexpressed Src and not the other members of the SFK (Yes/Fyn) at the long tubular endosomes and tubulovesicular structures (Reinecke et al., 2014b). Knockdown of MICAL-L1 impairs EGFR-induced Src activation in HeLa cells and therefore reduces Src localisation to focal adhesion structures (Reinecke et al., 2014b). Activated Src is transported from the ERC to the PM where they colocalise with adhesive structures, however, the absence of MICAL-L1 results in the accumulation of activated Src in the perinuclear region (Reinecke et al., 2014b). Therefore, MICAL-L1 is required for Src activation, transport from the ERC and subsequent localisation to focal adhesion structures.

Further experiments have established the role of MICAL-L1 in regulating FA turnover. Knockdown of MICAL-L1 in BJ cells moderately affects pY419 Src (Reinecke et al., 2014b). It also results in prominently larger FAs which could not turnover as the result of the failure of Src and vinculin recruitment by MICAL-L1 into these structures (Reinecke et al., 2014b). This was partially restored by reintroduction of a siRNA-resistant MICALL-L1 construct.

Moreover, MICAL-L1 depleted BJ cells fail to polarise properly on fibronectin as shown by the poor orientation of the Golgi apparatus to the area of the created wound and stress fibres not being perpendicular to the area of the created wound resulting in poor cell spreading and impairment in cell migration (Reinecke et al., 2014b).

MICAL-L1 is also involved in various aspect of the cell cycle. MICAL-L1 localises to ingression furrow and intercellular bridge during early and late cytokinesis respectively (Reinecke et al., 2014a). It regulates mitotic spindle length and mediates recycling endosome transport to the intercellular bridge independent of EHD1, RAB11 and RAB35 (Reinecke et al., 2014a). Furthermore, it is required for regulating kinetochore-microtubule dynamics. Silencing MICAL-L1 increases mitotic spindle length, produces longer/stable kinetochore fibres and failure of microtubules to terminate appropriately at kinetochore ends (Reinecke et al., 2014a).

1.7.3 EHD1

EHD1 is an endocytic adaptor protein which binds proteins containing NPF motifs. EHD proteins are different from other EH domain-containing proteins like Eps15 as they have their EH-domain at their C-terminus (Grant and Caplan, 2008). The EHD proteins have two helical domains, one at the N-terminus and the other between their ATP-binding G-domain and the EH-domain (Figure 1-9) (Grant and Caplan, 2008). The EH-domain of EHD1 interacts with the N-terminal NPF motif of SNAP29 (Xu et al., 2004). An earlier study also showed that EHD1, EHD1, EHD3, and even EHD1 lacking N or C-terminus interacts with SNAP29 (Rotem-Yehudar et al., 2001). EHD1 associates with the membrane through its nucleotide binding sites in the P-loop, whereas the EH domain, was suggested to be required for tubular membrane formation with the help of microtubules and nucleotide cycling of ARF6 (Caplan et al., 2002). In HeLa, COS7, and M1 cells but not CHO cells overexpression of GFP EHD1 shows extensive tubular membrane localisation (Caplan et al., 2002). However, overexpression of a C-terminal truncated EHD1 mutant (lacking the EH domain) produces vesicular rather than tubular structures (Caplan et al., 2002). The C-terminal domain of EHD1 is what enables it to associate with proteins such as

MICAL-L1 that facilitate its recruitment onto tubules (Sharma et al., 2009). Therefore, the absence of this domain prevents EHD1 tubular membrane association. Also, it has been shown that substitution of G65 to R65 in the P-loop domain of EHD1 renders the protein cytosolic (Caplan et al., 2002), likewise when K220 was mutated to N220 (Sharma et al., 2009). These regions harbour the ATP-binding domain which might enable EHD1 association with Rab proteins to enable its membrane localisation (Caplan et al., 2002, Grant and Caplan, 2008).

Recent studies have ruled out EHD1 involvement in tubular membrane formation as EHD1 only binds to pre-existing tubules enriched with MICAL-L1 and PACSIN2 (Sharma et al., 2009, Giridharan et al., 2013). EHD1 is involved in tubule vesiculation which requires close interaction between cPLA2 α and EHD1 (Cai et al., 2012). cPLA2 α and EHD1 moderate membrane scissions of GPI-APs containing tubules (Cai et al., 2012). There are four isoforms of EHD proteins, EHD1-4 (Naslavsky and Caplan, 2011). EHD1 and EHD3 bind strongly to MICAL-L1 with EHD4 binding moderately, whereas EHD2 does not bind at all (Sharma et al., 2009).

1.7.3.1 EHD1 function

EHD1 is required for recycling of both clathrin-dependent and -independent cargoes (Lin et al., 2001, Caplan et al., 2002, Jovic et al., 2007). In TRVb-1 cells, overexpression of a dominant negative RME-1/EHD1 slows down TF-R recycling from the ERC to PM but does not inhibit TF-R internalisation (Lin et al., 2001). Integrin β 1 recycling is impaired in EHD1 null fibroblasts and cells depleted of EHD1 (Jovic et al., 2007). EHD1 colocalises with ARF6 on the ERC and plays a role in MHC-Class 1 recycling (Caplan et al., 2002). Also, EHD1 depletion affects Src transport from the perinuclear region leading to its retention in the ERC (Reinecke et al., 2014b).

EHD1 is also involved in various aspect of mitosis including mitotic spindle orientation, and cell cycle regulation (Reinecke et al., 2014a). EHD1 is recruited to ingression furrow and intercellular bridge during early and late cytokinesis respectively with the aid of MICAL-L1 (Reinecke et al., 2014a). EHD1 mediates recycling endosomes transport to the intercellular bridge which is dependent on

MICAL-L1 (Reinecke et al., 2014a). Silencing EHD1 changes mitotic spindle orientation from 5° to greater than 10° (Reinecke et al., 2014a).

1.7.3.2 EHD paralogues (EHD 2-4) function

The other EHD paralogues (EHD 2-4) have all been implicated in the recycling of proteins. Depletion and overexpression of EHD2 impair both TF-R and Glut4 endocytosis (Guilherme et al., 2004). EHD3 which is the closest paralogue to EHD1 affects endosomal-Golgi transport (Naslavsky et al., 2009). EHD4 colocalises with EEA1, Rab5 and Arf6 endosomes (Sharma et al., 2008). EHD4 silencing accumulates TF-R, MHC1 and LDLR in EEA1/Rab5 positive structures (Sharma et al., 2008). EHD3 and EHD4 null mice show a characteristic smaller and paler kidney which may be as a result of defective VEGFR2 trafficking (George et al., 2011)

1.7.4 PACSIN2/Syndapin2

PACSIN2 is an F-BAR domain containing protein and is thought to be involved in membrane tubulation (Senju et al., 2011, Dawson et al., 2006, Wang et al., 2009). Bar proteins have a characteristic curved six α -helical coiled-coil domains that deposit positively charged residues on negatively charged phospholipid membranes to initiate membrane bending (Quan and Robinson, 2013). There are three F-BAR isoforms in mammals (PACSINs 1-3). They all have an N-terminal conserved F-Bar domain that binds to their SH3 domain to autoinhibit their activities. PACSIN 1 and 2 have one and three NPF motifs respectively (Figure 1-10). The NPF motif is absent in PACSIN 3. PACSIN 1 and 3 have distinct localisations. PACSIN 2 is ubiquitously expressed (Quan and Robinson, 2013). PACSIN1 is expressed in neurons, whereas PACSIN 3 can be found in heart and skeletal muscles (Quan and Robinson, 2013).

PACSIN2 contains an NPF motif which facilitates its binding to EHD1. PACSIN2's SH3 domain interacts with the PRD motif of MICAL-L1. The binding of PACSIN2 to MICAL-L1 helps recruit EHD1 to TRE. The interaction between PACSIN2 and MICAL-L1 stabilises the formation of tubular recycling endosomes (Giridharan et al., 2013).

1.7.4.1 PACSIN2 function

PACSIN2 is involved in curving caveolae from the PM which is required for internalising cargoes using caveolae-mediated pathway (Senju et al., 2011). Electron microscopy image shows that endogenous PACSIN2 localises to the neck of PM invaginations (caveolin-1 positive structures) which are characteristics of caveolae (Senju et al., 2011). Moreover, endogenous PACSIN2 colocalises with caveolin-1 to induce membrane tubulation (Senju et al., 2011). Knockdown of PACSIN2 increases the diameter and depth of PM invaginations that were positive for caveolin-1 (Senju et al., 2011). This is as a result of perturbation of dynamin recruitment to caveolae to excise the invaginated membranes (Senju et al., 2011). PACSIN2 depletion impairs cholera toxin B uptake which is mediated by caveolae endocytic pathway (Senju et al., 2011). These phenotypes were restored upon overexpression of wt PACSIN2 but not R254E mutants (deficient in membrane binding) (Senju et al., 2011).

PACSIN2 interaction with OCRL1 via IPIP27A and is required for the biogenesis of membrane transport carriers (Billcliff et al., 2016). Using GST-pull down assay coupled to MS analysis, PACSIN2 was identified to interact with IPIP27A (Billcliff et al., 2016). Further experiments using GFPTRAP IP of PACSIN2 or its SH3 domain also confirmed this interaction (Billcliff et al., 2016). PACSIN2 SH3 domain binds the PXXP motif of IPIP27A which links the former (PACSIN 2) to interact with OCRL1 (Billcliff et al., 2016). The absence of IPIP27A abrogates the interaction between PACSIN2 and OCRL1 (Billcliff et al., 2016). PACSIN2 stimulates OCRL1 phosphatase activities which are required for generating CIMPR carrier biogenesis (Billcliff et al., 2016). In COS7 cells, GFP PACSIN2 colocalises with OCRL1 (only in the presence of IPIP27A) at the TGN and recycling endosomes (Billcliff et al., 2016). Depletion of PACSIN2 reduces GFPCIMPR tubular membrane formation and also affects CD8-CIMPR reporter trafficking from the early endosomes to the TGN (Billcliff et al., 2016).

PACSIN2 regulates the dynamics of actin and microtubules through its association with N-WASP and tubulin respectively. The SH3 domain of PACSIN2 associates with the PRD of N-WASP (Quan and Robinson, 2013).

This provides an important link between endocytic machineries and actin dynamics that is needed for actin cytoskeleton organisation (Quan and Robinson, 2013). PACSIN2 has also been shown to interact with tubulin via its F-BAR domain to promote the assemble of microtubules (Quan and Robinson, 2013).

1.8 Rab11 recycling endosomes and Rab8/MICAL-L1 tubular recycling endosomes are distinct structures

The endocytic recycling compartment consists of a cluster of vesicles and tubules in the perinuclear region of the cell (Figure 1-11). Tubular recycling endosomes (TRE) emanate from this region and in HeLa cells can reach lengths of 10 μm (Xie et al., 2015). Classical recycling endosomes contain molecules such as the TF-R and LDL-R while TRE contains proteins such as MHC Class I and CD55/59. Rab11 and MICAL-L1 endosomal structures on the whole are distinct and are thought to be involved in the recycling of different cargo. Rab11-RE are required for the recycling of the TF-R from sorting endosomes to the ERC, whereas MICAL-L1 aids the recycling of CD59 and integrin beta one (Xie et al., 2015). Depletion of Rab11a or overexpression of a dominant negative of Rab11a (S25N) impairs TF-R recycling but not CD59 or integrin beta one recycling (Xie et al., 2015). Overexpression of a dominant negative form of myosin 5b which binds Rab11 blocks TF-R recycling but does not affect MICAL-L1 TRE (Xie et al., 2015). Surprisingly, depletion of MICAL-L1 affects the exit of TF-R from the ERC even though the proteins do not colocalise (Sharma et al., 2009, Ren et al., 1998). On the whole, the machinery of these endosomal compartments is also distinct. For example, Rab11a positive endosomes label for FIPs and KIF13A, whereas MICAL-L1 positive endosomes label for proteins such as Rab8a and Syndapin 2 (Goldenring, 2015). However, EHD1 and EHD3 are found on both types of endosomal structure. This may in part explain why overlapping phenotypes are sometimes observed when the endocytic recycling machinery is depleted.

1.9 The physiological relevance of the endocytic pathway

Endocytosis is required for several important physiological processes in the cell. It is required for cytokinesis, cell migration, maintenance of cell polarity, cell signal transduction and synaptic transmission (Doherty and McMahon, 2009, Sorkin and von Zastrow, 2009, Stenmark, 2009, Grant and Donaldson, 2009). For these reasons, defects in endocytosis are implicated in several disease conditions including cancers; neurodegenerative diseases (Alzheimer's, Huntington, Charcot-Marie-Tooth, Down syndrome, Carpenter syndrome, and); inherited disorders (Griscelli syndrome, Choroideremia), aneuploidy, obesity, type II diabetes and infectious diseases (Doherty and McMahon, 2009, Stenmark, 2009, Hutagalung and Novick, 2011).

Diseases associated with endocytic defects may be as a result of the failure of cargoes to internalise or recycled properly or malformation of the endocytic compartment or even cargoes delivered to inappropriate intracellular membrane compartments as a result of mutations in some core components of the endocytic machineries or core machineries being hijacked by pathogenic organisms. Aberrant expression of RABGTPases has been associated with cancer (Stenmark, 2009, Hutagalung and Novick, 2011). Overexpression of Rab5 and Rab25 is associated with poor prognosis of the lung, breast and ovarian cancer possibly due to their role in recycling receptors from the recycling endosomes (Stenmark, 2009). However, decreased EHD2 expression levels reduces E-cadherin protein levels which promote epithelial to mesenchymal transition in breast cancer (Shi et al., 2015). Moreover, Rab8 also mediates invasive behaviour of breast cancer due to increased exocytosis of MT1-MMP9. During cytokinesis EHD1, MICAL-L1, Rab11, Rab35 and Rab21 deliver materials to cleavage furrow to enable cell division and therefore their absence may be associated with aneuploidy (Reinecke et al., 2014a, Stenmark, 2009) . Rabs 1,3, 7, 11, 13 and 23 have been associated with several neurological diseases (Hutagalung and Novick, 2011). Overexpression of Rab1 reduces synucleinopathies in Alzheimer's disease. Overexpression of dominant negative Rab11 in mice brain recapitulates Huntington disease (Hutagalung and Novick, 2011).

Studies from RABGTPase mutants mice has also identified other physiological roles of Rabs which includes shortened circadian rhythm in Rab3A deficient mice, mal-functioned and -formed small intestine in Rab8A deficient mice (Stenmark, 2009). EHD3 deficient mice have malformed heart characterised by larger atria and ventricles and an overall increased heart weight to body ratio which affects cardiac function (Curran et al., 2014). EHD1 adult null mice males are infertile because of abnormal spermatogenesis and lack of mature spermatozoa (Rainey et al., 2010)

Endocytosis is also utilised by pathogenic microorganisms to gain access to the cellular machineries of the cell (Stenmark, 2009). *Helicobacter pylori* hijacks Rab7, whereas *Listeria monocytogenes* and *Salmonella typhimurium*, inhibit Rab5 activation and recruitment to prevent the engulfed (phagocytosed) bacteria from fusing with the lysosome to evade them (bacteria) from degradation (Stenmark, 2009, Hutagalung and Novick, 2011).

1.10 Protein modifications

Proteins can be modified either during (co-translational) or after (post-translational) synthesis. Acetylation, glycosylation, palmitoylation, phosphorylation, and ubiquitination are examples of post-translational modifications. The peptide bond, carboxyl- or amino-terminals and/ or individual amino acid side chains can be chemically modified (Wold, 1981, Walsh et al., 2005). Post-translational modifications play an important role in regulating the trafficking and function of intracellular proteins (Uy and Wold, 1977, Wold, 1981, Walsh et al., 2005). However, for the majority of proteins, we still do not have a complete understanding of their post-translational modifications and how this regulates their function. For the purpose of this thesis, I will elaborate more on two post-translational modifications; Palmitoylation and ubiquitination.

1.11 Palmitoylation

1.11.1 Definition and characteristics of palmitoylation

Palmitoylation is a reversible post-translational modification where a palmitic acid is covalently attached to a free cysteine residue (S-palmitoylation) (Resh,

2006b). Cysteine residues have distinct characteristics of being nucleophilic and redox sensitive. Thus allowing them to be amenable to post-translational modifications such as palmitoylation, prenylation, oxidation, nitrosylation, and glutathionylation (Chung et al., 2013). However, not all free cysteines are palmitoylated and in HRAS only two out of the six cysteines are palmitoylated (Misaki et al., 2010). Indicating that the sole presence of cysteines in a protein does not necessarily mean that protein is palmitoylated.

It has been estimated that 9-12% of the human proteome may undergo palmitoylation (Blanc et al., 2015). G-alpha coupled receptors, HRAS, NRAS, PSD95, STX19, STX11, SNAP25, SFKs, and TF-R have all been shown to be palmitoylated.

Palmitoylation affects the membrane targeting, trafficking and turnover of proteins (Figure 1-12). Palmitoylation mutants of SNAP25 fail to be trafficked correctly and fail to associate with the PM (Gonzalo and Linder, 1998). Similarly, HRAS palmitoylation mutant does not traffic properly from the Golgi to the PM (Misaki et al., 2010).

Alterations in palmitoylation have been associated with cancer, mental retardation, Alzheimer disease and Schizophrenia (Hornemann, 2014, Yeste-Velasco et al., 2015).

1.11.1.1 Palmitoylation is catalysed by palmitoyl acyltransferases (PATs)

There are 23 PATs encoded in the human genome and they are localised to various intracellular membranes including the ER, Golgi, and PM (Figure 1-12) (Fukata et al., 2004, Ohno et al., 2006). Palmitoyl acyltransferases are multi-spanning transmembrane proteins that have a conserved zDHHC or zDHYC motif (letter represent amino acids) (Prescott et al., 2009, Fukata et al., 2004). The DHHC motif was first identified in a human pancreatic cDNA library and shown to be highly conserved in all eukaryotes (Putilina et al., 1999). The zDHYC motif was identified in three yeast PATs proteins including; Akr1, Akr2 and Pfa5 (Mitchell et al., 2006). All the other remaining PATs proteins have the DHHC motif (Mitchell et al., 2006).

The PATs catalyse palmitoylation in a stepwise manner. The palmitate acyl group is attached to the cytosolic face of the enzyme, the PATs then transfer the acyl group to a specific cysteine in the substrate protein (Lemonidis et al., 2015). PATs may have overlapping substrate specificity. For example zDHHC 15, 7, 2, and 3 have been shown to catalyse PSD95 palmitoylation (Fukata et al., 2004). zDHHC2 is localised with AKAP79/80 on recycling endosomes to catalyse the latter's palmitoylation (Woolfrey et al., 2015). LCK, a member of SFKs, which mediates FAS signalling is dependent on zDHHC 21 mediated palmitoylation (Akimzhanov and Boehning, 2015). Moreover, knockout of zDHHC 3 and 7 relocalises GPCRs from the PM to the cytoplasm because they lose their palmitoylation (Tsutsumi et al., 2009).

Autoacylation, self-catalysed palmitoylation of the substrate, has also been reported to take place (Zeidman et al., 2009, Resh, 1999). 6XHis-tagged SNAP25 in the presence of palmitoyl-CoA was able to incorporate a very small amount of palmitate group even in the absence of PAT (Veit, 2000). This incorporation increased dramatically when SNAP25 was in a SNARE complex (Veit, 2000). Similarly, BET3 also incorporated palmitate efficiently even in the absence of a PAT (Kummel et al., 2006). However, it is unclear the physiological significance of this process.

1.11.1.2 Deacylation is catalysed by protein acyl- and palmitoyl-thioesterases

Palmitoylated proteins are deacylated by protein acyl thioesterases (APT1 and APT2) or protein palmitoyl thioesterases (PPT) (Conibear and Davis, 2010, Zeidman et al., 2009). APT1 and APT2 are cytosolic proteins that catalyse the removal of the acyl group from the palmitoylated protein. This process facilitates the recycling and effective turnover of proteins. APT1 has a broad substrate range catalysing the deacylation of several proteins including SNAP23, eNOS and VSV (Zeidman et al., 2009). APT2 deacylated GAP43 (Tomatis et al., 2010). Both APT1 and APT2 catalyses the deacylation of HRAS and NMNAT2 (Milde and Coleman, 2014). There is also a lysosomal localised palmitoyl thioesterases which is thought to play a role in protein degradation (Resh,

2006b, Zeidman et al., 2009). PPT1 has been shown to deacylate HRAS and G-alpha subunits (Zeidman et al., 2009).

1.11.2 Palmitoylation and protein trafficking

Attachment and subsequent removal of palmitate group from proteins is required for the proper trafficking of some s-acylated proteins (Figure 1-12) (Salaun et al., 2010). Palmitoylation has been shown to influence the trafficking of several proteins such as RAS, SFKs and SNAREs (Misaki et al., 2010, Akimzhanov and Boehning, 2015, Fukasawa et al., 2004). For the purpose of this thesis, I will elaborate further on the role of palmitoylation in the trafficking of RAS and SNARE proteins.

1.11.2.1 Palmitoylation and RAS trafficking

RAS proteins are vital for cell migration, cell proliferation and cell growth. Ras expression is commonly dysregulated in cancers such as colorectal, lung adenocarcinoma, melanoma and pancreas (Downward, 2003). There are three main isoforms H-, N- and K-RAS (Colicelli, 2004). All of them share a consensus CAAX motif in their C-terminal hypervariable region. This region undergoes several modifications including methylation, farnesylation, proteolysis and palmitoylation. Palmitoylation and depalmitoylation of RAS regulates its trafficking between the ER, Golgi, recycling endosomes, cytosol and PM (Misaki et al., 2010). The spatiotemporal distribution of RAS proteins influences their function (Hancock, 2003). HRAS, NRAS and KRAS 4A are palmitoylated but not KRAS4B (Hancock et al., 1990, Hancock et al., 1991). This modification segregates them into different membrane compartments. On the plasma membrane, whereas HRAS associates with lipid microdomains, KRAS 4B does not. RAS palmitoylation may occur during ER to Golgi trafficking and it becomes depalmitoylated at the PM and come back to the cytosol (Misaki et al., 2010). HRAS and NRAS palmitoylation is dependent on the attachment of palmitoyl group to its cysteines 181 and 184 (Misaki et al., 2010).

Farnesylation of RAS is thought to allow it to initially associate with intracellular membranes as proposed by the kinetic membrane trapping hypothesis (Shahinian and Silvius, 1995, Dunphy and Linder, 1998, Nadolski and Linder,

2007). Subsequently, RAS protein (HRAS and NRAS) is trapped into the membranes by palmitoylation to strengthen its membrane association (Shahinian and Silvius, 1995, Nadolski and Linder, 2007). The protein is recycled, depending on the cell requirement, from the PM via rapid depalmitoylation to the cytosol (Misaki et al., 2010).

1.11.2.2 Palmitoylation and SNAREs trafficking

SNAP25, SNAP23, YKT6, STX7, STX8, STX11 and STX19 are palmitoylated (Veit et al., 1996, Greaves et al., 2010, Fukasawa et al., 2004, He and Linder, 2009, Valdez et al., 1999, Prekeris et al., 2000, Kang et al., 2008).

SNAP25/23 palmitoylation is enhanced by zDHHC 3, 7 and 17 (Greaves et al., 2010). Palmitoylation mediates SNAP25 localisation on recycling endosomes, the TGN and PM (Greaves and Chamberlain, 2011b). Fully palmitoylated SNAP25 (four cysteines palmitoylated) is mostly associated with the PM (Greaves et al., 2009). However, when all the four cysteines are mutated to leucine it becomes cytosolic (Greaves et al., 2009). More importantly, when two of the four cysteines C90L and C88L, are mutated it becomes localised to the REs and TGN (Greaves and Chamberlain, 2011b). The study showed that SNAP25 is differentially localised depending on which cysteines are palmitoylated (Greaves and Chamberlain, 2011b).

YKT6 is a peripheral R-SNARE which cycles on and off membranes. Farnesylation at cysteine 195 and subsequent palmitoylation at cysteine 194 allow it to become stably associated with membranes (Fukasawa et al., 2004). The palmitoylation of Ykt6 is thought to regulate its fusogenic properties by changing it from a closed to open conformation (Fukasawa et al., 2004). A yeast strain carrying a temperature-sensitive Ykt6 mutant fails to survive in the absence of Ykt6 palmitoylation as it is unable to carry out its fusogenic functions (Fukasawa et al., 2004). Thus palmitoylation is essential for YKT6 function.

STX7 and STX8 are transmembrane-anchored Q-SNAREs which are palmitoylated at C239 and C214 respectively (He and Linder, 2009). Mutation of these residues mildly effects their trafficking and leads to an accumulation of STX7 at the PM (He and Linder, 2009).

The effect of palmitoylation on STX11 function is far more pronounced. In familial hemophagocytic lymphohistiocytosis type 4, STX11 is mutated so that it is lacking its cysteine-rich domain. This leads to the protein being degraded and the over- proliferation of NK cells (Hellewell et al., 2014, Halimani et al., 2014). Also, STX11 membrane binding and recruitment to immunological synapse is severely impaired (Hellewell et al., 2014). However, in other cell types such as HeLa and NRK cells, STX11 interaction with other SNARE proteins seems to be sufficient for its membrane targeting even in the absence of its cysteine-rich domain (Valdez et al., 1999, Prekeris et al., 2000).

1.11.3 Methods for studying palmitoylation

Palmitoylation in proteins can be prevented in several ways. These include mutating key cysteines required for palmitate attachment; mutating key hydrophobic amino acids within the cysteine-rich domains and using chemical inhibitors.

1.11.3.1 Mutation of key cysteine residue (s)

Cysteines are vital for palmitate incorporation. Using site-directed mutagenesis or other cloning techniques cysteines can be changed to alanine, leucine or serine and the effect on palmitoylation measured. Some PATs bind directly to the cysteines to incorporate the palmitate group. A study showed that zDHHC2 interaction with AKAP79/80 on recycling endosomes was abolished when C36 was mutated to A36 and C129 to A129 (Woolfrey et al., 2015). This confirms the requirement of cysteines for PATs attachment.

1.11.3.2 Chemical inhibitors

Chemical inhibitors of protein palmitoylation include 2-bromopalmitate, cerulenin, and tunicamycin (Resh, 2006b, Davda et al., 2013). 2-BP is structurally similar to palmitate with the exception of an added bromo group which prevents it from being degraded, and therefore cannot be metabolised. Once incorporated into the cell, it is converted to 2-BP-CoA which interferes with intracellular palmitoyl-CoA and several other enzymatic reactions (Resh, 2006b, Coleman et al., 1992). Because of its promiscuous nature, it is used in combination with other techniques to study palmitoylation in proteins.

1.11.3.3 Mutation of key hydrophobic amino acids

Many palmitoylated proteins have hydrophobic residues (tryptophan and phenylalanine) in close proximity to the palmitoylated cysteine residues. It has been proposed that these residues may help with the proteins initial association with membranes for subsequent palmitoylation. DeSouza et al., 2002 showed that pABP-L, AMPA receptor-binding protein, palmitoylation was blocked when tryptophan 4 was changed to alanine 4 (DeSouza et al., 2002). It is possible that the indole side chain facilitates polar-apolar interactions (Killian and von Heijne, 2000).

1.12 Ubiquitination

Ubiquitin, 8.5 kDa polypeptide, was first isolated and purified from a swine thymus (Goldstein et al., 1975). The study revealed that ubiquitin is conserved in a variety of cells and thus called “ubiquitous” immunopoietic polypeptide (UBIP) (Goldstein et al., 1975). Later, two studies identified an ATP- dependent proteolysis factor 1 and 2 from reticulocytes (Hershko et al., 1979, Ciechanover et al., 1980). As the name implies, APF-1 was shown to break down proteins in an ATP-dependent manner. Protein sequence analysis on APF-1 and ubiquitin showed that the two proteins were similar (Wilkinson et al., 1980).

Following the discovery of ubiquitin, several studies showed that ubiquitin works in complex with other enzymes including ubiquitin activating enzyme (E1), ubiquitin conjugating enzyme (E2), and ubiquitin ligase enzyme (E3) (Haas et al., 1982, Hershko, 1983, Ciechanover et al., 1981, Ciechanover et al., 1982, Ciechanover et al., 1980, Hershko et al., 1983). E1 was isolated from reticulocytes and purified using ubiquitin-sepharose in the presence of ATP and magnesium ions (Ciechanover et al., 1981, Ciechanover et al., 1982). E1 forms a stable complex with ubiquitin to activate the latter in the presence of ATP and magnesium ions to release two pyrophosphates in a stepwise manner. The interaction between E1 and ubiquitin leads to the formation of ubiquitin thioester and ubiquitin adenylate (Haas et al., 1982). Upon ubiquitin activation, it is transferred to E2. E2 binds ubiquitin in the presence of E1 and ATP (Ciechanover et al., 1982, Hershko et al., 1983). E2 then associates with E3; E3 binds to ubiquitin and ligates ubiquitin with a protein substrate. Ubiquitin forms

isopeptide linkage with the proteins by binding to key lysine residues on the target protein referred to as ubiquitination.

The stepwise attachment of E1, E2 and E3 to ubiquitin is required for the efficient ubiquitination of target proteins and their subsequent degradation by the 26S proteasome pathway (Hershko et al., 1983, Hershko and Ciechanover, 1992). It should be noted that ubiquitin might also conjugate directly with proteins via E2 only causing the protein to become monoubiquitinated (Hershko and Ciechanover, 1992). E3 promotes either monoubiquitination or polyubiquitination by the addition of several ubiquitin chains to the targeted protein (Hershko and Ciechanover, 1992). Ubiquitination is highly regulated. For example, the E3 ligase which is required for ubiquitination is kept in check. E3 ligase can be degraded by the proteasome via self-catalysed ubiquitination and/or an exogenous ligase (de Bie and Ciechanover, 2011). Moreover, there are approximately 600 E3 ligases which target specific substrates conferring specificity in the ubiquitination process (Deshaies and Joazeiro, 2009).

1.12.1 Importance of protein ubiquitination

Ubiquitination has both proteolytic and non-proteolytic functions (Figure 1-13) (MacGurn et al., 2012). At the plasma membrane, ubiquitination mediates the internalisation of receptors such as RTKs and GPCRs (MacGurn et al., 2012). In early endosomes ubiquitinated receptors interact with ESCRT components to target them into intraluminal vesicles for degradation in lysosomes (MacGurn et al., 2012). Ubiquitination also mediates the sorting of cargoes from the Golgi to endosomes.

Defects in ubiquitination play a role in cystic fibrosis, circulatory diseases, neuropathies, spermatogenesis disorders (MacGurn et al., 2012, Hao et al., 2015, Suresh et al., 2015).

1.12.1.1 Ubiquitination and protein degradation

De Duve et al., while analysing the intracellular distribution of enzymes observed that acid phosphatases were enclosed in the cytoplasmic granules of rat liver (De Duve et al., 1955). This cytoplasmic granule was later called lysosome. Lysosomes are present in different cells and function to store,

process and digest foreign substances endocytosed by the cells (De Duve and Wattiaux, 1966). Lysosomal proteases play a key major role in protein degradation; however, they are not the only pathway for protein degradation. Katunuma and colleagues also unravelled other forms of degradation independent of the lysosomal proteases, which they called group specific proteases of pyridoxal enzymes (Katunuma, 1973, Katunuma et al., 1973). In the mid-1970s studies began to show that there is yet other means of protein degradation which was to be called ubiquitin-mediated cell degradation.

The majority of cellular proteins are turned over by the proteasomal pathway (Lecker et al., 2006, Glickman and Ciechanover, 2002). The 26S proteasome consists of a 20S proteasome and a 19S regulatory particle. The 19S particle regulates the entry of the polyubiquitinated protein into the 20S particle where the proteins are digested into tiny peptides, which upon release are subsequently degraded by cytosolic peptidases (Lecker et al., 2006, Glickman and Ciechanover, 2002). There is always the need for the cell to maintain protein levels by degrading them so that there is a balance between amounts being synthesised and degraded (MacGurn et al., 2012). Defects in this pathway are associated with cancer, Alzheimer disease and Angelman's syndrome (Myung et al., 2001)

1.12.1.2 Nonproteolytic functions of ubiquitination

Ubiquitination does not always necessary lead to protein degradation, studies have shown that ubiquitin may control membrane trafficking, protein kinase activity, DNA repair, chromatin dynamics (Chen and Sun, 2009, Acconcia et al., 2009). Ubiquitin aids EGFR, PDGFR internalisation and sorting (Acconcia et al., 2009). During sorting in the early endosomes non-ubiquitinated receptors are mostly recycled back to the PM or to other intracellular compartments (Acconcia et al., 2009). Endosomal sorting complexes required for transport (ESCRT) recognise and bind to ubiquitin on receptors and cargoes. The ESCRT complex sorts ubiquitinated proteins into intraluminal vesicles generating multivesicular bodies, which then releases their content into the lysosome for degradation (Acconcia et al., 2009).

Even though beta2-adrenergic receptors can be internalised with or without ubiquitination, the receptor's internalisation and degradation is reduced by proteasomal inhibitors (Shenoy et al., 2001). Studies from yeast also provide evidence for the role of ubiquitination in trafficking. Ubiquitination of ste2P increases the latter's internalisation and endocytosis (Hicke and Riezman, 1996). Ubiquitination of steP2 and ste6 targets the proteins to the vacuole for degradation (Hicke and Riezman, 1996, Kolling and Hollenberg, 1994).

1.12.2 Characteristics of ubiquitination

Ubiquitination can be in different forms; mono, multi-mono and polyubiquitination (Komander, 2009, Ikeda and Dikic, 2008). Monoubiquitination is characterised by a single ubiquitin attached to a protein substrate. Multi-mono ubiquitination involves many ubiquitin attached to different lysine of its substrate. Polyubiquitination is whereby many ubiquitin attaches to a single lysine residue of its substrate. Polyubiquitination could be homotypic if the several ubiquitin linkages are derived from the same lysine in the ubiquitin. Meanwhile, polyubiquitination may be heterotypic in that case the ubiquitin linkage to its substrate is derived from different ubiquitin lysine. Mono or multi-mono ubiquitination has been linked to receptor protein internalisation, example RTKs, and their subsequent degradation via the lysosomal pathway (Haglund et al., 2003). Polyubiquitination especially, mediated by ubiquitin K48 is mostly associated with proteasomal protein degradation (Thrower et al., 2000). K63 linked ubiquitination plays a role in the DNA damage response, DNA repair, histone ubiquitination, cytokine signalling, and endocytic recycling of proteins (Komander, 2009, Ikeda and Dikic, 2008). The remaining lysines in ubiquitin have also been linked to a variety functions. K11 linked ubiquitination is much pronounced in the endoplasmic reticulum-associated degradative pathway; K6 for DNA repair; and K29/K33 are essential for AMPK ubiquitination (Komander, 2009, Ikeda and Dikic, 2008).

1.12.3 Analysing ubiquitinated proteins using mass spectrometry approach

Ubiquitin has seven lysines (K6, K11, K27, K29, K33, K48 and K63) and glycines at position 75 and 76. Each of these lysines is capable of forming

isopeptide bonds with the glycines 75, and 76. The addition of trypsin to proteins prepped for mass spectrometry creates diglycine signature peptide as a result of isopeptide-linked ubiquitin cleavage (Kirkpatrick et al., 2005). Mass spectrometry analysis of ubiquitinated proteins produces $_{-GG}$ signature peptides, which adds 114.0429 Da on lysine residues that have the potential to be ubiquitinated. Afterwards, using database search like MAXQUANT or MASCOT, the identity of the ubiquitinated lysine could be determined (Cox and Mann, 2008). Using tandem mass spectrometry analysis, six lysine residues (692, 713, 730, 843, 905, and 946) on EGFR were identified as being ubiquitinated (Huang et al., 2006).

1.12.4 Deubiquitination

Deubiquitination is the removal of ubiquitin from its target substrate catalysed by deubiquitinases. Ubiquitin carboxyl-terminal hydrolase is one of the earliest studied deubiquitinases (Wilkinson, 1997). It was first purified from rabbit reticulocytes and shown to hydrolyse glutathione and thiol esters of ubiquitin and so was referred to as ubiquitin carboxyl-terminal esterase (Rose and Warms, 1983). It was later reported that this enzyme also hydrolyses the lysine isopeptide linkage formed between ubiquitin and its target protein substrate (Pickart and Rose, 1985). There are approximately 100 DUBs in human and 20 in yeast, which targets more than 600 E3 ubiquitin ligases and their substrates (MacGurn et al., 2012). Ubiquitin can be recycled by deubiquitinating enzymes. Based on their proteolytic mechanisms, DUBs can be classified as either cysteine- or metallo- proteases. The cysteine DUBs are the most abundant and widely studied (Nijman et al., 2005, Reyes-Turcu et al., 2009). The cysteine DUBs proteases form a covalent bond with ubiquitin to break the bond between ubiquitin and its target proteins. The ubiquitin is then released from the DUBs by interaction with water (Nijman et al., 2005). DUBs metalloproteases rather form a non-covalent bond with ubiquitin to break the latter from its target proteins. The ubiquitin becomes free from the DUBs via proton transfer from water molecules (Nijman et al., 2005). The cysteines DUBs proteases are grouped into ubiquitin specific proteases (USP), otubain protease, ubiquitin C-terminal hydrolases and Machado-Joseph disease protease (Nijman et al., 2005). The

USPs is the most abundant. DUBs functions partake in the activation of ubiquitin proprotein, recycle ubiquitin, reverse ubiquitination , and regeneration of monoubiquitin (Reyes-Turcu et al., 2009). Due to their cellular importance, DUBs activities are highly regulated. They are regulated by self-ubiquitination (themselves undergoing ubiquitination) and phosphorylation (Reyes-Turcu et al., 2009). Moreover, DUBs are inactive until they become associated with ubiquitin.

1.13 The crosstalk between palmitoylation and ubiquitination

Palmitoylation and ubiquitination affect the trafficking of proteins. Palmitoylation deficient proteins tend to be less stable and are sometimes targeted by ubiquitin for degradation. Yeast SNARE Tlg1 palmitoylation mutant is recognised by Tul1 - and Bsd-2 - dependent ubiquitination system for degradation (Valdez-Taubas and Pelham, 2005). Oncoprotein TBC1D3 becomes mislocalised and subsequently degraded by CUL7 E3 ligase complex, when its palmitoylated cysteines 318 and 325 are changed to serine (Kong et al., 2013). TEM8 binds to the protective antigen domain of anthrax toxin which is required for anthrax toxin endocytosis. The absence of palmitoylation causes TEM8 to become degraded which was rescued by MG132 (Abrami et al., 2006). Palmitoylation deficient TEM8 no longer associated with anthrax toxin that affected anthrax toxin endocytosis (Abrami et al., 2006). In addition, loss of palmitoylation in CCR5, a G-protein coupled receptor, causes it to be degraded in the lysosome (Percherancier et al., 2001). These studies show that palmitoylation and ubiquitination are interlinked to regulate the stability and trafficking of proteins. Palmitoylation has been shown to affect the distribution of gp78 an E3 ubiquitin ligase required for ubiquitination (Fairbank et al., 2012). Gp78 palmitoylation is catalysed by several ZDHHCs 2, 6, 11, 13 and 24. Palmitoylation of gp78 regulates its ER distribution required for it to function in the ERAD pathway (Fairbank et al., 2012). Therefore crosstalk exists between palmitoylation and ubiquitination functions.

1.14 Research question

A significant amount of progress has been made in elucidating the cellular machinery required for biosynthetic and endocytic transport over the last 40 years. However, it is far from clear how these pathways are coordinated and or regulated. Works from several groups have shown that SNAP29 and STX19 play a role in biosynthetic transport. Our lab has found that a pool of SNAP29 and STX19 are localised to endocytic recycling tubules suggesting that they may also be involved in endocytic trafficking. The aim of this thesis was to elucidate the role of SNAP29 and STX19 in post-Golgi transport. I have been addressing four main questions during my PhD.

- 1) Where is STX19 and SNAP29 localised within the cell?
- 2) What is the role of palmitoylation in regulating STX19 trafficking and stability?
- 3) What machinery regulates STX19 and SNAP29 trafficking and function?
- 4) What pathways do STX19 and SNAP29 function on?

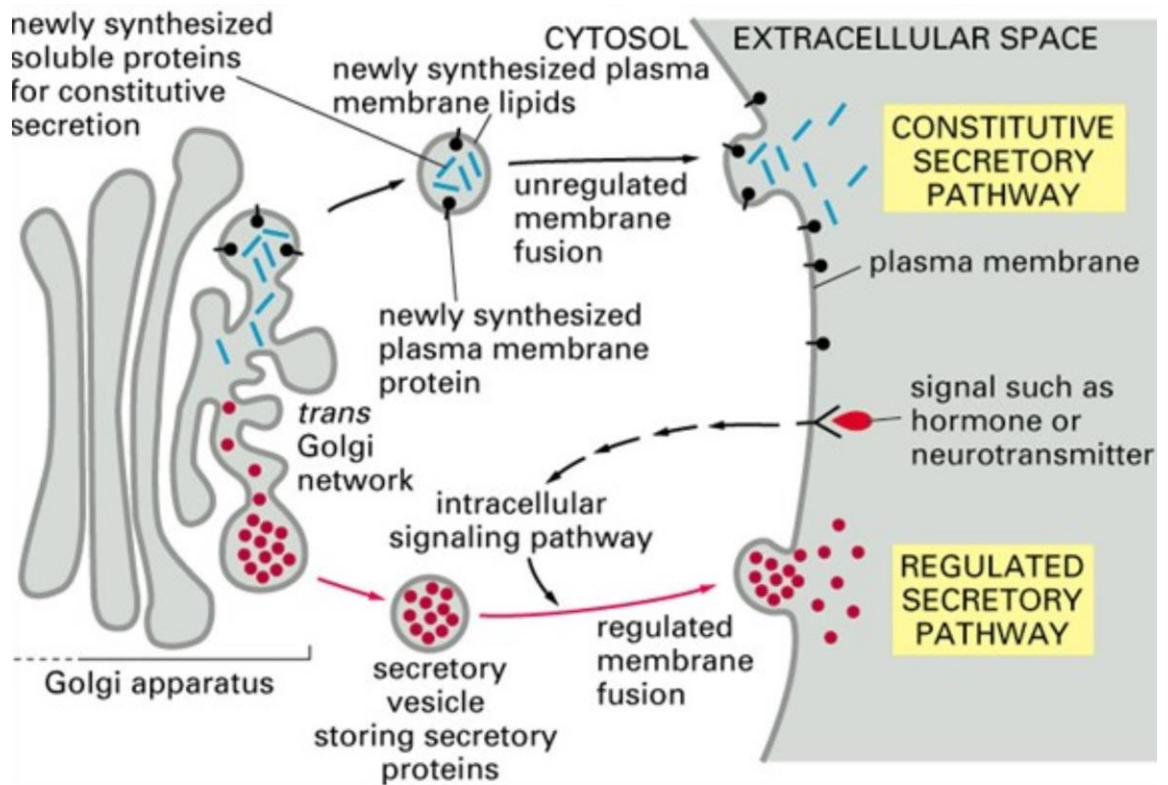


Figure 1-1 The biosynthetic pathway.

Diagram adapted from (Alberts et al., 2015)

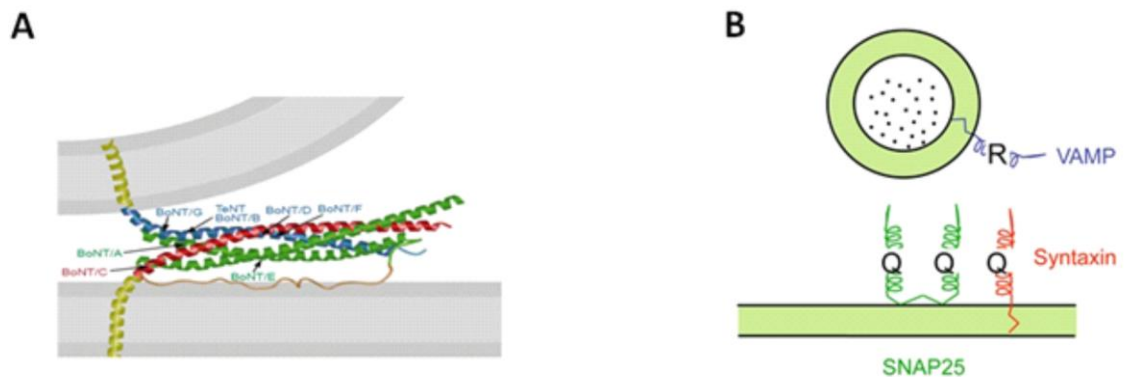


Figure 1-2 Model of the neuronal SNARE complex.

(A) The yellow helix shows hypothetical transmembrane domains of STX1A (Red) and VAMP2/Synaptobrevin II (Blue) with green loops indicating the two SNARE motifs of SNAP25. Adapted from (Sutton et al., 1998). (B) The R-SNAREs are attached to the vesicle and the Q-SNAREs on the target membrane. Adapted from the unpublished diagram of Andrew Peden.

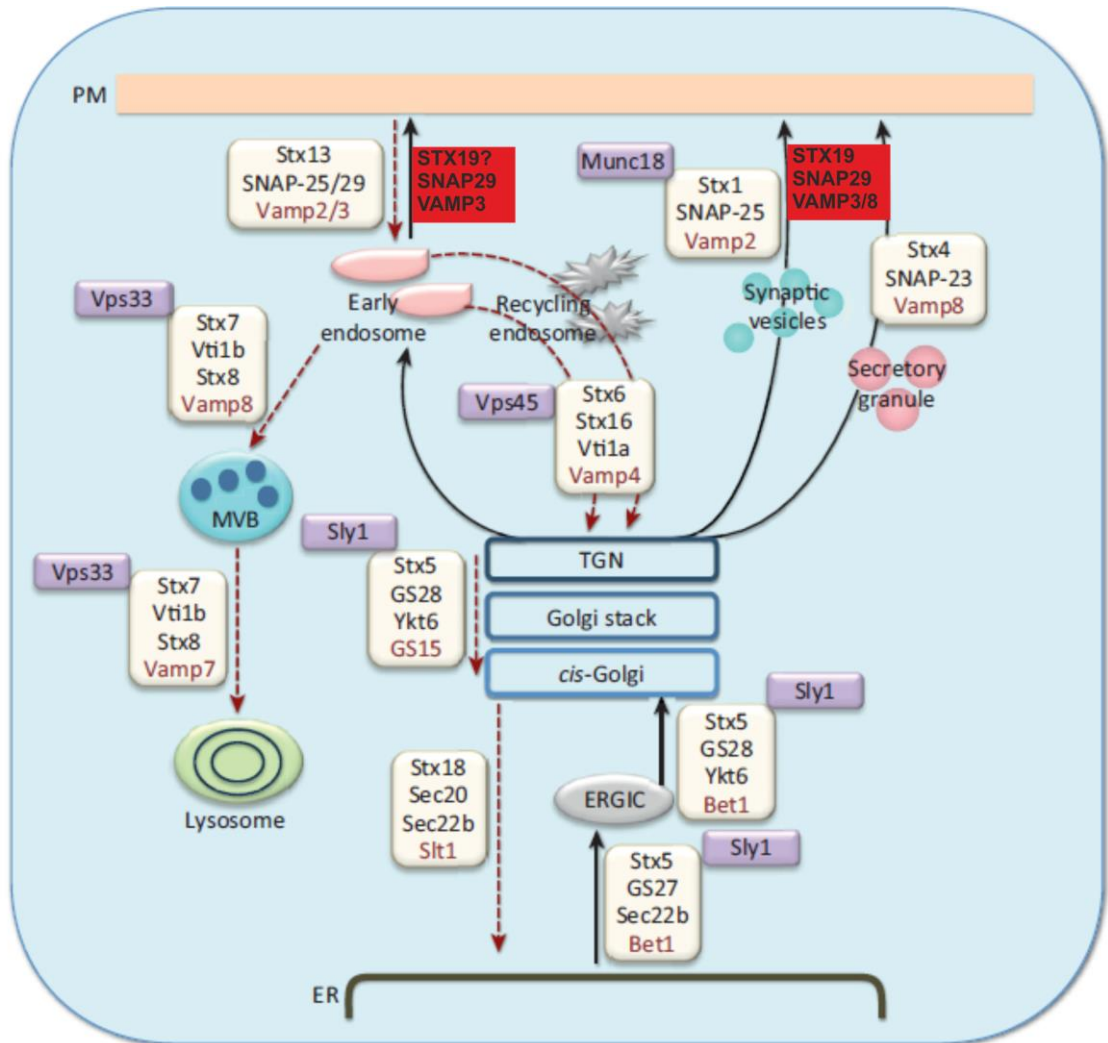


Figure 1-3 A simplified cartoon showing the role of SNAREs in the biosynthetic and endocytic pathways.

Modified diagram from (Hong and Lev, 2014)

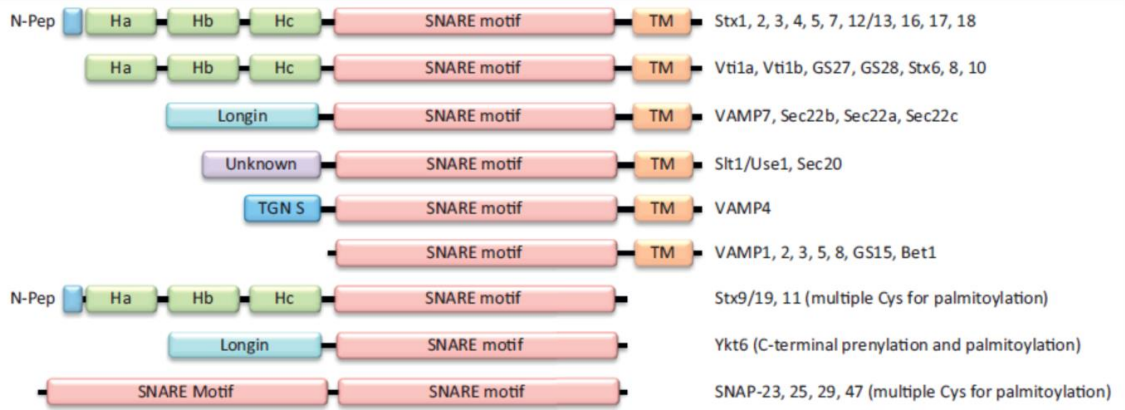


Figure 1-4 A cartoon showing domains of SNARE proteins.

Adapted from (Hong and Lev, 2014).

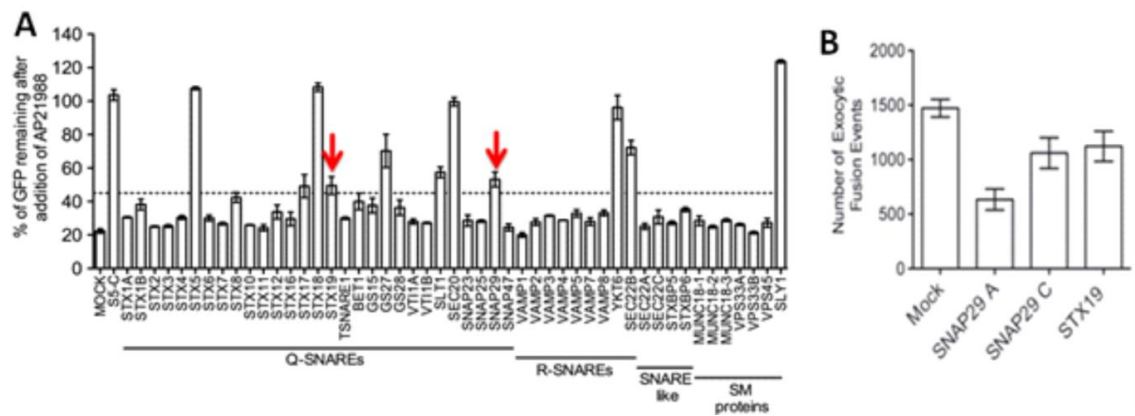


Figure 1-5 A targeted siRNA screen identifies SNAREs and SM proteins required for secretion.

HeLa-M cells expressing GFP-FM4-hGH secretion reporter construct were transfected with an ON-TargetPlus SMARTpool siRNA and then incubated with AP21988 (1 μ M) for 80 min at 37 $^{\circ}$ C and their mean fluorescence determined using flow cytometry. STX19 and SNAP29 have been highlighted with a red arrow. All values above the dotted line represent twice that of the mock-transfected cells. (B) Depletion of STX19 and SNAP29 reduces the number of vesicles fusing with the plasma membrane as measured by TIRF. Figures adapted from (Gordon et al., 2010).

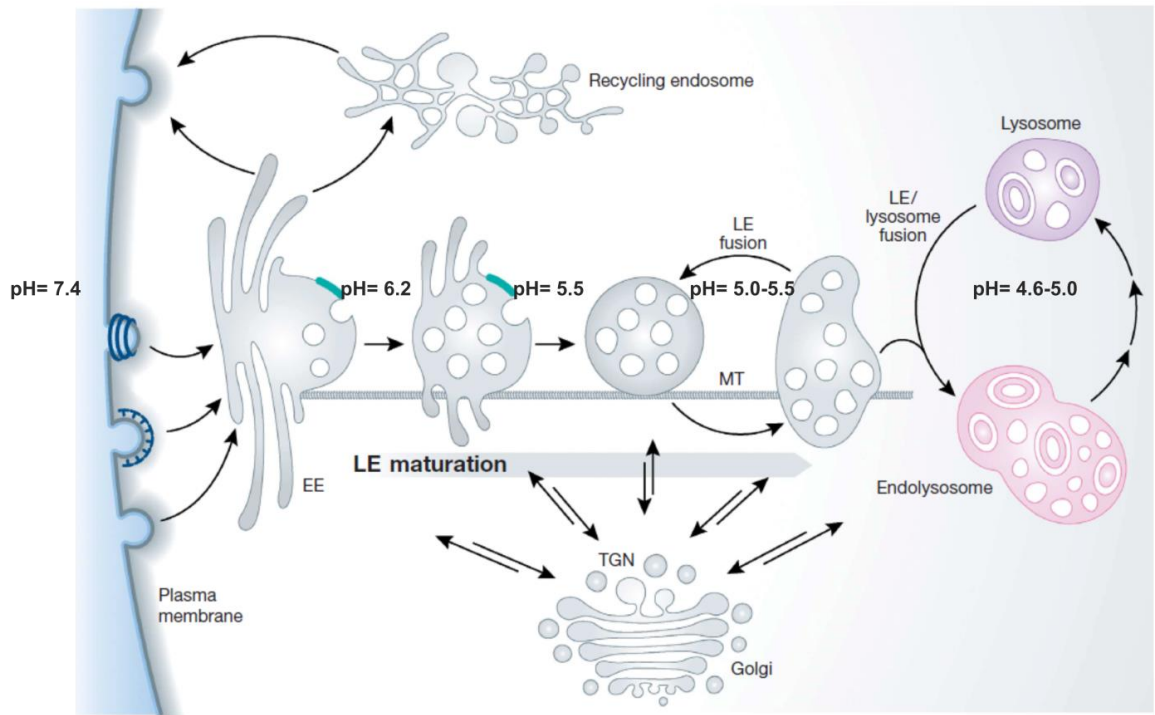


Figure 1-7 The endosomal compartments.

A modified diagram from (Huotari and Helenius, 2011).

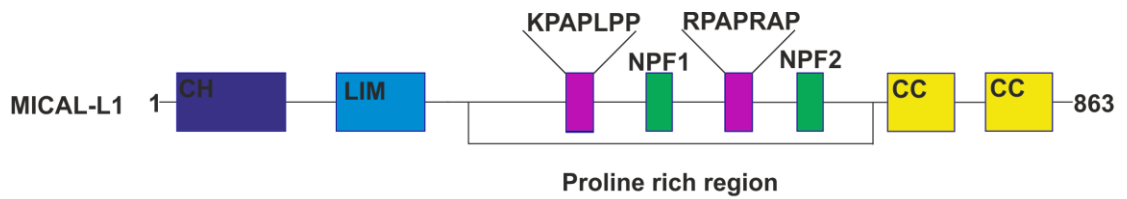


Figure 1-8 Cartoon of MICAL-L1.



Figure 1-9 Cartoon of EHD1.



Figure 1-10 Cartoon of PACSIN2.

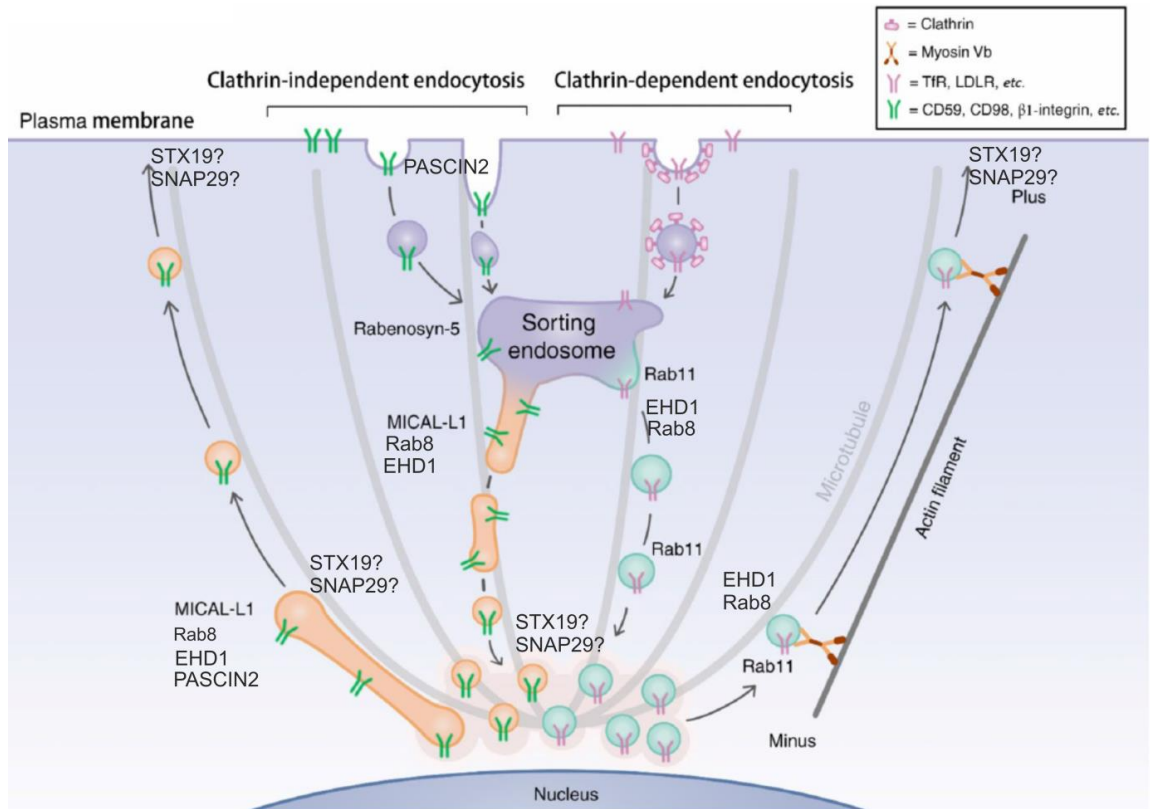


Figure 1-11A modified diagram of MICAL-L1 tubular- and Rab11- recycling endosomes.

Diagram adapted from (Xie et al., 2015).

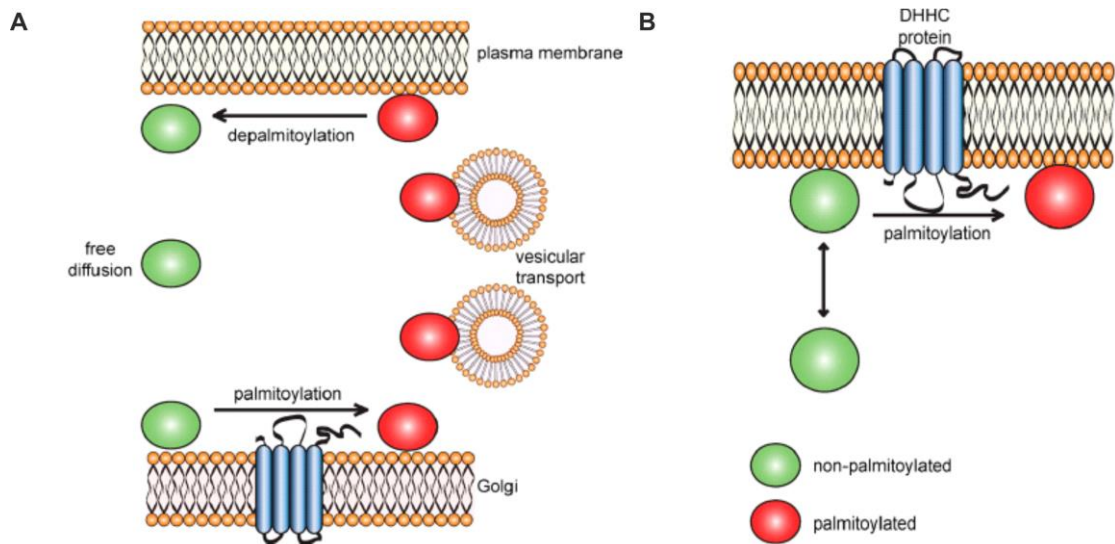


Figure 1-12 Palmitoylation influences the trafficking of protein.

A) Palmitoylation at the Golgi B) Palmitoylation at the plasma membrane.
Diagram adapted from (Salaun et al., 2010).

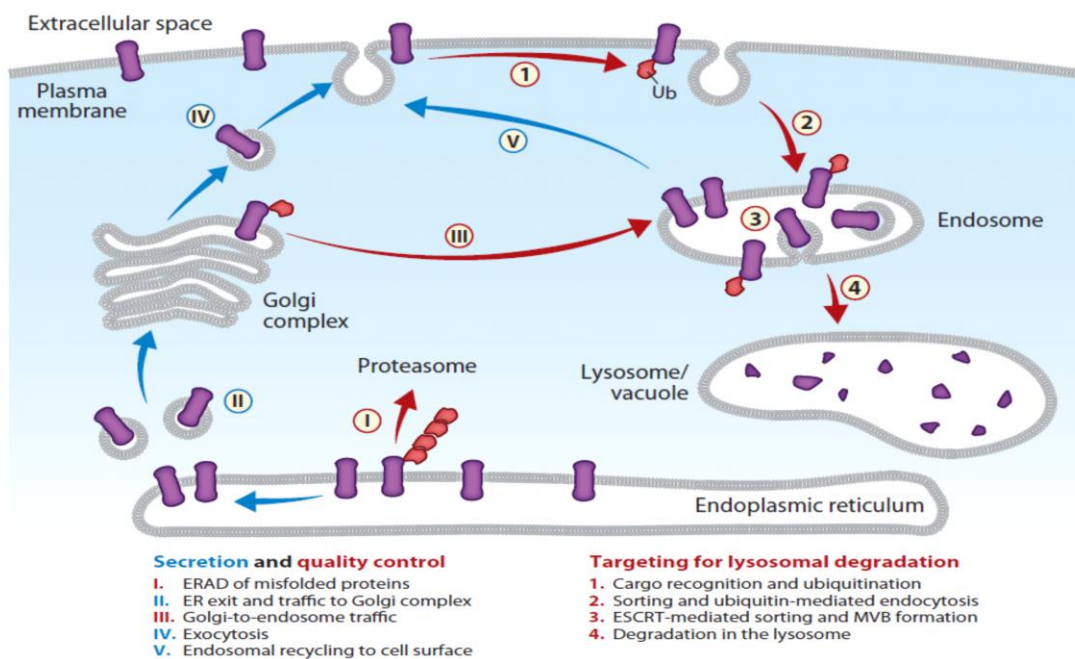


Figure 1-13 Ubiquitination influences the trafficking of proteins.

Adapted from (MacGurn et al., 2012)

2 Chapter Materials and Methods

2.1 Common Reagent and Antibodies

The antibodies and reagents used in this thesis were either purchased from reputable sources, gifts from colleagues or made in-house. Antibodies were used according to the manufacturer's instructions unless otherwise stated. Table 2-1 provides a full list of the antibodies used, their source and appropriate dilutions. The remaining tables provide a list of reagents used, their composition and source. All primers were designed in-house and purchased from Sigma. All restriction enzymes were purchased from New England Biolabs, UK.

2.2 Plasmids Preparation and Analysis

2.2.1 Transformation

Plasmid DNA spotted on filter paper was resuspended in 50 μL of ddH₂O. Lyophilised plasmids were centrifuged for 1 minute at 12,000 rpm and then reconstituted with an appropriate volume of ddH₂O. The DNA was transformed into bacteria as follows:

1. Competent bacteria were thawed on ice for 10 minutes.
2. 1-2 μL of the plasmid DNA (not exceeding 100 ng) was added to 50 μL of cells and the tube flicked gently.
3. The cells were incubated on ice for 30 minutes, heat shocked for 30 seconds at 42 °C and then returned onto ice for 5 minutes.
4. Transformations with ampicillin resistant plasmids were directly spread on the agar plate. Transformations with kanamycin or chloramphenicol resistant plasmids were recovered by adding 950 μL of fresh bacteria culture media to the cells and then incubated for 1 hour at 37 °C while shaking in KS 4000i control incubator (IKA, UK) before plated on their respective agar plate.
5. The transformed bacteria were grown overnight at 37 °C.

2.2.2 Plasmid isolation

Plasmid DNA was isolated from bacteria using GeneJET miniprep or maxiprep kits (Thermo Scientific, KO503/KO492) according to the manufacturer's instruction.

2.2.2.1 Miniprep preparation

1. Single colonies were selected and inoculated into 3 mL bacteria media containing the selective antibiotic and then grown overnight at 37 °C at 250 rpm in KS 4000i control incubator (IKA, UK).
2. Bacteria were pelleted by centrifugation at 4000 rpm for 10 minutes.
3. The bacterial pellet was resuspended in 250 µL of resuspension solution. The bacteria were lysed with the addition of 250 µL of lysis solution. The chromosomal DNA and proteins were precipitated by the addition of 350 µL of neutralisation solution. The insoluble precipitate was pelleted by centrifugation at 12,000 rpm for 10 minutes.
4. The DNA was then purified using a GeneJET spin column. The columns were washed two times with wash solution containing ethanol.
5. The column was centrifuged to remove excess wash solution and the DNA eluted with 50 µL of ddH₂O.
6. The concentration of the purified plasmid DNA was measured using a NANODROP LITE Spectrophotometer (Thermo Scientific, USA). In some instances, the DNA was sequenced using the University of Sheffield's Core Genomic Facility, Medical School.

2.2.2.2 Maxiprep preparation

Maxipreps were used to obtain high-quality plasmid DNA for cell transfection.

1. Single colonies were inoculated into 3 mL bacteria media containing the selective antibiotic and grown for 8 hours at 37 °C at 250 rpm. The starter culture was then transferred into 1 L conical flask containing 250 mL media with the required antibiotic and grown overnight at 37 °C at 200 rpm in INNOVA 44 shaker incubator (New Brunswick Scientific, Eppendorf AG, Germany).
2. Bacteria were pelleted by centrifugation using Beckman Avanti centrifuge at 5 Kg for 10 minutes.

3. The bacterial were resuspended in 6 mL of resuspension solution and lysed by the addition of 6 mL of lysis solution. The chromosomal DNA and proteins were precipitated by the addition of 6 mL of neutralisation solution.
4. 0.8 mL of endotoxin binding reagent was added. The insoluble precipitate was pelleted by centrifugation at 20,000 rpm for 40 minutes using Avanti J-26 XP centrifuge (Beckman Coulter, USA).
5. The supernatant was mixed with equal volume of 96% ethanol. The DNA was then purified using a GeneJET spin column. The columns were washed once with wash solution containing isopropanol and then two times with wash solution containing ethanol.
6. The column was centrifuged for 10 minutes to remove excess wash solution and the DNA was eluted with 1 mL of ddH₂O.
7. The concentration of the purified plasmid DNA was measured using a NANODROP LITE Spectrophotometer (Thermo Scientific, USA) and stored at -20 °C for the subsequent experiment.

2.2.3 Cloning

The majority of cloning was performed as outlined below.

1. DNA amplification using PCR
2. DNA purification
3. TOPO cloning
4. Transformation of TOPO clones
5. Mini prepping TOPO clones
6. Restriction digests of TOPO clones
7. DNA sequencing of TOPO clones
8. Restriction digest of TOPO clones to move inserts into expression vectors
9. DNA purification
10. Ligating inserts with expression vector
11. Transformation of ligation reaction
12. Mini prepping samples
13. Restriction digests of samples from step 12

14. Maxi prepping samples from step 13

I will briefly explain the steps. I have already explained some of the steps in earlier sections. The main aim of the TOPO cloning is to facilitate DNA sequencing. Once, the sequences were verified, they were moved into their respective vectors. For transient expression, genes were cloned mostly into pIRESNEO vector and/or EGFP vectors and pLXIN-MOD vector for stable retroviral selection. Antibiotic selection markers and restriction sites are shown in (Table 2-2; Table 2-13).

2.2.3.1 DNA amplification and Gel electrophoresis

The DNA was amplified using the primers described in Table 2-11 and the reaction was carried in PTC-100 Programmable Thermal Controller (MJ Research Inc, USA). The PCR settings are stated in Table 2-6 and Table 2-8. The amplified DNA was mixed with 10X DNA loading dye and run using Fisher Biotech Electrophoresis FB650 system (Fisher scientific, USA) on an agarose gel stained with SYBR Safe DNA gel stain. Quick-load 2-log DNA ladder was used to estimate the molecular weight of the PCR product. The DNA bands were separated at a constant voltage of 110 V in 1X TBE buffer. The BioRAD Gel Doc EZ Imager (BioRAD, USA) was used to detect the separated DNA bands and further analysis was carried out with Image Lab 5.0 (BioRAD, USA).

2.2.3.2 DNA purification from agarose gel slices

DNA was extracted from gel slices using QIAquick gel extraction kit (QIAGEN, UK) according to the manufacturer's instruction with some modifications.

1. The DNA fragment was excised from the gel into an Eppendorf tube using a clean razor blade (Fisher Scientific, USA) while the DNA bands were observed under LED illuminator (GeneFlow, Nippon Genetics Europe, Taiwan).
2. 400 μ L of buffer QG was added to the excised fragment and then incubated for 10 minutes at 50 °C with intermittent vortexing to facilitate dissolution.
3. 200 μ L of isopropanol was added to the dissolved fragment and mixed immediately.

4. The mixture was transferred into the QIAquick spin column and centrifuged at 12,000 rpm for 1 minute.
5. The flow-through was discarded and the column washed with 500 μ L of QG buffer (12,000 rpm for 1 minute).
6. The flow-through was discarded.
7. 750 μ L of buffer PE was added and incubated for 5 minutes and then centrifuged and the flow-through discarded.
8. The spin column was centrifuged one more time to remove excess wash buffer.
9. The DNA was eluted with 30 μ L of ddH₂O.

2.2.3.3 TOPO TA Cloning

TOPO cloning was performed using the TOPO TA Cloning Kit (Invitrogen). 1 μ L of the TOPO vector and 1 μ L of salt solution were combined and added to 4 μ L of the amplified and purified PCR product. The reaction was left at RT for 30 minutes and transformed into One Shot Mach1-T1 competent cells (Invitrogen, USA) as outlined above.

2.2.3.4 Restriction digests

Restriction digests were performed using enzymes and buffers purchased from New England Biolabs. The DNA, buffer and enzymes were combined according to the manufacturer's instructions and incubated at 37 °C for 2-3 hours.

2.2.3.5 Oligo annealing

To generate the GFPSTX19-tail and STX13 transmembrane domain expression constructs oligo annealing was performed. 5 μ L of each of the oligos 100 μ M (forward and reverse primer) were mixed with 5 μ L of 10X EcoR1 buffer and 35 μ L of distilled water into PCR tubes. The mixture was then heated to 95 °C for 2 minutes and cooled to 25 °C over 45 minutes. 1 μ L of the annealed oligo was diluted with 10 μ L of distilled water and 6 μ L of this used for the ligation reaction.

2.2.3.6 Klenow treatment

To remove the sticky ends produced using restriction enzymes Klenow treatment was performed. 0.5 μ L of DNA polymerase I, Large (Klenow)

Fragment and 1 µL of 2 mM DNTPs was added to the restriction digest. The mixture was incubated at RT for 20 minutes. The DNA was then purified using QIAquick gel extraction kit. This approach was used to clone BIRA*MICALL1 and GFP-tagged STX19.

2.2.4 Multiple sequence alignment of human STX19

The cysteine-rich domain of human STX19, 275-294 aa was compared to 10 different species using BLASTP (Basic local alignment search tool-Protein) from the National centre for biotechnology information website (Government, 2015) (see below for species used). Reference protein was selected from the database drop-down menu. The algorithm parameter was set to maximum 500.

1. *Cavia porcellus* (Guinea pig)
2. *Gorilla gorilla* (Gorilla)
3. *Felis catus* (Cat)
4. *Gallus gallus* (Chicken)
5. *Python bivittatus* (Snakes)
6. *Capra hircus* (Goat)
7. *Homo sapiens* (Human)
8. *Physetter catodon* (Whales)
9. *Eptesicus fuscus* (Bat)
10. *Xenopus laevis* (Frog)

BoxShade 3.21 was used to construct the sequence alignment of the 10 selected organisms (Hofmann and Baron, 2015). The settings used from the BoxShade 3.21 included:

- Output format RTF_new
- Font Size 10
- Consensus line with symbols
- Fraction of sequences 1.0

All other settings were by default.

2.3 Cell Culture and transfection

2.3.1 Tissue culture media preparation

DMEM was used for most cells lines unless otherwise stated. 50 mL fetal bovine serum (Life technologies, Brazil) together with 5 mL of 100 U/mL Penicillin, 100 µg/mL Streptomycin and 2 mM L-Glutamine (Sigma, UK) were filtered using 0.2 µm sterile filter cups and then added to 500 mL media.

2.3.2 Cells culture

Cells were grown at 37 °C in a humidified incubator (5% CO₂). Cells were passaged when approximately 80 to 90% confluent. Spent media was removed from the cells, washed once with PBS and 1 mL trypsin-EDTA (Sigma, USA) added (10 cm plate). The cells were incubated for 5 minutes and once the cells were detached they were resuspended in 10 mL fresh media. Most cells were split 1:5. When setting up coverslips for microscopy; 1 mL of cell suspension was mixed with 11 mL of fresh media and 1 mL aliquoted into each well of a 12 well plate. For six-well plate; 1 mL of cell suspension was mixed with 11 mL of fresh media and then 2 mL aliquoted into each well.

2.3.3 Using automatic cell counter

The Bio-Rad cell counter was used to count the cells according to the manufacturer's instructions.

1. 10µL of trypan blue dye was added to 10 µL of cell suspension and mixed thoroughly.
2. 10 µL of the mixture was added to either side of the cell counting chamber and the chamber inserted into the cell counter.
3. The cell counter distinguishes between live and dead population and give the total number of cells in each chamber.
4. The readings from both sides of the counting chamber were added and average calculated. This gives a rough estimation of the total amount of cells.

2.3.4 Cell freezing

A 10 cm plate of cells was washed once with PBS and trypsinized for 5 minutes at 37 °C. The cells were resuspended in 10 mL of media and pelleted by centrifugation at 1500 rpm for 5 minutes. The supernatant was removed and the cells resuspended in 3 mL of freezing media. The cells were then aliquoted into cryovials. The cells were frozen slowly using an isopropanol bath at -80 °C. Cells were either stored at -80 °C (short term) or in a liquid nitrogen cell bank (long term).

2.3.5 Cell transfection

The majority of cell transfections were performed using polyethylenimine (PEI) unless otherwise stated.

2.3.5.1 Preparing PEI

A 1mg/ml stock solution of PEI was prepared using a protocol adapted from a Cold Spring Harbour protocol (Protocols, 2006).

1. 50 mg of PEI was added to 45 mL of ddH₂O in a clean glass beaker.
2. The pH of the solution was adjusted to pH < 2.0 by the addition of approximately 80 µL of 12 M HCl.
3. The mixture was stirred for 2 hours until the PEI was completely dissolved.
4. The pH of the solution was adjusted to pH 7.0 by the addition of approximately, 50 µL of 10 M NaOH.
5. The final volume of the solution was adjusted to 50 mL and sterilised using a 0.2 µm filter. The solution was aliquoted into 1.5 mL Eppendorf tubes and stored either at 4 °C (short term) or -20 °C (long term).

2.3.5.2 DNA transfection

Cells were grown to 60% confluency and on the day of the transfection the media replaced with antibiotic-free media. The ratio of DNA to PEI used was 1:5 and the amount of DNA used adjusted to the surface area of the dish (see Table 2-17). DNA and PEI were diluted with Opti-MEM and incubated for 5 minutes at RT. The DNA and PEI were combined and vortexed vigorously for 30 seconds and incubated for 20 minutes at RT. The DNA/PEI complexes were

added to the media and distributed evenly across the cells by swirling. Cells were analysed between 24-48 hours post transfection.

2.3.5.3 siRNA transfections

siRNA transfections were carried out in six-well plates using Oligofectamine or lipofectamine RNAiMAX according to the manufacturer's instruction. 2×10^5 cells were seeded in a six-well plate and grown overnight. The next day the cells were transfected with 100 nM siRNA as follows:

1. 10 μ L of the 20 μ M stock siRNA was mixed with 150 μ L Opti-MEM.
2. 6 μ L of Oligofectamine was mixed with 34 μ L Opti-MEM in a separate Eppendorf tube.
3. The siRNA and the Oligofectamine were incubated for 5 minutes at RT.
4. The siRNA and the Oligofectamine were combined together in an Eppendorf tube, mixed thoroughly and incubated for 20 minutes at RT.
5. The mixture was then added to cells and incubated for 96 hours.
Knockdown efficiency was determined by immunofluorescence microscopy and immunoblotting.

2.3.6 Generating stable cell lines using viral transduction

Stable cell lines were generated by transducing cells with a replication-incompetent retrovirus derived from the Moloney Murine Leukaemia Virus. Virus was generated by transiently transfecting HEK cells with three plasmids:

- 1) Transfer plasmid (pLXIN-MOD). This plasmid was derived from pLXIN vector (Clontech) and had been modified so that the polylinker contains additional multiple cloning sites. The transfer vector also carries a neomycin resistance gene enabling cell selection using G418 (Geneticin).
- 2) The Gag and Pol plasmid (psPAX2).
- 3) Envelope plasmid (pMD2.G). The viral envelope used was from the vesicular stomatitis virus glycoprotein (VSVG).

The plasmids were combined at a ratio of 2:1:1 (transfer plasmid, Gag/Pol and VSVG envelope) and transfected into HEK cells as indicated above. 24 hours after transfection the media on the packaging cells was replaced with 15 mL of

fresh media and the cells transferred to 32 °C for another 24 hours. The cells to be transduced were plated into a six-well plate so that they were at approximately 60% confluency on the day of the infection.

1. The viral media was collected from the HEK cells using 20 mL syringe and 15 µL of polybrene (5 mg/mL) was added to the tip of the syringe and sucked into the viral media and mixed thoroughly.
2. The viral media was filtered through 0.45 µm filter (to remove cell debris).
3. The media was removed from the cell to be transduced and washed once with PBS. 2 mL of the filtered viral media was added to each well of the six-well plate.
4. The plate was sealed with parafilm and centrifuged for 90 minutes at 2500 rpm.
5. The parafilm was removed and the plate returned to the incubator.
Excess viral media was stored at -80 °C

24 hours post infection the transduced cells were passaged onto a 10 cm plate and the appropriate selectable marker added. If puromycin was being used, the cells were allowed to grow for a further 24 hours before it was added. To determine the transduction efficiency some of the cells were transferred onto coverslips in a 12-well plate.

2.4 Microscopy

2.4.1 Immunofluorescence protocol

Approximately, 2×10^5 cells were seeded onto coverslips (15 mm No.1 VWR, Germany) in a 12-well plate and grown overnight at 37 °C with 5% CO₂.

1. Cells were initially fixed by directly adding 4% paraformaldehyde (in PBS) to the culture media for 1 minute. The PFA was added to cells as soon as they were removed from the incubator to preserve membrane structures. After 1-minute the media was removed.
2. The fixation solution was again added to cells and incubated at RT for 15 minutes.
3. The fixation solution was removed and the cells washed once with PBS.

4. The PBS was removed and quenching solution (0.1 M glycine in PBS) was added to the cells and incubated at RT for 5 minutes.
5. The quenching solution was removed and cells washed once with PBS.
6. The PBS was removed and the cells were permeabilized with either 0.1% saponin buffer or 0.2% Triton X-100 buffer prepared with PBS and 5% FBS.
7. A humidified chamber was made by soaking tissue paper with water and placing it in a plastic dish. Parafilm was then placed on top of the tissue paper.
8. The respective primary antibody was prepared in the permeabilization buffer at their appropriate concentrations as indicated in the Table 2-1
9. 50 to 100 μ L of the primary antibody solution was aliquoted onto the parafilm depending on the size of the coverslips.
10. The coverslips were gently removed from the 12 well dish with forceps and excess permeabilization buffer drained off using tissue paper. The side containing the cells were placed on the primary antibody and incubated at RT for 1 hour.
11. The coverslips were gently removed and excess primary antibody was drained off and then washed three times with the permeabilization buffer.
12. The cells were incubated with their appropriate secondary antibody at RT for 40 minutes in the same manner to the primary antibody and then washed three times with the permeabilization buffer and then once with PBS.
13. The cells were mounted onto 1.0 – 1.2 mm microscope slides (Fisherbrand, UK) with Prolong Gold anti-fade reagent with DAPI (Molecular probes by life technologies, USA). Then observed with 60X oil immersion objective using a Motorized Olympus BX61 wide field epifluorescence microscope (Olympus, UK) unless otherwise stated.

2.4.2 Preparing samples for 3D-SIM OMX

Samples were prepared as outlined in section 2.4.1, however; 22 mm No. 1.5H high precision microscope coverslips (VWR, Germany) and 0.8-1.0 mm microscope slides (Fisherbrand, UK) were used. Samples were imaged at least

48 hours after mounting to reduce the risk of a reflective index mismatch between the mounting media and immersion oil. Dr Darren Robinson (Light Microscopy Facility Manager, Department of Biomedical Science, The University of Sheffield) performed the OMX imaging.

2.4.3 Stochastic Optical Reconstitution Microscopy (STORM)

Samples were prepared as outlined in section 2.4.1. However, after the terminal wash with PBS, gold nanoparticles were added onto the coverslips to serve as fiducial markers for 30 minutes at RT and then washed with PBS. The coverslips were mounted with 5 μ L of imaging buffer containing 100 mM β -mercaptoethylamine, with 0.5 mg/mL glucose oxidase and 0.04 mg/mL catalase. The β -mercaptoethylamine helps the dyes stay in the 'dark state' for longer. The glucose oxidase and catalase serve as oxygen scavenging system to stop the samples from bleaching quickly. Nail polish was then used to seal the coverslips onto the slides. The sample was imaged at 20-50fps for 10,000-20,000 frames. Mary Snape (PhD student, Physics Department, The University of Sheffield) performed the STORM imaging.

2.4.4 Chemical inhibitors

2.4.4.1 Proteasome inhibitor treatment (MG132)

HeLaM cells were treated with 5 μ M of MG132 (Cayman Chemical, USA) for 8 hours (stock concentration 1 mM in ethanol).

2.4.4.2 2-bromopalmitate (2-BP) treatment

HeLaM cells were treated with a range of different concentrations of 2-bromopalmitate (Sigma, USA) (50 μ M, 100 μ M, and 150 μ M) for 8 hours (stock concentration 100 mM in DMSO).

2.4.5 Antibody uptake Assay

HeLaM cells were grown on coverslips, transferred to a prewarmed/humidified chamber and incubated with 50 μ L of media containing antibodies against CD29, CD55, CD59, MHC1, and TF-R (see Table 2-1 for dilutions). The coverslips were then incubated at 37 $^{\circ}$ C, for various times (10, 30 and 60 minutes) to allow for the internalisation of the antibodies. The coverslips were gently removed from the chamber and excess media wiped off using tissue

paper. The cells were then fixed and processed as in Section 2.4.1. During the immunofluorescence staining, the internalised antibodies were co-stained with STX19.

2.5 Protein preparation and analysis

2.5.1 GFP-binding protein expression and purification

The expression and purification of the GFP-binding protein were performed as described in (Kweon et al., 2003a, Rothbauer et al., 2008) but with some modifications.

The GFP-Trap plasmid was transformed into BLD21-gold (DE3) pLysS competent as in section (2.2.1). A single colony was selected and used to inoculate a 5 mL starter culture and grown overnight at 37 °C (2xTY media and 50 µg/mL kanamycin). The culture was poured into a 100 mL Schott bottle with 50 mL of 2xTY and 50 µg/mL kanamycin and incubated at 37 °C for 4 hours. The culture was diluted into 500 mL of 2xTY and 50 µg/mL kanamycin in a 2 L flask and grown at 37 °C until the optical density (OD) at 600 nm reached between 0.6 and 0.8. This occurred after 1.5 hours. Protein expression was induced by the addition of 0.5 mL of 100 mM IPTG. The culture was grown for a further 16 hours at 22 °C.

2.5.1.1 Bacteria culture cell lysis and coupling of proteins onto Nickel-NTA agarose beads

1. Bacteria were harvested by centrifugation at 5 Kg for 15 minutes using Avanti J-26 XP centrifuge (Beckman Coulter, USA). The supernatant was discarded and the cells transferred onto ice.
2. The pellet was resuspended using 5 mL of lysis buffer and transferred into a 50 mL Falcon tube. The original tube containing the bacteria was rinsed with an extra volume of 5 mL of lysis buffer. 250 µL of Roche complete protease inhibitor cocktail was added (50X stock of 1 tablet/1 mL dH₂O).
3. The Falcon tube was snap frozen at -80 °C for 15 minutes and then put in RT water until it thawed (10-20 minutes).

4. 12 μL of 1 M MgCl_2 stock and 0.01 g deoxyribonuclease I (Sigma, USA) was added and rocked at RT for 10 minutes.
5. Triton X-100 was added to make a final concentration of 2% (1.5 mL of 20%) and rotated at 4 °C for 20 minutes.
6. 0.5 mL of HIS-tagged Nickel-NTA agarose beads (Qiagen, Germany) were pipetted into a 15 mL falcon tube washed by resuspending in low salt buffer, spun at 2000 rpm for 1 minute and then supernatant poured off. This was repeated twice.
7. Lysates from step 5 were pelleted by centrifugation at 7,000 rpm for 20 minutes at 4 °C. 10 μL of the supernatant (Input) was saved for gel analysis (Figure 2-1).
8. The supernatant was incubated with the beads for 1.5 hours at 4 °C while being rotated.
9. The beads were pelleted at 2000 rpm for 1 minute. 10 μL of the supernatant (Flow-through) was saved for gel analysis (Figure 2-1).
10. The beads were washed twice as in step 6 using a high salt buffer.
11. The beads were washed twice as in step 6 using a low salt buffer.
12. The beads were resuspended in 7 mL of low salt buffer and 10 μL was saved for gel analysis (Pull down) (Figure 2-1).
13. 3.3 μL of 4X loading buffer was added to the samples saved for gel analysis and loaded on SDS-PAGE gel followed by coomassie staining.
14. The beads were filled with glycerol to reach a maximum 15 mL and mixed well on a shaker before storing at 4 °C.

2.5.1.2 Protein elution and purification

1. The beads washed three times with 15 mL of buffer A and then resuspended in 1.5 mL of buffer A containing 250 mM imidazole to elute the protein from the beads.
2. The beads were centrifuged at 2000 rpm and the supernatant taken. 5 μL was saved for gel analysis.
3. The concentration of the protein was measured using a NANODROP LITE Spectrophotometer (Thermo Scientific, USA) to confirm that the protein had been effectively eluted from the beads.

4. The protein was concentrated using 10 kDa Generon membrane vivaspin (Sartorius Stedium Biotech GmbH, Gottingen, Germany) as the protein size is 13 kDa and then purified by AKTA Fast protein liquid chromatography (AKTA, Buckinghamshire, UK) fitted with Superdex 200 Increase 10/300 GL gel filtration column (GE Healthcare Bio-Sciences AB, Uppsala, Sweden).
5. The purified protein had a peak of 2000 mAU over three fractions (22, 23, and 24) 0.5 mL each. The protein purification was performed together with Charlotte Lesse (A postdoc student, The University of Sheffield, Prof Bazbek Daveletov Lab) (Figure 2-2).

2.5.1.3 Coupling of GFP-binding protein onto NHS-activated Sepharose 4 Fast Flow

The purified proteins was coupled onto NHS-activated Sepharose 4 Fast Flow (GE Healthcare Life Sciences, Uppsala, Sweden) as the manufacturer's instructions.

1. The NHS-activated Sepharose 4 resin was thoroughly mixed and 7 mL of the resin pelleted at 2000 rpm for 1 minute (yields 4 mL of packed resin).
2. The resin was washed 5 times with 40 mL of 1 mM HCl.
3. After the final wash, the purified protein was added to the resin and incubated for 4 hours at RT on an end-over-end rotator.
4. The resin was blocked by incubation with 0.1 M Tris pH 8.5 for 2 hours at RT. Non-coupled protein was removed by washing the resin three times with 0.5 M NaCl pH 4.5 and then three times with PBS.
5. After the last wash and centrifugation step an equal volume of PBS / 20% ethanol was added to the resin. The resin was aliquoted and stored at 4 °C for subsequent use (Figure 2-2).

2.5.2 Bio-Rad protein assay (Bradford assay)

The assay was performed according to the manufacturer's instructions.

1. Two-fold serial dilutions of bovine serum albumin were prepared in the sample buffer (the same buffer as the protein sample). Serial dilutions used were 4, 2, 1, 0.5, 0.25, 0.125, 0.0625, and 0.03125 mg/mL.

2. 10 μ L from each of the serial dilutions were taken and 1 mL of Bio-Rad protein assay solution (Bio-Rad laboratories GmbH, Germany) was added.
3. The mixture was aliquoted into cuvettes, vortexed gently and then incubated for 5 minutes.
4. Absorbance was read at OD600 using Bio-Rad SmartSpec Plus Spectrophotometer (Bio-Rad, USA).
5. The values obtained were used to plot a standard curve and the protein concentrations inferred from the graph.

2.6 Affinity capture of biotinylated proteins

The process of capturing biotinylated proteins for analysis by mass spectrometry was performed following the protocol developed by the Davies laboratory with few minor modifications. The key steps are as follows:

1. Growing cells
2. Collection of cells
3. Lysis of cells
4. Incubation with streptavidin beads
5. Elution
6. Western blot
7. Mass spectrometry

2.6.1 Growing HA-tagged BIRA*STX19

HeLaM stable cell line expressing HA-tagged BIRA*STX19 cells were grown in T175 flasks overnight. The cells were incubated with 50 μ M of biotin (Sigma, USA) for 24 hours. The stock biotin concentration was 50 mM.

2.6.2 Collection and lysis of cells

Cells were removed from the incubator and quickly placed on ice and washed three times with ice-cold PBS. Cells were scraped in 10-15 mL of cold PBS with the aid of Cell scraper (Fisher Scientific, China) and transferred into a centrifuge tube. The cells were washed three times with 5 ml of cold PBS (pelleted at 2500 rpm for 5 minutes). The cell pellets were resuspended in 1 mL of RIPA lysis

buffer and passed through QIASHredder (QIAGEN GmbH, Hilden, Germany) via centrifugation. This process was repeated three times. The samples were then incubated at 4 °C on an end-to-end rotating device (NeoLab Migge, Heidelberg, Germany) for 20 minutes, followed by centrifugation at 13,000 rpm for 15 minutes. 5% of the supernatant was transferred into a new Eppendorf tube and labelled as input. The remaining supernatant was used for the next step.

2.6.3 Incubation with streptavidin beads

The streptavidin agarose beads (Solulink, USA) were vortexed to mix the beads and 60 µL transferred into 1.5 mL Eppendorf tube. The beads were pelleted by centrifuging at 8000 rpm for 3 minutes and washed twice with 1 mL of ice-cold TBS pH 7.4 and once with 1 mL of RIPA buffer. The cell supernatant generated as in section (2.6.1) was added to the beads and then incubated at 4 °C for 3 hours with continual mixing. Afterwards, the beads were pelleted at 8000 rpm for 3 minutes and 5% of the supernatant transferred into a new Eppendorf tube and labelled as flow-through. The beads were washed three times with RIPA buffer and a further two times with TBS (5 minutes at 4 °C for each wash). The Input, Flow-through and Beads were resuspended in 50 µl of 2x SDS-PAGE sample buffer, 5% β-mercapto-ethanol and boiled at 100 °C for 10 minutes for Western blot analysis. Samples for mass spectrometry were resuspended in 4X NuPAGE LDS Sample Buffer, 50 mM TCEP (Tris (2-carboxyethyl) phosphine hydrochloride). Samples were stored at -20 °C for further analysis.

2.6.4 Western blotting

Western blotting involved the following steps:

1. casting gels
2. running samples
3. transfer of samples
4. staining
5. blocking
6. primary antibody incubation
7. secondary antibody incubation
8. detection

2.6.4.1 Casting gels

Polyacrylamide gels were cast by first pouring the separating gel (see Table 2-20 for percentages). The separating gel was overlaid with isopropanol to reduce the introduction of oxygen which might otherwise interfere with the solidification of the gel. After the gel had polymerised the isopropanol was washed away with water. The water was removed using chromatographic paper (GE Healthcare Life Sciences, China). The stacking gel (Table 2-20) was added and a comb (10-15 well) inserted. Gels were used within 3 days of preparation. Precast gels (NuSep Limited, Homebush, Australia) were also used for preparing samples for mass spectrometry to reduce keratin contamination.

2.6.4.2 Electrophoretic separation and transfer of samples

For 10 well gels, a maximum of 20 μL of sample was loaded and 15 μL loaded for 15-well gels to prevent the sample spilling into the other wells. 5 μL of protein ladder was loaded in both the first and the last well. Empty or distorted wells were loaded with 1X sample buffer. Samples were run using a Fisher Biotech electrophoresis power pack (Fisher Scientific, Pittsburgh, USA) at 120 V until they reached the separating gel (10-15 minutes). The voltage was then increased to 200 V and ran until the dye reached the very bottom of the gel (approximately 60 minutes). Once the gel had finished running the proteins were either directly stained (see section 2.6.4.3) or electrophoretically transferred onto a 0.45 μm PVDF membrane (GE Healthcare Life Sciences, Germany). The PVDF membrane was first immersed in methanol for 30 sec and then placed onto a transfer cassette (containing transfer sponge, and Whatman paper) already immersed in the transfer buffer (Table 2-20). Samples were transferred using either a low molecular weight transfer buffer (<100 kDa) or high molecular weight transfer buffer (>100 kDa). The high molecular weight transfer buffer contains 0.1% SDS to aid the transfer of large proteins. The transfer was performed overnight in a cold room using a Bio-Rad PowerPac HC (Bio-Rad, USA) at 100 mA.

2.6.4.3 Protein visualisation

To confirm that the gels had run correctly or that the transfer had been successful the proteins were visualised using either SimplyBlue SafeStain or Ponceau-S.

➤ SimplyBlue SafeStain

The gel was washed rapidly three times and once slowly (5 minutes) with ddH₂O. The gel was incubated with SimplyBlue SafeStain (Invitrogen, California, USA) at RT for 1 hour. The dye was removed and the gel was washed quickly three times and slowly three times (10 minutes) with ddH₂O until clear bands were observed. The gel was left in ddH₂O and imaged with EPSON scanner (EPSON Perfection 4990 Series, California, USA) and/or Gel Doc EZ Imager (Bio-Rad laboratory Inc, USA)

➤ Ponceau-S staining

PVDF membranes were immersed in methanol for 30 seconds and transferred into the Ponceau-S (Cayman Chemical Company, USA) stain for 30 seconds. The membrane was removed and washed with water. Membranes were left to dry on a Whatman paper and then prepared for the next step.

2.6.4.4 Blocking

The majority of membranes were blocked using 5% milk powder (Table 2-20). Blocking was performed at RT for 30 minutes on a shaker. The blocking buffer was changed every 15 minutes during the blocking period. For detecting biotinylated proteins using streptavidin-HRP, 2.5% bovine serum albumin was used as the blocking agent (Table 2-20).

2.6.4.5 Primary and secondary antibody incubation

After blocking, the membranes were probed with specific antibodies (Table 2-1) diluted in blocking buffer. The primary antibody incubation lasted for 1 hour at RT on a shaker. The primary antibody was removed and the membrane washed quickly three times and slowly three times (5 minutes per wash) using blocking buffer. The membrane was then incubated with the appropriate secondary antibody (Table 2-1) diluted in blocking buffer for 40 minutes at RT. The secondary antibody was removed and the membrane washed quickly three times and slowly three times (5 minutes per wash) using blocking buffer.

2.6.4.6 Detection

The probed membranes were washed thoroughly with PBS and excess PBS removed by placing the membranes on Whatman paper. The damp membranes were then incubated with Clarity ECL Western blot Substrate for 5 minutes at RT. The excess substrate was removed and the signal detected using either X-ray film (Fujifilm) or with LiCOR c-DiGiT camera-based detection system (LiCOR Inc., Lincoln, USA). Densitometry analyses were performed using Image Studio Lite Ver 4.0

2.7 Mass spectrometry

Samples that were prepared for MS analysis were BIRA*STX19 to detect potential interacting partners of STX19 (sections 5.2.2; 5.2.3). GFPSTX19 (full-length and tail constructs) were prepared to identify putative palmitoylation and ubiquitination sites in STX19 (sections 4.2.8; 4.2.11). BIRA*STX19 samples were prepared as in section (2.6). GFPSTX19 (full-length and tail constructs) samples were as in section (2.6) Affinity capture of biotinylated proteins but with few exceptions:

- The cells were transfected with GFPSTX19 (full length or tail constructs).
- GFPTRAP beads were used to capture and purify the samples instead of streptavidin agarose beads.
- No biotin was used.

The mass spectrometry analysis was performed using two complementary processes including:

- In-gel sample analysis
- On resin digest

2.7.1 In-gel sample analysis

Biotinylated samples generated from BIRA-SRX19 were processed by the in-gel sample analysis. The in-gel sample analysis involves the following steps:

1. Alkylation
2. Gel purification
3. Staining

4. Destaining whole gel
5. Slicing
6. Destaining sliced gel
7. Digestion
8. Extraction

2.7.1.1 Alkylation and running samples

TCEP treated samples generated as in section (2.6.3) were alkylated with 50 mM iodoacetamide (Sigma, USA) and incubated in dark on a shaker (600 rpm) at 70 °C for 10 minutes. The samples were shaken for a further hour at RT. Samples were double loaded onto a precast gel and ran at 160 V for 70 minutes until the samples had effectively separated but have not yet reached the bottom of the gel.

2.7.1.2 Staining, destaining and slicing gels

The gel was washed with water and stained using colloidal coomassie blue (manufacturer's instruction) for 3 hours at room temperature. The stain was removed and the gel was washed with water. The gel was destained overnight using a solution of 40% methanol and 10% acetic acid in ddH₂O. The gel was first sliced into lanes, then sliced into six sections and each section further sliced into cubes (approximately 36 cuboids). The gel slicing was performed in a laminar flow hood. The scalpel and forceps used to slice the gel were cleaned with ethanol and wiped dry between gel slices. The gel fragments were transferred into labelled Eppendorf tube containing 0.5 mL destaining solution (Table 2-23).

The gel fragments were destained further using 0.5 mL Ammonium bicarbonate/ acetonitrile solution (Table 2-23) and incubated at RT on a shaker (600 rpm) for 1 hour. The gel fragments were centrifuged at 1000 rpm for 1 minute and the solution removed by pipetting (aspiration was avoided as to reduce the possibility of losing the gel fragments). The destaining step was repeated several times until the gel was free from any stain. The terminal destaining step was done with 500 µL of 100% acetonitrile and incubated at RT for 15 minutes on a shaker. The acetonitrile solution was removed and the gel fragments

allowed drying at RT. The dried gel fragments were stored at 4 °C until the digestion step.

2.7.1.3 Trypsin digestion and peptide extraction

200 µL of the trypsin digest solution (Table 2-23) was added to the dried gel pieces and incubated for 1 hour at 37 °C (shaken at 800 rpm). The digestion was continued overnight at 25 °C. Peptides were extracted from the gel fragments as follows:

1. 100 µL of acetonitrile was added to each of the samples and incubated at 37 °C for 20 minutes on a shaker at 800 rpm.
2. The samples were centrifuged at 1000 rpm for 1 minute and the supernatant transferred into a fresh Eppendorf tube and stored at -20 °C.
3. 50 µL of 0.5% formic acid was added to the samples and then incubated at 37 °C for 20 minutes on a shaker (800 rpm) followed by addition of 100 µL of acetonitrile.
4. Samples were incubated for another 20 minutes and centrifuged to collect the supernatant.
5. The supernatant was added to the previously collected supernatant and stored at -20 °C.
6. The formic acid and acetonitrile incubation steps were repeated twice.
7. Following the terminal collection of the supernatant, the gel pieces were stored at 4 °C and the supernatant dried using a Speed-Vac at 30 °C overnight (NB: the Eppendorf tube remained opened during the centrifugation step) .
8. Dried peptides obtained after sample preparations were suspended in 0.5% formic acid for 10 minutes at RT with gentle shaking and filtered to remove any gel piece that would block the MS column. Dr Mark Collins (Lecturer, The University of Sheffield, UK) ran the samples on the Orbitrap Elite™ Hybrid Ion Trap-Orbitrap Mass Spectrometer (Thermo Scientific, USA) and analysed the MS data using Mascot (Matrix Science) and MaxQuant (Cox and Mann, 2008) software.

2.7.2 On-resin sample analysis

The on-resin digest method, provided by Dr Mark Collins (Lecturer, The University of Sheffield, UK), was used to identify palmitoylation sites in GFPTRAP IP STX19.

2.7.3 On-resin digest of palmitoylation sites in GFPTrap IP STX19

Samples were prepared as in section (2.6; 2.7). The samples were prepared as follows:

1. GFPTRAP STX19 beads were incubated with 50 μ L of 50 mM TCEP and 50 mM iodoacetamide in 50 mM Tris pH 8. The incubation was performed in the dark at RT for 30 minutes. The beads were washed five times with 200 μ L of 50 mM Tris pH 7.5.
2. 50 μ L of 1M hydroxylamine pH 7.5 was added to one set of the beads and incubated for 1 hour at room temperature. The control beads were resuspended in 50 μ L of 50 mM Tris pH 7.5.
3. Both the treated and the control beads were washed three times with 100 μ L of 50 mM Tris pH 7.5.
4. The protein was eluted from the beads by adding 50 μ L of 8 M Guanidine-HCl and heated at 95 $^{\circ}$ C for 10 minutes.
5. The eluted proteins were collected and transferred to a fresh Eppendorf tube. Both the residual beads and the eluted proteins were stored at -20 $^{\circ}$ C for digestion.
6. The eluted proteins were digested with 1 μ g of trypsin for 4 hours at 37 $^{\circ}$ C and then at 25 $^{\circ}$ C overnight. This was followed by mass spec analysis as explained in section (2.7.1.3)

2.7.4 PEG Switch whole cell lysate assay

The PEG Switch assay was performed as described previously (Howie et al., 2014a, Burgoyne et al., 2013b) with some minor modifications:

1. HeLaM cells were grown on 10 cm plates overnight and transfected with EGFP3STX19, EGFP3STX19 tail, EGFPHRAS, EGFP3STX19 Tr2 and EGFP3 vector for 48 hours.

2. The plates were washed three times with ice-cold PBS and cells scraped off using cell scraper. The cells were pelleted by spinning at 2500 rpm for 5 minutes.
3. The cells were washed three times with 5 mL of PBS.
4. The cells were resuspended in 200 μ L lysis buffer pH 7.4 (2.5% SDS, 100 mM HEPES, 1 mM EDTA and 100 mM maleimide), and incubated on a shaker (800 rpm) at 40 °C for 4 hours.
5. Excess unreacted maleimide was removed by acetone precipitation. The acetone precipitation protocol was based on a protocol by (Wessel and Flugge, 1984). Acetone was precooled overnight at -20 °C. 800 μ L of the acetone was added to 200 μ L of the lysed cells, vortexed vigorously and incubated for 1 hour at -20 °C. The protein was pelleted by centrifugation for 10 minutes at 12,000 rpm. The supernatant was discarded. The pellet was washed five times with 70% acetone and dried for 5 minutes to allow the acetone to evaporate.
6. The pellet was solubilised with 200 μ L of 1% SDS, 100 mM HEPES, and 1 mM EDTA pH 7.4 and incubated on a shaker (800 rpm) at RT.
7. The sample was divided into two (100 μ L each). 100 μ L of 4 mM 5 kDa PEG-maleimide; 400 mM hydroxylamine-HCl pH 7.4 was added to one set of the samples. The other 100 μ L was incubated with 100 μ L 4 mM 5 kDa PEG-maleimide containing 200 mM Tris pH 7.4 instead of hydroxylamine-HCl to serve as negative control. The reaction was left on a shaker at RT for 2 hours.
8. 70 μ L of 4X SDS sample buffer was added to each of the samples and incubated on a shaker at RT for 30 minutes.

2.7.5 Palmitate labelling coupled to click chemistry

The palmitate labelling coupled to click chemistry was performed as described previously with some modifications: in (Martin and Cravatt, 2009, Yap et al., 2010).

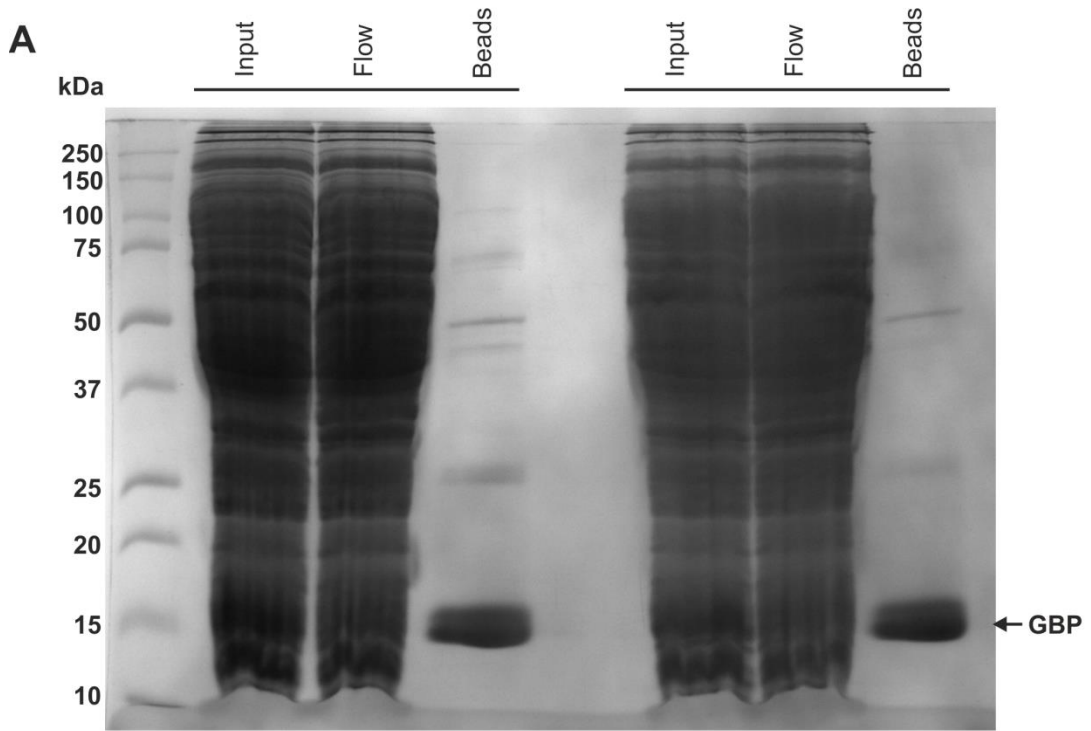
2.7.5.1 Metabolic labelling

HEK293T cells were seeded onto a 24-well plate, grown overnight and transfected with GFPSTX19 or GFPSTX19tail together with the 23 HA-tagged

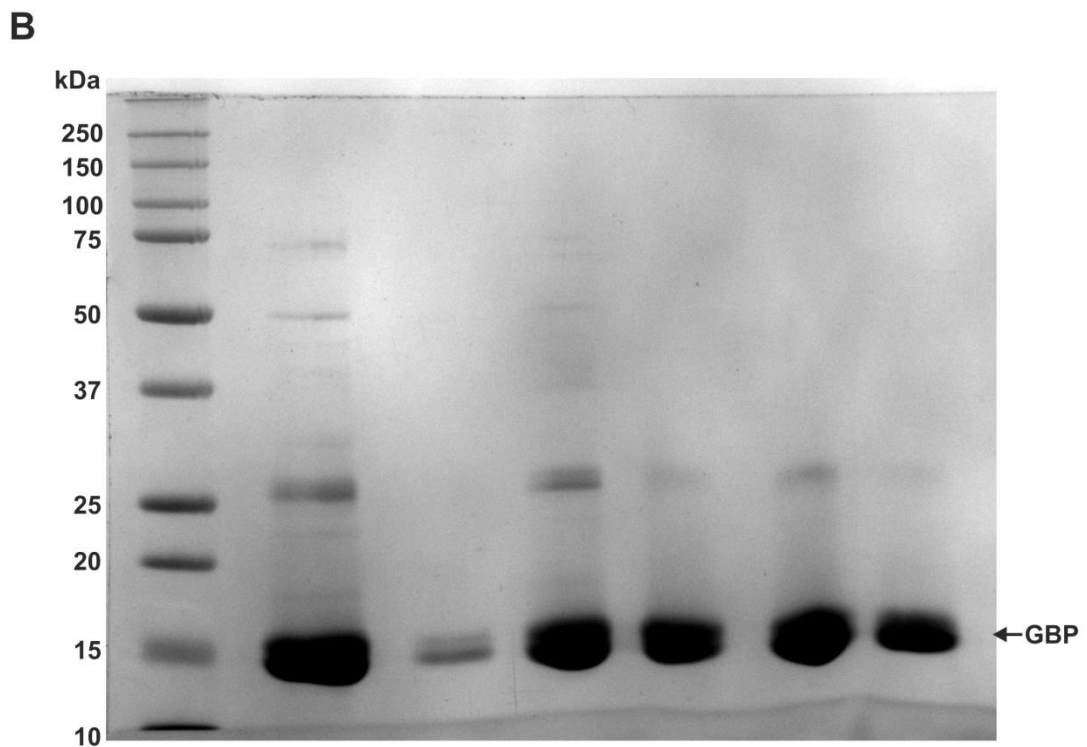
palmitoyl acyltransferases library. The ratio of the substrate to the PATs was 1 to 2 (0.8ug substrate + 1.6 ug HA-zDHHHC). 24-hours post transfection, the cells were serum-starved in DMEM containing 1% fatty-acid free BSA for 30 minutes at 37 °C. The cells were then incubated in DMEM 1% fatty-acid free BSA containing 50-100 µM palmitic acid azide for 3 hours at 37 °C. The cells were washed two times with ice-cold PBS and then lysed on ice with 100 µL of 50 mM Tris pH 8.0 containing 0.5% SDS and protease inhibitors.

2.7.5.2 Click chemistry

The click reaction mix and ascorbic acid were freshly prepared on the day of the experiment. To 100 µL of cell lysate, 80 µL of click reaction mix was added (0.125 µL alkyne dye, 10 µL CuSO₄ and 0.4 µL Tris [(1-benzyl-1H-1,2,3-triazol-4-yl)methyl]amine TBTA in ddH₂O) and vortexed. To this 20 µL of 40 mM ascorbic acid added. The final concentrations of the reagents were 2.5 µM alkyne Dye, 2 mM CuSO₄, 0.2 mM TBTA and 4 mM Ascorbic Acid; total volume including lysate was 200 µL. The samples were vortexed and incubated for 1 hour at RT with end-over-end rotation. After the click reaction, the proteins were precipitated using methanol/chloroform or acetone and the pellet allowed air-drying for 5 minutes. The pellets were resuspended in 100 µL of 1x SDS sample buffer containing 25 mM DTT and 10-15 µL of this separated by precast SDS-PAGE gel (4-20%). This was followed by immunoblotting as explained in section (2.6.4).



GFP Binding Protein (GBP) after coupling onto His-tagged Nickel beads

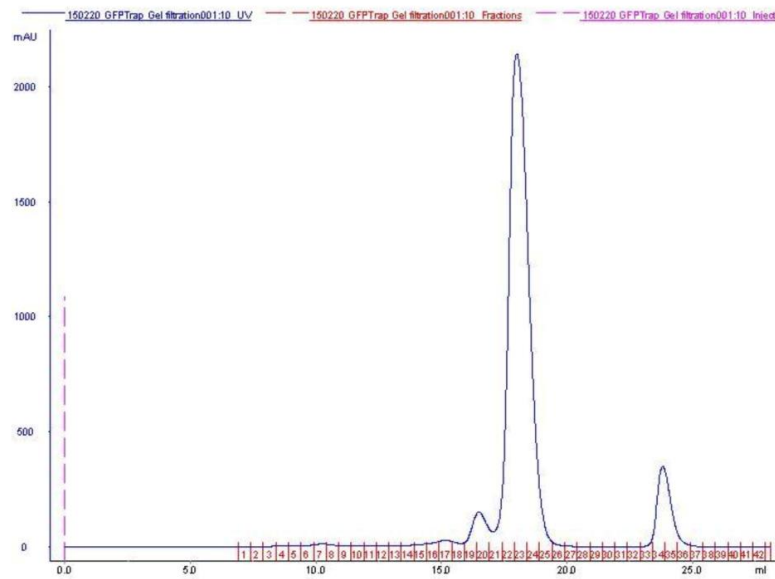
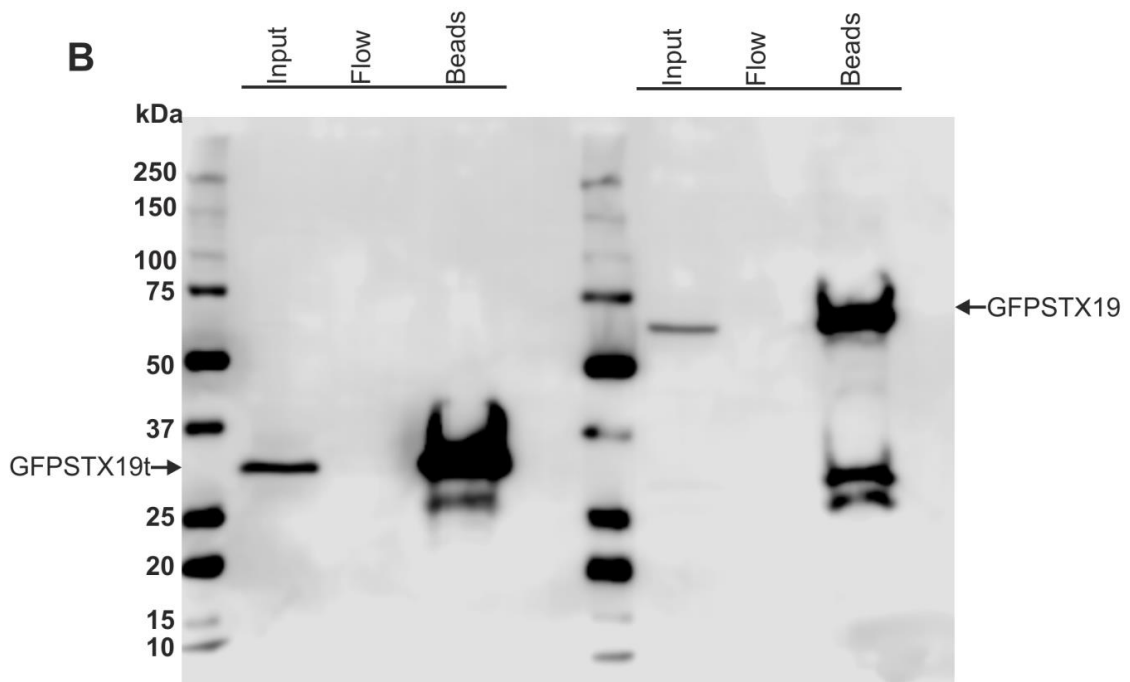


Purified GFP Binding Protein (GBP) after passing through 10 kDa MWCO membrane vivapsin

Figure 2-1 The purification of the GFP-binding protein (GBP).

The His-tagged GBP (13 kDa) was transformed into BLD21-gold (DE3) pLysS

competent cells and then grown in 500 mL culture media at 37 °C for 1.5 h . The culture was induced with 100 mM of Isopropyl β -D-1-thiogalactopyranoside (IPTG) when the optical density of the culture had reached between 0.6 and 0.8. After about 16 h, the bacteria was pelleted, lysed and purified on Nickel-NTA agarose beads **A)** Coomassie staining of the purified GBP plasmid **B)** Coomassie staining of the purified GBP plasmid after concentrating with 10 kDa molecular weight cut-off (MWCO) membrane vivaspin

A**Chromatographic peaks of the GBP****B****Validating the efficiency of the GBP coupled onto NHS-activated sepharose beads****Figure 2-2 Ultrapurification, coupling and validation of the efficacy of the GBP.**

After concentrating the GBP as explained before, the samples were further purified using AKTA Fast protein liquid chromatography. The purified GBP was coupled onto NHS-activated Sepharose 4 Fast Flow. **A)** The chromatographic peaks of the purified GBP. **B)** HeLaM cells were seeded overnight into 10 cm plates and then transfected with either GFPSTX19t or GFPSTX19. 48 h post

transfection, the cells were collected, lysed and trapped onto the GFP beads. The purified samples were blotted with anti-GFP followed by rabbit HRP. Western blots were detected using LI-COR Image Studio Digits Ver 4.

The generation of STX19 and SNAP29 antibodies was synthesised as explained before (Gordon et al., 2010, Gordon et al., 2009). Refer to pages 105-106 for a detailed explanation.

Table 2-1 Antibodies

Antigen	Source	Usage	Host species
Primary antibodies			
RAB8A	ProteinTech Europe Cat No. 555296-1- AP	WB (1/1000); IF (1:200)	Rabbit
STX19	A. Peden	WB (1/500); IF (1:200)	Rabbit
Anti-HA	BioLegend Cat No. MMS-101R	WB (1/2000); IF (1:200)	Mouse
SNAP29	A. Peden	WB (1/300); IF (1:200)	Rabbit
MICALL1	Abnova Cat No. H00085377-B01P	WB (1/500); IF (1:200)	Mouse
AF 488 conjugated CD29	Invitrogen Cat No. CD292920	IF (1:200)	Mouse
AF 488 conjugated CD59	AbD Serotec Cat No. MCA1054A488	IF (1:200)	Mouse
CD59	Sigma Cat No. SAB4700207	IF (1:200)	Mouse
FITC labelled CD55	BD Biosciences Cat No. 555693	IF (1:50)	Mouse
FITC labelled CD77	BD Biosciences Cat No.	IF (1:25)	Mouse

	551353		
AF 488 conjugated HLA-ABC	BD Biosciences Cat No. 560169	IF (1:25)	Mouse
MYC 9E10	Made in house	IF (1:500)	Mouse
PASCIN2	Abgent Cat No. AP8088b	WB (1/1000); IF (1:500)	Rabbit
EHD1 (EPR4954)	Abcam Cat No. ab109311	WB (1/1000); IF (1:100)	Rabbit
Dystonin	Abcam Cat No. ab55654	IF (1:50)	Mouse
γ-Adaptin		WB (1/2000)	Mouse
MACF1-4 (D-10)	Santa Cruz Biotechnology Cat No. sc-377534		Mouse
GLUT1	Abcam Cat No. ab15309		Rabbit
Src (36D10)	Cell signal Cat No. 2109		Rabbit
Secondary antibodies			
Alexa Flour 488	Invitrogen Molecular Probes	IF (1:1000)	Mouse
Alexa Flour 488	Invitrogen Molecular Probes	IF (1:1000)	Rabbit
Alexa Flour 594	Invitrogen Molecular Probes Cat No. A11032	IF (1:1000)	Mouse

Alexa Flour 594	Invitrogen Molecular Probes	IF (1:1000)	Rabbit
Alexa Fluor 647	Invitrogen Molecular Probes	IF (1:800)	Rabbit
Cy3	Invitrogen Molecular Probes	IF (1:1000)	Mouse
Streptavidin 594	Dr Jason King (The University of Sheffield)	IF (1:1000)	Rabbit
HRP (FC-specific fragment)	Jackson ImmunoResearch Laboratories Cat No. 115-035-008	WB (1/5000)	Mouse
GFP	Abcam Cat No. ab6556	WB (1:2000); IF (1:1000)	Rabbit
HRP (FC-specific fragment)	Jackson ImmunoResearch Laboratories Cat No. 111-035-008	WB (1:5000)	Rabbit
Streptavidin HRP		WB (1/5000)	
StrepTactin-HRP conjugates	Bio-Rad Cat No. 161-0380	WB (1/5000)	

Table 2-2 Antibiotics

Antibiotic stock	Working concentration	Composition	Recipe (source)
10 mL Ampicillin	100 µg/mL	100 mg/mL Ampicillin dH ₂ O	Dissolve 1 g Ampicillin sodium salt (Fisher, BP1760-5) in 10 mL dH ₂ O. Filter through 0.22 µm filter before use. Make 1 mL aliquot, store at -20 °C.
10 mL Kanamycin	50 µg/mL	50 mg/mL Kanamycin disulfate salt dH ₂ O	Dissolve 0.5 g Kanamycin disulfate salt (MERCK, EC 223-347-1) in 10 mL dH ₂ O. Filter through 0.22 µm filter before use. Make 1 mL aliquot, store at -20 °C.
10 mg/mL Puromycin	10 µg/mL	10 mg/mL Puromycin dH ₂ O	Dissolve 0.1 g puromycin in 10 mL dH ₂ O. Filter through 0.22 µm filter before use. Make 0.5 mL aliquot, store at -20 °C.
Geneticin (G418)	500 µg/mL	50 mg/mL	As supplied (gibco by life technologies,

			10131-019)
Hygromycin B	250 µg/mL	50 mg/mL	As supplied (Invitrogen, 10687-010)
L-Glutamine penicillin Streptomycin (100 mL)	2 mM L-Glutamine 100 U/mL Penicillin 100 µg/mL Streptomycin	10000 U/mL Penicillin 10 mg/mL Streptomycin 200 mM L-Glutamine	Make 5 mL aliquot of 100 mL L-Glutamine - penicillin - Streptomycin solution (Sigma, G1146-100ML) Store at -20 °C

Table 2-3 Plasmid media and Reagents.

Media/Reagents	Composition	recipe
Agarose gel (100 mL)	1% agarose powder 10% Tris-Borate-EDTA (TBE) ddH ₂ O	1 g agarose powder (Fisher Scientific, BP1356-100) 10 mL 10X TBE (Fisher BioReagents, BP13334) Add ddH ₂ O to 100 mL. Microwave 90 seconds. Cool to 50 °C, add 1 µL sybr safe, shake gently and pour into gel cast.
LB media pH8.0 (1 L)	0.5% Sodium chloride 1% Tryptone 0.5% Yeast extract 5 M NaOH ddH ₂ O	5 g Sodium chloride (Fisher Scientific, S/3120/60) 10 g Tryptone (Fluka Analytical, T9410-1KG) 5 g Yeast extract (Sigma, 41625-1KG)

		<p>Add ddH₂O to 1 L. Stir 10 minutes and adjust to pH 8.0 with 5 M NaOH (Thermo Scientific, S/4920/60).</p> <p>Autoclave to sterilise media.</p>
Agar plate pH8.0 (1 L)	<p>0.5% Sodium chloride 1% Tryptone 0.5% Yeast extract 1.5% Agar 5 M NaOH ddH₂O</p>	<p>5 g Sodium chloride (Fisher Scientific, S/3120/60) 10 g Tryptone (Fluka Analytical, T9410-1KG) 5 g Yeast extract (Sigma, 41625-1KG) 15 g Agar (Fluka Analytical, 05040-1KG)</p> <p>Add ddH₂O to 1 L. Stir 10 minutes and adjust to pH 8.0 with 5 M NaOH (Thermo Scientific, S/4920/60)</p> <p>Autoclave to sterilise media.</p> <p>Allow agar media to cool down to 50 °C, add required antibiotic and poured into sterile bacteria culture plate.</p> <p>Store solidified agar plate at 4 °C</p>
5 M Sodium hydroxide (10 mL)	<p>20% Sodium hydroxide ddH₂O</p>	<p>2 g NaOH (Thermo Scientific, S/4920/60) 10 mL ddH₂O</p>

Table 2-4 PCR mix.

Reverse primer (10 μ M)	2.5 μ L
Forward primer (10 μ M)	2.5 μ L
DNA template	1.0 ng
2x ReadyMix PCR Master Mix	25 μ L
ddH ₂ O	To 50 μ L

Table 2-5 Oligo annealing mixture.

Reverse primer (100 μ M)	5 μ L
Forward primer (100 μ M)	5 μ L
10x Ecor1 buffer	5 μ L
ddH ₂ O	35 μ L

Table 2-6 PCR program.

Step		Temperature	Duration	Cycle
1		95 °C	2 minutes	
2		95 °C	25 seconds	35
3		60 °C	35 seconds	35
5		72 °C	5 minutes	
6		4 °C	∞	

Table 2-7 PCR master mix for generating a site-directed mutation in MICALL1.

Reagent	Volume
Q5 Hot Start High-Fidelity 2x Master Mix	25 μ L
Reverse primer (10 μ M)	2.5 μ L
Forward primer (10 μ M)	2.5 μ L
DNA template	1.0 ng

Nuclease-free water	Add to make total volume of 30.0 μ L
---------------------	--

Table 2-8 PCR program for generating a site-directed mutation in MICALL1.

Step	Temperature	Duration	Cycle
1	98 °C	30 seconds	
2	98 °C	25 seconds	25
3	61 °C	30 seconds	25
4	72 °C	4 minutes	25
5	72 °C	2 minutes	
6	4 °C	∞	

Table 2-9 Ligation reaction mixture

Reagent	Volume
Vector	1 μ L
Insert	6 μ L
T4 5x ligase buffer	4 μ L
DDH ₂ O	8 μ L
T4 Ligase	1 μ L

Table 2-10 Restriction digest mixture.

Reagents	Amount
DNA	1.5 μ g – 3.0 μ g
Restriction enzyme (1)	1.5 μ L
Restriction enzyme (2)	1.5 μ L
Buffer (10x)	3.0 μ L
Water	Add to make total volume of 30.0 μ L

Table 2-11 Primers.

Primer name	Sequence (5 to 3')
5 Xho1 HA STX19	CTCGAGATGTACCCCTACGACGTCCCCGACTACGCAAAGAC CGACTTCAAG
3 Not1 STX19 WT	GCGGCCGCTTATTTTGTAGCTACAGCATGGACAGCACC
Primers used to generate HA-STX19 with the cysteine-rich domain mutated to leucines	
3 Not1 STX19 M1	GCGGCCGCTTATTTTGTAGCTAAGGAGTGGACAGCACCAACAA CACAGTACTCTGCAAGGATTTCTTTTTTTGTATTTTAC
3 Not1 STX19 M2	GCGGCCGCTTATTTTGTAGCTACAGCATGGAAGGAGCCAACAA CACAGTACTCTGCAAGGATTTCTTTTTTTGTATTTTAC
3 Not1 STX19 M3	GCGGCCGCTTATTTTGTAGCTACAGCATGGACAGCACCAAGAA GCAGTACTCTGCAAGGATTTCTTTTTTTGTATTTTAC
3 Not1 STX19 M4	GCGGCCGCTTATTTTGTAGCTAAGGAGTGGAAAGGAGCCAACAA CACAGTACTCTGCAAGGATTTCTTTTTTTGTATTTTA
3 Not1 STX19 M5	GCGGCCGCTTATTTTGTAGCTACAGCATGGAAGGAGCCAAGA AGCAGTACTCTGCAAGGATTTCTTTTTTTGTATTTTAC
3 Not1 STX19 M6	GCGGCCGCTTATTTTGTAGCTAAGGAGTGGACAGCACCAAGA AGCAGTACTCTGCAAGGATTTCTTTTTTTGTATTTTAC
3 Not1 STX19 M7	GCGGCCGCTTATTTTGTAGCTAAGGAGTGGAAAGGAGCCAAGA AGCAGTACTCTGCAAGGATTTCTTTTTTTGTATTTTAC
Primers used to generate HA-STX19 with cysteine-rich domain truncated	
3 STX19 T1	CTCTGCAAGGATTTCTTTTTTTGTATTTTACTTCCTTGTGT CTCTGTTCAATCTCTGAAAG
5 STX19 T1	CTTTCAGAGATTGAACAGAGACACAAGGAAGTAAAATACA AAAAAAGAAATCCTTGCAGAG
3 Not1 STX19 T2 (273-294 truncated)	GCGGCCGCTTATACAGCTAGTCCAATTTCTC
Primers used to generate HA-STX19 with specified mutations	
5 Xho1 STX19	CTCGAGATGTACCCCTACGACGTCCCCGACTACGCAGCAGCA

KDR(2-4) AAA(2-4)	to	GCACTTTCAAGAACTAAAGCAGAGAACAAAGG
3 Not1 P (289) R(289)	STX19 to	GCGGCCGCTTATTTTGTAGCTACAGCATCGACAGCACC
3 Not1 W(286) R(286)	STX19 to	GCGGCCGCTTATTTTGTAGCTACAGCATGGACAGCATCGACAAC ACAGTACTCTGC
3 Not1 P(289) R(289); W(286) R(286)	STX19 to	GCGGCCGCTTATTTTGTAGCTACAGCATCGACAGCATCGACAAC ACAGTACTCTGC
3 STX19/STX13 tail	Not1	TCACTTCGTTTTATAAACTAGCCAGATAATAAGTCCCAAGATTA GAATAATCACTGACAGGACAAGCACCAGGATACACATTCTTTTT TTGTATTTTACAGCTAGTCC
Primers used to generate C-terminal HA-tagged STX19		
5 Xho1 STX19	STX19	GGCTCGAGCTATGAAAGACCGACTTCAAGAACTAAAGC
3 STX19	Not1 HA	GCGCGGCCGCTTATGCGTAGTCGGGGACGTCGTAGGGGTATT TTGAGCTACAGCATGGACAGCACC
Primers used to generate HA-tagged STX19		
5 STX19	Xho1 HA	CTCGAGATGTACCCCTACGACGTCCCGACTACGCAAAGAC CGACTTCAAG
3 STX19	Not1	GCGGCCGCTTATCTTTTTTTGTATTTTACAGCTAGTCC
Primers used to generate HA-tagged BirA*		
5 BirA*	Xho1	CTCGAGATGAAGGACAACACCGTGCCC
3 BirA*	EcoR1 HA	CGGGGACGTCGTAGGGGTACATGAATTCCTTCTCTGCGCTTCT CAGGG
Primers used to generate STX19 tail (274-294) constructs		
5 STX19 tail	Xho1	TCGAGAAAAAAGAAATCCTTGCAGAGTAC TGTGTTGTTGGTGCTGTCCATGCTGTAGCT CAAATAAG

3 EcoR1 STX19 tail	AATTCTTATTTTGAGCTACAGCATGGACAGC ACCAACAACACAGTACTCTGCAAGGATTC TTTTTTTC
5 XhoI STX19 tail W(286) to R(286)	TCGAGAAAAAAGAAATCCTTGCAGAGTAC TGTGTTGTCGATGCTGTCCATGCTGTAGCT CAAATAAG
3 EcoR1 STX19 tail W(286) to R(286)	AATTCTTATTTTGAGCTACAGCATGGACAGC ATCGACAACACAGTACTCTGCAAGGATTC TTTTTTTC
5 XhoI STX19 tail SS (292-3) to AA (292-3)	TCGAGAAAAAAGAAATCCTTGCAGAGTAC TGTGTTGTTGGTGCTGTCCATGCTGTGCAG CAAATAAG
3 EcoR1 STX19 tail SS (292-3) to AA (292-3)	aattcTTATTTtgctgcACAGCATGGACAGCACC AACAACACAGTACTCTGCAAGGATTTCTTTT TTTc
5 XhoI STX19 tail KKR to DDD (275-277)	TCGAGGACGACGACAATCCTTGCAGAGTAC TGTGTTGTCGATGCTGTCCATGCTGTAGCT CAAATAAG
3 EcoR1 STX19 tail KKR (275-277) to DDD (275-277)	AATTCTTATTTTGAGCTACAGCATGGACAGC ATCGACAACACAGTACTCTGCAAGGATTGT CGTCGTCC
5 XhoI STX19 tail KKR (275-277) to AAA (275-277)	TCGAGGCAGCAGCAAATCCTTGCAGAGTAC TGTGTTGTTGGTGCTGTCCATGCTGTAGCT CAAATAAG
3 EcoR1 STX19 tail KKR (275-277) to DDD (275-277)	AATTCTTATTTTGAGCTACAGCATGGACAGC ACCAACAACACAGTACTCTGCAAGGATTTG CTGCTGCC
5 XhoI STX19 tail KK (275-277) to RR (275-277)	TCGAGCGACGAAGAAATCCTTGCAGAGTAC TGTGTTGTTGGTGCTGTCCATGCTGTAGCT CAAATAAG
3 EcoR1 STX19 tail KK (275-277) to RR (275-277)	AATTCTTATTTTGAGCTACAGCATGGACAGC ACCAACAACACAGTACTCTGCAAGGATTC

	TTCGTCGC
5 XhoI STX19 tail Ks (274-294) to Rs (274-294); Cs (274-294) to Ls (274-294) except C (280)	TCGAGCGACGAAGAAATCCTTGCAGAGTAC TGCTTCTTTGGCTCCTTCCACTCCTTAGCTC ACGATAAG
3 EcoRI STX19 tail Ks (274-294) to Rs (274-294); Cs (274-294) to Ls (274-294) except C (280)	AATTCTTATCGTGAGCTAAGGAGTGGAAGG AGCCAAAGAAGCAGTACTCTGCAAGGATTT CTTCGTCGC
5 XhoI STX19 tail PP (279/289) to AA (279/289)	TCGAGAAAAAAGAAATGCTTGCAGAGTAC TGTGTTGTTGGTGCTGTGCATGCTGTAGCT CAAATAAG
3 EcoRI STX19 tail PP (279/289) to AA (279/289)	AATTCTTATTTTGAGCTACAGCATGCACAGC ACCAACAACACAGTACTCTGCAAGCATTCT TTTTTTC
5 XhoI STX19 tail Cs (274-294) to Ls (274-294) except C (280); W(286) to R(286)	TCGAGAAAAAAGAAATCCTTGCAGAGTAC TGCTTCTTAGACTCCTTCCACTCCTTAGCTC AAAATAAG
3 EcoRI STX19 tail (274-294) to Ls (274-294) except C (280); W(286) to R(286)	AATTCTTATTTTGAGCTAAGGAGTGGAAGG AGTCTAAGAAGCAGTACTCTGCAAGGATTT CTTTTTTTC
5 XhoI STX19 tail Cs (274-294) to Ls (274-294) except C (280)	TCGAGAAAAAAGAAATCCTTGCAGAGTAC TGCTTCTTTGGCTCCTTCCACTCCTTAGCTC AAAATAAG
3 EcoRI STX19 tail (274-294) to Ls (274-294) except C (280)	AATTCTTATTTTGAGCTAAGGAGTGGAAGG AGCCAAAGAAGCAGTACTCTGCAAGGATTT CTTTTTTTC
Primers used to generate GFP-STX13 transmembrane domain	
5 XhoI STX13	TCGAGATGTGTATCCTGGTGCTTGTCTGTGAGTG ATTATTCTAATCTTGGACTTATTATCTGGCTAGTTTA TAAACGAAGTGAG
3 EcoRI STX13	AATTCTCACTTCGTTTTATAAACTAGCCAGATAATAA GTCCAAGATTAGAATAATCACTGACAGGACAAGCA CCAGGATACACATC

Primers used to generate GFP-MICALL1 coiled-coil domain	
5 Xho1 MICALL1 coiled-coil	CTCGAGAAGGTCCAGGCTGACCAGTACATC CC
Primers used to generate GFP-MICALL1 with NPF motifs changed to AAA	
5 mut1 neb	GAGGAGGAGGAGGAGGAC
3 mut1 neb	ATAGGGTTTGGACTCCAG
5 mut2 neb	AACCGGAAGCCATCACCT
3 mut2 neb	CTCCTTGCAGGAGGACTTTAC
Primers used to generate MYC-EHD1	
5 EcoR1 myc EHD1	GAATTCATGGAACAAAACACTCATCTCAGAA GAGGATCTGTTCAGCTGGGTGAGCAAG
3 Not1 EHD1	GCGGCCGCTCACTCGTGCCTCCGTTTGG
Primers used to generate HA-SNAP29	
5 EcoR1 SNAP29	GAATTCATGTCAGCTTACCCTAAA
3 HA Not1 SNAP29	GCGGCCGCTCAAGCGTAATCTGGAACATC GTATGGGTAGAGTTGTGCGAACTTTTCTTTC
Sequencing primers	
STX19 internal reverse	GACCACTGAAGATGGACC
BirA* internal	CCAGGACCGCAAGCTGGC
STX19	GAGATGTCTGAAGAAG
EGFP-C3	GACAACCACTACCTGAGC
mCherry-C3	GGACATCACCTCCCAC
MICAL R	GGCCTTGGGTCCATCGGC
MICAL 1	GGCCCTTCTCACAGCC
MICAL 2	GCCACCAAGCCAGGACAG
MICAL 3	GGACCAGGGGCAGCTCAG
MICAL 4	CCGTGAGGATGACATGCTG
EHD1	CGACGCCACAAGCTGG
pIRES-NEO F	GGTACCGAGCTCGGATCG

Table 2-12 Common expression vectors used in this study.

Vectors	Selectable markers
pIRES-NEO	Ampicillin
pLXIN-MOD	Ampicillin
EGFP-C3	Kanamycin
EGFP-C1	Kanamycin
mCherry-C3	Kanamycin

Table 2-13 Expression constructs generated during this study.

Plasmid	Vector	Restriction sites	Cloning technique
GFP-tagged and CHERRY-tagged MICALL1	EGFP-C3 mCherry-C3	Xho I EcoR I	PCR was used to introduce an Xho I and EcoR I site at the 5 and 3' end of MICALL1. The PCR product was Topo cloned and sequenced. MICALL1 was then cloned into the expression vectors using Xho I and EcoR I.
GFP-tagged MICALL1 (NPF motifs mutated to AAA)	EGFP-C3	Xho I EcoR I	GFP-tagged MICALL1 with the NPF motifs mutated to AAA was generated using Q5 Site-Directed Mutagenesis Kit. Xho I and EcoR I sites were introduced by PCR and the product cloned into the expression vector.
GFP-tagged and CHERRY-tagged MICALL1 (coil-coiled domain)	EGFP-C3 mCherry-C3	Xho I EcoR I	The coiled-coil domain of MICALL1 was generated by PCR and Topo cloned and sequenced. The fragment was cloned into the expression vectors using Xho I and

			EcoR I
GFP-tagged STX19	EGFP-C3	Xho I	GFP-tagged STX19 was generated by restriction digest of pLXINSTX19 with NotI and EGFP-C3 empty vector with EcoR I, Klenow-treated and then digested with Xho I separately. The DNA was cloned into the EGFP-C3 vector using Not I.
HA-tagged STX11	pIRES-NEO	Not I EcoR I	HA-tagged STX11 was generated by PCR, Topo cloned and sequenced. The insert was cloned into a pIRESNEO using Not I and EcoR I.
Mutant HA-tagged STX19 (M1-M7, Tr)	pIRES-NEO	Not I EcoR I	Mutant forms of HA-tagged STX19 were generated by PCR (see table). The PCR products were Topo cloned and sequenced. The inserts were cloned into pIRES-NEO using Not I and EcoR I.
HA-tagged STX19 (coil-coiled domain absent)	pIRES-NEO	Not I EcoR I	HA-tagged STX19 without its coil-coiled domain was generated by PCR. The PCR product was topo cloned and sequenced. The DNA was cloned into a pIRESNEO using Not I and EcoR I.
HA-tagged STX19/13 hybrid	pIRES-NEO	Not I BamH I	HA-tagged STX19/13 hybrid was generated by replacing STX19's cysteine-rich domain with STX13 transmembrane domain and introduction of Not I and BamH I sites into STX19 by PCR. The DNA

			was cloned into a pIRESNEO using Not I and BamH I.
HA-tagged BIRA*STX19	pIRES-NEO	Xho I Not I	HA-tagged BIRA*STX19 was generated by introducing Xho I and EcoR I site into BIRA* and EcoR I and Not I sites into STX19 by PCR. The DNA was cloned into a pLXIN retroviral expression vector using Xho I and Not I.
MYC-tagged EHD1	pIRES-NEO	Not I EcoR I	MYC-tagged EHD1 was generated by introducing an EcoR I and Not I site into EHD1 by PCR and then cloned into a pIRES-NEO expression vector.
MYC-tagged FKBPSTX19	pLXIN-MOD	Xho I Not I	MYC-tagged FKBPSTX19 was generated by introducing Xho I and EcoR I site into the FKBP fragment and EcoR I and Not I sites into the STX19 by PCR. The DNA was cloned into a pLXIN retroviral expression vector using Xho I and Not I.

Table 2-14 Constructs obtained commercially or gift.

Plasmid	Selectable marker	Restriction sites	Source
pCAG-mGFP	Ampicillin	EcoR1/Not1	Addgene (14757). GFP fused with GAP43 palmitoylation sequence (Matsuda and Cepko, 2007)
pCDNA3-EGFP CDC42	Ampicillin	HindIII/Xho1	Addgene (12599) (Nalbant et al., 2004).

pCDNA3-EGFP RAC1	Ampicillin	HindIII/Xho1	Addgene (13719) (Kraynov et al., 2000).
pEF-Bos-HA-tagged zDHCs (1-23)	Ampicillin	BamH1/BamH1	A kind gift from Dr Luke Chamberlain (University of Strathclyde, Glasgow, Scotland) (Fukata et al., 2004)
EGFPC3 vector	Kanamycin	Multiple cloning sites	A kind gift from Dr Mathew Seaman (University of Cambridge, Cambridge, United Kingdom)
His-tagged GFP-binding protein	Kanamycin		

Table 2-15 Cells media composition.

Cells	Media composition
HeLaM, TIFF and A431	500 mL DMEM + 10% FBS + 5 mL PSG (Penicillin, Streptomycin, L-Glutamine)
MDCK	500 mL MEM + 10% FBS + 5 mL PSG + 5 mL 100x NEAA (Non-essential amino acids)
RPE	500 mL RPMI F1/2 + 10% FBS + 5 mL PSG + 17 mL 7.5% NaHCO ₃
HT29	500 mL MEM + 10% FBS + 5 mL PSG + 5 mL 100x NEAA (Non-essential amino acids)
Hap1	500 mL IMDM + 10% FBS + 5 mL PSG

Table 2-16 Cell culture media and reagents.

Media/Reagents	Composition	Recipe/Source
DMEM (500 mL)	1X Dulbecco's Modified	As supplied (gibco life

	Eagle Medium 0.45% D-Glucose 0.45% Pyruvate	technologies, 31966-047)
MEM(500 mL)	1X Minimum essential media	As supplied (gibco life technologies, 31095-052)
RPMI F1/2(500 mL)	1X Roswell Park Memorial Institute medium	As supplied (gibco life technologies, 121875-091)
IMDM(500 mL)	1X Iscove's Modified Dulbecco's medium L-Glutamine 25 mM HEPES	As supplied (gibco life technologies, 21980-032)
100X MEM NEAA	100X non-essential amino acid	Add 5 mL to 500 mL of media (gibco life technologies, 11140-035)
PBS pH 7.4 (500 mL)	Phosphate Buffered Saline without Calcium and Magnesium	As supplied (gibco life technologies, 10010-056)
1X Trypsin-EDTA	0.5 g porcine trypsin 0.2 g EDTA 4Na/L Hanks' solution	As supplied (Sigma, T3924-100ML)
Fetal bovine serum (500 mL)	Heat inactivated Fetal bovine serum	Fetal bovine serum (Sigma, F9665) Make 50 mL aliquot and store at -20 °C.
7.5% sodium bicarbonate solution	7.5 g sodium bicarbonate ddH ₂ O	Add 17 mL to 500 mL of media (gibco life technologies, 25080-060)

DMEM R10K8 (500 mL)	SILAC DMEM 13C and 15N labelled arginine 13C and 15N labelled lysine	As supplied (Dundee cell products, LM015-500 mL)
DMEM R0K0 (500 mL)	Control SILAC DMEM	As supplied (Dundee cell products, LM014-500 mL)
Dialyzed fetal bovine serum	10 kDa MWCO fetal bovine serum	As supplied (Dundee cell products, DS1003)
Dimethyl sulphoxide hybrid-Max	Dimethyl sulphoxide	As supplied (Sigma, D2650-100 mL)
Trypan blue dye (0.4%)	TC10 Trypan Blue Dye, 0.4% in 0.81% sodium chloride and 0.06% potassium phosphate dibasic solution	As supplied (BIO-RAD, 145-0013)

Table 2-17 Transfection mixture.

Plate	DNA concentration	PEI concentration	Total Opti-MEM volume
12-well	0.5 µg	2.5 µg	100 µL
6-well	1.0 µg	5.0 µg	200 µL
10 cm	10.5 µg	52.5 µg	500 µL
T175	25.0 µg	125 µg	800 µL

Table 2-18 Transfection reagents.

Buffer Stock	Composition	Recipe (source)
Linear polyethyleneimine	7-8% poly(2-ethyl-2-oxazoline)	As supplied (Polysciences Inc., 23966)
Oligofectamine	Oligofectamine	As supplied (Invitrogen)

		by life technologies, USA, 12252-011)
Polybrene (10 mL)	0.05% Hexadimethrine bromide dH ₂ O	50 mg Hexadimethrine bromide (Sigma, H9268-10G) Add 10 mL dH ₂ O, filter and store at 4 °C.
Lipofectamine2000	Lipofectamine	As supplied (Invitrogen by life technologies, USA, 11668-027)

Table 2-19 Cell culture materials.

Item	Catalogue Number	Source
MCO-18AIC Incubator		Panasonic biomedical service
Cell counter		BIO-RAD TC20 Automated Cell Counter, Singapore
ESCO Class II Biological Safety Cabinet		Walker safety cabinets limited, UK
1.8 mL Nunc Cryotube Vials	377267	Thermoscientific, Denmark
Powder free nitrile examination gloves		Barber HealthCare Limited, Leyburn, UK
Dual chamber cell counter slides	145-0011	BIO-RAD, USA
Pipette tips (RNase, DNase, DNA and Pyrogen free 10 µL, 200 µL, and 1 mL)	S1111-1720 S1111-0706 S1112-1720	STARLAB GmbH, Ahrensburg, Germany
Centrifuge tube (15 mL and 50 mL)	E1415-0200 E1450-0200	STARLAB International GmbH, Hamburg, Germany
1 mL sterile pipette	86.1251.001	SARSTEDT AG and Co.,

		Numbrecht, France
Syringe (20 mL and 50 mL)	300613 300865	BD Plastipak, Spain
2 mL sterile aspirator pipette	E48601211	STARLAB, France
15 mm No.1 microscope cover glass	ECN631-1579	VWR, Germany
0.45 µm Minisart syringe filter	16555-K	Sartorius Stedium Biotech GmbH, Germany
0.2 µm Minisart syringe filter	17823-K	Sartorius Stedium Biotech GmbH, Germany
Stericup and Steritop 0.22 µm sterilised vacuum driven filtration system	SCGPU02RE	GP Millipore Express Plus Membrane, China
150 cm ² canted neck flask	355001	BD Falcon, USA
10 cm ² plate	353003	BD Falcon, USA
Disposable serological pipette 5 mL, 10 mL and 25 mL	4051 4101 4489	Corning Inc, USA

Table 2-20 Western blot buffers.

Buffer stock	Composition	Recipe (source)
RIPA lysis buffer (50 mL)	50 mM Tris (pH 7.4) 150 mM NaCl 1 mM EDTA (pH 8.0) 1% NP-40 0.5% Sodium deoxycholate 0.1% SDS 1 tablet Protease cocktail inhibitor	2.5 mL 1 M Tris (Sigma, T1503-1KG) (pH 7.4) 2.5 mL 3.125 M NaCl (Fisher Scientific, S/3120/60) 100 µL 0.5 M EDTA (Fisher Scientific, D/0700/53) (pH 8.0)

	ddH ₂ O	<p>5 mL 10% NP-40 (BioVision Inc, 2111-100)</p> <p>0.25 g Sodium deoxycholate (Acros Organics, 218590250)</p> <p>250 µL 20% SDS (Fisher Scientific, BP 1311-1)</p> <p>1 tablet Protease cocktail inhibitor (Roche Diagnostics, 11836170001)</p> <p>Add ddH₂O to 50 mL</p> <p>NB: Tablet added just before use</p>
1X Tris buffer pH 7.4 (50 mL)	<p>50 mM Tris (pH 7.4)</p> <p>150 mM NaCl</p> <p>1 tablet Protease cocktail inhibitor</p> <p>ddH₂O</p>	<p>2.5 mL 1 M Tris (Sigma, T1503-1KG) (pH 7.4)</p> <p>2.5 mL 3.125 M NaCl (Fisher Scientific, S/3120/60)</p> <p>1 tablet Protease cocktail inhibitor (Roche Diagnostics, 11836170001)</p> <p>Add ddH₂O to 50 mL</p>
Separating buffer (500 mL)	<p>3 M Tris-HCl (pH 8.9)</p> <p>11.6 M HCl</p> <p>ddH₂O</p>	<p>183 g Trizma (Sigma, T1503-1KG)</p> <p>20 mL 11.6 M HCl (Fisher, HOURS/1200//PB17)</p> <p>Add ddH₂O to 500 mL</p> <p>Stir thoroughly</p> <p>pH 8.9</p>

		Store at 4 °C
Stacking buffer(500 mL)	1 M Tris-HCl (pH 6.8) 11.6 M HCl ddH ₂ O	61 g Trizma (Sigma, T1503-1KG) 30 mL – 40 mL 11.6 M HCl (Fisher, HOURS/1200//PB17) Add ddH ₂ O to 500 mL Stir thoroughly pH 6.8 Store at 4 °C
30% acrylamide	30% acrylamide 37.5:1 bis-acrylamide solution	As supplied (Bio-Rad, 161-0158)
20% SDS (1 L)	200 g sodium dodecyl sulfate ddH ₂ O	As supplied (Fisher Scientific, BP 1311-1)
10% APS (10 mL)	10% Ammonium persulfate ddH ₂ O	1 g APS (Sigma, A3678-25G) 10 mL ddH ₂ O Aliquot and store at -20 °C
TEMED	99% N,N,N',N'-Tetramethylethylenediamine	As supplied (Sigma, T7024-25ML)
Running buffer (10 L)	25 mM Tris 192 mM Glycine 0.1% (w/v) SDS ddH ₂ O	1 L 10X TGS (Bio-Rad, 161-0772) 9 L ddH ₂ O Shake vigorously
1 mL 4X Laemmli sample buffer	277.8 mM Tris-HCl (pH 6.8) 4.4% LDS 44.4% (w/v) glycerol 0.02% bromophenol blue	450 µL 4X Laemmli sample buffer (Bio-Rad, 161-0747) 100 µL β-mercapto-

		ethanol (Sigma, M6250-100ML) 450 µL ddH ₂ O Use immediately
2X Laemmli sample buffer (1 mL)	65.8 mM Tris-HCl (pH 6.8) 2.1% SDS 26.3% (w/v) glycerol 0.01% bromophenol blue	950 µL 2X Laemmli sample buffer (Bio-Rad, 161-0737) 50 µL β-mercapto-ethanol (Sigma, M6250-100ML) Use immediately
4x NuPAGE LDS sample buffer (1 mL)	NuPAGE LDS	500 µL 4x NuPAGE LDS sample buffer (Novex by life technologies, NP0007) 100 µL TCEP (Sigma 646547-10X1ML) 400 µL ddH ₂ O Use immediately
Precision Plus Protein Standard	62.5 mM Tris-HCl (pH 6.8) 2% SDS 30% (w/v) glycerol 50 mM DTT 5 mM EDTA 0.02% NaN ₃	As supplied (Bio-Rad, 161-0374) Aliquot into 5-10 µL Store at -20 °C
Low molecular weight transfer buffer (5 L)	0.6% Trizma 0.3% Glycine 20% Methanol ddH ₂ O	30 g Trizma (Sigma, T1503-1KG) 15 g Glycine (Fisher Scientific, G/0800/60) 1 L Methanol (Fisher Scientific, M/4056/17) Add ddH ₂ O to 5L

		Stir 2-3 hours
High molecular weight transfer buffer (5 L)	0.6% Trizma 0.3% Glycine 20% Methanol 0.5% SDS ddH ₂ O	30 g Trizma (Sigma, T1503-1KG) 15 g Glycine (Fisher Scientific, G/0800/60) 1 L Methanol (Fisher Scientific, M/4056/17) 25 mL 20% SDS (Fisher Scientific, BP 1311-1) Add ddH ₂ O to 5L Stir 2-3 hours
Ponceau-S stain (500 mL)	0.1% Ponceau-S sodium salt 5% acetic acid	0.05 g Ponceau-S (Cayman Chemical Company, 14330) 25 mL acetic acid (Fisher, A/0360/PB15) Add ddH ₂ O to 500 mL
Simply Blue SafeStain	Coomassie dye	As supplied (Invitrogen, LC6060)
Milk blocking buffer (500 mL)	5% Skim milk powder 1% Tween-20 PBS ddH ₂ O	25 g Skim milk powder (Fluka Analytical, 70166-500G) 5 mL Tween-20 (NBS Biologicals, 17767-B) 50 mL 10X PBS (Fisher Scientific, BP399-4) Add ddH ₂ O to 500 mL Stir 5-15 minutes
Bovine serum albumin blocking buffer (200 mL)	2.5% BSA PBS 0.4% Triton X-100 ddH ₂ O	5 g BSA (Fisher Scientific, BP1600-100) 20 mL 10x PBS (Fisher Scientific, BP399-4)

		4 mL 20% Triton X-100 Add ddH ₂ O to 500 mL Stir 5-15 minutes
--	--	--

Table 2-21 Immunofluorescence buffers.

Buffer Stock	Composition	Recipe (source)
0.2% Triton X-100 buffer (200 mL)	0.2% Triton X-100 5% Fetal bovine serum PBS dH ₂ O	0.4 mL 100% Triton X-100 10 mL FBS (Sigma, F9665) 20 mL 10X PBS (Fisher Scientific, BP399-4) Add dH ₂ O to 200 mL
0.1% saponin buffer(1L)	Saponin powder from quillaja bark 5% Fetal bovine serum PBS dH ₂ O	1 g saponin (Sigma, S4521-2G) 50 mL FBS (Sigma, F9665) 100 mL 10X PBS (Fisher Scientific, BP399-4) Add dH ₂ O to 1L Filter through 0.22 µm sterile filter cup and stored at 4°C.
4% fixation solution (50 mL)	4% formaldehyde PBS dH ₂ O	20 mL 10% formaldehyde methanol-free UltraPure EM Grade (Polysciences Inc, 04018) 5 mL 10X PBS (Fisher Scientific, BP399-4) Add dH ₂ O to 50 mL
0.1 M quenching solution (50 mL)	0.1 M glycine PBS	0.375 g glycine (Fisher Scientific, G/0800/60)

	dH ₂ O	5 mL 10X PBS (Fisher Scientific, BP399-4) 45 mL ddH ₂ O
--	-------------------	---

Table 2-22 GFP-binding protein expression and purification buffers.

Buffer Stock	Composition	Recipe (source)
500 mL Buffer A	20 mM HEPES (pH 7.3) 100 mM NaCl	10 mL 1 M HEPES (Sigma, H0887) 10 mL 5 M NaCl (Fisher Scientific, S/3120/60) Add dH ₂ O to 500 mL
500 mL Lysis buffer	20 mM HEPES (pH 7.3) 500 mM NaCl 1 mM EDTA 20 mM imidazole	10 mL 1 M HEPES (Sigma, H0887) 50 mL 5 M NaCl (Fisher Scientific, S/3120/60) 1 mL 0.5M EDTA (Fisher Scientific, D/0700/53) 10 mL 1 M imidazole (BDH Laboratory supplies, 286874D) (Added just before use) Add dH ₂ O to 500 mL
500 mL Low salt buffer	20 mM HEPES (pH 7.3) 100 mM NaCl 0.1% Triton X-100 1 mM EDTA 30 mM imidazole	10 mL 1 M HEPES (Sigma, H0887) 10 mL 5 M NaCl (Fisher Scientific, S/3120/60) 2.5 mL 20% Triton X-100 1 mL 0.5M EDTA (Fisher Scientific, D/0700/53) 15 mL 1M imidazole (BDH Laboratory supplies, 286874D)

		(Added just before use) Add dH ₂ O to 500 mL
500 mL High salt buffer	20 mM HEPES (pH 7.3) 1M NaCl 0.1% Triton X-100 1 mM EDTA 30 mM imidazole	10 mL 1 M HEPES (Sigma, H0887) 100 mL 5 M NaCl (Fisher Scientific, S/3120/60) 2.5 mL 20% Triton X-100 1 mL 0.5 M EDTA (Fisher Scientific, D/0700/53) 15 mL 1M imidazole (BDH Laboratory supplies, 286874D) (Added just before use) Add dH ₂ O to 500 mL

Table 2-23 Mass spectrometry analysis buffers.

Buffer Stock	Composition	Recipe (source)
0.5 mL elution buffer	50 mM TCEP 50 mM iodoacetamide NuPAGE LDS Sample Buffer (4X)	50 µL 0.5M TCEP (Sigma 646547-10X1ML) 4.624 mg iodoacetamide (Sigma GERPN6302) 450 µL Sample Buffer (4X) (NP0008)
Methanol/Acetic acid destaining solution (500 mL)	50% dH ₂ O 40% Methanol 10% Acetic acid	250 mL dH ₂ O 200 mL Methanol HiPerSolv CHROMANORM for HPLC (VWR Chemicals, 152506X) 50 mL Acetic acid 99% Hipersolv

		CHROMANORM (VWR Chemicals, 84874.260)
Ammonium bicarbonate/Acetonitrile destaining solution (50 mL)	50 mM Ammonium bicarbonate 50% Acetonitrile 50% dH ₂ O	0.19 g Ammonium bicarbonate (Sigma , 09830-500G) 25 mL Acetonitrile isocratic grade HiPerSolv CHROMANORM for HPLC(VWR Chemicals, 20048.420) 25 mL dH ₂ O
Hydroxylamine hydrochloride/N-ethylmaleimide solution (10 mL)	1 M Hydroxylamine-HCl 50 mM N-ethylmaleimide 4 N NaOH dH ₂ O	1.389 g Hydroxylamine-HCl (Sigma , 159417-100G) 0.062 g N-ethylmaleimide (Sigma , E3876-5G) 4 mL dH ₂ O 4.5 mL 4 N NaOH (Thermo Scientific, S/4920/60)
200 µL Trypsin digest solution	0.5 µg trypsin/sample 50 mM ammonium bicarbonate solution	Add 200 µL HPLC grade water to 100 µg Trypsin-ultra (NEW ENGLAND BioLabs, P8101S). Take 1 µL and mix with 10 µL Ammonium bicarbonate solution

Table 2-24 PEG Switch buffer.

Buffer Stock	Composition	Recipe (source)
5 mL Lysis buffer	2.5% SDS	0.625 mL 20% SDS

	100 mM Hepes 1 mM EDTA 100 mM maleimide dH ₂ O	(Fisher Scientific, BP 1311-1) 0.5 mL 1M Hepes (Sigma, H0887) 10 µL 0.5 M EDTA (Fisher Scientific, D/0700/53) 0.5 g maleimide (Sigma , 129585-2G) Add dH ₂ O to 5 mL. pH 7.4
5 mL Resolubilisation buffer	1% SDS 100 mM Hepes 1 mM EDTA 100 mM maleimide dH ₂ O	0.25 mL 20% SDS (Fisher Scientific, BP 1311-1) 0.5 mL 1M Hepes (Sigma, H0887) 10 µL 0.5 M EDTA (Fisher Scientific, D/0700/53) 0.5 g maleimide (Sigma , 129585-2G) Add dH ₂ O to 5 mL. pH 7.4
5 mL PEG/ Hydroxylamine-HCl	4 mM Methoxypolyethylene glycol maleimide (PEG) 400 mM hydroxylamine-HCl dH ₂ O	0.1 g Methoxypolyethylene glycol maleimide (Sigma, 63187-1G) 0.14 g hydroxylamine-HCl (Sigma , 159417-100G) Add dH ₂ O to 5 mL. pH 7.4
PEG/Tris	4 mM PEG	0.1 g PEG (Sigma,

	400 mM Tris dH ₂ O	63187-1G) 2 mL 1 M Tris (Sigma, T1503-1KG) Add dH ₂ O to 5 mL. pH 7.4
--	----------------------------------	--

Table 2-25 Palmitate labelling coupled to click chemistry buffers.

Reagent	Composition	Recipe (Source)
100 mL 1% Fatty-acid free BSA	1% Fatty-acid free BSA DMEM	1g fatty-acid free BSA (Sigma, A7030) 100 mL DMEM (gibco life technologies, 31966-047)
100 mL 4 mM IR800 Palmitic acid-azide dye	Palmitic acid-azide DMSO	0.12 g palmitic acid-azide (synthesised by Professor Nicholas C. O. Tomkinson and Dr Kevin R. Munro, Department of Pure and Applied Chemistry, University of Strathclyde, Glasgow, UK). 100 mL DMSO (Sigma, D2650-100 mL) Store at -20 °C
1 mL IRDye 800CW Alkyne Infrared Dye	Lyophilised alkyne ddH ₂ O	0.5 mg lyophilised alkyne (LICOR Bioscience, 929-60002) 1 mL ddH ₂ O Mix and store in dark at -20 °C
500 mL 40 mM CuSO ₄	Powdered copper sulphate pentahydrate	3.2 g copper sulphate (Sigma, 451657)

	ddH ₂ O	Add dH ₂ O to 500 mL and store at RT
10 mL 100 mM TBTA	Powdered Tris [(1-benzyl-1H-1,2,3-triazol-4-yl)methyl]amine DMSO	0.53 g Tris [(1-benzyl-1H-1,2,3-triazol-4-yl)methyl]amine (Sigma, 678937-50MG) Dissolve in 10 mL DMSO and store at -20 °C
1 mL 40 mM Ascorbic acid	Crystalline powdered L-(+)-Ascorbic acid ddH ₂ O	0.007 g L-(+)-Ascorbic acid (Alfa Aesar, A15613) 1 mL ddH ₂ O Prepared fresh

Table 2-26 Chemical inhibitors.

Name	Function	Source	Working concentration
MG132	Inhibits proteasomal degradation	(Cayman Chemical, USA) Cat No. 10012628	5 µM
2-bromopalmitate	Inhibits palmitoylation	(Sigma, USA) Cat No. 238422-10G	100 µM
Cycloheximide	Inhibits newly synthesised proteins	(Sigma, USA) Cat No. C-7698	100 µg/mL

The 8-80 amino acid of STX19 and the full-length protein of SNAP29 (that is 1-258 aa) were respectively cloned into PGEX-KG vector. The GST-fused STX19 and SNAP29 plasmids were transformed individually into BL21-gold (DE3) pLysS competent cells as explained before in section (2.5.1). The bacterial lysates generated from the GST-fused proteins were lysed and coupled onto Glutathione cellulose beads, eluted and then dialysed using ice-cold PBS in Por

tubing with a molecular weight cut-off (MWCO) of 6-8 kDa to remove unwanted protein contaminants. The Bio-Rad protein assay as explained before in section (2.5.2) was used to determine the concentration of the GST-fused purified proteins. To determine the correct size of the proteins, the proteins were run on an SDS-PAGE gel and their bands examined accordingly. The purified GST-fused proteins were aliquoted and sent to Proteintech (Manchester, United Kingdom) for mass production of appropriate rabbit polyclonal antibodies against our protein. Antibodies generated were aliquoted into 1.5 mL Eppendorf tubes in 0.5 mL fractions and mixed thoroughly with an equal volume of glycerol. The antibodies were stored at -80 °C for long-term storage and -20 °C for short-term storage. The SNAP29 rabbit polyclonal antibody generated works well for both immunofluorescence and Western blotting, however, the STX19 rabbit polyclonal antibody works well for only immunofluorescence. Notwithstanding the STX19 antibody can detect blot for overexpressed recombinant STX19

3 Chapter Where is STX19 localised in mammalian cells?

3.1 Introduction

SNAREs and RABs play a key role in membrane tethering and fusion (Gurkan et al., 2005). SNAREs are localised to every membrane of the biosynthetic and endocytic pathways (Jahn and Scheller, 2006, Kloepper et al., 2007). During membrane fusion, the SNAREs on opposing membranes come together and zipper up to form a four helical complex. This is thought to generate the force needed to pull the membranes together and promote fusion. Qa-SNAREs such as STX11 or STX19 and R-SNARE such as VAMP3 or VAMP8 contribute one SNARE motif; whereas SNAP29 or SNAP25 contribute two motifs by virtue of them have two SNARE motifs each.

The Tang lab was the first to clone and characterise Syntaxin 9 (Wang et al., 2006). Following the reclassification of SNAREs, STX9 was renamed STX19 (Kloepper et al., 2007). Overexpressed MYC-tagged STX19 was found to be localised to the PM and punctate vesicles in HeLa and MDCK (Wang et al., 2006). The antibody they generated against STX19 was unable to detect endogenous STX19 so its intracellular distribution is unknown. This chapter addresses the intracellular distribution of STX19 and its role in post-Golgi trafficking. My research has shown that a pool of STX19 is localised to the Golgi and tubular recycling endosomes. Depletion of STX19 causes the loss of recruitment of tubular recycling endosomal markers and perturbs the integrity of the Golgi morphology. My results suggest that STX19 plays an important role in the fusion of vesicles emanating from the perinuclear region with the PM.

In this chapter I have:

1. Determined the intracellular distribution of STX19 in a panel of different cell types.
2. Determined the intracellular distribution of overexpressed STX19.
3. Performed a colocalisation studies on STX19 with a variety of endocytic and biosynthetic markers.

4. Used RNAi to examine the role of STX19 in endocytic and biosynthetic transport.

3.2 Results

3.2.1 Endogenous STX19 is localised to tubules and vesicles

To gain insight into the intracellular localisation of STX19 a panel of cell lines were stained for endogenous STX19. The cells were selected in part because they have high levels of STX19 mRNA based on Nextbio Illumina data (Kupersmidt et al., 2010). An affinity-purified rabbit polyclonal antibody raised against the cytoplasmic domain of STX19 was used for the localisation studies. I observed that the antibody labelled several membranous structures including tubules, vesicles, Golgi and the plasma membrane (Figure 3-1). The tubular staining was mostly evident in HeLaM, BXPC3, Ht29 and to a less extent in A431 cells (Figure 3-1). In confluent CACO-2 cells, I also observed that endogenous STX19 is enriched in the basolateral plasma membrane (Figure 3-1). In some cells, large punctate structures are observed in the cytoplasm (Figure 3-1). At present, it is unclear what these structures are. To determine if this STX19 staining was specific I used RNAi to deplete STX19 in HeLaM cells. In the depleted cells the STX19's tubular, vesicle and Golgi staining were lost (Figure 3-8). This indicates that the tubular, vesicular and Golgi staining is specific.

3.2.2 Overexpressed STX19 localises to similar cellular compartment as endogenous STX19

To validate the STX19 immunostaining, I overexpressed a variety of tagged STX19 constructs in HeLaM cells (GFP-STX19, GFPSTX19t, mCherry-STX19t (t denotes tail- which is the STX19 275-294 amino acid sequence), HA-STX19 and STX19-HA). All of the STX19 constructs showed a similar localisation to endogenous STX19 and were found on tubules, vesicles, Golgi and the PM (Figure 3-2). This data suggests that tagged STX19 traffics in a similar way as the untagged protein. However, all of the tagged constructs gave significant plasma membrane staining. This may in part be caused by overexpression of the tagged protein. These data strongly suggest that our STX19 antibody staining is specific.

3.2.3 STX19 colocalises with the tubular recycling endosomal markers RAB8 and MICAL-L1

MICAL-L1 and RAB8 have been studied extensively and have been shown to localise to the tubular recycling endosomes (Sharma et al., 2009, Giridharan et al., 2013, Rahajeng et al., 2012). I have confirmed the staining patterns of MICAL-L1 and RAB8 in HeLaM cells. HeLaM cells were stained against STX19, SNAP29, RAB8 and MICAL-L1. SNAP29, RAB8 and MICAL-L1 were all localised to tubular structures reminiscent of that seen with endogenous STX19 staining (Figure 3-4). The tubular staining in RAB8 and MICAL-L1 were longer than those seen with SNAP29 (Figure 3-4). To determine whether STX19 tubular staining colocalises with MICAL-L1 and RAB8, I have performed colocalisation studies using both endogenous STX19 and overexpressed STX19. HeLaM cells were stained with both endogenous STX19 and endogenous MICAL-L1. Both STX19 and MICAL-L1 stained tubules (Figure 3-5). Endogenous STX19 colocalises with endogenous MICAL-L1 at the perinuclear Golgi area and on the tubular recycling endosomes (Figure 3-5). I have also transfected HeLaM cells with GFPSTX19 and co-stained the cells for endogenous RAB8. Both the overexpressed STX19 and endogenous RAB8 were found localised to the tubular recycling endosomes and the perinuclear Golgi area (Figure 3-5). Overall, my studies show that there is a pool of STX19 that colocalises with RAB8 and MICAL-L1 on the TRE.

3.2.4 STX19 colocalises with GPI-anchored proteins on TRE

MICAL-L1 and RAB8 are involved in the recycling of TF-R, integrin β 1 (CD29), GPI-anchored proteins (CD55, CD59) and EGFR (Sharma et al., 2008, Giridharan et al., 2013, Xie et al., 2015). I hypothesise that since STX19 also colocalises with MICAL-L1 decorated tubules, internalised CD55, CD59 and CD29 might also colocalise with STX19. To confirm this, I performed antibody uptake assay. HeLaM cells were pulsed for 1 h with CD55, CD59 and CD29 and then stained endogenously for STX19. After 1 h uptake, the internalised CD55 and CD59 were seen on the tubules and have reached the perinuclear Golgi region (Figure 3-6). Both CD55 and CD59 colocalise with STX19 on the tubules and the perinuclear Golgi region (Figure 3-6). However, CD29 upon

internalisation were found on punctate vesicles (Figure 3-6) most likely Rab11 recycling endosomes (Powelka et al., 2004, Bridgewater et al., 2012). My data does not show any convincing colocalisation between CD29 and STX19 (Figure 3-6). The colocalisation between CD55, CD59 and STX19 suggests that STX19 might also be required for the trafficking of GPI-anchored proteins.

3.2.5 STX19 colocalises with proteins involved in cell migration

MICAL-L1 and Rab8 have been shown to have a role in regulating integrin trafficking and cell migration (Sharma et al., 2009, Reinecke et al., 2014b). To elucidate whether STX19 also may have a role in this process, I have determined whether transfected STX19 colocalises with this machinery. HRAS, RAC1 and CDC42 are all small GTPases that have been shown to be required for regulating cell migration (Hood and Cheresch, 2002). HeLaM cells were cotransfected with mCherrySTX19t together with GFP HRAS, GFP RAC1, or GFP CDC42. From the cotransfection experiments, STX19 colocalises with HRAS, RAC1 and CDC42 on the tubules, Golgi and the PM (Figure 3-7). STX19 colocalisation with these proteins suggests that STX19 might be involved in the trafficking of materials that are required for cell migration. A pool of STX19 is localised to microdomains in tubular recycling tubules

To obtain a more detailed understanding of STX19 localisation, I have used super-resolution imaging. I used Stochastic Optical Reconstitution Microscopy (STORM) and Structured Illumination Microscopy (SIM). Using the STORM and SIM, I observed that STX19 is localised to puncta or microdomains on the tubular recycling endosomes (Figure 3-3). Using conventional wide field microscopy endogenous STX19 shows continuous staining along the tubular recycling endosomes (Figure 3-3). The vesicles spanned from the perinuclear region to the plasma membrane (Figure 3-3).

3.2.6 Investigating the function of STX19 using RNAi

To gain insight into the role of STX19 in endocytic trafficking I have used RNAi to deplete STX19. An RT-PCR validated Smartpool targeting STX19 (Gordon et al., 2010) was used and the siRNA tested individually (Oligo 9, 10, 11 and 12) or in combination. The effectiveness of the siRNA was monitored by immunofluorescence microscopy. Using a double transfection strategy, it was

observed that the Smartpool efficiently depleted STX19. siRNAs 10 and 12 reduced endogenous STX19 staining (Figure 3-8). However, siRNA 11 had no effect on STX19 staining (Figure 3-8). Surprisingly, I observed that siRNA 9 upregulates STX19 levels (Figure 3-8). With siRNA 10, it was observed that the cell morphology significantly changed with the cells becoming larger, more spread out and polarised with several protruding edges (Figure 3-8). With siRNA 12, the cells became more slender and there was a significant reduction in cell number possibly suggesting non-specific toxicity (Figure 3-8). So we decided to use siRNA 10 for subsequent experiments.

3.2.7 STX19 depletion affects endosomal markers and endocytic cargoes

I have shown that STX19 colocalises with MICAL-L1 and RAB8 on tubular recycling endosomes (Figure 3-5). We hypothesised that STX19 depletion might affect the localisation of MICAL-L1 and RAB8. I found that in STX19 depleted cells there was a dramatic reduction in the amount of MICAL-L1 and RAB8 tubular staining (Figure 3-9). There was also a reduction in SNAP29 tubular staining (Figure 3-9). However, PACSIN2 was still localised to the tubular recycling endosomes suggesting that this compartment was still present (Figure 3-9). I also stained for both early (RAB5 and EEA1) and late (CD63) endosomal markers. In the control cells, RAB5 stained punctate structures characteristic of the early endosomes (Figure 3-9). Some of the cells also stained tubular structures perhaps tubular recycling endosomes emanating from the sorting endosomes (Figure 3-9) (Huotari and Helenius, 2011, Galvez et al., 2012, Xie et al., 2015). There was no gross change in RAB5 localisation in the STX19 depleted cells except for the fact that the staining became more spaced out perhaps as a result of the cells being larger (Figure 3-9). A similar phenotype was also observed for EEA1 (Figure 3-10). In some cells there also appeared to be a reduction in the number of RAB5 tubules (Figure 3-9). I also looked at the steady-state localisation of CD63 (a late endosomal marker). In the STX19 depleted cells there was an accumulation of CD63 signal in small punctate vesicles dispersed through the cytoplasm (Figure 3-10). This suggests that STX19 may perturb the trafficking endocytic cargoes. To investigate this further, I have looked at the effect of cargoes that trafficked through the endosomal

compartments by staining for GLUT1 and TF-R. GLUT1 has been shown to be a retromer-dependent cargo that cycles between the PM and endosomes (Steinberg et al., 2013, Hesketh et al., 2014). In the control cells, GLUT1 was localised to the PM and perinuclear recycling endosomes (Figure 3-10). However, in the STX19 depleted cells GLUT1 is lost from the plasma membrane and accumulate in the perinuclear region suggesting an impairment in GLUT1 recycling (Figure 3-10). Also, I looked at the steady-state localisation of TF-R which is internalised via clathrin-mediated endocytosis and then recycled through the endosomal compartment and the endocytic recycling compartment to the PM (Grant and Donaldson, 2009, Maxfield and McGraw, 2004). In the control cells the TF-R was found predominantly in perinuclear recycling endosomes and endosomal tubules (Figure 3-10). However, in the STX19 depleted cells the TF-R was found in small puncta dispersed through the cytoplasm and in long tubular structures (Figure 3-10). This data suggests that STX19 depletion might impair TF-R recycling. Overall, my data suggests that STX19 is required for the correct trafficking of a wide variety of endocytic cargoes. However, care must be taken when interpreting these observations as we need to show that the observed phenotypes are not off target.

3.2.8 STX19 depletion affects the localisation of post-Golgi VAMPs

A previous study in our lab showed that STX19 can form SNARE complexes with SNAP29, SNAP23, SNAP25, VAMPs 3 and 8 (Gordon et al., 2010). I have also confirmed this interaction in both Bio-ID and GFPTrap IP experiments (sections 5.2.3; 5.2.5). I have observed that STX19 depletion reduces SNAP29 tubular membrane localisation (Figure 3-9) so I have also investigated whether STX19 depletion alters the localisation of VAMPs (3, 4, and 8). In control cells VAMPs 3 and 4 are localised to the TGN and endosomes; and VAMP8 is localised to perinuclear endosomes. In the depleted cells VAMP4 staining was significantly reduced and VAMP8 was redistributed to punctuate vesicles scattered through the cytoplasm (Figure 3-11). These results suggest that STX19 may be required for the correct recycling of VAMPs 4 and 8. The observed phenotypes are consistent with STX19 have a general role in endocytic recycling.

3.2.9 STX19 depletion alters the steady-state localisation of proteins which cycle between the Golgi and endosomes

A pool of STX19 is localised to the Golgi region (Figure 3-1; Figure 3-2). We, therefore, investigated the effect of STX19 depletion on Golgi morphology by staining for GM130 and P230 (Munro and Nichols, 1999, Nakamura et al., 1995). In control cells, GM130 and P230 all gave reticular staining with a compact morphology (Figure 3-12). In the STX19 depleted cells; the Golgi was less compact and more spread out (Figure 3-12). However, the overall integrity of the Golgi looked intact.

I next examined whether the localisation of proteins which traffick between the TGN and endosomes was affected (TGN46, CD-MPR and CI-MPR (Duncan and Kornfeld, 1988, Ghosh et al., 2003). In the control cells, CI-MPR and CD-MPR were mostly localised to a perinuclear region, however, in the depleted cells both CI-MPR and CD-MPR appeared more dispersed (Figure 3-12). This suggests that STX19 may be required for the correct trafficking of CI-MPR and CD-MPR. This is consistent with a previous genome-wide RNAi screen that identified STX19 as having a role in endosome-to-Golgi retrieval (Breusegem and Seaman, 2014). Interestingly, TGN46 staining appeared to be unaffected suggesting that STX19 is not involved in its trafficking.

3.2.10 STX19 depletion affects focal adhesion dynamics

In STX19 depleted cells, we observed that the cells became larger and had multiple membrane lamellipodia (Figure 3-8). To gain insight into these phenotypes, we looked at the effect of STX19 depletion on the localisation of integrins and vinculin. Integrins play a crucial role in cell adhesion and migration by connecting the extracellular matrix to the actin cytoskeleton via recruiting proteins including; paxillin, talin and vinculin (Hood and Cheresh, 2002, Humphries et al., 2007, Bridgewater et al., 2012, Geiger et al., 2009). I observed that in the STX19 depleted cells the adhesive structures formed by vinculin became larger compared to control cells (Figure 3-13). The vinculin focal adhesive structures were mostly found in the protruding edges (lamellipodia) of the STX19 depleted cells. I also looked at the trafficking of integrin $\beta 1$, $\alpha 2$, $\alpha 3$ and $\alpha 5$. Integrins exist as heterodimers; integrin $\beta 1$ can form

a dimer with integrin $\alpha 2$, $\alpha 3$ and $\alpha 5$ (Hood and Cheresch, 2002, Hynes, 2002). HeLaM cells were allowed to internalise integrin $\beta 1$, $\alpha 2$, $\alpha 3$ and $\alpha 5$ for 1 hour and then chased for 30 minutes. In the control cells, integrin $\beta 1$ and $\alpha 5$ were found localised to adhesive structures on the cell surface, whereas integrin $\alpha 2$ and $\alpha 3$ were localised to punctate structures most likely Rab11 recycling endosomes (Bridgewater et al., 2012) (Figure 3-13). In the STX19 depleted cells there is a dramatic increase in the observed signal for all the integrin subunits examined. At present it is unclear whether this simply reflects increased integrin recycling or an overall upregulation of the subunits. In the depleted cells $\alpha 2$, $\alpha 3$ and $\alpha 5$ accumulated in large punctate structures. There is also an accumulation of $\beta 1$, $\alpha 2$ and $\alpha 5$ in tubular structures (Figure 3-13). Overall, my data suggests that STX19 may be playing an important role in regulating integrin trafficking.

3.3 Discussion

3.3.1 Summary of results

My results show that endogenous STX19 is predominantly localised to tubular recycling endosomes and the Golgi region in HeLaM cells. A pool of STX19 colocalises with MICAL-L1, RAB8 and endocytosed GPI-anchored proteins (CD55 and CD59). STX19 also colocalises with machinery required for cell motility and polarisation such as HRAS, CDC42 and RAC1. Depletion of STX19 interferes with the recruitment of endocytic machinery (MICAL-L1, SNAP29 and Rab8) and alters the trafficking of endocytic cargoes (such as integrins, GLUT1 and transferrin). Thus, STX19 may play a role in cell migration by regulating the trafficking of integrins and the machinery involved in their sorting. My data suggests that STX19 has a multifunctional role in post-Golgi trafficking.

3.3.2 The cellular localisation pattern of STX19

The cellular distribution pattern of STX19 has been poorly characterised. This is partly due to lack of appropriate antibodies. To overcome this our lab has generated a rabbit polyclonal antibody to STX19 which I have used for immunolocalisation studies. I have stained a panel of different cells to examine STX19 cellular localisation. My immunolocalisation studies show that STX19 is localised at the Golgi region and long branched tubules (Figure 3-1). In HeLaM and BXPC3 cells these tubules could be observed to span the whole length of

the cell (Figure 3-1). The STX19 positive tubules predominantly emanate from the perinuclear region of the cell (Figure 3-1; Figure 3-3). These tubules colocalises with endocytic tubular recycling markers such as MICAL-L1 and RAB8 (Figure 3-5) and endocytosed CD55 and CD59 (Figure 3-6). However, we saw very limited colocalisation with CD29 (Figure 3-6) or the transferrin receptor (data not shown). This colocalisation data suggests that STX19 may be playing a role in the fusion of tubular recycling endosomes with the PM or be involved in the fusion of vesicles within TRE.

At present, it is unclear why we are unable to detect plasma membrane staining for endogenous STX19 in some cell types. It is possible that STX19's expression level is too low or these cells are missing factors required for retaining STX19 at the PM. In polarised CACO-2 cells; we could observe plasma membrane staining of STX19 which colocalises with beta-catenin (data not shown). Previous studies using immunohistochemistry analysis from mouse skin tissue shows that STX19 colocalises with ZO-1 at tight junctions (Wang et al., 2006).

We have also used SIM and STORM super-resolution microscopy to dissect the true nature of STX19 tubular staining. I observed that the STX19 staining is not continuous but is localised to puncta on these tubules (Figure 3-3). At present, it is unclear whether these puncta are microdomains or are tethered vesicles as proposed by (Xie et al., 2015). This question can only be properly addressed using electron microscopy. These pilot experiments suggest that two colour SIM may be useful for studying the recruitment of endocytic machinery to these structures.

3.3.3 Depletion of STX19 interferes with the endocytic pathway

A pool of STX19 colocalises with MICAL-L1 and RAB8 on TRE suggesting that STX19 may have a role in endocytic trafficking (Figure 3-5). In STX19 depleted cells MICAL-L1 and RAB8 are lost from TRE but not PACSIN2 (Figure 3-9). This data suggests that STX19 may play a role in the recruitment of MICAL-L1 and RAB8 onto TRE. This phenotype is specific as the localisation of the early endosomal markers RAB5 and EEA1 are not affected. However, it is unclear whether STX19 and MICAL-L1/Rab8 directly interact with each other.

MICAL-L1 and RAB8 have been shown to be involved in regulating endocytic recycling (Sharma et al., 2009, Cai et al., 2012) so we looked at the steady-state localisation of a series of endocytic cargo. We observed that loss of STX19 caused dramatic changes in the steady-state localisation of GLUT1, transferrin receptor, and integrins. We also observed changes in the localisation of CD and CI-MPR two proteins which traffic through the endocytic system. In most cases, the perinuclear pool of these markers is lost suggesting a general defect in recycling. We also observed significant changes in the levels of the late endosomal marker CD63 in the depleted cells. It is likely that some of the observed phenotypes are indirect and reflect global changes in endocytic trafficking. However, my data suggests that STX19 is playing an important role in the endocytic pathway. My data does not allow me to determine whether STX19 is functioning at the plasma membrane, Golgi or TRE.

3.3.4 STX19 may play a role in cell migration by regulating the trafficking of integrins

STX19 depleted cells become larger and more polarised suggesting that STX19 may be playing a role in cell adhesion and migration. To examine this, I have looked at the trafficking of integrins and the machinery involved in forming focal adhesions. Depletion of STX19 severely perturbed integrin β 1, α 2, α 3 and α 5 trafficking and vinculin focal adhesive structures became larger compared to control cells (Figure 3-13). It is unclear how depletion of STX19 is causing these phenotypes. Is STX19 directly involved in the fusion of integrins with the plasma membrane or does it have a role in trafficking proteins which regulate integrin function? Excitingly, my studies have shown that STX19 colocalises with a variety of small GTP-binding proteins including CDC42, RAC1, HRAS and RAB8 (Figure 3-5; Figure 3-7). RAC1 and CDC42 are involved in the formation of lamellipodia and filopodia respectively and are required for cell migration (Sadok and Marshall, 2014). HRAS is involved in the exocytic delivery of vesicles to the PM (Goodwin et al., 2005). HRAS, RAC and CD42 also play a role in regulating integrin affinity for the extracellular matrix and integrin avidity (integrin clustering) (Hood and Cheresh, 2002). The proper regulation of these proteins is required for cell migration (Hood and Cheresh, 2002). Thus, it is

possible that depletion of STX19 may be altering the function of CDC42, RAC1, HRAS and RAB8. It will be interesting to determine whether CDC42, RAC1, HRAS and RAB8 also regulate STX19 trafficking.

3.3.5 Depletion of STX19 alters the morphology of the biosynthetic pathway and changes the levels of key factors which function on this pathway

Previously, our lab identified that the depletion of STX19 reduces the delivery of biosynthetic cargo to the plasma membrane (Gordon et al., 2010). However, its role in post-Golgi trafficking was not examined in great detail. In order to examine this further, I depleted STX19 and stained the cells with various markers of the biosynthetic pathway. In cells depleted for STX19, I observed that the Golgi and TGN had become elongated and more spread out (Figure 3-12). Suggesting, that STX19 might be required for the maintenance of the correct morphology of the Golgi. However, this phenotype may simply reflect the fact that the cells have become larger and more spread out. I also observed that proteins such as CD-MPR and CI-MPR became more dispersed and less concentrated in the perinuclear/Golgi region. This data is consistent with (Breusegem and Seaman, 2014) studies. Thus STX19 may have a role in the fusion of endosomal material with the TGN.

I have also determined if STX19 is involved in VAMP trafficking. STX19 directly interacts with VAMPs 3 and 8. These VAMPs are enriched on secretory carriers and also mediates fusion of endosomal compartments (Jahn and Scheller, 2006, Hong and Lev, 2014). STX19 depletion causes the dispersion of VAMPs 3 and 8 and loss of VAMP4 staining from the TGN (Figure 3-11). The change in VAMP8 staining is very dramatic with a significant proportion of VAMP8 accumulating in peripheral structures. This phenotype is similar to what is seen with other endocytic proteins suggesting that loss of STX19 is perturbing endocytic recycling. I have also examined machinery involved in vesicle tethering at the plasma membrane in STX19 depleted cells. RAB8 has been shown to be required for the docking and fusion of secretory vesicles via its interaction with MICAL3 and ELKS (A RAB6-cortical interacting factor).

Depletion of STX19 causes a dramatic reduction of RAB8 (Figure 3-9). Thus the docking of secretory vesicles may be perturbed. This data suggests that it is possible that STX19 is not directly involved in secretion but is indirectly altering the levels of machinery which function on this pathway.

3.3.6 Future experiments

A major caveat of this study is that I have not repeated the RNAi experiments using alternate siRNA or rescued the phenotypes. This is extremely important as it is well known that siRNA can cause off-target phenotypes (Jackson and Linsley, 2010, Fedorov et al., 2006, Qiu et al., 2005). To address this issue, I have generated several siRNA-resistant STX19 expression constructs with differing expression levels. In the future, I plan to use them transiently or to generate stable cell lines. If this approach does not work it may be useful to use an alternative approach such as CRISPR-CAS9 to knock out STX19. It will also be important to quantify these phenotypes and repeat the RNAi in a more physiologically relevant cell line such as CACO-2 cells.

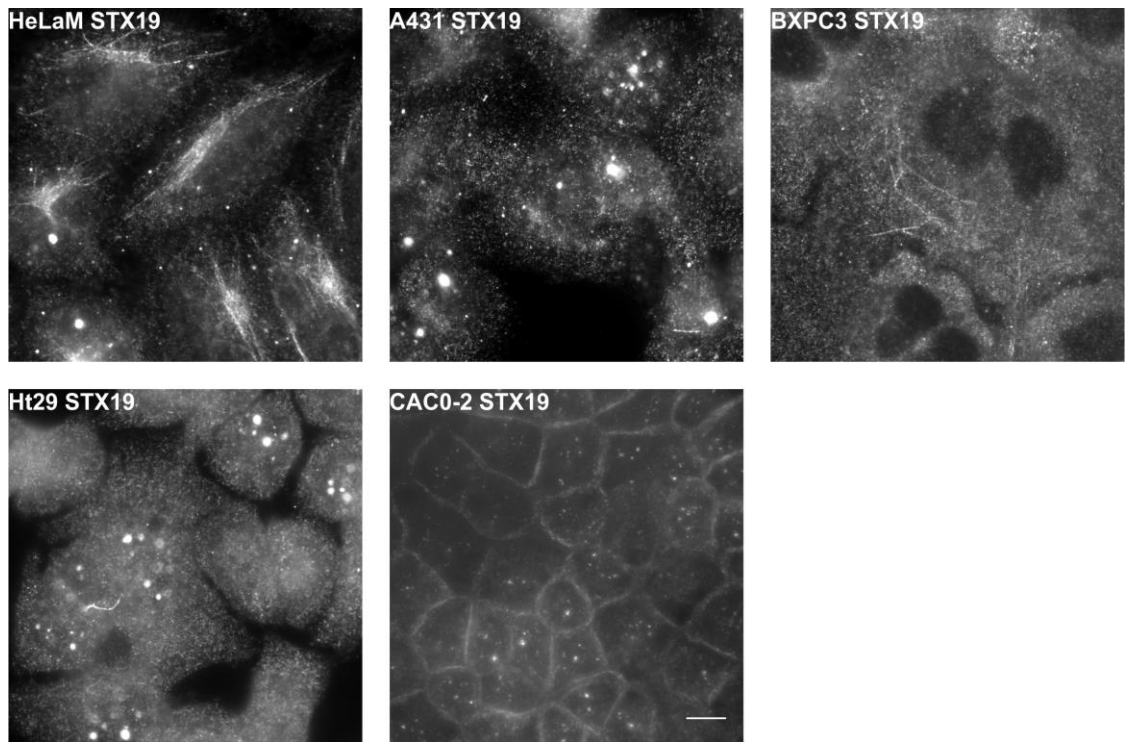


Figure 3-1 A pool of endogenous STX19 is localised to long branched tubular structures.

Different cells types were grown on coverslips. CACO-2 cells were grown on Transwell membrane filters for 16 days. All cells were fixed in 4% PFA, except CACO-2 which was fixed in -20 °C prechilled methanol. The cells were washed, permeabilized with 0.1% saponin and stained with anti-STX19 followed by donkey anti-rabbit 488 nm. Images were obtained from wide field microscope at x60 oil immersion. Scale bar = 10 μ m.

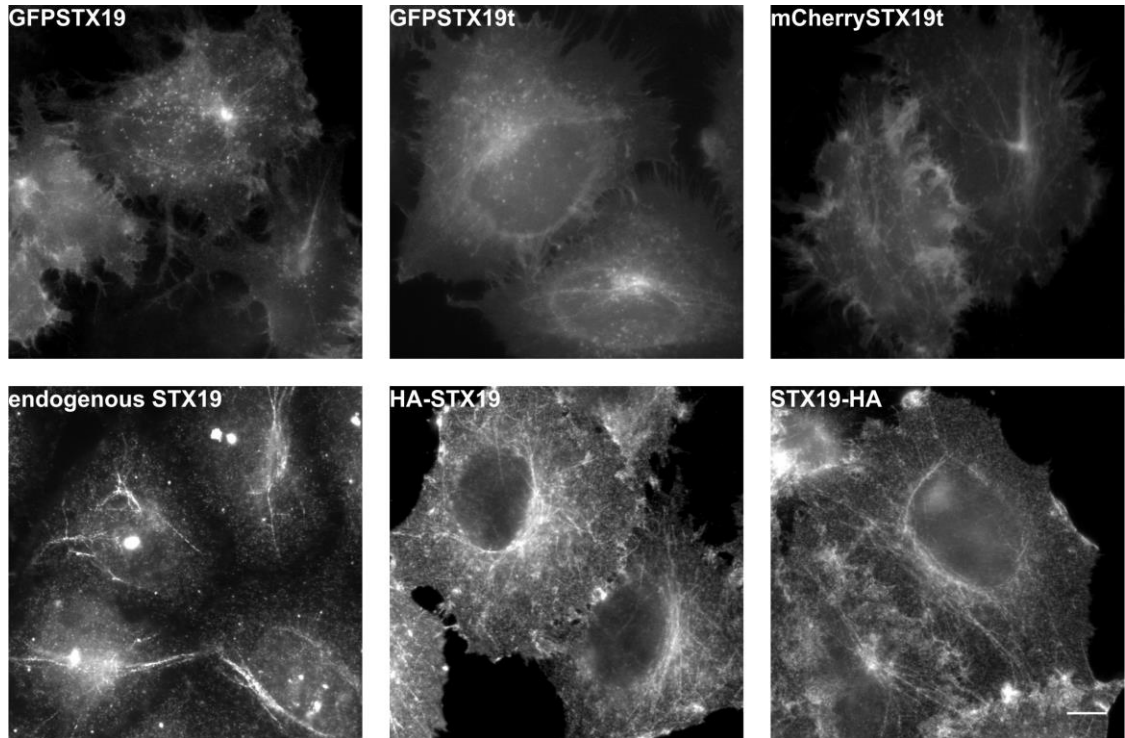


Figure 3-2 Transfected STX19 is localised to long tubular structures and the plasma membrane.

HeLaM cells were grown overnight on coverslips and then transfected with either with GFPSTX19, GFPSTX19t or mCherrySTX19t. 24 h post transfection, the cells were fixed, washed, permeabilized with 0.1% saponin and stained with anti-HA (only for the HA-STX19 and STX19-HA), followed by goat anti-mouse 594 nm. Untransfected cells were stained against STX19 followed by donkey anti-rabbit 488 nm. Images were obtained from wide field microscope at x60 oil immersion. Scale bar = 10 μ m.

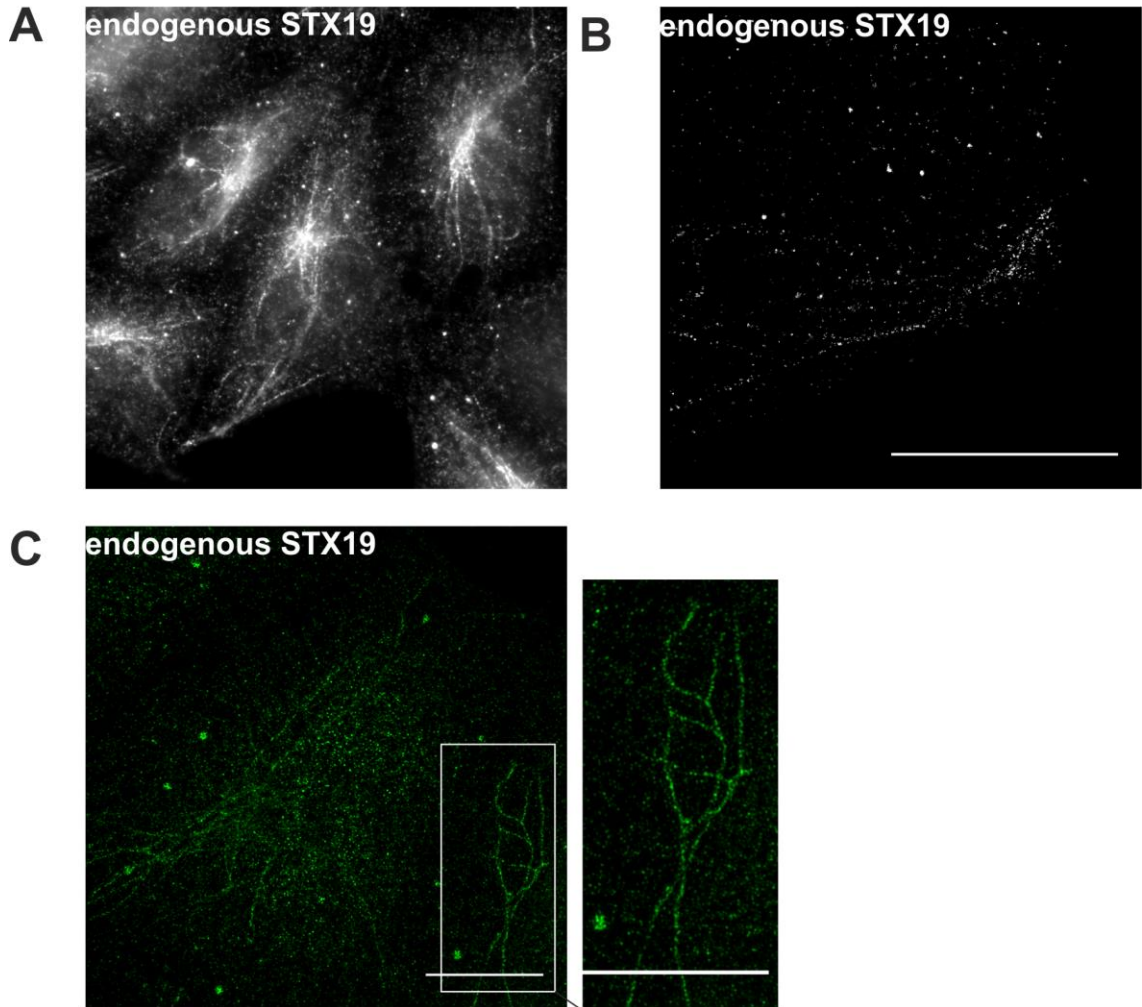


Figure 3-3 STX19 is localised to punctate structures on TREs.

HeLaM cells were grown on coverslips. The cells were fixed, washed, permeabilized with 0.1% saponin and stained with anti-STX19 followed by donkey anti-rabbit Alexa 488 nm. The cells were mounted with ProLong Gold antifade reagent with DAPI and then observed using **(A)** Wide field microscopy **(C)** OMX. **(B)** The cells were stained with anti-STX19 followed by anti-rabbit Alexa 647 nm and mounted with a buffer containing 100 mM β -mercaptoethylamine, with 0.5 mg/mL glucose oxidase and 0.04 mg/mL catalase. The image was taken using the STORM. Scale bar = 10 μ m.

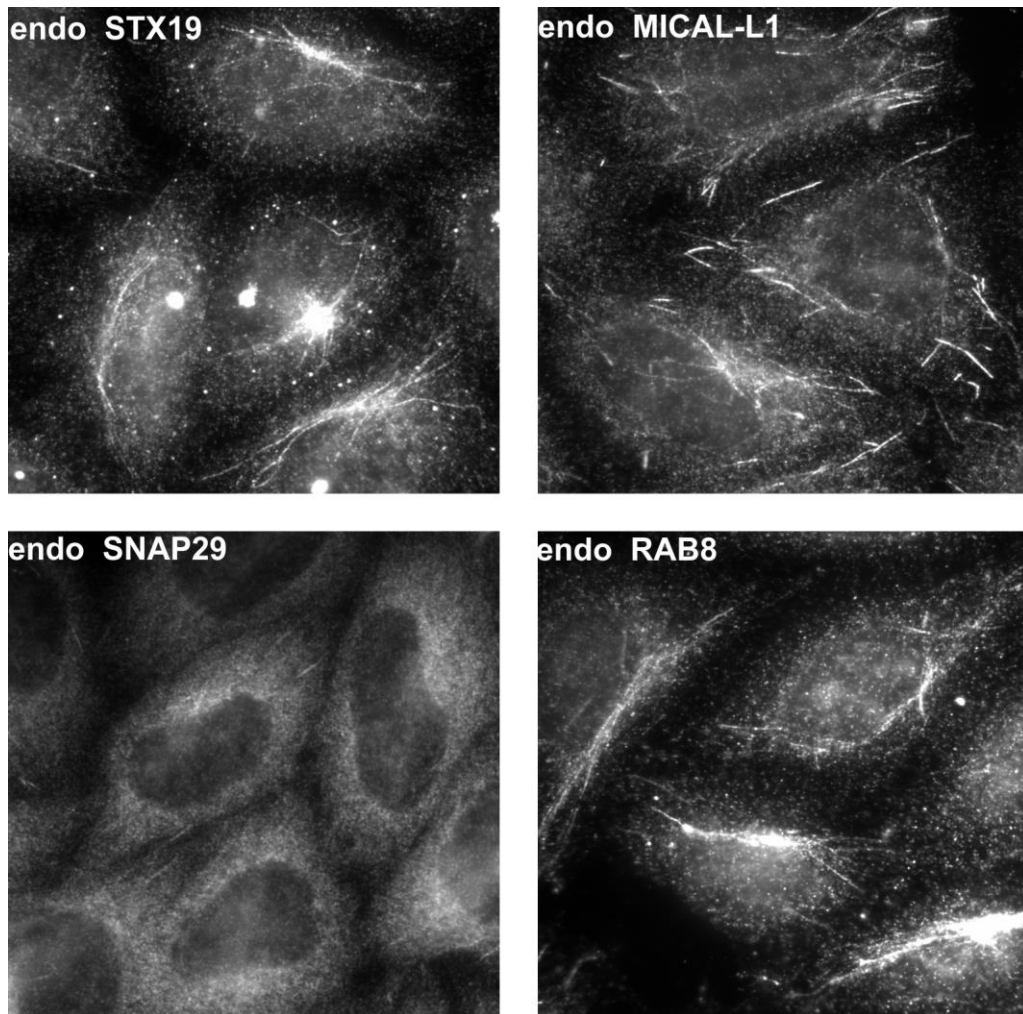


Figure 3-4 Testing tubular recycling endosomal marker antibodies in HeLaM cells.

HeLaM cells were grown overnight on coverslips. The cells were fixed, washed, permeabilized with 0.1% saponin and stained with anti-STX19, anti-SNAP29, anti-MICAL-L1 and anti-RAB8 followed by goat anti-rabbit 594 nm or goat anti-mouse 594 nm. Images were obtained from wide field microscope at x60 oil immersion. Scale bar = 10 μ m.

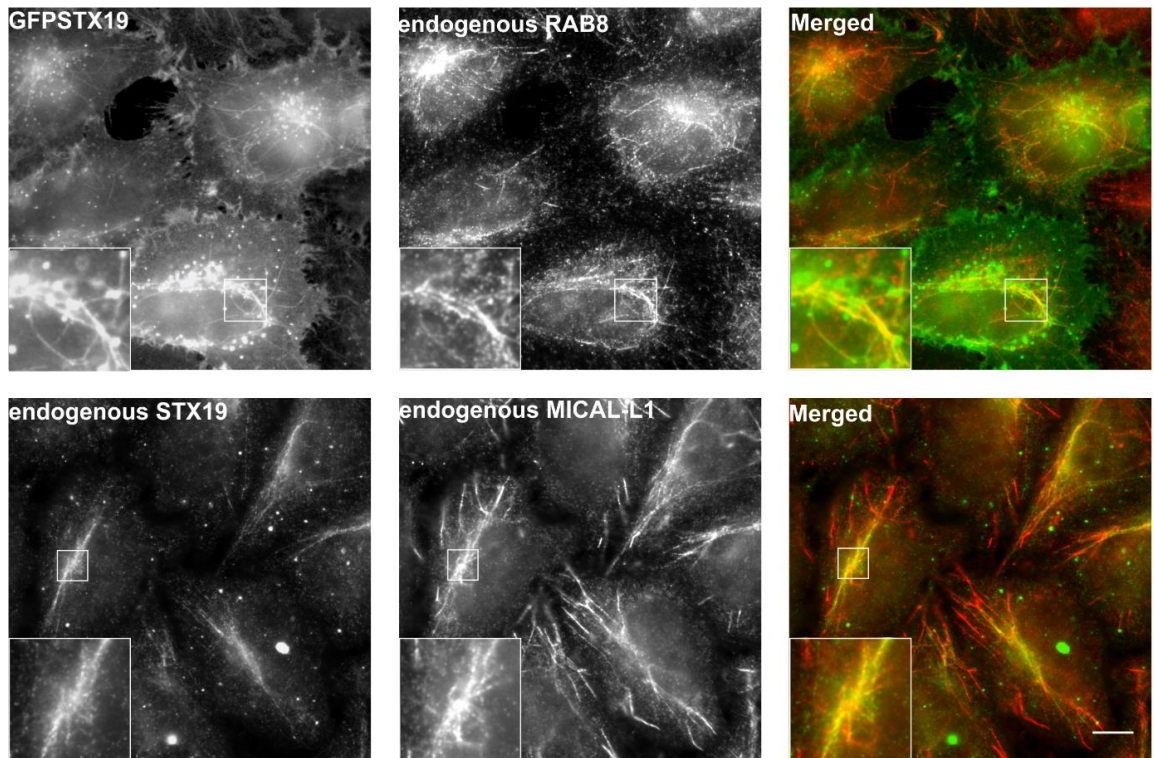


Figure 3-5 STX19 colocalises with RAB8 and MICAL-L1.

HeLaM cells were grown on coverslips overnight and transfected with GFPSTX19 or untransfected. The cells were fixed, washed, permeabilized with 0.1% saponin. The transfected cells were stained with anti-RAB8 followed by goat anti-rabbit Alexa 594 nm. The untransfected cells were costained with anti-STX19 and anti-MICAL-L1 followed by donkey anti-rabbit Alexa 488 nm and goat anti-mouse Alexa 594 nm. Images were obtained from wide field microscope at x60 oil immersion. Scale bar = 10 μ m.

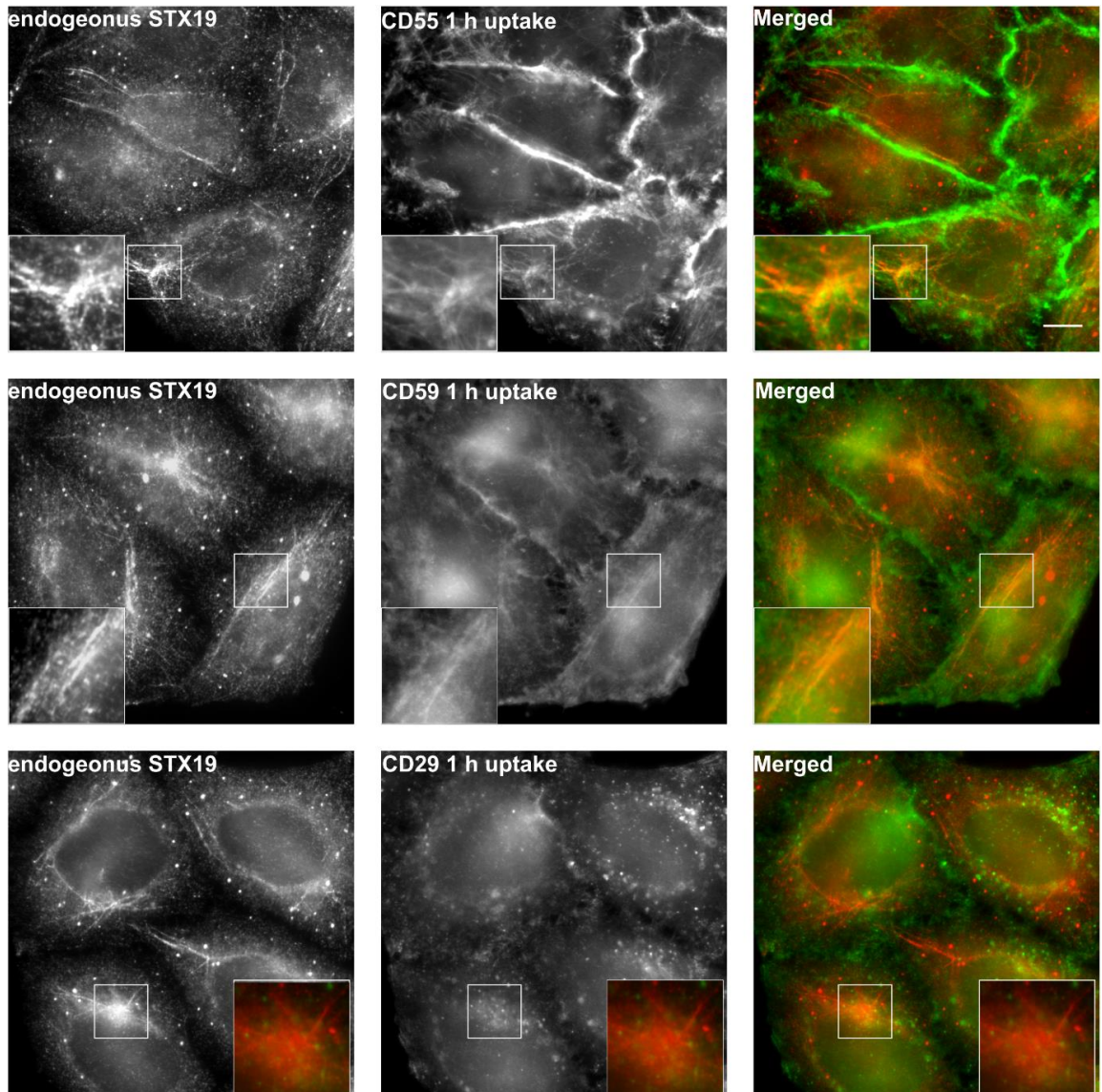


Figure 3-6 STX19 colocalises with internalised CD55 and CD59.

HeLaM cells were grown overnight on coverslips and then pulsed for 1 h with goat anti-mouse Alexa 488 nm conjugated CD55, CD59, and CD29. The cells were fixed, washed, permeabilized with 0.1% saponin and stained with anti-STX19, followed by goat anti-rabbit 594 nm. Images were obtained from wide field microscope at x60 oil immersion. Scale bar = 10 μ m.

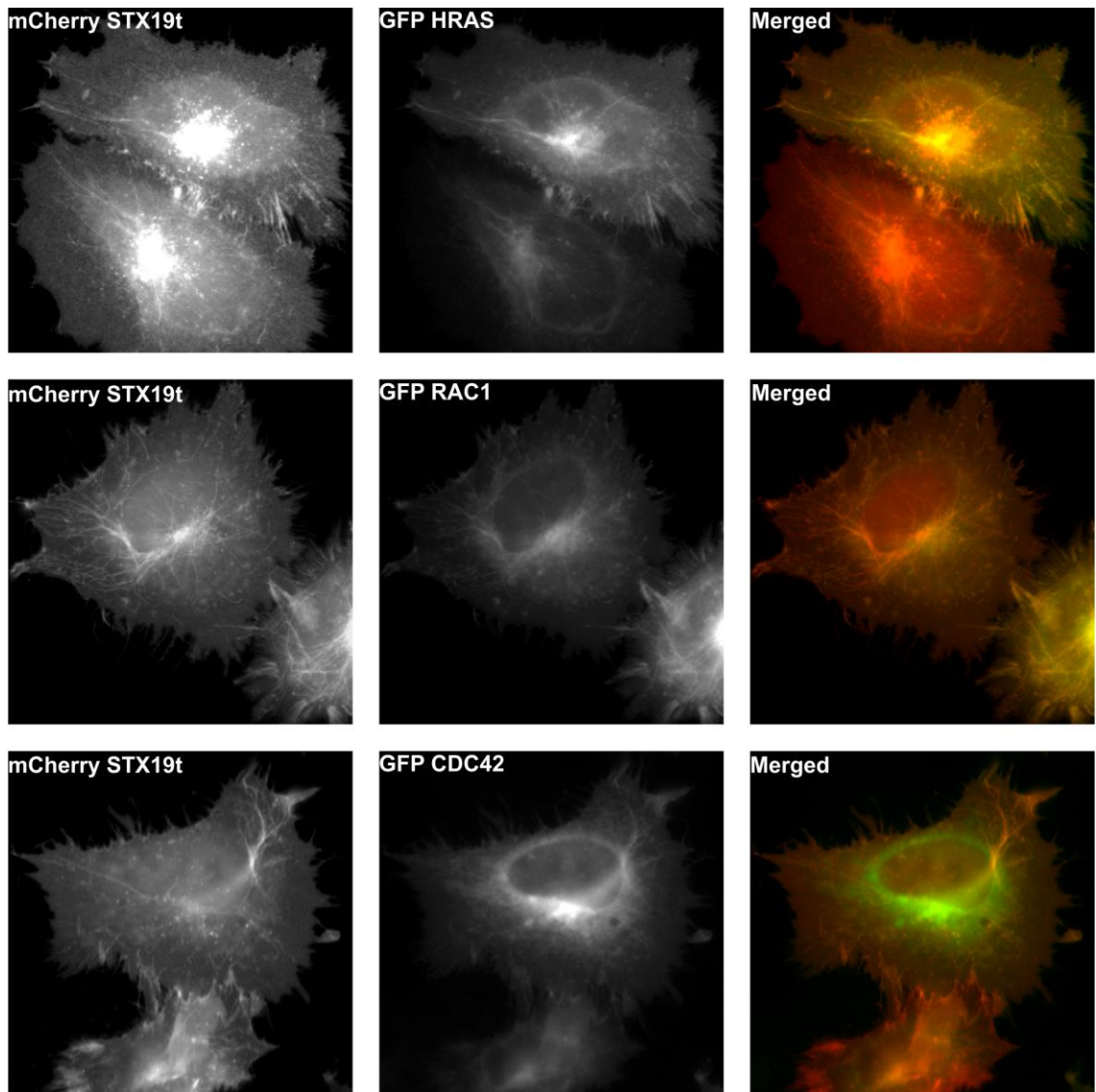


Figure 3-7 Overexpressed STX19 colocalises with HRAS, RAC1 and CDC42.

HeLaM cells were grown overnight on coverslips and then cotransfected with mCherry STX19t and either GFP HRAS, GFP RAC1 or GFP CDC42. 24 h post transfection, the cells were fixed, washed, and permeabilized with 0.1% saponin. Images were obtained from wide field microscope at x60 oil immersion.

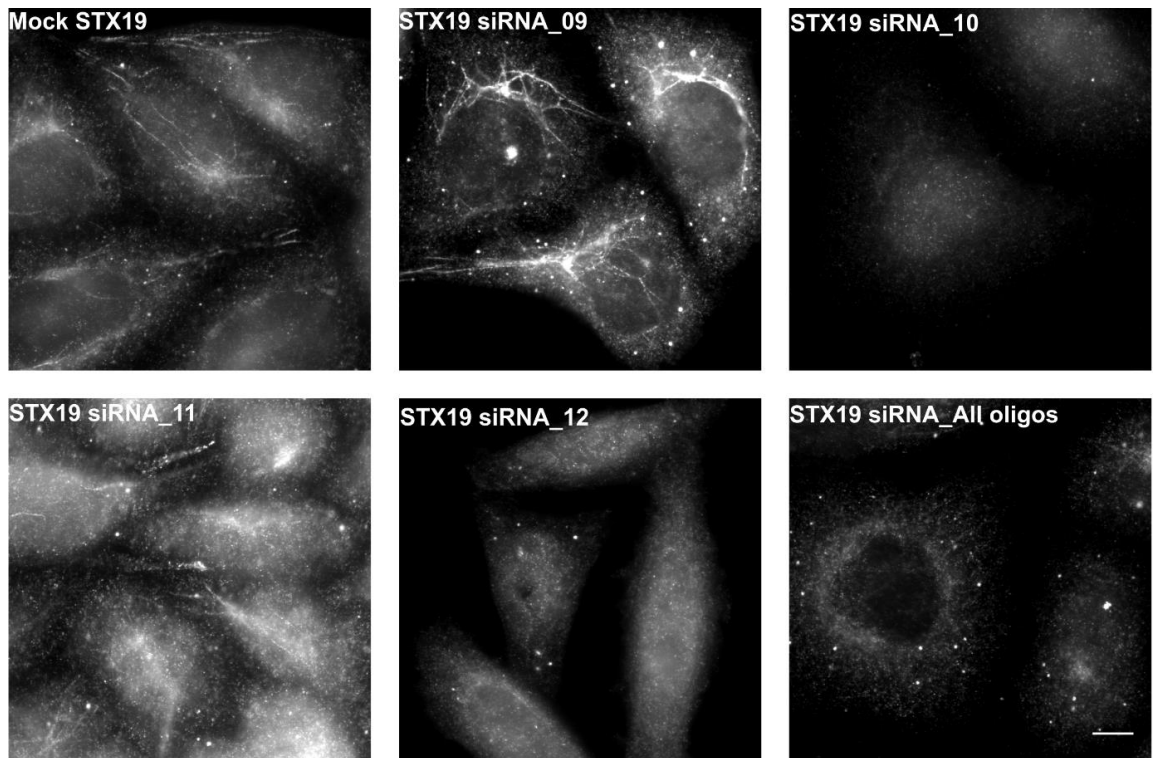
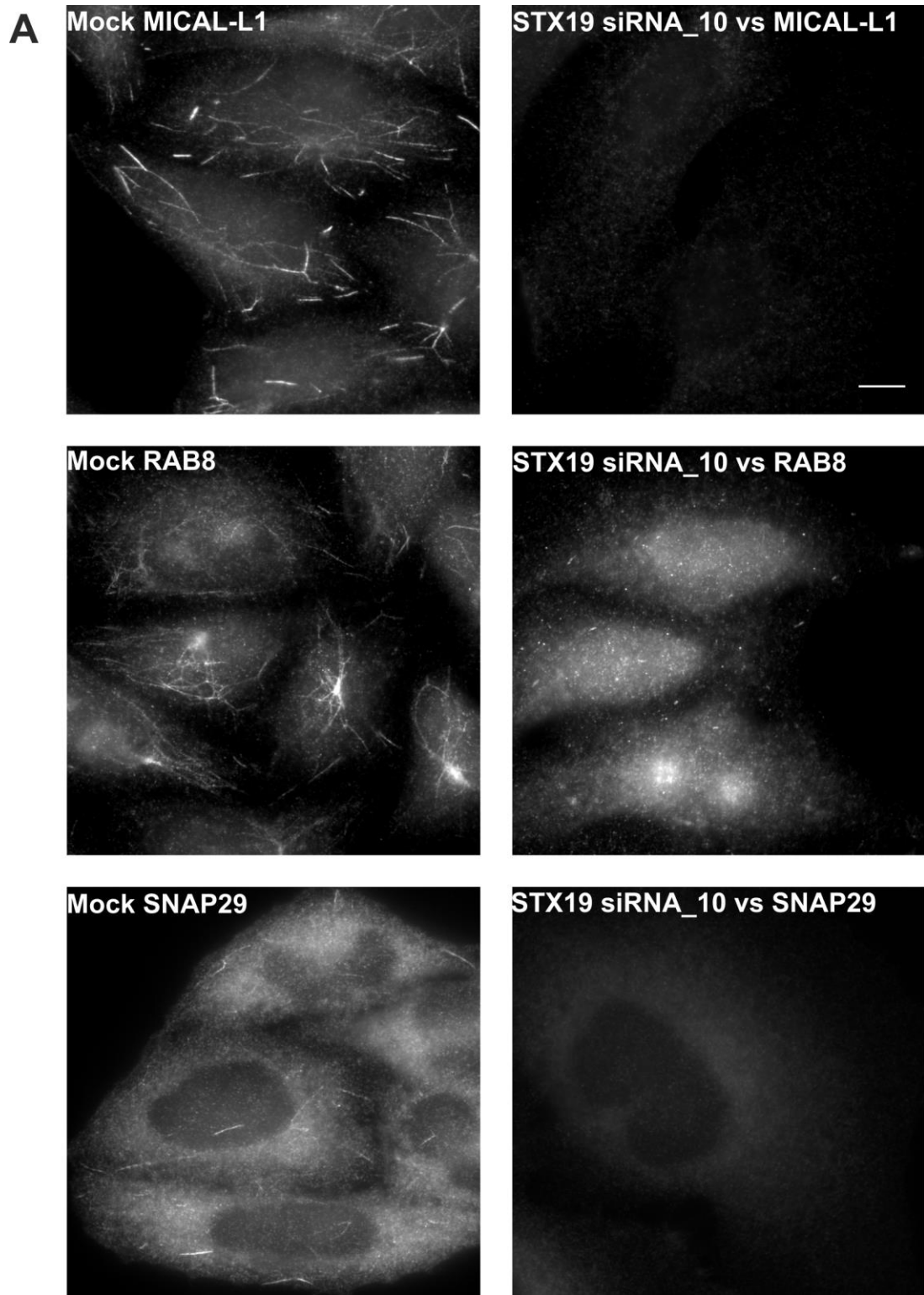


Figure 3-8 STX19 can be depleted using RNAi.

HeLaM cells were grown overnight in six-well plates and transfected with four different STX19 siRNA oligos using 96 h double transfection approach or mock transfected with lipofectamine RNAiMAX transfection reagent. The cells were transfected after 24 h and again after 48 h of seeding and then passaged after 96 h onto coverslips. The cells were fixed, washed, permeabilized with 0.1% saponin and stained with anti-STX19 followed by goat anti-rabbit Alexa 488 nm. Images were obtained from wide field microscope at x60 oil immersion. Scale bar = 10 μ m.



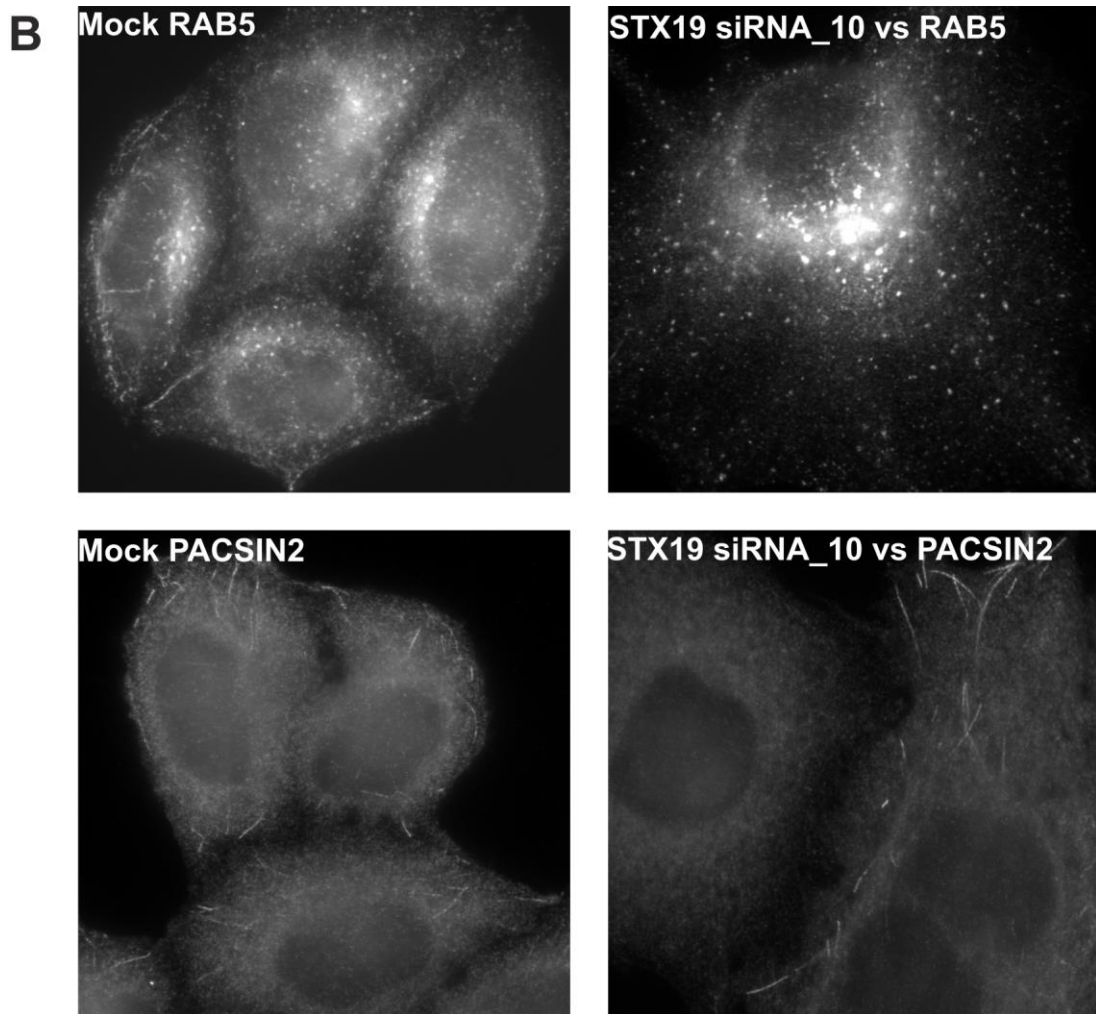


Figure 3-9 STX19 depletion affects the recruitment of RAB8 and MICAL-L1 to tubular recycling endosomes.

HeLaM cells were transfected with STX19 siRNA oligo_10 or mock transfected with lipofectamine RNAiMAX transfection reagent. The cells were fixed, washed, permeabilized with 0.1% saponin and stained with **(A)** MICAL-L1, RAB8, or SNAP29 **(B)** RAB5 or PACSIN2 or followed by goat anti-rabbit Alexa 488 nm or goat anti-mouse Alexa 594. Images were obtained from wide field microscope at x60 oil immersion. Scale bar = 10 μ m.

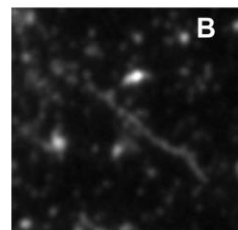
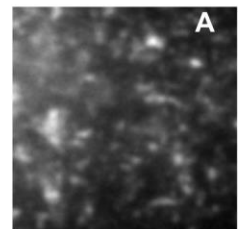
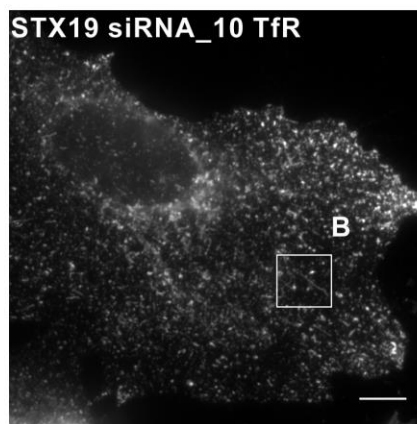
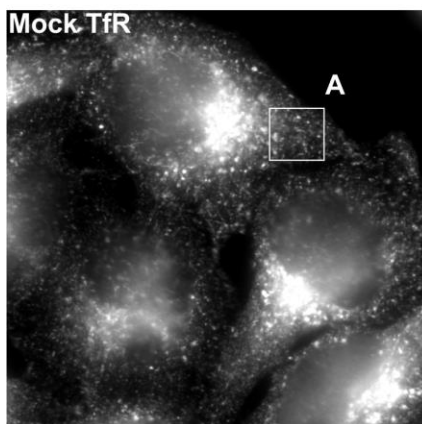
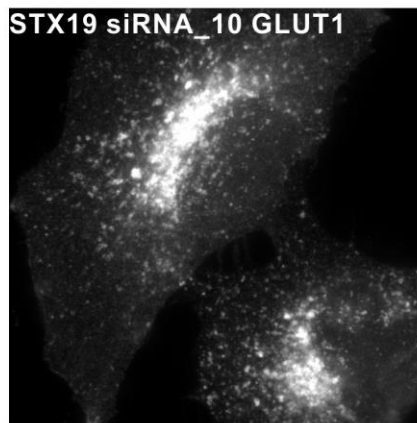
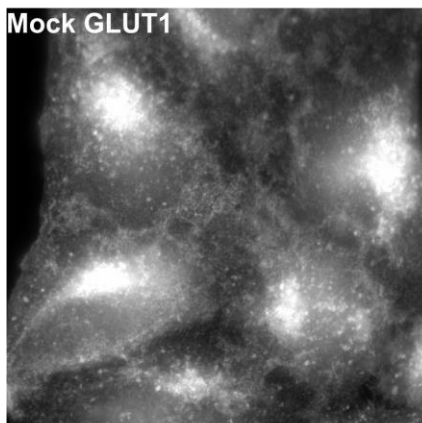
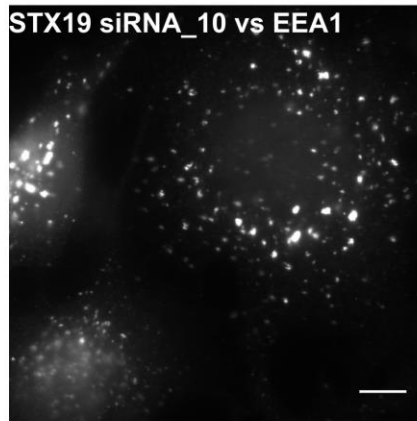
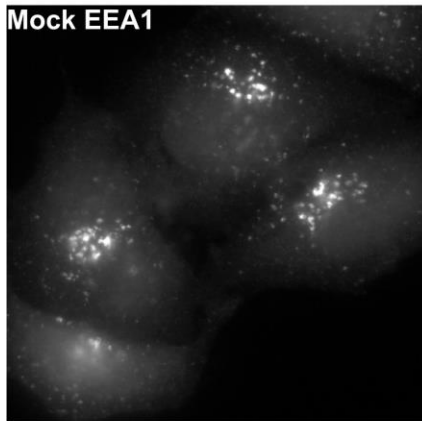
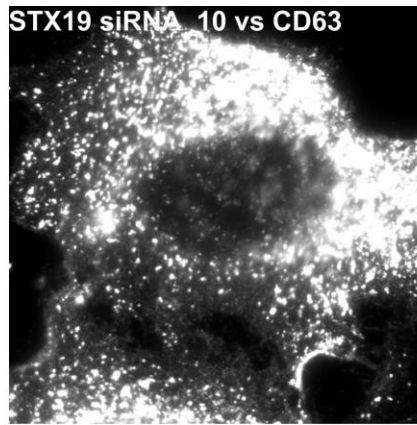
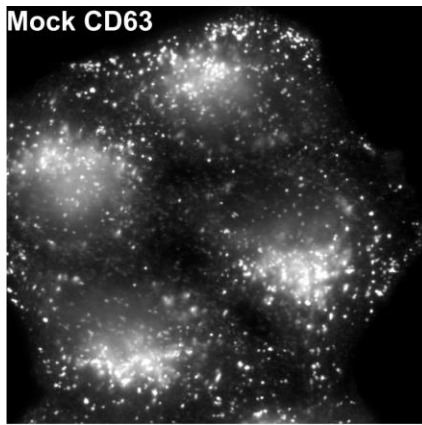


Figure 3-10 Depletion of STX19 leads to a defect in endosomal recycling.

HeLaM cells were transfected with STX19 siRNA oligo_10 or mock transfected with lipofectamine RNAiMAX transfection reagent. The cells were fixed, washed, permeabilized with 0.1% saponin and stained with anti-CD63, anti-EEA1, anti-GLUT1, or human anti-TF-R followed by either goat anti-mouse Alexa 594 or mouse anti-human Alexa 594 nm. Images were obtained from wide field microscope at x60 oil immersion. Scale bar = 10 μ m.

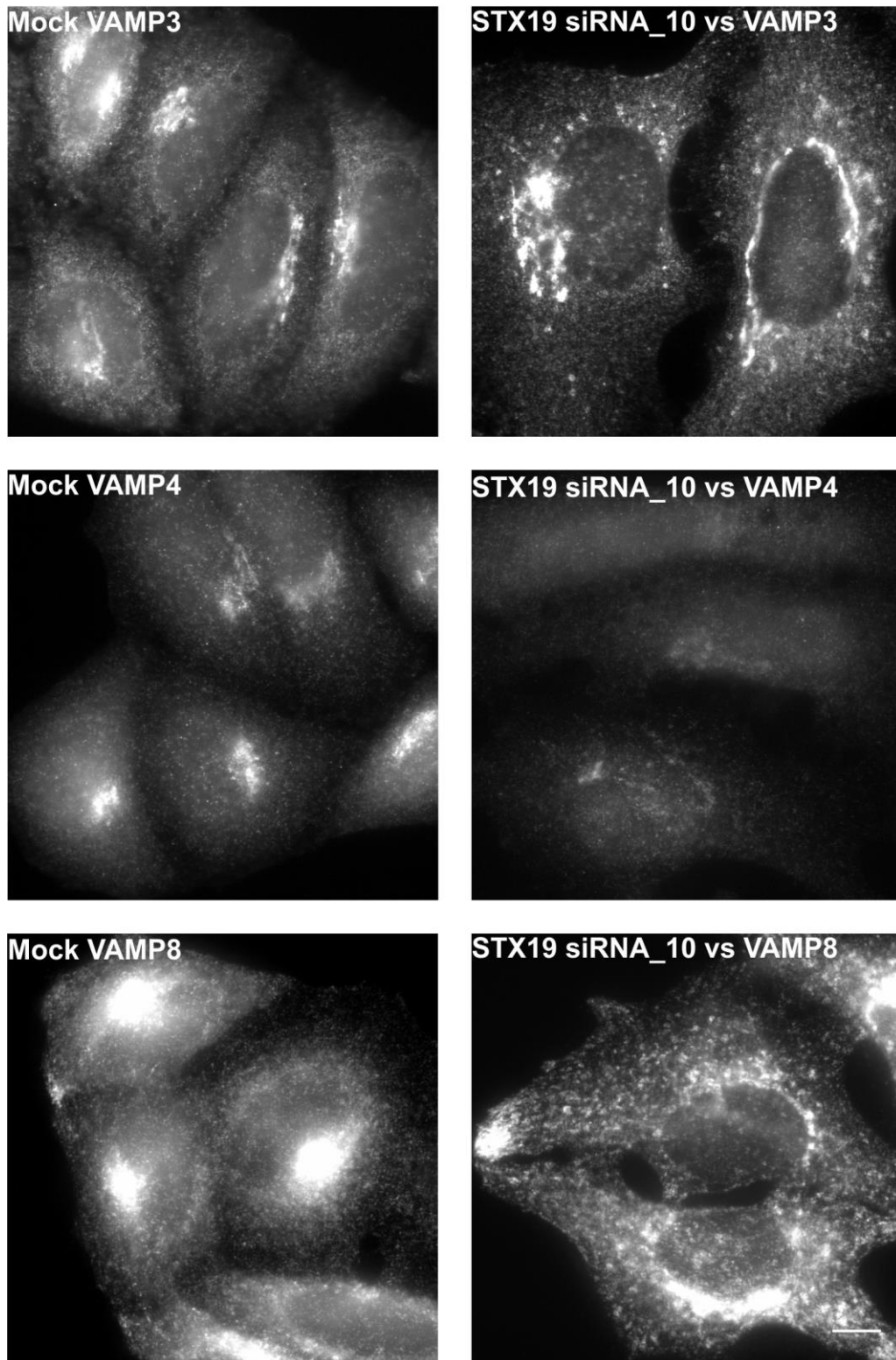
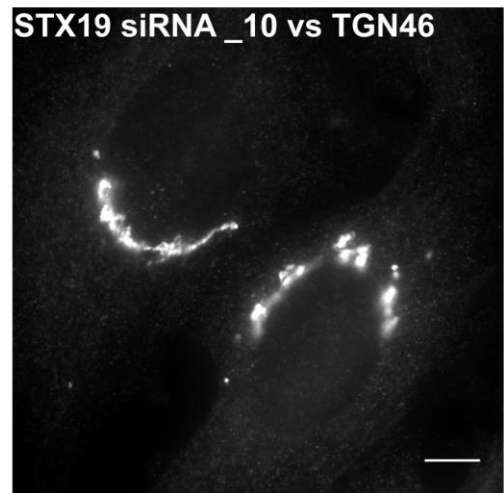
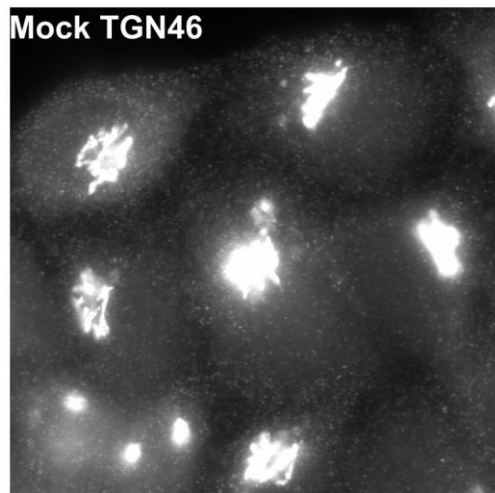
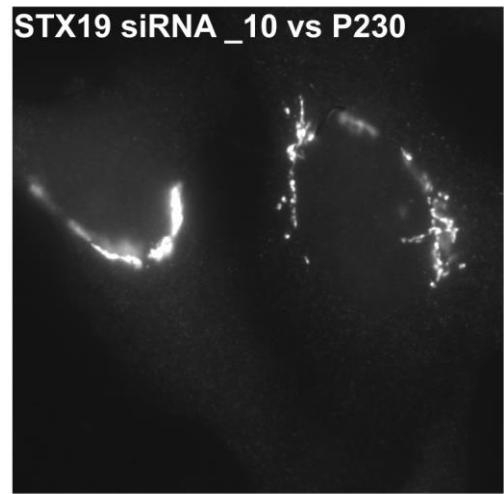
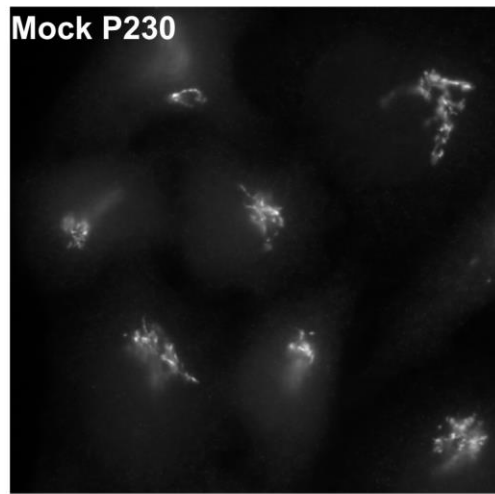
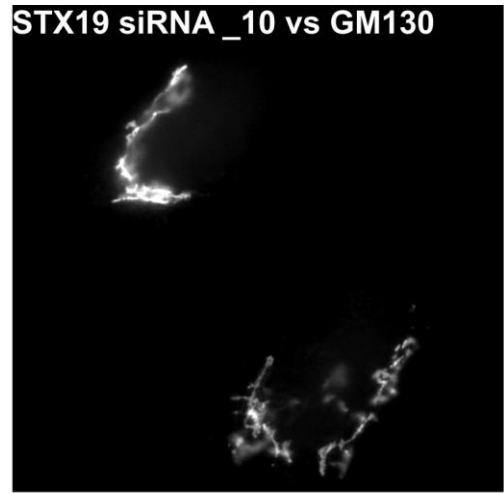
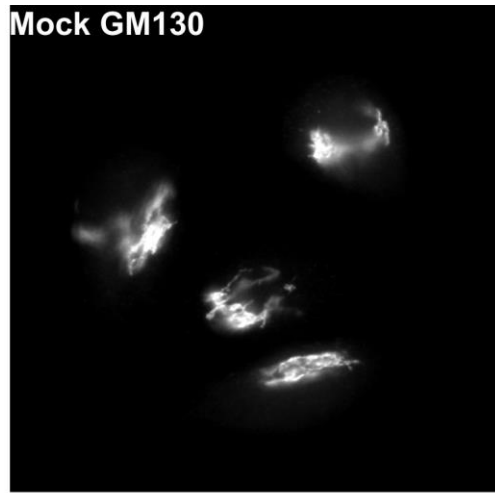


Figure 3-11 STX19 depletion affects R-SNARE localisation.

HeLaM cells were transfected with STX19 siRNA oligo_10 or mock transfected with lipofectamine RNAiMAX transfection reagent. The cells were fixed, washed, permeabilized with 0.1% saponin and stained with VAMPs (3, 4 and 8)

followed by goat anti-rabbit Alexa 488 nm. Images were obtained from wide field microscope at x60 oil immersion. Scale bar = 10 μ m.

A



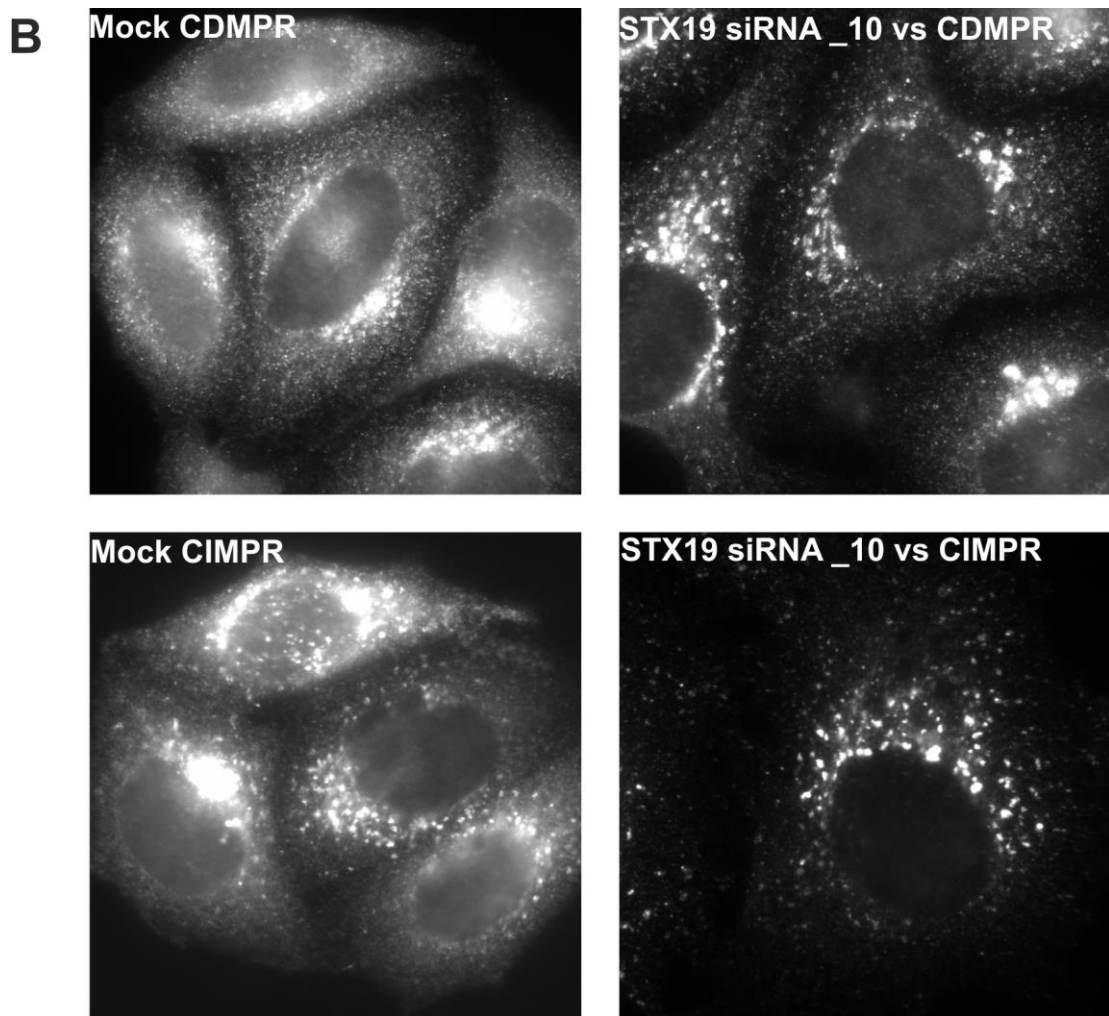
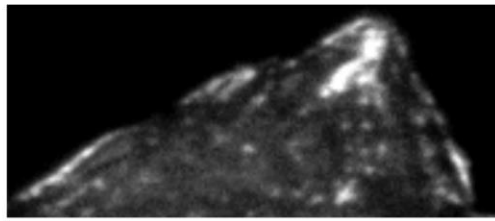


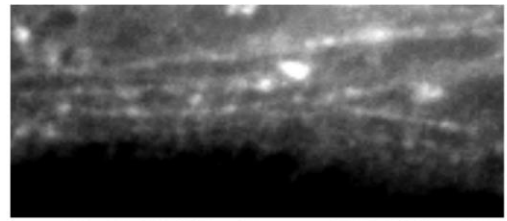
Figure 3-12 STX19 depletion affects Golgi morphology and the distribution of CD- and CI-MPR.

HeLaM cells were transfected with STX19 siRNA oligo_10 or mock transfected with lipofectamine RNAiMAX transfection reagent. The cells were fixed, washed, permeabilized with 0.1% saponin and stained with **(A)** GM130, TGN46, P230, **(B)** CDMPR or CIMPR followed by goat anti-rabbit Alexa 488 nm or goat anti-mouse 594. Images were obtained from wide field microscope at x60 oil immersion. Scale bar = 10 μ m.

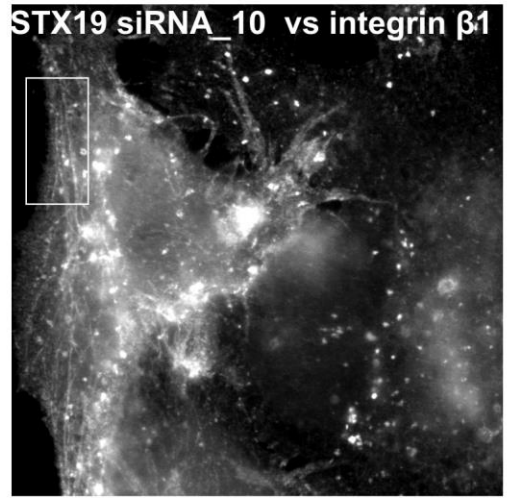
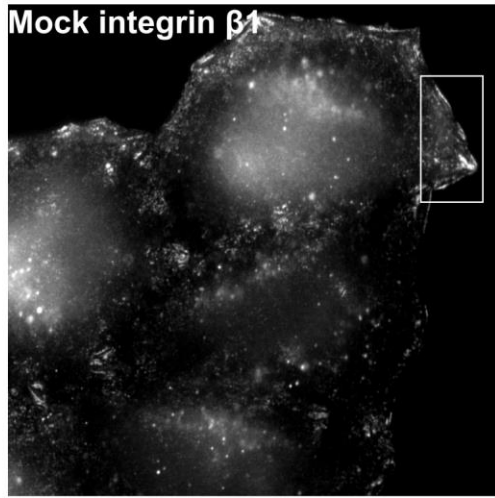
A



Mock integrin $\beta 1$

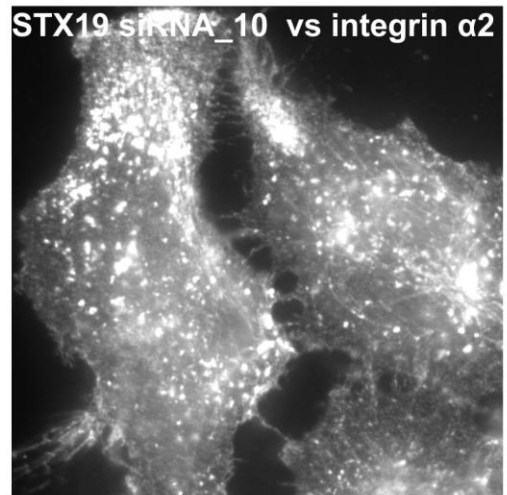
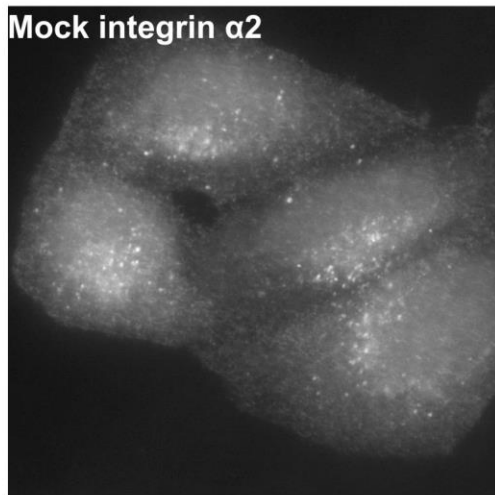


STX19 siRNA_10 vs integrin $\beta 1$



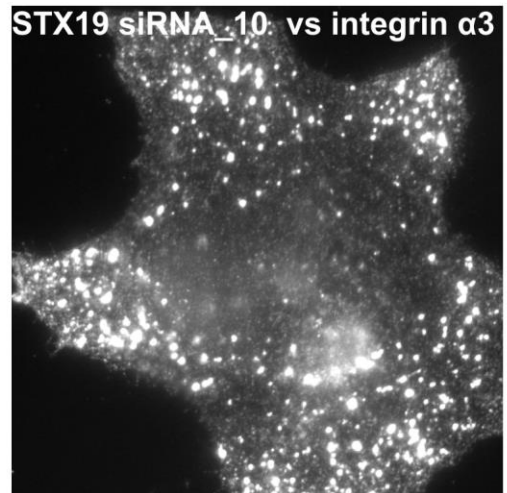
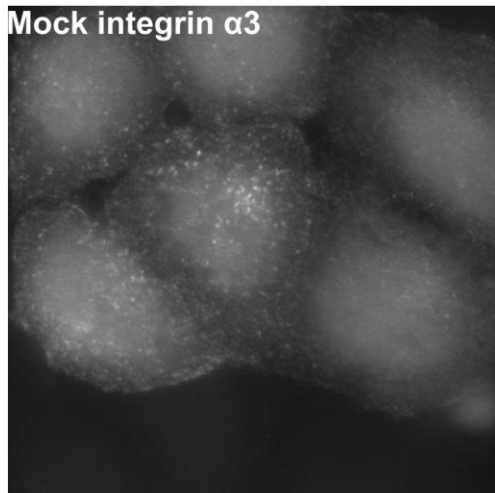
Mock integrin $\alpha 2$

STX19 siRNA_10 vs integrin $\alpha 2$



Mock integrin $\alpha 3$

STX19 siRNA_10 vs integrin $\alpha 3$



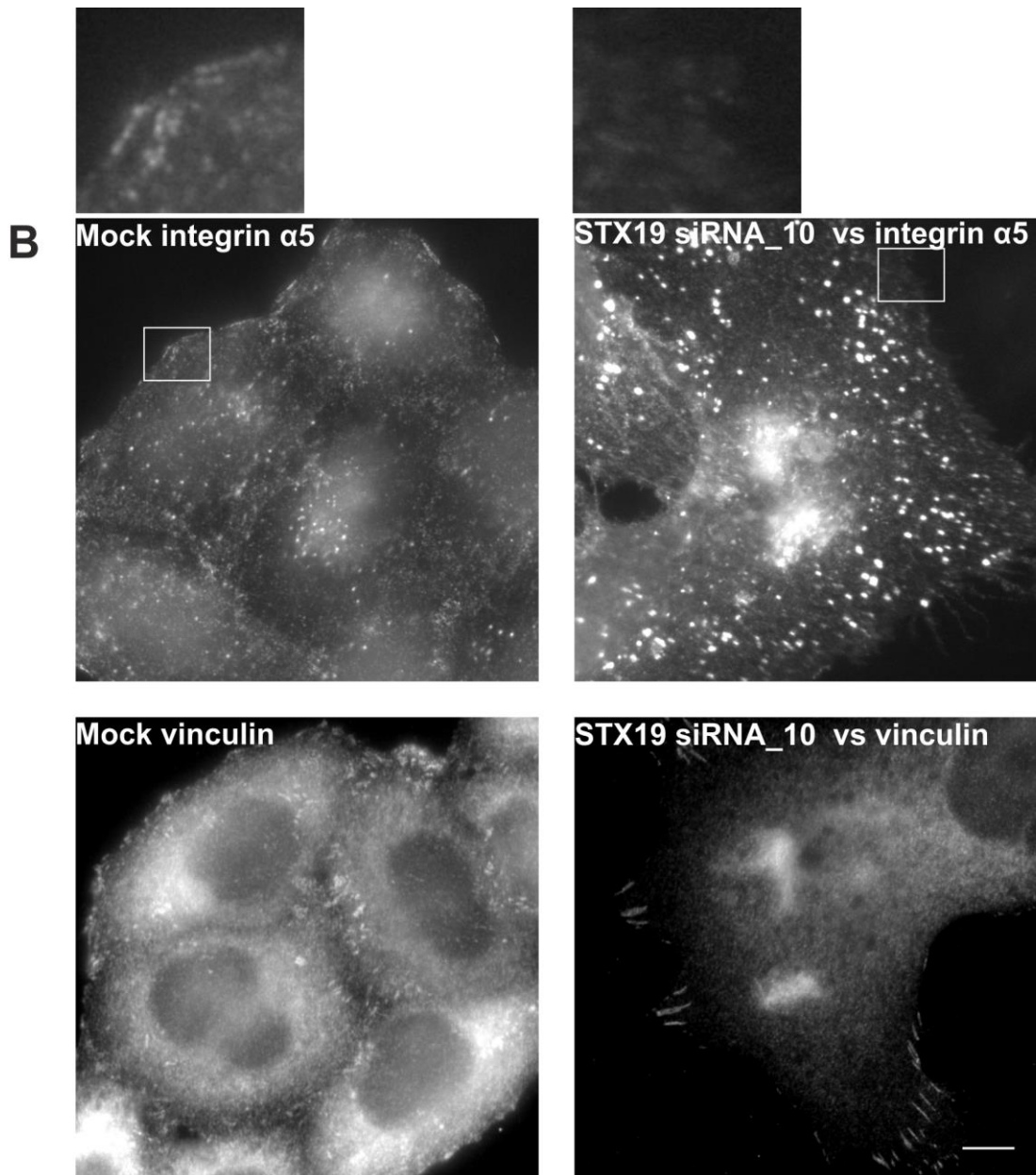


Figure 3-13 STX19 depletion affects integrin trafficking and focal adhesion dynamics.

HeLaM cells were transfected with STX19 siRNA oligo_10 or mock transfected with lipofectamine RNAiMAX transfection reagent. The cells were pulsed with Alexa 488 nm **(A)** integrin β 1, α 2, α 3 or **(B)** α 5 for 1 h at 37 °C, acid stripped for 1 min at rt and chased for 30 min 37 °C. They were then fixed, washed and permeabilized with 0.1% saponin. **(B)** For vinculin staining, the cells were fixed with -20 °C ice-cold methanol for 10 min, washed, permeabilized with 0.1% saponin and stained with vinculin followed by goat anti-mouse 594. Images were obtained from wide field microscope at x60 oil immersion. Scale bar = 10 μ m.

4 Chapter How is STX19 targeted to post-Golgi membranes?

4.1 Introduction

4.1.1 Investigating the role of palmitoylation in STX19 trafficking

The proper targeting of proteins to membranes can play an important role in regulating their function. Post-translational modifications like glypiation, palmitoylation, myristoylation, and prenylation (farnesylation and geranylgeranylation) facilitate protein membrane attachment (Cross, 1987, Resh, 1999, Zhang and Casey, 1996). HRAS and NRAS undergo farnesylation and then palmitoylation which promotes their trafficking from the ER to the Golgi and then to the PM (Hancock et al., 1991, Misaki et al., 2010). In SRC family kinases, myristoylation and palmitoylation are required for their transport from the perinuclear region of the cell and segregation into rafts and non-rafts membrane compartments (Seong et al., 2009, Shima et al., 2003, Akimzhanov and Boehning, 2015, Resh, 1999).

Studies have shown that SNARE proteins membrane association is promoted by the presence of transmembrane domains, interaction with other SNARE proteins and post-translational modifications including farnesylation and palmitoylation (Watson and Pessin, 2001, Fdez et al., 2010, Fukasawa et al., 2004, Greaves and Chamberlain, 2011b). SNAP25 membrane association is differentially regulated by the number of cysteines that undergo palmitoylation (Greaves and Chamberlain, 2011b). This determines whether it remains solely on the PM or on intracellular membrane compartments or the cytosol (Greaves and Chamberlain, 2011b). The trafficking of the R-SNARE YKT6 is controlled by both farnesylation and palmitoylation (Fukasawa et al., 2004). STX11 like STX19 are both Qa-SNARE that lacks a transmembrane domain but has a conserved cysteine-rich domain at their C-terminus, which has biochemically been shown to be palmitoylated (Kang et al., 2008). In natural killer cells, mutant STX11 lacking the cysteine-rich domain results in familial hemophagocytic lymphohistiocytosis type 4 due to STX11 trafficking defect (Hellewell et al., 2014).

I hypothesise that C-terminal cysteine-rich domain of STX19 is critical for STX19 palmitoylation and that palmitoylation is important for STX19 membrane targeting. However, it is unclear whether this modification is the sole determinant in regulating STX19 localisation. To address this, I have performed the following experiments:

1. Generated CLUSTALW alignment of STX19 cysteine-rich region to determine its conservation in different organisms
2. Developed truncation mutants to determine which domains are important for STX19 membrane association.
3. Performed PEG switch assay to confirm the palmitoylation of STX19.
4. Treated cells with 2-bromo palmitate (a pharmacological inhibitor of palmitoylation), to observe changes in STX19 membrane targeting.
5. Changed cysteines in the cysteine-rich region to leucine, to determine their effects on STX19 membrane targeting.
6. Fused the cysteine-rich region to GFP, to determine whether it targets properly as the full-length protein.
7. Performed mass spectrometry analysis on STX19, to identify the cysteine that are palmitoylated.
8. Mutated the hydrophobic region within the cysteine-rich region, to determine if it plays a role in STX19 palmitoylation.
9. Co-transfected HEK cells with GFPSTX19 full-length with the 23 PATs library and GFPSTX19 cysteine-rich region only also with the 23 PATs library followed by performing palmitate labelling, to identify which palmitoyl acyltransferases catalyses STX19 palmitoylation.
10. Mapped ubiquitination sites to check the role of ubiquitination in STX19 trafficking.

4.2 Results

4.2.1 STX19's cysteine-rich domain is highly conserved

Human STX19 is a Qa-SNARE having a cysteine-rich region at its C-terminus (Figure 4-1) (Wang et al., 2006). I have investigated the conservation of this

domain by comparing the sequence of STX19 from 10 different species using BLASTp (protein Basic Local Alignment Search Tool), CLUSTAL 2.1 multiple sequence alignment followed by BoxShade analysis. In the majority of the species, there is an upstream basic patch (K/R) followed by series of cysteine region separated by a bulky hydrophobic residue (W/F) and a proline (Figure 4-1). Interestingly, RAS also has a basic patch upstream of its palmitoylation signal which has been shown to be important for its trafficking (Schmick et al., 2014, Misaki et al., 2010). Consensus residues are indicated as “*” (Figure 4-1). To investigate the importance of this region in STX19 palmitoylation and trafficking, I have generated a series of mutation constructs and determined their localisation.

4.2.2 Mapping STX19 domain required for membrane association

To gain insight into how STX19 might be targeted to membranes, I have made several mutant constructs and determined how they affect STX19 targeting onto membranes. STX19 has a predicted Habc domain, a coiled-coil domain and a C-terminal cysteine-rich region (Figure 4-1). To identify which of the domains are required for STX19 membrane association, I have made three different STX19 constructs;

- without the coiled-coil domain
- cysteine-rich region replaced with STX13's transmembrane domain
- without the cysteine-rich region (1-277 amino acid only)

HeLaM cells were transfected with these constructs and immunolocalisation studies performed. The microscopy experiments show that wild-type STX19 is predominantly localised to the PM and TRE (Figure 4-2). This localisation is similar to that of endogenous STX19 (Figure 3-1). However, the tagged constructs show greater plasma membrane staining (Figure 4-2). The coiled-coil mutant has similar staining pattern as the wild-type STX19 indicating that the STX19 coiled-coil domain is dispensable for STX19's membrane association (Figure 4-2). However, STX19 no longer remained associated with the PM and TRE when the cysteine-rich domain was removed indicating that the cysteine-rich domain is essential for its targeting (Figure 4-2). Most Qa-SNAREs including STXs 1, 2, 3, and 13 (but not STXs 11 and 19) have a transmembrane

domain for membrane association (Hong and Lev, 2014). I investigated whether the transmembrane domain could enable STX19 cysteine-rich domain truncated mutant to associate with membranes. The STX19/13 hybrid was effectively targeted to the PM as the wild-type STX19 but its association with the TRE was significantly reduced (Figure 4-2).

Overall, my results show that both the wild-type STX19 and STX19 without the coiled-coil domain localises properly to membranes (tubular recycling endosomes and plasma membrane) (Figure 4-2). The absent of the coiled-coil domain slightly reduced STX19's TRE localisation by 10.4%; $P = 0.1591$ (Table 4-1). However, STX19's TRE localisation was reduced by 50.83% in the STX19/13 hybrid and 86.79% in the STX19 with the cysteine-rich region truncated which are statistically significant with $P = 0.0377$ and 0.0002 respectively (Table 4-1).

4.2.3 A PEG (polyethylene glycol)-switch assay shows that STX19 is palmitoylated

Previous studies have used PEG switch assay to determine the palmitoylation state of HRAS (Burgoyne et al., 2013a, Howie et al., 2014b). I have also used this approach to further confirm the palmitoylation state of STX19. The PEG switch assay involves maleimide treatment of cell lysates to block free cysteines, hydroxylamine to cleave thioester bond and the addition of 5 kDa polyethylene glycol which reacts with the free cysteines and causes an increase in molecular weight. This increase in MW can simply be detected as a mobility shift on an SDS gel (Burgoyne et al., 2013a, Howie et al., 2014b). HEK cells were transfected with GFP-STX19, GFP and GFP-HRAS as negative and positive control respectively. In the GFP transfected cells there was no mobility shift in either the control or hydroxylamine-treated cell lysates (Figure 4-3). However, in the GFP-HRAS transfected cells, there was a band shift for the cell lysates treated with hydroxylamine (Figure 4-3). This shows that the PEG assay was working properly. Then, I tested the PEG assay on wild-type GFPSTX19 full-length protein (1-294 aa), GFPSTX19 tail (cysteine-rich domain 274-294 aa only) and GFPSTX19 without the cysteine-rich domain (1-277). The Western blot data shows that there was a mobility shift in both GFPSTX19 full-length

protein and the GFPSTX19 tail but not when the cysteine-rich region was truncated (Figure 4-3). These results indicate that STX19 is palmitoylated.

4.2.4 STX19 membrane localisation is inhibited by 2-bromopalmitate

My results so far have shown that STX19 is palmitoylated. To further determine the effect of palmitoylation on STX19 membrane localisation, I have used 2-bromopalmitate. Palmitoylation can be inhibited by 2-bromopalmitate (Resh, 2006b). 2-BP is structurally similar to palmitate, however; the bromo group attached prevents it from degradation and cannot be metabolised. Once incorporated into the cell, it interferes with intracellular palmitoyl-CoA, therefore preventing palmitoylation to take place (Resh, 2006b). I have tested the effect of 2-BP on GFPSTX19 full-length protein GFPSTX19 tail and endogenous STX19. In the control cells, the GFPSTX19 and GFPSTX19 tail were localised to TREs and PM, whereas, endogenous STX19 was localised to TREs (Figure 4-4). When the cells were treated with 100 μ M 2-BP, STX19 lost its TRE and PM staining and became mostly cytosolic (Figure 4-4). My results clearly show that 2-BP affects wild-type GFPSTX19, GFPSTX19 tail, and endogenous STX19 membrane localisation (Figure 4-4). The percentage of STX19 localised to membranes were reduced significantly with P values of 0.0173, 0.0064, and 0.0033 corresponding respectively to wild-type GFPSTX19, GFPSTX19 tail, and endogenous STX19 (Table 4-2). The expression levels of STX19 from cells transfected with the GFPSTX19 tail was also dramatically reduced in a dose-dependent manner with P values of 0.1038, 0.0037 and 0.0000 denoting 50 μ M, 100 μ M and 150 μ M of 2-BP respectively (Table 4-2; Figure 4-4). This data indicates that palmitoylation is regulating the stability and membrane targeting of recombinant and endogenous STX19.

To gain an insight into which of the cysteines are important for STX19 targeting to membranes. I have mutated pairs of cysteines in the cysteine-rich region by replacing them with leucine residues (Resh, 1999). HeLaM cells were transfected with wild-type STX19 or mutants (M1, M2, M3, M4, M5, M6, M7, and Tr). The wild-type STX19 remains associated with the TREs and the PM (Figure 4-5). The mutants M1, M2 and M3 which were all single paired cysteines changed to leucines also localises properly to the TREs and the PM similar to

the wild type STX19 (Figure 4-5). The doubled mutants M4 and M6 but not M5 associated poorly with the TREs and PM (Figure 4-5). When all the cysteines in the cysteine-rich domain were either changed to leucines or truncated, STX19 became completely cytosolic (Figure 4-5). The data shows that mutating the cysteine-rich region (M4, M6, M7, Tr with P values of 0.0069, 0.0035, 0.0004 and 0.0004 respectively) drastically affects the membrane targeting of STX19 (Table 4-3).

4.2.5 STX19 cysteine residue mutants (M4, M6, M7, and Tr) cause the protein to be degraded

From the immunolocalisation studies it became apparent that interfering with palmitoylation significantly reduced the levels of recombinant STX19. My results show that mutants (M4, M6, M7, and Tr) cause STX19 to be degraded and also make the protein cytosolic (Figure 4-5). To investigate this further, I have transfected HeLaM cells with wt STX19 or mutants (M1, M2, M3, M4, M5, M6, M7, and Tr) in the presence or absence of 5 μ M MG132 and whole cell lysates prepared. MG132 is a proteasomal inhibitor that protects a protein from degradation (Lee and Goldberg, 1998). Western blotting was performed and the blots quantified. The wild-type STX19 expression level was fairly similar to the mutants (M1, M2, M3, and M5) (Figure 4-6). However, the levels were significantly reduced in mutants M4, M6 and Tr and completely lost in M7 (Figure 4-6) (P values of 0.0041, 0.0249, 0.00002 and 0.0036 respectively (Table 4-4). The addition of MG132 rescues the mutant constructs from degradation as shown in (Table 4-4; Figure 4-6). This suggests that the mutant constructs are being targeted for degradation by the proteasomal pathway.

4.2.6 The cysteine-rich region of STX19 is necessary and sufficient for STX19's membrane localisation

Mutations in the cysteine-rich domain affected STX19 targeting to membranes; I hypothesised that this region alone might be sufficient for STX19's membrane localisation. To test this, I tagged GFP with STX19's cysteine-rich domain (KKRNPCRVLCCWCCPCCSSK) and then transfected it into HeLaM cells. I observed that the construct localises to similar compartment as full-length STX19 (Figure 4-7). In addition, when the cysteines were mutated to leucines (to

recapitulate cysteine mutant in STX19 full-length protein; Figure 4-5) the construct became degraded (Figure 4-7). Interestingly, when the tryptophan residue only was mutated to either alanine or arginine the protein became cytosolic but not degraded (Figure 4-7).

4.2.7 STX19's tryptophan-286 and Proline-289 might be required for its initial membrane targeting

From the CRUSTALW alignment of STX19 in different organisms, I observed that proline 279 and 289 and tryptophan 286 are conserved (Figure 4-1). To understand the role of these amino acids contribution to STX19 membrane targeting, I have mutated the tryptophan 286 to either alanine 286 or arginine 286. STX19 W286R/A localises to the PM and TREs similar to the wild-type STX19 (Figure 4-9). Also, STX19 P289R and STX19 P289A + P279A all targets properly to the PM and TREs (Figure 4-9). To gain further insight into the role of W286 and P289, I mutated the tryptophan 286 together with the proline 289 both to arginine to form W286R + P289R. This mutant construct mostly remains cytosolic and had reduced PM and TRE staining compared to the wild-type STX19 (Figure 4-9). My data shows that W286 or P289 on its own does not greatly influence STX19 membrane targeting in the context of the full-length protein. However, with the STX19 tail construct W286R makes the protein cytosolic and protects it degradation (Figure 4-7). These data suggest that the proline and the tryptophan residues might aid STX19 initial membrane attachment for subsequent palmitoylation.

4.2.8 STX19's cysteines 284, 285, 287, 288 and 290 are palmitoylated

STX19 has seven cysteines in the conserved cysteine-rich domain at its C-terminus. To identify which of the seven cysteines in the cysteine-rich domain are palmitoylated I have used mass spectrometry. HEK cells were transfected with GFPSTX19 or GFPSTX19 tail and then immuno-isolated using GFPTRAP beads. The samples were all treated with Tris (2-carboxyethyl) phosphine hydrochloride [TCEP] and iodoacetamide to reduce and alkylate the cysteines making them freely available for further modification upon addition of hydroxylamine. From the mass spectrometry chromatographic peak upon trypsin cleavage in the control sample, the peptide identified from the

reconstruction of the b- and y-series was “LCCWCCPCCSSK”. The y- and b-series identified peptides “LCCWCCPCS” and “CWCCCSS” respectively (Figure 4-8). Using carbamidomethylation as a fixed modification due to the presence of iodoacetamide in all the samples (both treated and control) all the six cysteines identified were equally modified (alkylated) (Figure 4-8). However, in the hydroxylamine treated samples with the exception of C291 all the other cysteines were modified (Figure 4-8). Thus my studies show that C284, C285, C287, C288, and C290 have a 99% probability of being palmitoylated. Dr Mark Collins (The University of Sheffield, UK) helped in the MS analysis.

4.2.9 Identifying palmitoyl acyltransferases required for STX19 palmitoylation

Palmitoylation in mammals is catalysed by 23 palmitoyl acyltransferases (PATs) (Fukata et al., 2004, Lemonidis et al., 2015). PATs have a conserved zDHHC motif and are located in the ER, Golgi and PM (Chamberlain et al., 2013, Fukata et al., 2004, Ohno et al., 2006). To identify which of the PATs may be involved in STX19 palmitoylation, I have performed immunolocalisation studies in HeLaM cells and palmitate labelling coupled to click chemistry (Palmitate labelling performed in collaboration with Dr Jennifer Greaves, Strathclyde Institute of Pharmacy and Biomedical Sciences).

HeLaM cells were transfected with HA-tagged PATs known and their localisation determined. The zDHHCs had varied and overlapping intracellular membrane localisation patterns (Figure 4-10; Figure 4-11; Table 4-5). The Golgi localised PATs include zDHHCs (3, 5, 7, 9 and 11); the ER localised PATs were zDHHCs (4, 6,7,10 and18) whereas zDHHCs 2, 5, 10 and 23 were localised to the PM (Figure 4-10; Figure 4-11; Table 4-5). Some of the PATs zDHHCs (2, 5, 9 and 14) were localised to the tubular recycling endosomes (Figure 4-10; Figure 4-11; Table 4-5). I investigated whether endogenous STX19 colocalises with the PATs that were found on the TRE. I observed that endogenous STX19 colocalises with the zDHHCs (2, 5, 9 and 14) on the tubular recycling endosomes (Figure 4-12).

4.2.10 Palmitate labelling click chemistry identifies palmitoyl acyltransferases involved in STX19 palmitoylation

To identify the PATs that potentially catalysed STX19 palmitoylation, we have cotransfected either GFPSTX19 or GFPSTX19 tail together with a 23 PAT library in HEK cells. The cells were allowed to incorporate a biorthogonal palmitate (palmitic acid azide). The amount of palmitate incorporated was determined using click chemistry in a reaction containing a copper catalysed azide-alkyne dye that enables the protein to fluoresce. The samples were blotted for GFP to determine the expression level of the STX19 constructs, full-length GFPSTX19 (Figure 4-13) or GFPSTX19 tail (Figure 4-14). The samples were also probed for HA to check that the HA-tagged zDHHCs were properly expressed. The slight differences in the expression levels of GFPSTX19 and GFPSTX19 tail for the individual lanes might be as a result of the cotransfection assay (Figure 4-13; Figure 4-14). The click indicates the incorporation of the 17-ODYA (the palmitic azide) which is dependent on the expression levels of the HA-tagged zDHHCs and the ability of STX19 to act as a substrate for the zDHHCs (Figure 4-13; Figure 4-14). In most instances the higher the expression levels of the zDHHCs the higher the amount of 17-ODYA it incorporated (Figure 4-13; Figure 4-14). Thus, the amount of 17-ODYA incorporated were normalised to the expression levels of the zDHHCs to reduce biases in the 17-ODYA incorporated into either GFPSTX19 or GFPSTX19 tail (Figure 4-13; Figure 4-14). There was a significant increase in the amount of the palmitate incorporated into STX19 when STX19 was cotransfected with zDHHCs 1, 2, 3, 6, 7, 11, 14, and 15 (Figure 4-13). However, in the STX19 tail, we identified zDHHCs 2, 3, 7, 11, and 15 (Figure 4-14). This shows that there is an overlap in zDHHCs, which catalyses STX19 and STX19 tail palmitoylation. The fact that GFPSTX19 full-length protein was catalysed by more zDHHCs than GFSTX19 tail could be as a result of the additional domains in the wild-type STX19.

4.2.11 Mapping STX19 ubiquitination site

Blocking STX19 palmitoylation causes STX19 to become degraded indicating that palmitoylation regulates STX19 stability. This degradation is rescued by the addition of MG132 (Figure 4-6) indicating that STX19 most likely undergoes

ubiquitination and degradation by the proteasome. To test whether STX19 is ubiquitinated, cells were transfected with GFPSTX19 and treated with or without 5 μ M MG132. GFP-Trap IPs were performed and followed by mass spectrometry. In the first set of experiment, we identified an ubiquitination site at K206 and a phosphorylation site at S197 (Figure 4-15). To investigate the role of these residues in STX19 degradation, I have replaced K206 with arginine in a mutant STX19 construct that is constitutively degraded STX19 Tr2 (1-273 aa). I have also substituted S197 to leucine in wt STX19. I predicted that K206R mutant will rescue Tr2 from degradation and S197L will cause wt STX19 to undergo degradation. From the immunolocalisation studies both the wt STX19 and the STX19 S197L mutant was localised to TREs and the PM. In addition, both the STX19 Tr2 and K206R were localised to the cytosol and degraded. Therefore both the K206R and S197L did not behave as we had expected. So, we performed a second round of proteomic analysis to determine if we have missed other ubiquitination sites. K158 of STX19 is ubiquitinated. However, we did not perform a further study on this new ubiquitination site.

To gain insight into other motifs that might be relevant to STX19 degradation, I have scanned STX19 using the “Eukaryotic Linear Motif” database (Dinkel et al., 2016). The database identified an “MKDR” motif which is at the N-terminus of STX19. From the database, this motif has been predicted to initiate protein degradation via the N-end rule pathway (Dinkel et al., 2016, Tasaki and Kwon, 2007). I mutated the “KDR” motif to “AAA” and compared its localisation pattern with wt STX19. Both the wt STX19 and the KDR to AAA mutant are targeted properly to PM and TREs (Figure 4-16). Thus the “KDR” motif to “AAA” did not have any effect on STX19. My previous data show that STX19 M4, M6, M7 and Tr causes STX19 to be degraded (Figure 4-5; Figure 4-6). So, I wondered if this mutant (KDR to AAA) could rescue STX19 M7 and Tr mutants from degradation. To confirm this, I made an STX19 mutant construct that encodes both the KDR to AAA and M7 or Tr, however, STX19 still remain degraded (Figure 4-16).

4.3 Discussion

4.3.1 Summary of results

My data has shown that the highly conserved cysteine-rich domain (KKRNPCRVLCCWCCPCCSSK) of STX19 is necessary and sufficient for STX19 palmitoylation and membrane targeting. Blocking palmitoylation by mutating key cysteine residues in this region (especially M4, M6, M7 and Tr mutants) causes STX19 to be degraded and also blocks the ability of the protein to associate efficiently with membranes. In support of this observation, inhibition of palmitoylation using 2BP alters the steady-state localisation of endogenous as well as recombinant STX19. Using mass spectrometry, we have identified C284, C285, C287, C288 and C290 to be palmitoylated. Using palmitate labelling click chemistry, we have identified zDHHCs 1, 2, 3, 6, 7, 11, 14, and 15 as enhancing recombinant STX19 palmitoylation. We have also identified two novel ubiquitination sites in STX19, K-158 and K-206 and several phosphorylation sites at S- 24, 60, 83,112, 178,197, and 210.

4.3.2 Palmitoylation targets STX19 to the PM and TRE

Palmitoylation regulates the trafficking of several proteins such as SNAP25, HRAS, and SKFs (Chamberlain et al., 2013, Salaun et al., 2010, Misaki et al., 2010). Palmitoylation in HRAS targets it to Rab11 positive recycling endosomes and the plasma membrane (Misaki et al., 2010). My results indicate that the cysteine-rich domain of STX19 is necessary and sufficient for targeting STX19 to the plasma membrane and TREs. Substitution of STX19's cysteine-rich region with STX13's transmembrane domain reduces the targeting of STX19 to tubular recycling endosomes (Figure 4-2). This observation strongly suggests that palmitoylation is allowing STX19 to access this compartment. At present, it is unclear how palmitoylation is regulating the sorting of STX19. It is possible that the palmitoylation allows STX19 to associate with lipid microdomains (Resh, 2006a, Lingwood and Simons, 2010). However, we cannot rule out that other proteins may be playing a role in regulating its correct trafficking.

4.3.3 Multiple cysteines are required for STX19 palmitoylation.

My data has shown that five cysteines in STX19 are palmitoylated. However, it is clear that not all of the palmitoylated cysteines play an equivalent role in STX19 targeting and trafficking. Mutating the cysteine pairs individually in STX19 did not cause any gross change in the localisation or membrane association of STX19. However, when 4 cysteines were mutated together significant changes in STX19 localisation and membrane targeting were observed. Similar results have been also observed with SNAP25 where not all of the palmitoylated cysteines play equivalent roles in membrane targeting, C88A contributed to about 65% loss in the SNAP25b membrane targeting, whereas C90A contributed to less than 5% (Greaves et al., 2009). Also, loss in SNAP25b membrane targeting was visibly clear only when all the four cysteines were replaced with leucine or alanine (Greaves et al., 2009). This further explains why M7 and Tr membrane targeting was greatly reduced or lost in comparison to where four (M5, M4, M6) or two cysteines (M1, M2, M3) were replaced with leucine (Figure 4-4). In the current study, whereas M1, M2, M3 and M5 there was not any great decrease in STX19 membrane association; M4 and M6 there was about 70% lost which was further increased into a complete cytosolic pool of STX19 in M7 and Tr mutants (Figure 4-5).

4.3.4 How is STX19 initially targeted to membranes?

It remains unclear how STX19 is initially recruited onto the membrane for it to become palmitoylated. HRAS utilises its farnesylation in the CAAX box for initial membrane targeting. Most SNAREs associate with membrane via their transmembrane domain. Examples include STX13, STX7, STX8 or farnesylation as in YKT6 before undergoing palmitoylation (He and Linder, 2009, Fukasawa et al., 2004). STX19 initial membrane association could be driven by its N-terminal peptide interaction with Munc18-2 (STXBP2) for it to become palmitoylated. Indeed, Munc18-2 has been shown to chaperone STX11 to the plasma membrane where it becomes palmitoylated (Dieckmann et al., 2015). In FHL5 cytotoxic lymphocyte which lacks Munc 18-2, STX11 is lost from the plasma membrane (Dieckmann et al., 2015). Similarly, Munc 18-1 chaperones STX1 to the PM, apical and basolateral membranes (Han et al.,

2011). My results strongly suggest that tryptophan-286 might serve as an initial membrane targeting signal for the STX19 tail but not full-length STX19. In STX19 tail, W286R makes the protein cytosolic, whereas in the full-length protein STX19 still remains membrane associated (Figure 4-7; Figure 4-9) This suggests that full-length STX19 may have an additional membrane targeting signal including perhaps its interaction with Munc18-2 via its N-terminal peptide or via its interaction with other SNARE proteins. Indeed we and others have identified that STX19 interacts with Munc 18-2/STXBP2 (Table 5-3) (Huttlin et al., 2015). Future experiments will require truncating the N-terminal peptide that is required for STX19's interaction with Munc18-2 to see if any at all there is an effect on STX19 membrane localisation.

4.3.5 Palmitoyl acyltransferases (1, 2, 3, 6, 7, 11, 14, and 15) catalyse STX19 palmitoylation

To identify the palmitoyl transferase which palmitoylates STX19 I have performed immunolocalisation and palmitoylation assays in HEK and HeLM cells using recombinant zDHHCs.

4.3.5.1 PAT assays

To identify the PATs that catalyse STX19 palmitoylation I have performed a screen where I co-expressed the 23 PATs with GFPSTX19 full-length or GFPSTX19 tail and used click chemistry to measure palmitate incorporation. zDHHCs 1, 2, 3, 6, 7, 11, 14, and 15 increase STX19 full-length protein palmitoylation (Figure 4-13) and zDHHCs 2, 3, 7, 11, and 15 increase STX19 tail palmitoylation (Figure 4-14). The greatest increase of palmitate incorporation in STX19 full-length protein was seen with zDHHCs 2, 3, 7, 15 and to a less extent with zDHHCs 6, 11 and 14 (Figure 4-13). The amount of palmitate incorporated by zDHHC7 was approximately 5.5 fold (Figure 4-13).

ZDHHCs 2, 3, 7, 15 and 17 have previously been shown to palmitoylate SNAP25 whereas zDHHCs 3, 7, 15 and 17 palmitoylate cysteine string protein (Greaves et al., 2010, Greaves et al., 2008). ZDHHCs 3 and 7 have been shown to have a broad range of substrate specificity towards other palmitoylated proteins including HRAS, SNAP25, SNAP23, phosphatidylinositol 4-kinase II α (Fukata et al., 2004, Greaves and Chamberlain, 2011a, Lu et al.,

2012). ZDHHC 2 and 15 palmitoylate PSD-95, HRAS, AKAP79/150 (Fukata et al., 2004, Woolfrey et al., 2015). Not many substrates have been identified for zDHHC 14 which is known to increase the aggressiveness of gastric cancer by regulating the expression levels of MMP-17 and integrins alpha 5 beta 1 (Oo et al., 2014). ZDHHC 6 is specifically targeted to ER by its dilysine motif at its C-terminus (Gorleku et al., 2011). ZDHHC 6 regulates calnexin palmitoylation by attaching palmitate to calnexin's C502 and C503 which is vital for the latter's ribosome-translocon complex formation important for protein folding (Lakkaraju et al., 2012). ZDHHC 11 is unique as no substrate has been identified yet and its aberrant expression is associated with bladder cancer (Yamamoto et al., 2007).

At present, it is unclear why there are differences in the enzymes which palmitoylate the tail and full-length STX19 constructs (Figure 4-13; Figure 4-14). Both proteins are efficiently targeted to membranes and traffic to the plasma membrane and TRE (Figure 4-2; Figure 4-7). One possible explanation for this difference is that the ZDHHCs may be recognising motifs in STX19 outside the cysteine-rich domain. For example, zDHHC6 has an SH3 domain, zDHHC 13, 17 have Ankyrin repeats and zDHHC 5, 8, 14 have PDZ domains. When the Ankyrin repeat domain of zDHHC 17 was transported onto zDHHC 3, zDHHC 3 was then able to palmitoylate huntingtin as effectively as zDHHC 17 (Huang et al., 2009).

4.3.5.2 Colocalisation studies

To validate the biochemical PAT data I have performed colocalisation studies on endogenous STX19 and recombinant PATs. The Intracellular localisation of recombinant zDHHCs in HEK, COS and yeast cells have been well characterised (Fukata et al., 2004, Ohno et al., 2006, McCormick et al., 2008). However, the intracellular localisation of zDHHCs in HeLaM cells has not been studied. I have transfected HA-tagged zDHHCs (1-23) in HeLaM cells and costained them with endogenous STX19. As previously reported zDHHCs 3, 4, 7, 15, 17, and 18 are localised to the Golgi; zDHHCs 5, 20 are localised to the plasma membrane; zDHHCs 6, 10 and 19 are found at the ER (Figure 4-10; Figure 4-11; Figure 4-12). In HEK cells, none of the zDHHCs were shown to be

localised to tubular recycling endosomes (Ohno et al., 2006). In HeLaM cells, I have identified zDHHCs 2 and 14 to colocalise with endogenous STX19 on the tubular recycling endosomes (Figure 4-12) potentially supporting the biochemical data. Interestingly, zDHHCs 5 and 9 also colocalise with endogenous STX19 on tubular recycling endosomes, however, they did not palmitoylate STX19 in the HEK cells (Figure 4-12; Figure 4-13; Figure 4-14).

One significant limitation of my PATs experiments is they were all performed with overexpressed recombinant tagged zDHHCs. Thus it is possible that the tagging and overexpression is altering the specificity and localisation of the enzymes. However, the fact that STX19 colocalises with zDHHC 5 and 9 but is not palmitoylated by them argues that there is some specificity in the biochemical experiments. To address these issues, it will be important in the future to use siRNA to deplete the appropriate zDHHCs and determine if they affect the palmitoylation of endogenous STX19. However, one significant issue with this approach is that there is a high level of redundancy between several of the zDHHCs.

4.3.6 Palmitoylation regulates STX19's stability

Palmitoylation is not only required for regulating the trafficking of proteins but also plays an important role in maintaining protein stability (Linder and Deschenes, 2007). Tlg1 which is required for Golgi to endosomal transport in yeast when not palmitoylated becomes targeted by Tul1 E3 ligase for degradation (Valdez-Taubas and Pelham, 2005). STX19 appears to behave in a similar manner and becomes degraded when not palmitoylated. My Western blot data shows that the levels of STX19 palmitoylation-deficient mutants M8, M4, M6, M7, Tr and Tr2 were significantly reduced (Figure 4-5; Figure 4-6; Figure 4-7). Also, when GFPSTX19 tail was treated with 100 μ M 2BP the protein became degraded (Figure 4-4). These data indicate that cytoplasmic, non-palmitoylated STX19 is targeted for degradation. This degradation can be blocked by the treatment with 5 μ M MG132 (Figure 4-6), suggesting the involvement of ubiquitination and the 26S proteasome. Although the mutants were rescued from degradation in the presence of MG132, this did not increase

their membrane attachment as the mutants did not harbour the required cysteines for their membrane association.

At present, it is unclear why cytosolic STX19 is a target for degradation. It is likely that cytoplasmic STX19 may be toxic to cells and it has been shown for other SNAREs that cytoplasmic SNARE domains act in a dominant negative fashion (Scales et al., 2000, Pulido et al., 2011). From our biochemical data, we propose that STX19 contains at least two degrons. The first degron is formed when the cysteine-rich domain of STX19 is not palmitoylated (Figure 4-4)(Figure 4-5; Figure 4-6; Figure 4-7). The second degron is upstream of this and its effect can be observed in the truncation mutants (the truncation mutant is almost as efficiently degraded as M7).

In an attempt to identify the second degron, I performed a motif scan of STX19 (Dinkel et al., 2016). At the N-terminus of STX19, there is an “MKDR” motif which is predicted to initiate protein degradation (Dinkel et al., 2016). This motif is also found in STX1, STX11, STX2 and STX4 which is part of the N-terminal peptide domain of Qa_SNAREs that associates with Sec1/Munc18-like proteins (Baker and Hughson, 2016, Rathore et al., 2010, Hu et al., 2011). Following removal of the methionine from the “MKDR” motif by N-met aminopeptidase or endopeptidase exposes the lysine or arginine residues to UBR-BOX1 that initiates an E3 ubiquitin ligase degradation of the protein (Tasaki and Kwon, 2007, Varshavsky, 2011).

To determine the role of the “MKDR” motif in regulating STX19 stability, the KDR was changed to AAA. Immunolocalisation studies show that the KDR to AAA mutants targets to membranes properly as the wt STX19 (Figure 4-16). So we predicted that when the KDR to AAA mutants was combined with either of the STX19 degradative mutants M4, M6, M7, or Tr, it should rescue them from degradation. However, when we made a STX19 mutant construct containing either the KDR to AAA and M7 or KDR to AAA and Tr, nothing happened (Figure 4-16). The combined mutant was equally degraded as the M7 only (Figure 4-16) indicating that this motif is not important for the degradation of the mutant STX19 constructs.

STX19 contains 16 lysine residues so it is possible that anyone of them is playing a key role in its degradation and be subject to ubiquitination. Therefore, I performed a GFPTRAP IP of STX19 in the presence or absence of 5 μ M MG132 to identify any possible ubiquitination site. We identified lysine-206 (K-206) and a phosphorylation site at S197 in the sample treated with MG132 only and not the untreated sample (Figure 4-15). From the peptides identified, the phosphorylation inhibited ubiquitination and vice versa (Figure 4-15). This further strengthens the fact that K-206 is an actual ubiquitination site for STX19. Studies have revealed a dynamic interaction between phosphorylation and ubiquitination (Hunter, 2007). Phosphorylation may either interfere with ubiquitin ligase activity or generate a phosphodegron to bring about protein degradation (Hunter, 2007). However, mutating these residues did not have any effect on STX19 degradation.

4.3.7 FUTURE EXPERIMENTS

My studies have shown that when STX19 is not palmitoylated it becomes degraded most likely via ubiquitination. Our data suggests that non-palmitoylated STX19 contains at least two degrons. The first is found in the cysteine-rich C-terminal domain and the second is located upstream of this. However, it is unclear what are the key lysines residues involved in this process and what are the ubiquitin ligases mediating this process. Our initial attempts have identified K206 residue to be ubiquitinated. However, mutating it does not block the degradation of STX19. This suggests that other residues may be playing a role in this process. To investigate this further we can generate a STX19 construct where all of the lysines have been mutated. Our yeast two-hybrid screen and Bio-ID proteomic studies have identified several ubiquitin ligases which might be targeting STX19. It will be interesting to determine if they are involved in STX19 degradation.

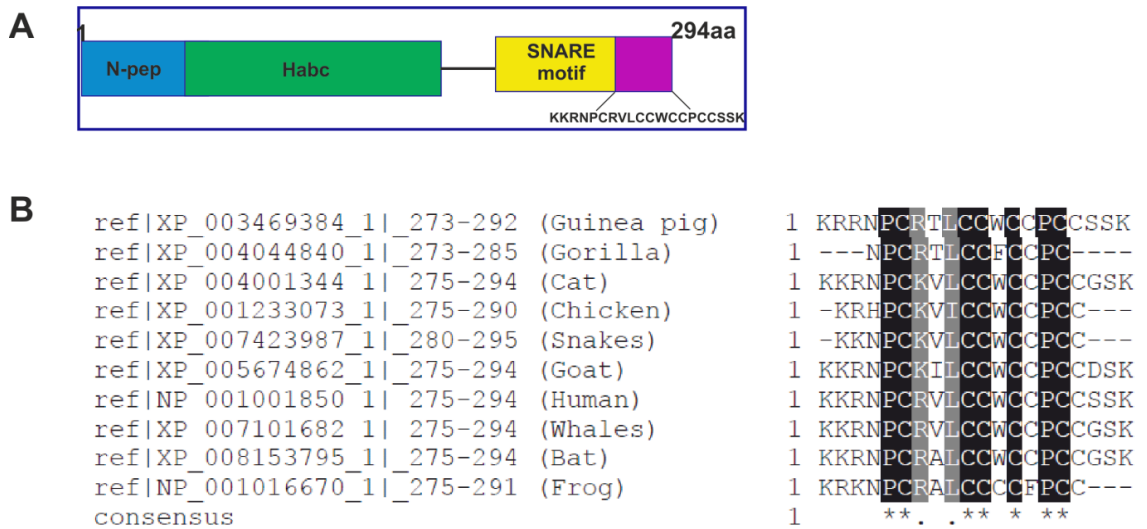


Figure 4-1 STX19 cysteine-rich region is conserved in different species.

A) Domain structure of STX19. B) BoxShade Analysis of STX19 conserved cysteine-rich domain from different organisms.

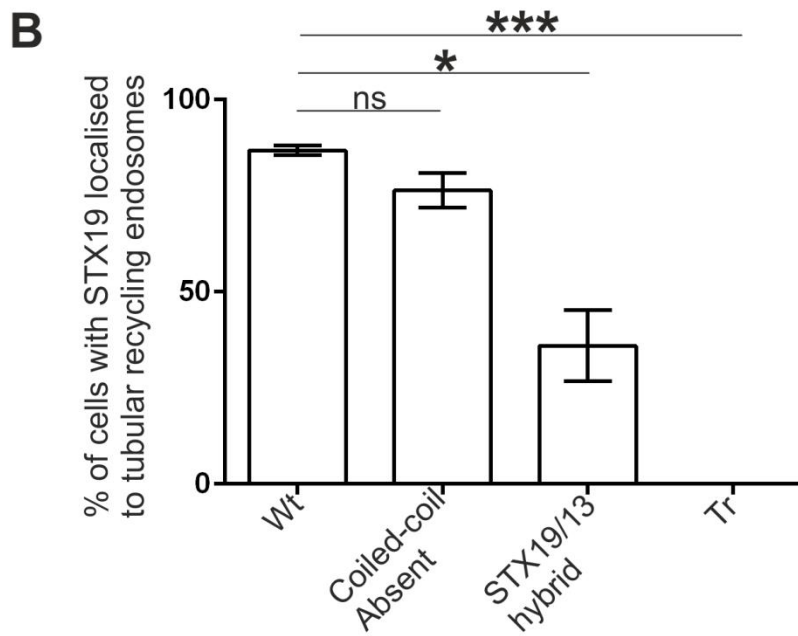
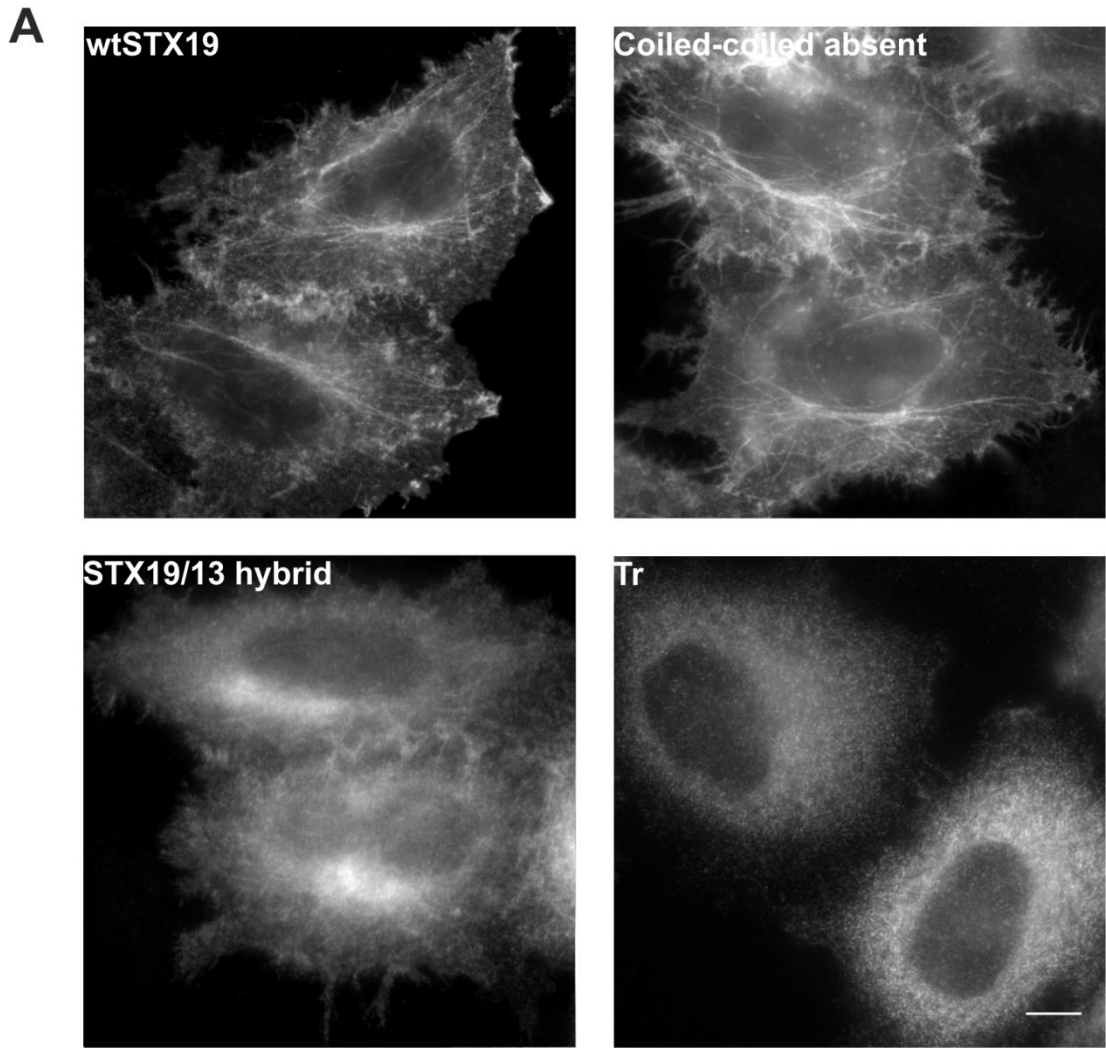


Figure 4-2 Mapping STX19 domain required for membrane association.

A) HeLaM cells were grown overnight on coverslips and then transfected with either HA-tagged STX19 wt, HA-tagged STX19 (without coiled-coil domain), HA-tagged STX19 (with STX13 transmembrane) or HA-tagged STX19 (without CRVLCCWCCPCC). 24 h post transfection, the cells were fixed, washed, permeabilized with 0.1% saponin and stained with anti-HA followed by goat anti-mouse Alexa 594 nm. **B)** Approximately 250 cells were counted and the percentage of cells showing STX19 tubular recycling endosomes localisation quantified (ns = not significant; * = $P < 0.05$; *** = $P < 0.01$). Error bar indicates means \pm SEM from three independent experiments. Images were obtained from wide field microscope at x60 oil immersion. Scale bar = 10 μ m.

Table 4-1 Quantification of STX19 domain tubular recycling endosome localisation.

Repeats	Wt	Coiled-coil absent	STX19/13 hybrid	Tr
1st Quantification	88.57	82.35	37.03	0.000
2nd Quantification	87.5	67.64	19.44	0.000
3rd Quantification	84.31	79.17	51.42	0.000
P-value		0.1591	0.0377	0.0002

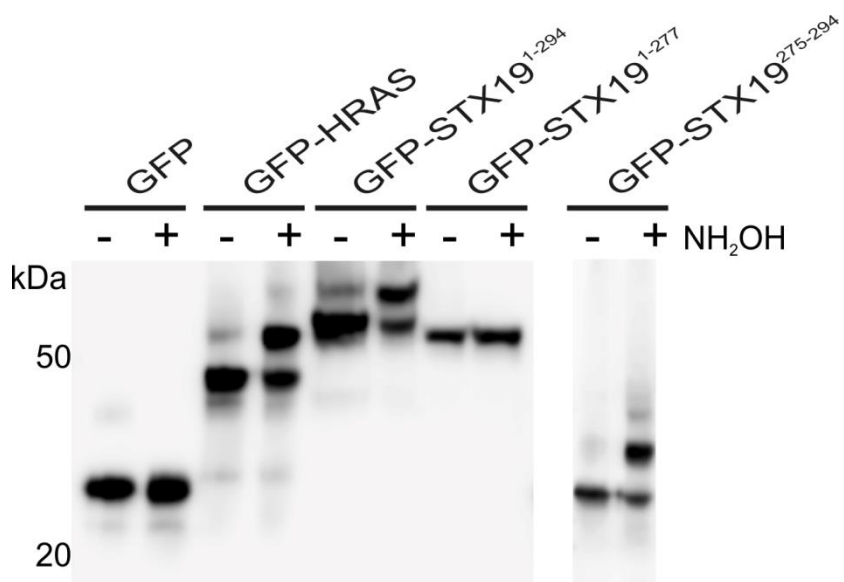


Figure 4-3 PEG switch assay confirms the palmitoylation state of STX19.

HEK cells were grown overnight on six cm plates and then transfected with either GFP only, GFP-tagged HRAS, STX19 full-length protein, truncated STX19 (274-294 removed) (Tr2), and STX19 tail only. 48 hours posttransfection, the cells were lysed in the presence of 2.5% SDS and maleimide and then incubated at 40 °C for 4 hours. Excess unreacted maleimide was removed by acetone precipitation and the cell lysates treated with 200 mM hydroxylamine or 200 mM NaCl as control. The lysates were blotted with anti-GFP rabbit antibody followed by rabbit HRP.

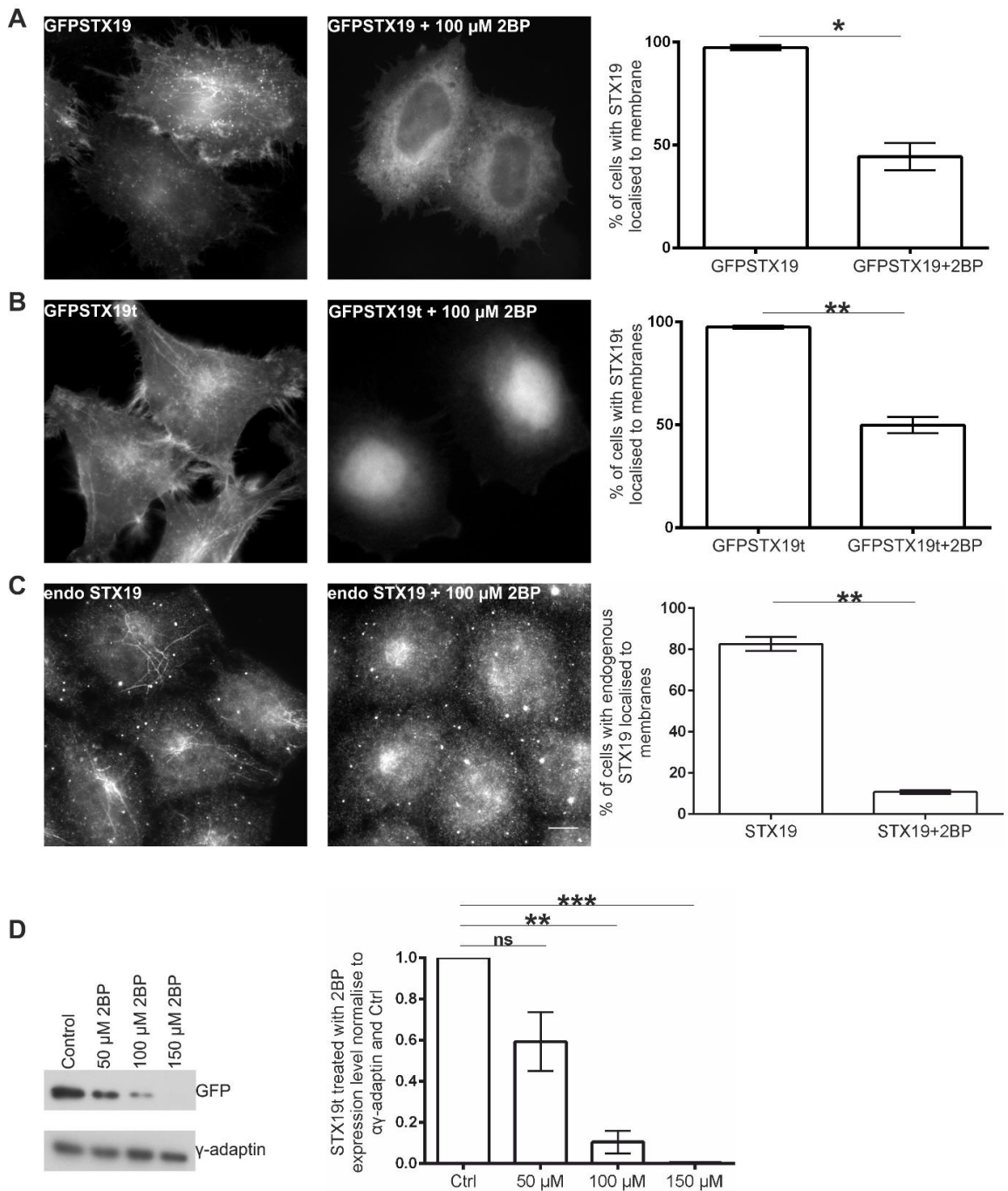


Figure 4-4 STX19 membrane localisation is dependent on its palmitoylation.

A, B and C) HeLaM cells were grown on coverslips and then treated with or without 100 μ M 2 BP overnight. **A and B)** Cells transfected with either GFPSTX19 or GFPSTX19t. 8 h posttransfection the cells were treated with or without 100 μ M 2 BP. 24 h posttransfection the cells were fixed and washed. **C)** Non-transfected cells treated with or without 100 μ M 2 BP overnight were fixed, washed and stained with anti-STX19 followed by anti-rabbit Alexa 488 nm. **A, B and C)** A total of 300 cells were counted and the number of cells with membranes quantified. **D)** HeLaM cells were seeded overnight into 6 cm plates and then transfected with GFPSTX19 tail. 8h posttransfection, the cells were

treated with or without 2 BP at different concentrations. Whole cell lysates were collected 24 h post- transfection and WB performed. The lysates were blotted with anti-GFP rabbit antibody followed by rabbit HRP. Mouse anti-gamma-adaptin monoclonal antibody was used as a loading control. Western blots from three independent experiments were quantified using LI-COR Image Studio Digits Ver 4.0. (ns = not significant; * = $P < 0.05$; ** = $P < 0.01$; *** = $P < 0.001$). Images were obtained from wide field microscope at x60. Error bar indicates means \pm SEM from three independent experiments. Scale bar = 10 μ m.

Table 4-2 Quantification of STX19 membrane localisation with or without 2 BP.

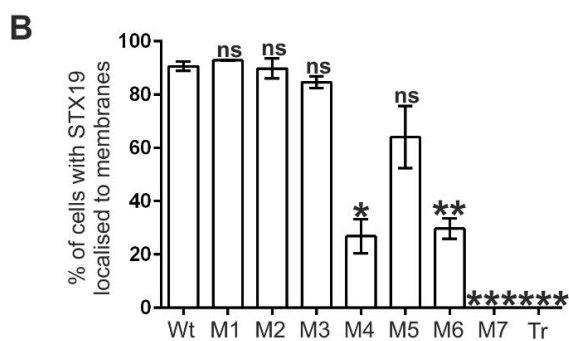
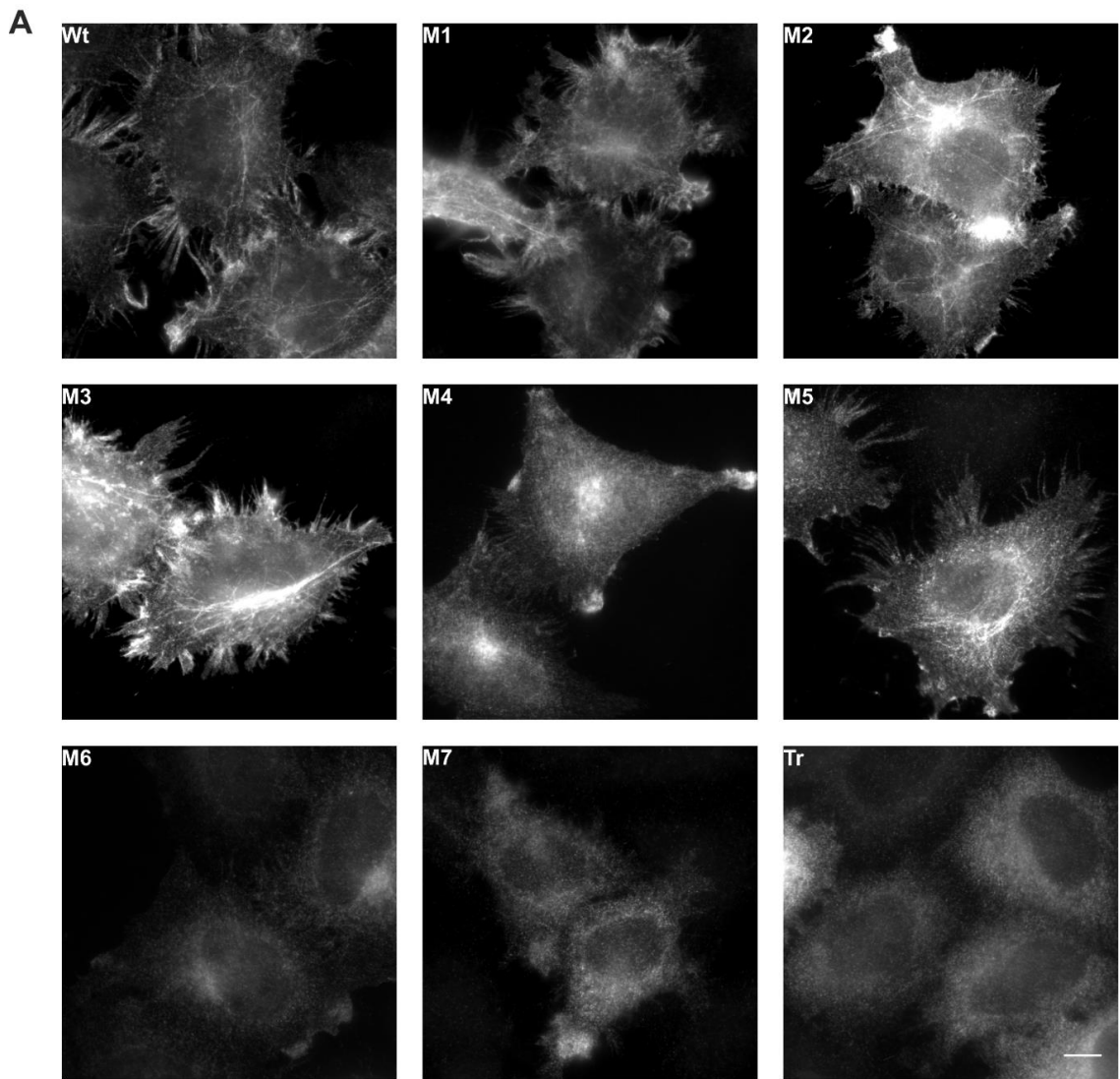
A) By microscopy. **B)** Expression levels of GFPSTX19t.

A

Repeats	GFPSTX19		GFPSTX19t		endo STX19	
	No	100 μ M	No	100 μ M	No	100 μ M
1st Quantification	98.96	50.00	96.62	42.42	85.00	11.00
2nd Quantification	95	51.64	99.20	51.55	87.00	9.00
3rd Quantification	98.13	31.33	96.46	55.56	76.00	12.00
P-value		0.0173		0.0064		0.0033

B

Repeats	Control	50 μ M	100 μ M	150 μ M
1st Quantification	1	0.3328	0.0108	0.0033
2nd Quantification	1	0.8248	0.1028	0.0028
3rd Quantification	1	0.6196	0.2003	0.0076
P-value		0.1038	0.0037	0.0000



C

Wt	CRVLCCWCCPCCSSK
M1	CRVLCCWCCP LL SSK
M2	CRVLCCW LL PCCSSK
M3	CRV LL WCCPCCSSK
M4	CRVLCCW LL PLSSK
M5	CRV LL W LL PCCSSK
M6	CRV LL WCCP LL SSK
M7	CRV LL W LL PL LL SSK
Tr	1-CRVLCCWCCPCCSSK

Figure 4-5 STX19's cysteine-rich domain is required for its correct membrane localisation.

A) HeLaM cells were grown overnight on coverslips and then transfected with either HA-tagged STX19 wt, or mutants (M1, M2, M3, M4, M5, M6, M7, Tr). 24 h post transfection, the cells were fixed, washed, permeabilized with 0.1% saponin and stained with anti-HA followed by goat anti-mouse Alexa 594 nm. **B)**

Approximately 200 cells were counted and the percentage of cells showing STX19 membrane localisation quantified (ns = not significant; * = $P < 0.05$; ** = $P < 0.01$; *** = $P < 0.001$). **C)** The sequence of mutant constructs. Images were obtained from wide field microscope at x60 oil immersion. Error bar indicates means \pm SEM from three independent experiments. Scale bar = 10 μ m.

Table 4-3 Quantification of STX19 paired cysteine mutants.

Repeats	Wt	M1	M2	M3	M4	M5	M6	M7	Tr
1st Quantification	94	93.22	94.74	85.71	38.04	60	34.48	0	0
2nd Quantification	88	92.5	92.31	87.9	26.55	46.23	32.43	0	0
3rd Quantification	90	92.97	82.4	80.36	16	86	22.11	0	0
P-value		0.291	0.8321	0.1813	0.0069	0.1472	0.0035	0.0004	0.0004

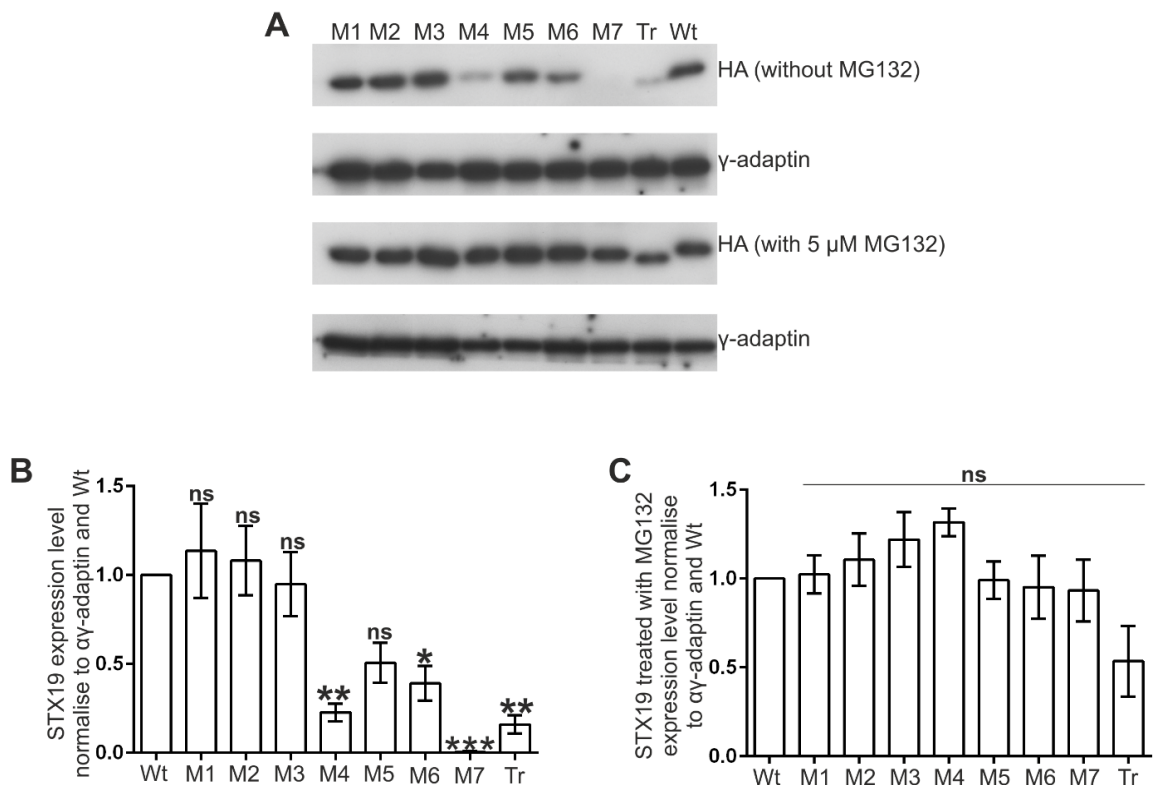


Figure 4-6 Blocking palmitoylation causes STX19 to be degraded.

A) HeLaM cells were grown overnight on 10 cm plates and then transfected with either HA-tagged STX19 wt or HA-tagged STX19 mutants (M1, M2, M3, M4, M5, M6, M7, and Tr). 8h posttransfection, the cells were treated with or without 5 μ M MG132. Whole cell lysates were collected 24 h post transfection and WB performed. The lysates were blotted with anti-HA mouse antibody followed by mouse HRP. Mouse anti-gamma-adaptin monoclonal antibody was used as a loading control. **B and C)** Western blots from three independent experiments were quantified using LI-COR Image Studio Digits Ver 4.0. (ns = not significant; * = $P < 0.05$; ** = $P < 0.01$; *** = $P < 0.001$). Error bar indicates means \pm SEM from three independent experiments.

Table 4-4 Quantification of STX19 mutants Western blot.**A) Cells without MG132. B) Cells treated with 5 μ M MG132****A**

Repeats	Wt	M1	M2	M3	M4	M5	M6	M7	Tr
1st Quantification	1	0.8784	0.8513	0.8649	0.3243	0.7297	0.5811	0.0000	0.2027
2nd Quantification	1	0.8627	0.9216	0.6863	0.1961	0.3922	0.2549	0.0000	0.0588
3rd Quantification	1	1.6667	1.4708	1.2938	0.1601	0.3955	0.3371	0.0132	0.2184
P-value		0.6595	0.7185	0.8012	0.0041	0.0477	0.0249	0.0000	0.0036

B

Repeats	Wt	M1	M2	M3	M4	M5	M6	M7	Tr
1st Quantification	1	0.8923	1.1159	1.0166	1.4363	1.0207	0.7707	0.9363	0.9338
2nd Quantification	1	1.2378	1.3549	1.5195	1.3439	1.1549	1.3073	1.2329	0.3159
3rd Quantification	1	0.9400	0.8474	1.1227	1.1713	0.7959	0.7772	0.6302	0.3567
P-value		0.8485	0.5446	0.2879	0.0550	0.9359	0.8115	0.7377	0.1453

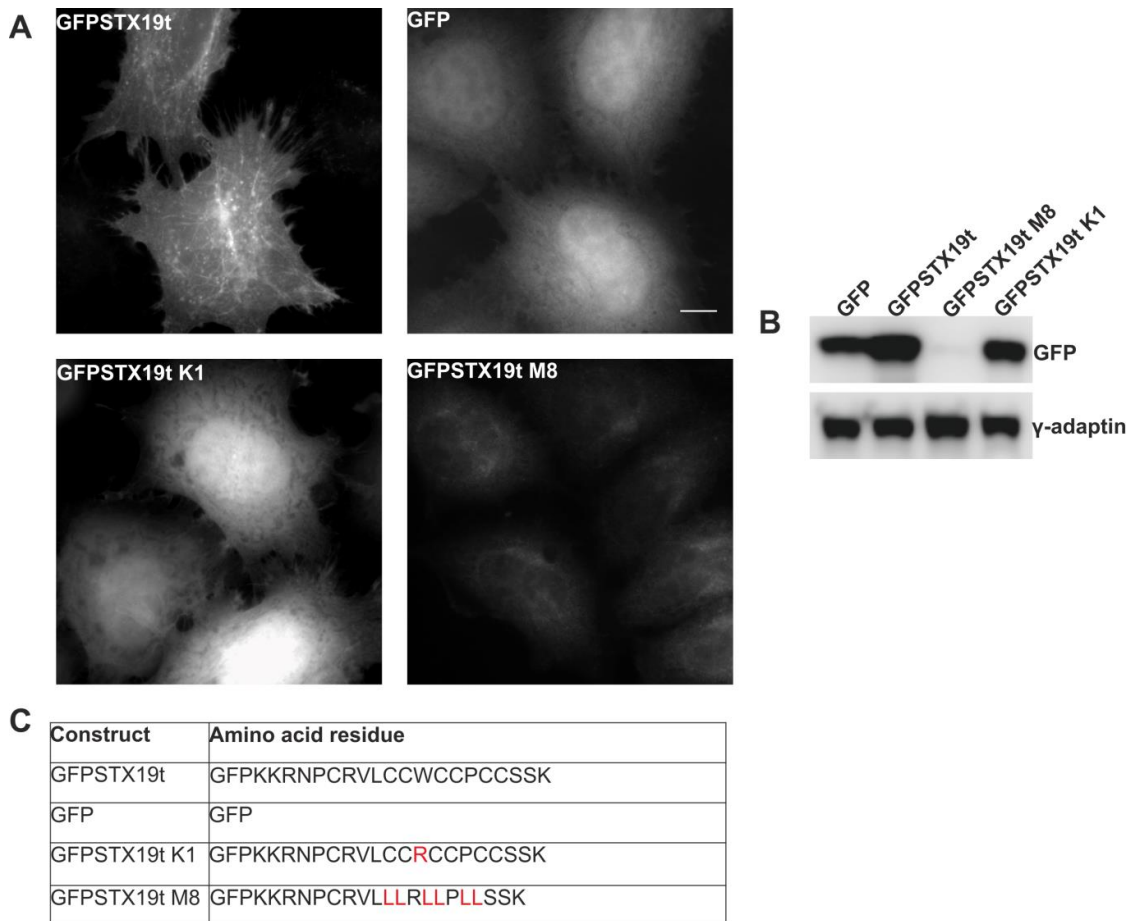


Figure 4-7 The cysteine-rich domain of STX19 is necessary and sufficient for STX19's membrane localisation.

A) HeLaM cells were grown overnight on coverslips and then transfected with either GFPSTX19t, GFP vector only, GFPSTX19t K1 or GFPSTX19t M8. 24 h post transfection, the cells were fixed, washed, permeabilized with 0.1% saponin. Images were obtained from wide field microscope at x60 oil immersion. Scale bar = 10 μ m. **B)** HeLaM cells were grown overnight on 6 cm plates and then transfected with either GFPSTX19t, GFP vector only or its mutants. Whole cell lysates were collected 24 h post transfection and WB performed. The lysates were blotted with anti-GFP rabbit antibody followed by rabbit HRP. Mouse anti-gamma-adaptin monoclonal antibody was used as a loading control. **C)** Sequences used in tagging experiments.

effectively alkylated. **C)** Shows cysteines that were cleaved as a result of hydroxylamine treatment to indicate that the cysteines contain a probable palmitoylation site.

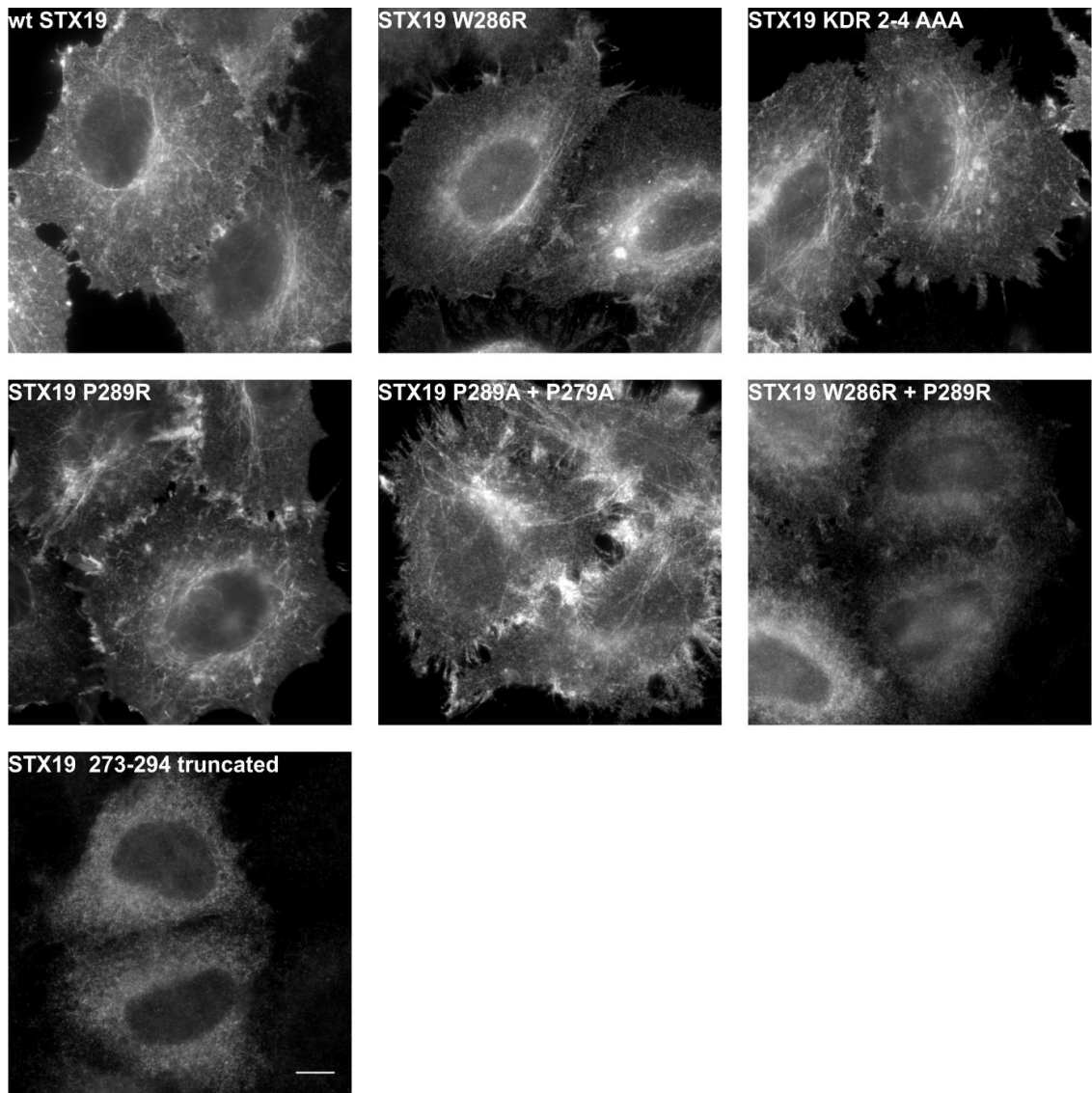


Figure 4-9 STX19's tryptophan-286 and Proline-289 might be required for its initial membrane targeting.

HeLaM cells were grown overnight on coverslips and then transfected with either HA-tagged STX19 wt, or other mutants as indicated above. 24 h post transfection, the cells were fixed, washed, permeabilized with 0.1% saponin and stained with anti-HA followed by goat anti-mouse Alexa 594 nm. Images were obtained from wide field microscope at x60 oil immersion. Scale bar = 10 μ m.

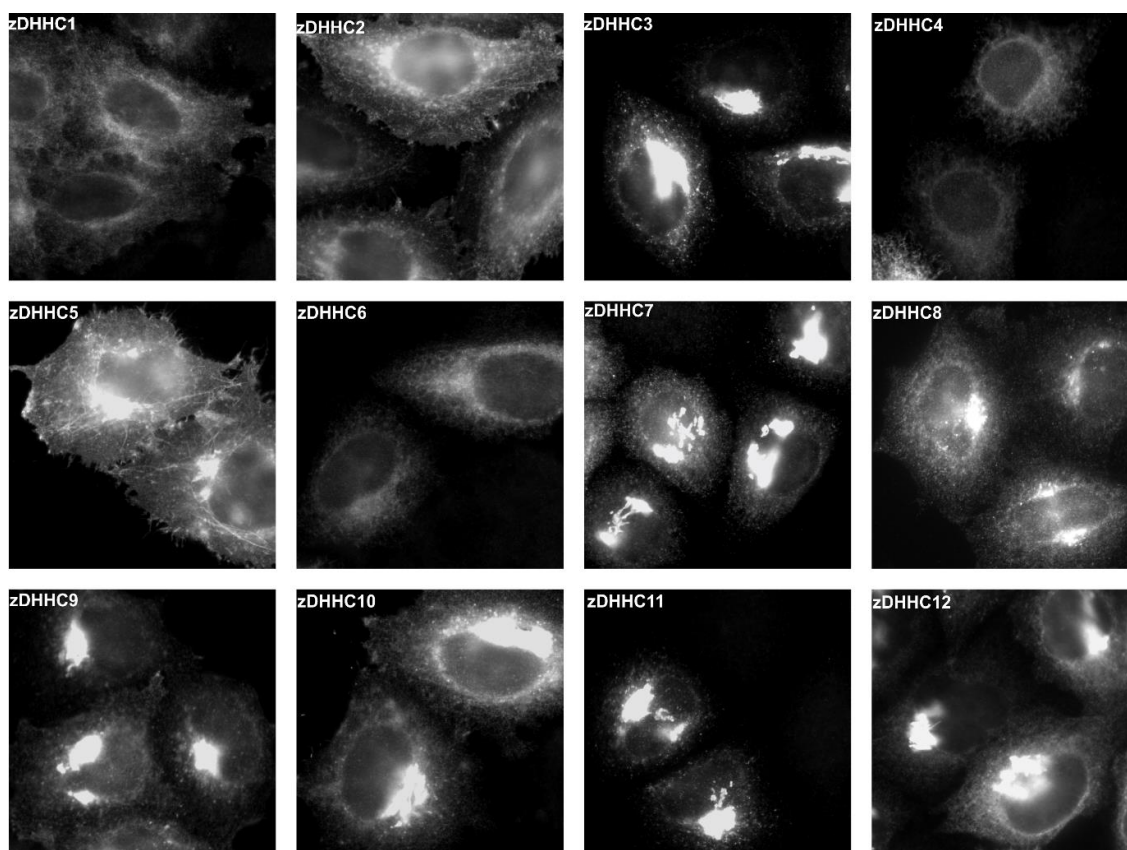


Figure 4-10 PATs (1-12) are distributed on different intracellular organelles.

HeLaM cells were grown on coverslips overnight and transfected with the HA-tagged PATs (1-12). The cells were fixed, washed, permeabilized with 0.1% saponin and stained with anti-HA followed by anti-mouse Alexa 595 nm. Images were obtained from wide field microscope at x60 oil immersion.

Table 4-5 localisation of PATs in different intracellular compartments.

Localisation	Palmitoylacyltransferases
Golgi	3, 5, 7, 9,10,11,12,13,14,15,16,17,18,19, 21, 22, 23
ER	4, 6, 7,10,18,19, 21, 23
Tubules	2, 5, 9, 14
PM	2, 5, 10, 23
Cytosolic	1, 20

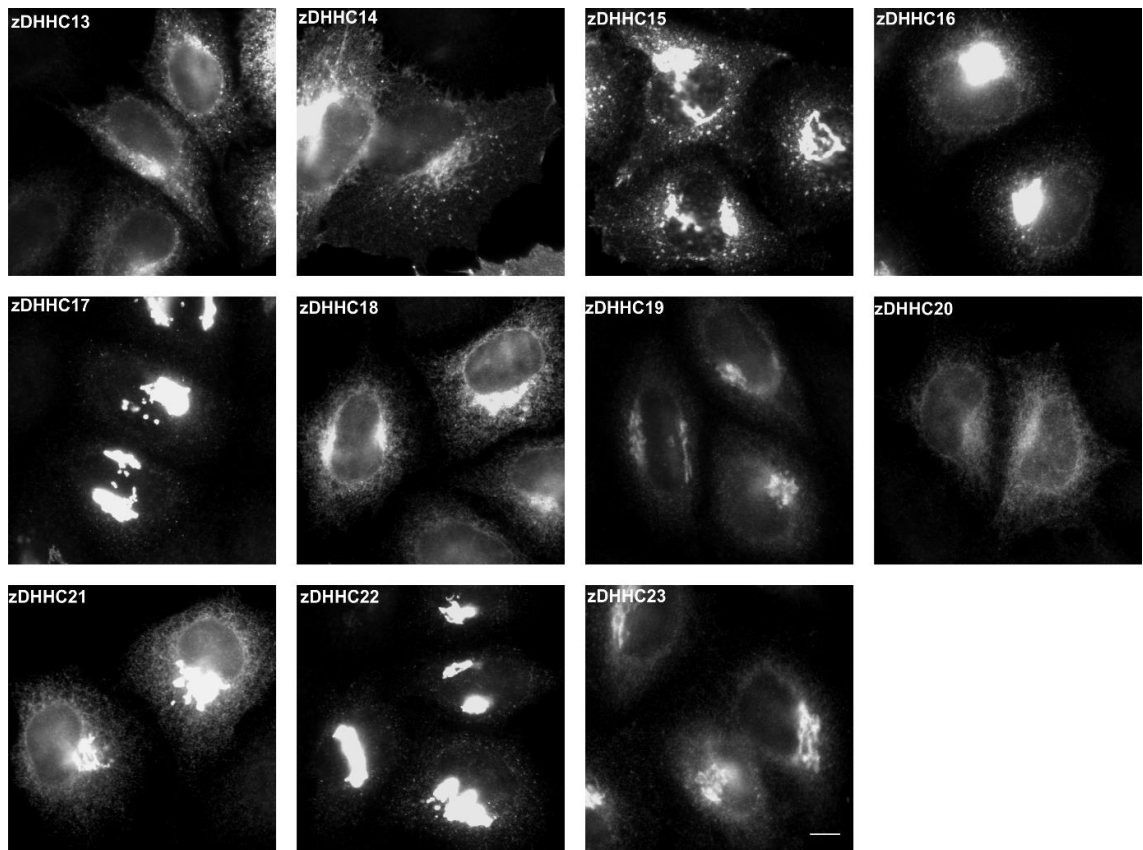


Figure 4-11 PATs (13-23) are distributed on different intracellular organelles.

HeLaM cells were grown on coverslips overnight and transfected with the HA-tagged PATs (13-23). The cells were fixed, washed, permeabilized with 0.1% saponin and stained with anti-HA followed by anti-mouse Alexa 595 nm. Images were obtained from wide field microscope at x60 oil immersion. Scale bar = 10 μ m.

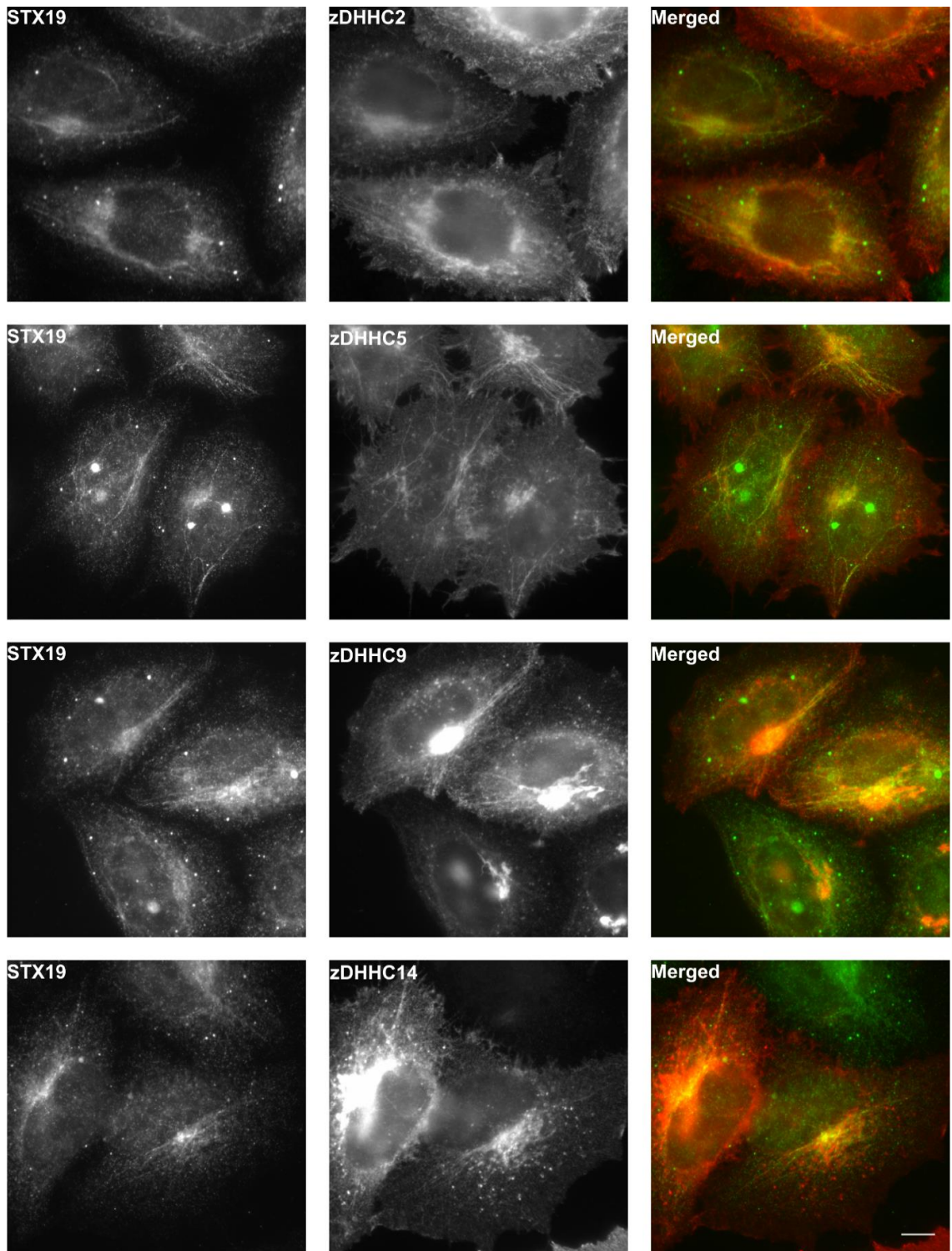
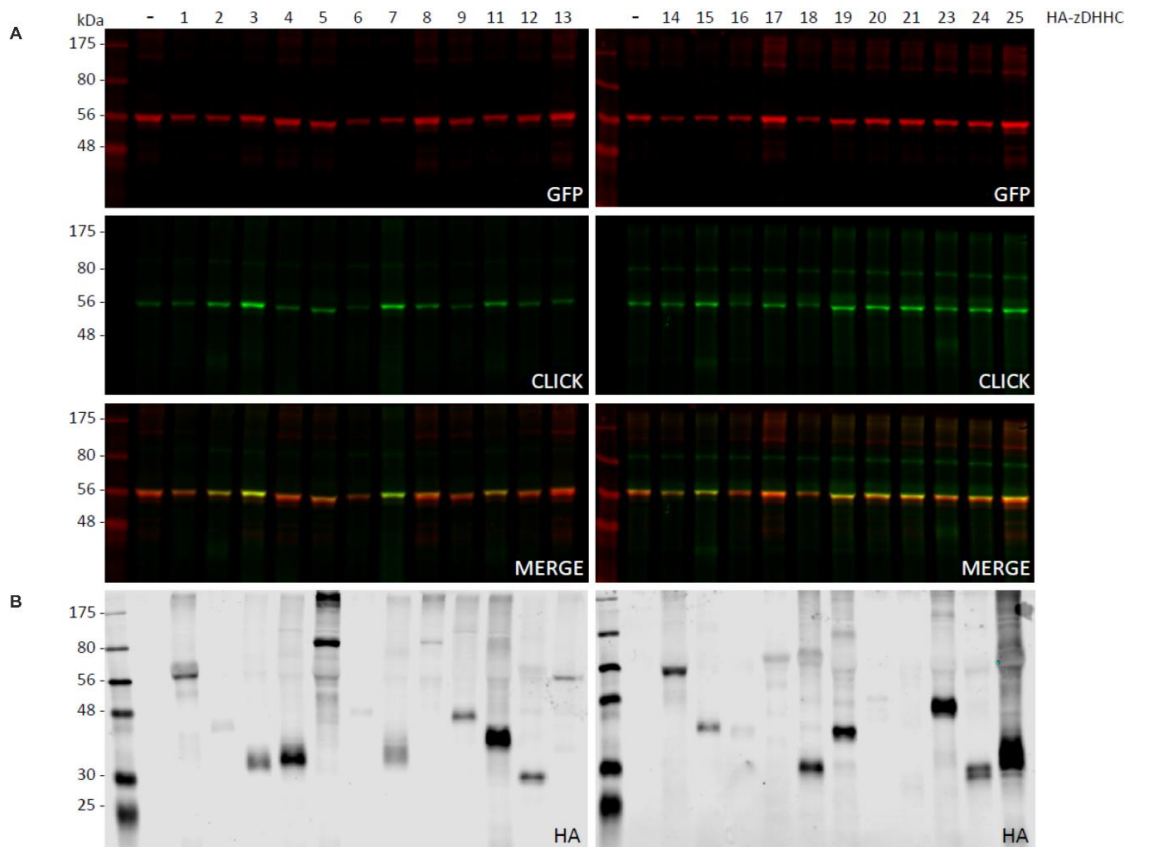


Figure 4-12 STX19 colocalises with zDHHCs (2, 5, 9 and 14).

HeLaM cells were grown on coverslips overnight and transfected with the 23 HA- tagged PATs. The cells were fixed, washed, permeabilized with 0.1% saponin and costained with anti-HA and anti-STX19 followed by anti-mouse Alexa 595 nm and anti-rabbit Alexa 488 nm. Images were obtained from wide field microscope at x60 oil immersion.

EGFP-Syntaxin19 + HA-zDHHCs



C S-acylation of EGFP-Syntaxin19

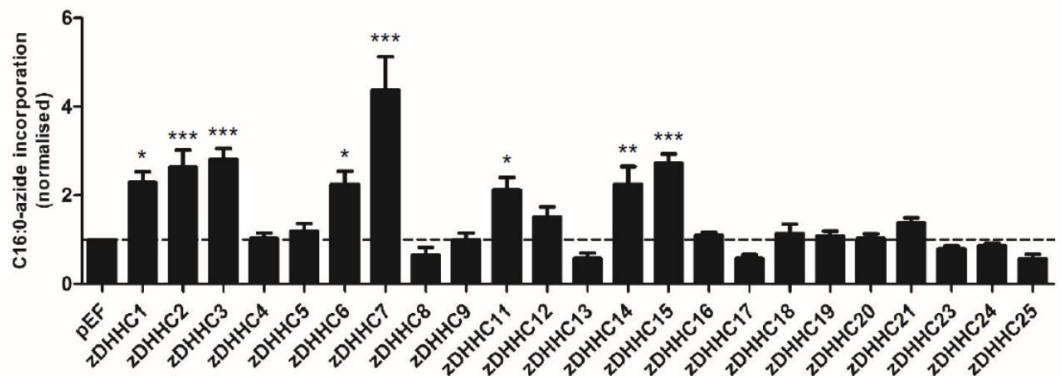


Figure 4-13 PATs involved in STX19 palmitoylation.

HEK cells were grown overnight in a 24 well plate and then cotransfected with GFPSTX19 and the 23 HA-tagged PATs library. 24 h posttransfection, the cells were incubated with 100 μ M palmitic acid azide for 3 hours at 37 $^{\circ}$ C. The cells were washed, lysed and incubated with the click reaction mixture (2.5 μ M alkyne Dye, 2 mM CuSO₄, 0.2 mM TBTA and 4 mM Ascorbic Acid) for 1 h. The samples were then acetone precipitated and resuspended in 1X SDS buffer. **A**) The expression levels of STX19 as shown by the amount of palmitate incorporated following the click reaction. **B**) Immunoblot of individual HA-tagged

PATs library. **C)** Quantification of the individual PATs contribution to the palmitoylation state of STX19. Western blots from four independent experiments were quantified using LI-COR Image Studio Digits Ver 4.0. (ns = not significant; * = $P < 0.05$; ** = $P < 0.01$; *** = $P < 0.001$).

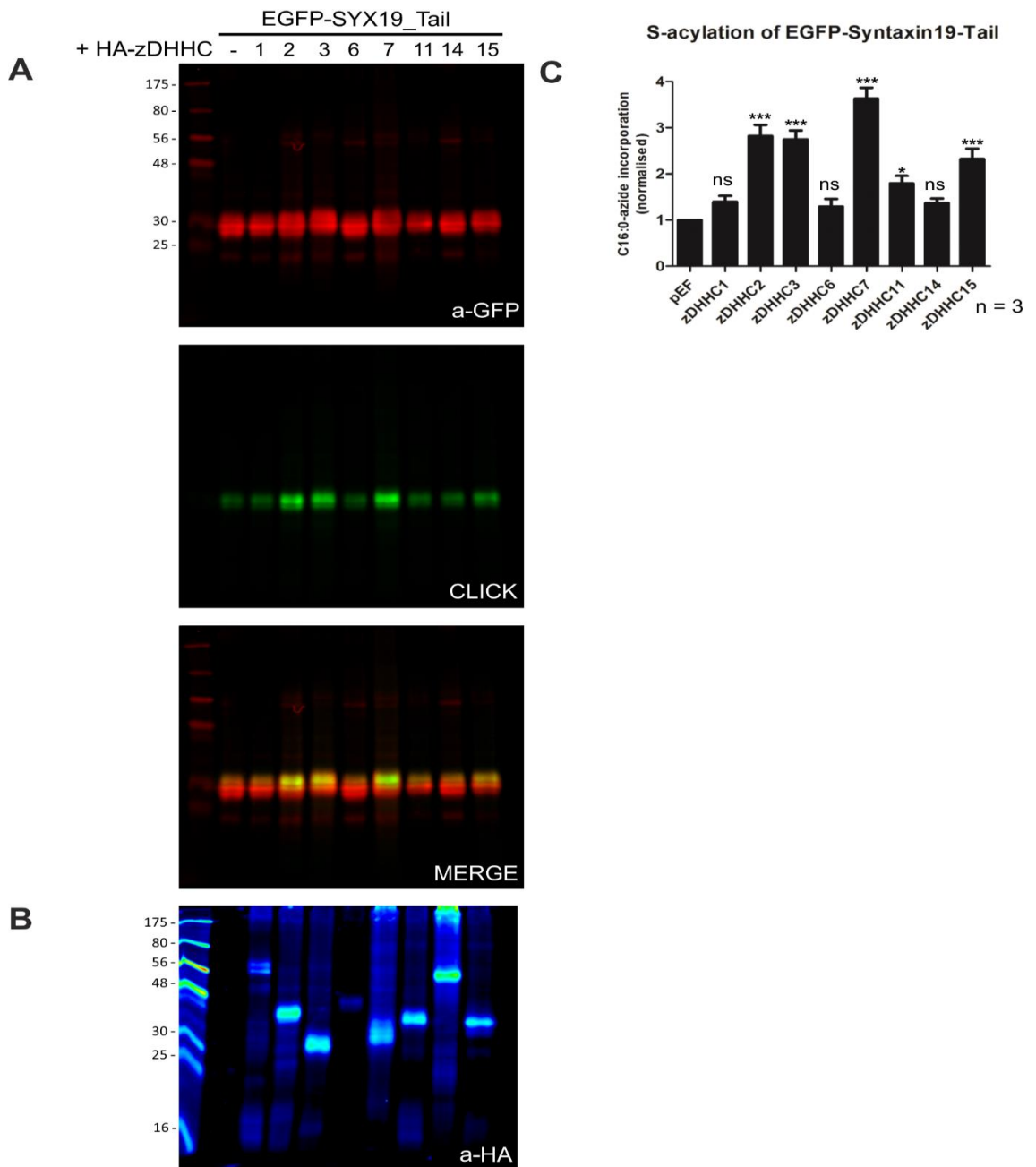


Figure 4-14 PATs involved in STX19 tail palmitoylation.

The experiment was performed as described earlier **A)** The expression levels of the STX19 tail as shown by the amount of palmitate incorporated following the click reaction. **B)** Immunoblot of individual HA-tagged PATs library. **C)** Quantification of the individual PATs contribution to the palmitoylation state of the STX19 tail. Western blots from four independent experiments were quantified using LI-COR Image Studio Digits Ver 4.0. (ns = not significant; * = $P < 0.05$; ** = $P < 0.01$; *** = $P < 0.001$).

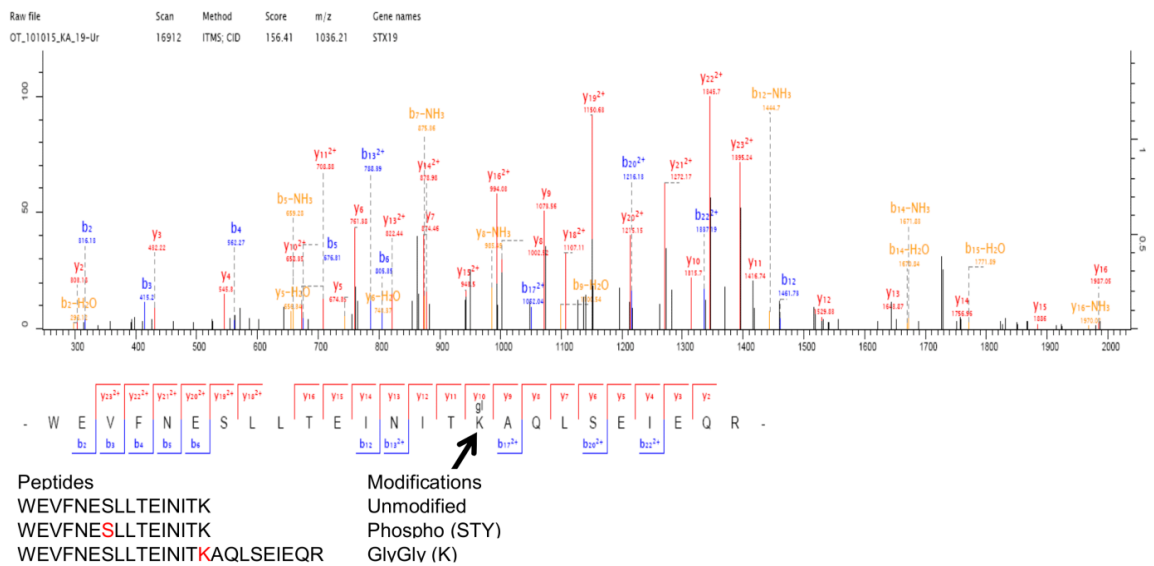


Figure 4-15 Prediction of STX19 ubiquitination sites.

HEK293T cells were seeded overnight into T175 flasks and then transfected with GFPSTX19 for 48 h. 4 h prior to sample collection, the cells were treated with or without 5 μ M MG132. The cells were collected, lysed with RIPA buffer and trapped onto GFP beads. 50 mM of TCEP and 50 mM chloro-iodoacetamide (pH 8) was added to the beads to reduce and alkylate the cysteines. Beads were washed with 50 mM Tris (pH 7.5). On-resin trypsin digest was performed and samples were run on Mass Spectrometer. Further analysis including peptide identification and modification was performed using MaxQuant (Cox and Mann, 2008). Arrow points toward modified lysine by glycine.

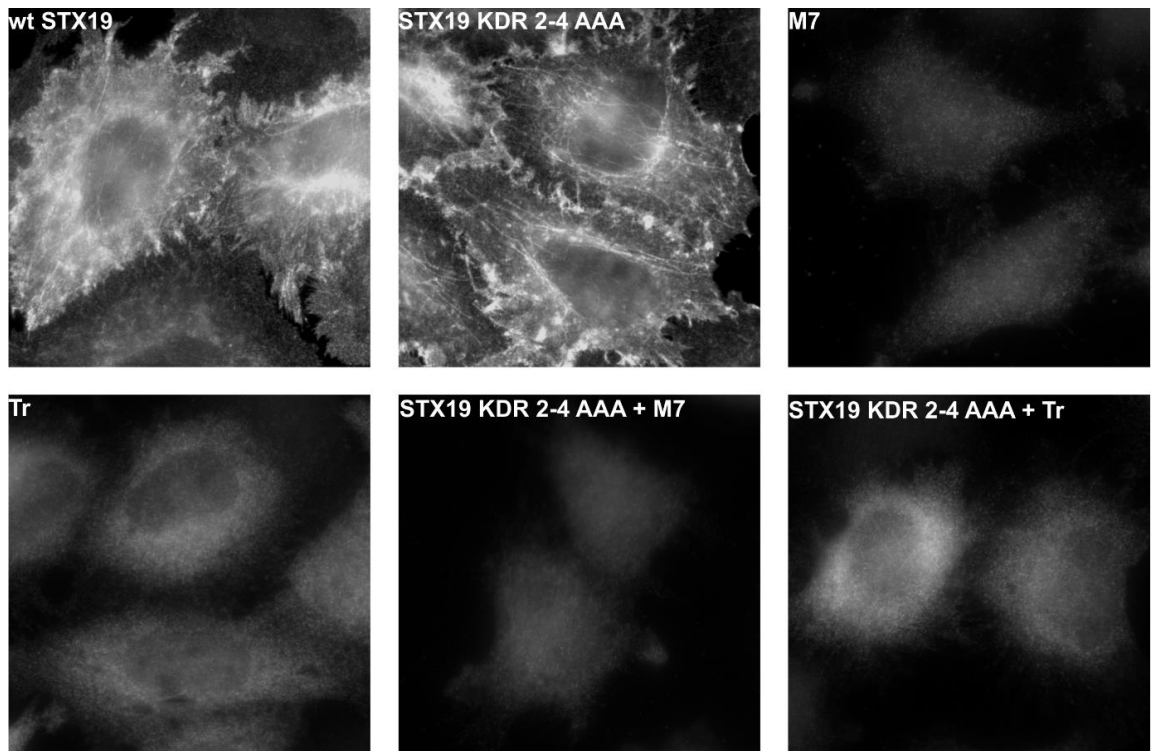


Figure 4-16 Mapping STX19 ubiquitination sites.

HeLaM cells were grown overnight on coverslips and then transfected with either HA-tagged STX19 wt, or its mutants. 24 h post transfection, the cells were fixed, washed, permeabilized with 0.1% saponin and stained with anti-HA followed by goat anti-mouse Alexa 594 nm. Images were obtained from wide field microscope at x60 oil immersion.

5 Chapter Identifying STX19 protein interacting partners

5.1 Introduction

Proteins do not function alone they form transient or stable complexes with each other. These interactions can play an important role in regulating the trafficking and function. For example, the interaction between VARP and VAMP7 regulates VAMP7's trafficking between the endosomes and the trans-Golgi network (Schafer et al., 2012, Hesketh et al., 2014). Identifying the interaction network of a protein may also give important clues to which processes and pathways the protein function on. For example, VARP binds VPS29 a subunit of the retromer complex (Hesketh et al., 2014). The retromer complex has been shown to play an important role in endosome to TGN and endosome to PM sorting (Hesketh et al., 2014).

Several approaches have been developed to identify protein interacting partners. Notable among them include yeast two-hybrid screening, affinity capture mass spectrometry approaches (Glutathione sepharose transferases pull down, co-immunoprecipitation) and biotinylation proximity dependent assays (Bio-ID). All these approaches have their advantages and limitations.

Yeast two-hybrid screening is a very useful tool to identify and map millions of novel protein interactions (Fields and Song, 1989). However, this technique is limited by the complexity of the cDNA library, inability to express the bait proteins and high positive and false negative rates (Huang et al., 2007). Affinity capture mass spectrometry overcomes the limitation of inappropriate folding of some proteins in the yeast system. However, it is limited by the expression levels of the proteins in the cell lysate, the affinity of the proteins for the beads and the stringency of the washing conditions to reduce non-specific proteins from remaining bound to the beads.

Another approach developed for detecting protein interactors is Bio-ID. Bio-ID was first developed by Fernández-Suárez et al., 2008. BirA is a biotin ligase from *E. coli*. The authors fused BirA to a protein of interest and then attached Biotin acceptor tag (BAT) to another protein. If the proteins interact the BirA biotinylates the BAT which could then be detected by streptavidin staining (Fernandez-Suarez et al., 2008). The method was modified by Burke group, whereby they used a mutant version of BirA* (R118G) that can simply biotinylate any protein that is in close proximity (Roux et al., 2012).

The aim of this chapter is to identify and characterise the protein interaction network for STX19. I used the following approaches:

1. Yeast two-hybrid screen (Performed commercially by Hybrigenics Services SAS).
2. Bio-ID coupled to mass spectrometry using HeLaM stable cell line expressing HA-tagged BirA*STX19.
3. GFPTRAP-IPs using GFP-tagged STX19 to pull down STX19 protein interacting partners.
4. siRNA depletion of STX19 to examine the effect of STX19 depletion on some of the identified protein interactors.

5.2 Results

5.2.1 Identifying STX19 interacting partners using a yeast two-hybrid screen

A commercial Y2H screen was performed using STX19 as bait. Residues 1-279 were used as they do not contain the cysteine-rich domain which may interfere with the assay. STX19 was fused to the C-terminus of pB27 N-LexA vector and then expressed in yeast. 55.6 million potential interactions were screened using a Human colon library and 312 colonies grew under the selection conditions. The plasmid DNA was isolated from the yeast and sequenced. Out of the 312 colonies, 70 unique protein sequences were identified. The potential interacting partners were then categorised as either very high (2), high (8), good (6), moderate (41) and low (2) confidence interactors (Table 5-1). To validate these

potential interactions, we have used Bio-ID and conventional immunoprecipitations. The potential interacting proteins will be discussed in more detail later in the chapter.

Table 5-1 Shortlisted proteins from STX19 yeast two-hybrid screen results.

The selection was based on functional relevant to STX19.

Bait



Prey: Human Colon_RP1

Protein Name	Length (aa)	Function	Interaction domain (aa)	Independent clones
SNAP23	211	vesicle docking and membrane fusion	N/A ¹	1
VAMP7	260	early to late endosome fusion, exocytosis	N/A ²	3
TRIO	2999	Rho guanine nucleotide exchange factor, cell migration, cytoskeleton rearrangement	259-479	3
ZWINT	277	kinetochore formation and spindle checkpoint activity	63-277	1
DST	4499	microtubule and cytoskeleton organisation; cell polarity, adhesion and migration	3596-3708 4193-4362	6
MACF1	7391	Golgi to PM protein transport; microtubule and cytoskeleton organisation; adhesion and migration	3373-3509	13
DES	470	cytoskeleton and intermediate filament organisation	264-421	5
DMD	1225	constituent of the cytoskeleton	483-653	9
GOLGA4	2243	Golgi to PM protein transport; vesicle mediated transport	1135-1305	2
IFT57	429	cilium assemble; intercilary transport	244-330	9
GGA3	651	vesicle mediated and intracellular protein transport	41-170	2
COG5	860	ER to Golgi and intra-Golgi protein transport	102-176	21
ATP6V1E1	226	transferrin transport; macroautophagy	1-110	15
KIAA1033	1173	WASH complex; endosomal protein transport and organisation	N/A ³	4
KIF5B	963	vesicle transport along microtubule and cytoskeleton	524-687; 763-926	5
KIF3B	747	mitotic spindle assembly and organisation; vesicle mediated transport	427-641	1
KRT20	424	intermediate filament organisation; regulation of protein secretion	256-343	22
KANSL1L	987	histone acetyltransferase complex	307-435	9
PSMD7	324	protein polyubiquitination	148-316	2
RABEP1	862	membrane fusion and vesicle mediated transport	677-818	1
RASSF8	419	adherens junction maintenance	103-211	1
SEC10/EXOC5	708	exocyst complex, vesicle docking and protein transport	16-172	1
SEC8/EXOC4	974	exocyst complex, vesicle docking and protein transport	546-663	2
SEC6/EXOC3	745	exocyst complex, vesicle docking and protein transport	4-136	2
TLN1	2541	actin cytoskeleton organisation; integrin mediated cell adhesion	1899-2075	1
MOB4	225	membrane trafficking	69-212	1

NA¹ denotes coding sequence out of frame

NA² denotes coding sequence lies only in the 5' untranslated region (UTR)

NA³ denotes coding sequence lies in unidentified frame

5.2.2 Generating and testing BirA*STX19 for Bio-ID assay

The Y2H screen identified a large number of potential interacting proteins. This number was too large to validate using conventional approaches. To validate the Y2H data and identify proteins which may localise to the same compartment as STX19 I took a Bio-ID based approach (Roux et al., 2012, Firat-Karalar et al., 2014, Morriswood et al., 2013). I generated a viral expression construct where HA-tagged BirA* was cloned at the 5' end of STX19 (Figure 5-2). The construct was then transduced into HeLaM cells to generate a mixed population of cells stably expressing BirA*STX19. To determine if the STX19 construct was localised correctly and whether BirA* had enzymatic activity, I incubated cells with or without 50 μ M of biotin for 24 h and then performed immunolocalisation studies. The cells were stained with antibodies to HA and streptavidin to detect biotinylated proteins. As shown in Figure 5-3 the BirA*STX19 is localised to TRE and the plasma membrane (Figure 3-2). This localisation is very similar to that observed with HA- or GFP-tagged STX19 indicating that the BirA* tag is not altering the steady-state distribution of STX19. In the control cells, the streptavidin staining is localised to the mitochondria (Figure 5-3) (Roux et al., 2012). However, in the cells incubated with biotin, the staining is found predominantly on the plasma membrane and TRE (Figure 5-3). This observation indicates that the BirA* is active and biotinylated proteins that are localised to the same compartment as STX19.

To validate the localisation studies immunoblotting experiments were also performed. Whole cell lysates were prepared from control cells (non-transduced) and cells expressing BirA*STX19 either in the presence or absence of biotin. The samples were probed for HA and biotin. As predicted, we only detected a band at 71 kDa in the BirA*STX19 HeLaM clonal cells and not in the non-transduced cells (Figure 5-4). In the non-transduced cells and samples which were not incubated with biotin, the streptavidin-HRP only detected a small number of bands (Figure 5-4). However, in the BirA*STX19 sample, incubated with biotin, there was a dramatic increase in the number of bands detected (Figure 5-4). This data suggests that the BirA* tag on STX19 is active

and capable of biotinylating proteins. Overall my data suggests that the HA-tagged BirA*STX19 is localised correctly and is capable of biotinylating proteins.

5.2.3 Identifying STX19 interacting partners using Bio-ID approach

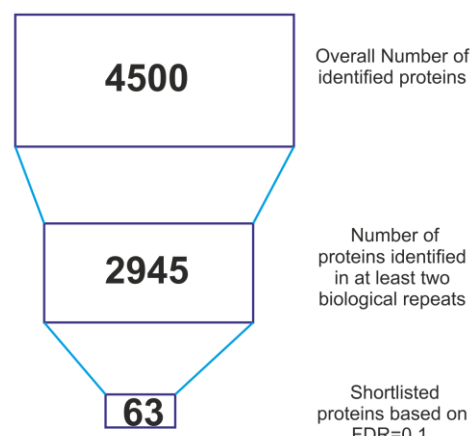
To identify proteins that are biotinylated as a result of the BirA*STX19, we have coupled our Bio-ID approach to mass spectrometry. BirA*STX19 HeLaM cells were cultured in four T175 flasks (two per group) with or without 50 μ M of biotin and then purified using streptavidin agarose beads. The samples were run on SDS gel and coomassie stained and then analysed and quantified using a label-free mass spectrometry-based approach (Figure 5-5) (Patel et al., 2009). We predict that proteins that either interact with or are in close proximity to STX19 will be biotinylated and should be significantly enriched compared to the no biotin control. We identified and quantified 2945 number of proteins in both the +/- biotin samples. From the four biological repeats, repeats 2, 3, and 4 had a normal distribution curve (**Figure 5-6**). Moreover, there was a good correlation within and among the groups (Figure 5-7). The correlation between the Intensity Biotin_rep4 versus Intensity Biotin_rep2, Intensity Biotin_rep3, Intensity Control_rep2, Intensity Control_rep3, and Intensity Control_rep4 were 0.874, 0.946, 0.848, 0.918, and 0.889 respectively (Figure 5-7). The correlation between the Intensity Biotin_rep3 versus Intensity Biotin_rep2, Intensity Biotin_rep4, Intensity Control_rep2, Intensity Control_rep3, and Intensity Control_rep4 were 0.865, 0.946, 0.841, 0.918, and 0.878 respectively (Figure 5-7). The correlation between Intensity Biotin_rep2 versus Intensity Biotin_rep3, Intensity Biotin_rep4, Intensity Control_rep2, Intensity Control_rep3, and Intensity Control_rep4 were 0.865, 0.874, 0.917, 0.868 and 0.832 respectively (Figure 5-7). Therefore, the biological repeats 2, 3, and 4 were used for the subsequent analysis.

STX19 was the most enriched protein with the highest average ratio of biotin to control (390.27) followed by SNAP23, NDRG1, ERBB2IP, VANGL, SLC30A1, STXBP5, SNAP25, TAP1, zDHHC5, ZWINT and SNAP29 in that order with average ratio of biotin to control 204.7, 83.8, 79.7, 66.274, 58.36, 48.79, 46.31, 40.08, 39, 34 and 31 respectively (Table 5-2). The 2945 number of proteins identified was shortlisted to 63 based on false discovery rate of 0.1. The

proteins shortlisted had an average ratio of biotin to control to be above 6.4 fold (Table 5-2). 46 out of the 63 shortlisted proteins all had their overall peptide identified to be unique to them (Table 5-2). Also, 35 out of 63 had a good coverage of above 10% (Table 5-2). This shows that above 70% of the selected proteins exceeds the threshold score value set in the Mascot.

Table 5-2 Shortlisted proteins from STX19 Bio-ID results.

Protein	Ratio biotin treated vs control	Mascot score	Number of peptides (Unique)	Coverage (%)
STX19	390.27	191.77	11(11)	38.4
SNAP23	204.7	323.31	16(16)	74.4
NDRG1	83.8	8.8682	4(4)	18
ERBB2IP	79.7	284.26	40(40)	36.3
VANGL1	66.274	153.13	16(16)	37
SLC30A1	58.36	20.01	6(6)	13.8
STXBP5	48.79	-2	5(1)	9.5
SNAP25	46.31	256.31	17(7)	64.1
TAP1	40.08	82.352	6(6)	14.4
ZDHHC5	39	42.13	13(11)	25
ZWINT	34.69	19.859	3(3)	13.4
SNAP29	31.29	23.278	6(6)	37.6
SLC4A7	27.63	19.277	9(2)	2.3
FAM83B	24.95	41.487	6(6)	9.2
ROR2	23.57	27.948	6(6)	8.9
PPF1BP1	23.14	63.735	12(10)	13.7
DMD	22.62	114.73	12(2)	2.6
NUBP2	19.46	27.138	5(5)	31.4
MTIF2	19.07	9.627	4(4)	7
PTRF	16.96	69.659	6(6)	19.5
MCM3AP	16.17	75.433	13(13)	11.2
TRIOBP	15.43	95.038	16(16)	9.4
PACSN3	15.2	51.975	5(5)	17.7
BEGAIN	15.2	15.129	7(7)	15.3
EPB41L2	15.15	154.16	23(23)	35.6
TNKS1BP1	14.15	157.8	21(21)	20.1
TOPBP1	13.61	14.919	6(6)	4.8
AHNAK	13.12	323.31	438(438)	83.3
FLNA	13.05	5.1641	149(2)	0.7
MCAM	12.18	15.608	8(8)	17.3
TRIO	11.97	18.765	6(6)	3.4
PALM	11.56	15.581	5(5)	20.4
AGPS	11.27	104.06	15(15)	28.6
MYO18A	11.03	18.814	9(9)	6.4
SCRIB	10.96	128.25	42(39)	27.4
SASS6	10.86	32.485	8(8)	22.5
GNPAT	10.44	11.304	3(3)	6.8
ZFP91-CNTF	10.33	11.748	2(2)	8.9
UTRN	10.17	93.661	20(19)	7.8
CYP51A1	9.93	5.853	2(2)	4.7
SPTBN2	9.63	32.965	20(13)	9.2
MINK1	9.61	27.363	10(4)	6.2
SUZ12	9.56	34.455	7(7)	16.2
VPS13C	8.8	28.467	12(12)	4.6
SLC3A2	8.66	323.31	41(27)	50.4
SNTB1	8.52	14.831	6(6)	16.5
SRCAP	8.42	13.398	6(6)	2.8
NF1	8.28	12.816	8(8)	3.7
SPG20	7.56	51.282	4(4)	9.5
EGFR	7.19	144.75	26(24)	25.7
NSF	7.1	38.512	16(16)	26.4
SBF1	6.78	63.506	13(13)	11.6
DST	6.61	322.16	34(32)	8.2
TARS2	6.58	20.667	8(8)	22.5
PRTFDC1	6.492	5.923	4(4)	21.3



5.2.4 Bioinformatics analysis of STX19 interacting partners

To gain insight into STX19 function, I have grouped putative STX19 interacting partners into classes, biological processes, cellular components, biochemical properties and palmitoylation state using the GENEONTOLOGY PANTHER

classification system from Gene ontology consortium, SwissPalm Database, and UniProt consortium (Ashburner et al., 2000, Gene Ontology, 2015, Blanc et al., 2015, UniProt, 2014). At present, it is unclear what percentages of these proteins directly interact with STX19 or are just in close proximity with STX19 so care must be taken when interpreting these results. I analysed 81 potential interacting partners (Y2H and Bio-ID) using both the Gene ontology and STRING consortia databases. I have identified five main groups including SNARE, membrane trafficking, non-motor actin binding, actin family cytoskeleton and cytoskeletal proteins contributing to 6%, 20%, 9%, 13% and 20% respectively (Figure 5-8). Some proteins were found in more than one class group (Figure 5-8). STX19, VAMP7, SNAPs 23, 25 and 29 were found both in the SNARE and membrane trafficking group (Figure 5-8). DST, MACF1, DMD, FLNA, UTRN, SPTBN2 and SNTB1 were found in non-motor actin binding, actin family cytoskeleton and cytoskeletal groups (Figure 5-8). Some proteins such as SCRIB, VANGL1, ZWINT1, ZDHHC5 and NDRG1 were not assigned to any group (Figure 5-8).

On the basis of biological processes, I have identified that most proteins were involved in protein transport followed by cytoskeletal organisation, exocytosis and membrane fusion in that order (Figure 5-9). This is consistent with what we think STX19's is likely to be doing. I have also provided a network of interaction between STX19 and the remaining proteins using the STRING consortium database (Franceschini et al., 2013). STX19 may potentially link several cellular components including cytoskeleton, cell junction, SNARE complex, focal adhesion, adheren junction and actin cytoskeleton (Figure 5-10; Figure 5-13).

The Bio-ID data does not allow you to determine whether the enriched proteins are in close proximity or are physically interacting with your bait protein. To try and gain an insight into this I have grouped my data based on how they interact with membranes. We predict that peripheral proteins are most likely to be the proteins that directly interact with STX19. We predict that transmembrane proteins are unlikely to be direct binding partners of STX19 and may be cargos which are on the same pathway as STX19. About 70% of the proteins are

predicted to either be peripheral membrane proteins or cytosolic. 15% of the enriched proteins are transmembrane (Figure 5-11; Table 5-4).

I have also mined my data to determine if palmitoylated proteins are enriched in the data. Based on my tagging studies it is clear that many palmitoylated proteins colocalise with STX19 so it is possible that they will be in close proximity with STX19. 42% of the enriched proteins were identified to be palmitoylated using the SwissPalm database (Table 5-4; Figure 5-12) (Blanc et al., 2015). Examining this list in more detail indicated that many non-palmitoylated proteins were included in the palmitoylated list indicating that these numbers were unreliable. Therefore, I narrowed the list down by focusing on proteins that have experimentally validated to be palmitoylated. 15% out of the total potential palmitoylated proteins had specifically targeted studies performed (Table 5-4; Figure 5-12). They include ZDHHC5, PALM, ERBB2IP and SNAPs 23, 25 (Table 5-4; Figure 5-12).

To bioinformatically validate my data, I have compared my Bio-ID and Y2H data to publicly available interaction data sets for STX19 (BioGRID, STRING consortium and HA-STX19 IPs) (Huttlin et al., 2015, Franceschini et al., 2013, Gordon et al., 2010). 23 out of the 88 interactions have been observed in two or more of the available data sets (Table 5-3). SNAP23 was found in all the studies, ZWINT, DST and VAMP7 were found in three of the data sets (Table 5-3). Using this approach, I have been able to generate a short list of high confidence interacting proteins that includes proteins such as SNAPs 23, 25 and 29; STXBP1, 2 and 5; VAMP7, DST, MACF1, TRIO, DMD, EXOC4.

Table 5-3 Shortlisted proteins based on current and previous studies.

Protein	Bio-ID	BioGRID	Yeast two-hybrid screen	HA-STX19 IP
SNAP23	Yes (204.7)	Yes	Yes	Yes
STXBP5	Yes (48.79)	Yes	No	No
SNAP25	Yes (46.31)	No	No	Yes
ZWINT	Yes (34.69)	Yes	Yes	No
SNAP29	Yes (31.29)	No	No	Yes
DMD	Yes (22.62)	No	Yes	No
TRIO	Yes (11.97)	No	Yes	No
DST	Yes (6.61)	No	Yes	Yes
STXBP1	Yes (5.59)	Yes	No	No
STXBP2	Yes (6.48)	Yes	No	No
TBK1	Yes (5.92)	Yes	No	No
VAMP7	Yes (1.8)	Yes	Yes	No
MACF1	Yes (1.29)	No	Yes	No
ATP6V1E1	Yes (2.88)	No	Yes	No
KIAA1033	Yes (1.39)	No	Yes	No
KIF5B	Yes (2.6)	No	Yes	No
PSMD7	Yes (2.51)	No	Yes	No
RABEP1	Yes (2.18)	No	Yes	No
EXOC4	Yes (6.36)	No	Yes	No
TLN1	Yes (1.75)	No	Yes	No
PRMT3	Yes (2.01)	Yes	No	No
KDM1A	Yes (2.68)	Yes	No	No
TP53RK	Yes (2.33)	Yes	No	No

Yes () = below the threshold FDR= 0.1. The () denotes ratio biotin

5.2.5 Validating yeast two-hybrid screen and Bio-ID data using GFPTRAP IP approach

From the Y2H and Bio-ID experiments, we have identified 81 candidate proteins. As a proof of principle, I have attempted to validate 3 potential interactions using a co-immunoprecipitation based approach.

I have developed a GFPTRAP IP approach. In this method, cells are transfected with GFP-tagged expression constructs and the tagged proteins immuno-isolated using a single chain anti-GFP antibody coupled to sepharose beads. To test this method, I have looked at SNARE interactions. HeLaM cells were transfected with GFPSTX19 and the STX19 immuno-isolated using

GFPTRAP beads. The Western blot analysis shows that GFPSTX19 was effectively trapped onto the beads (Figure 5-14). The samples were then blotted with antibodies against VAMPs 2, 3, 4, 7, 8 and SNAPs 23 and 29. STX19 was able to immunoprecipitate VAMPs 3 and 8; SNAPs 23 and 29 and to a less extent with VAMP7 (Figure 5-14). My results agree well with previous studies using either affinity capture mass spectrometry or HASTX19 proteomics (Gordon et al., 2010, Huttlin et al., 2015). At present it is unclear why our Bio-ID experiments did not detect VAMP3 and VAMP8. It is possible that the conditions used were not favourable for detecting SNARE complexes (experiments were performed in the absence of NEM).

5.2.5.1 ZWINT1

ZWINT1 was found both in the Y2H screen and was enriched in the BirA*STX19 treated group (Table 5-1; Table 5-2). GFPTRAP IPs were performed with STX19 and STX7 as a negative control. The samples were blotted for GFP and endogenous ZWINT1. ZWINT1 was immunoprecipitated only with STX19 indicating that the interaction was specific (Figure 5-15). This data strongly suggests that ZWINT1 is a real interacting partner of STX19.

5.2.5.2 MACF1 and DST

Attempts to co-immunoprecipitate endogenous MACF1 and DST with GFP-STX19 have proven to be technically challenging. Under the standard GFPTRAP conditions, MACF1 is not immuno-isolated with STX19 (Figure 5-16). At present, it is unclear why this is the case. It is possible that the interaction between MACF1 and STX19 is weak or transient.

To validate the Bio-ID experiments, I have determined whether MACF1 or DST are enriched in the Bio-ID pull downs based on immunoblotting. BirA*STX19 cells were incubated either with or without biotin for 24 hours and the biotinylated proteins isolated using streptavidin beads. The samples were then blotted for biotin, endogenous MACF1 and DST. MACF1 and DST were significantly enriched in the cells treated with biotin confirming the mass spectrometry analysis (Figure 5-17). However, we were unable to detect a band at the correct MW for DST in the cell lysate suggesting that care must be taken when interpreting the DST blotting result (Figure 5-17).

5.2.6 STX19 depletion affects the organisation of actin cytoskeleton

From our yeast two-hybrid screen and Bio-ID data, we have identified two spectraplakins: Dystonin (DST) and microtubule actin cross-linking factor (MACF1) as potential interacting partners of STX19. DST and MACF1 have been shown to be involved in regulating actin/microtubule dynamics and focal adhesion turnover (Roper et al., 2002, Brown, 2008, Wu et al., 2008, Ryan et al., 2012). We have also identified several other proteins that are involved in the organisation of the actin cytoskeleton including TRIO, DES, DMD, and TLN1 that may localise with or interact with STX19. To determine if STX19 plays a role in regulating the organisation of the cytoskeleton or the localisation of MACF1 and DST we depleted STX19 using siRNA. Cells were stained for MACF1, DST, tubulin and KRT20 as a marker of the microtubules and intermediate fibres respectively (Zhou et al., 2003). Depletion of STX19 causes a dramatic change in cell morphology (Figure 3-8). The cells become larger and develop well-organised lamellipodia. This type of phenotype is often observed when cells undergo an epithelial to mesenchymal transition (Mellman and Nelson, 2008, Bryant and Mostov, 2008). In addition to the gross changes in cell morphology, there are also dramatic changes in the organisation of the cytoskeleton (Figure 5-18). The intensity of the tubulin staining is dramatically increased in the STX19 depleted cells and DST cytoskeletal structures become large and robust (Figure 5-18). There is also a significant increase in KRT20 intermediate filament staining (Figure 5-18). Focal adhesion structures in the STX19 depleted cells may also become altered with the MACF1 positive structures becoming slightly longer in STX19 depleted cells (Figure 5-18). These observations suggest that STX19 might have a role in regulating cell polarity and cell migration. However, these phenotypes have only been observed using one siRNA so these results need to be confirmed either by expression of an RNAi-resistant form of STX19 or using an alternate siRNA. In addition, more detailed and quantitative analysis must be performed before any strong conclusions can be drawn.

5.3 Discussion

5.3.1 Summary of results

I have used both Y2H and Bio-ID analysis to identify novel STX19 interacting partners. I have identified more than 75 novel proteins that may interact or colocalise with STX19 including NDRG1, ERBB2IP, VANGL1, ZDHHC5, MACF1, DST. SNAP23, ZWINT1, DST, DMD, MACF1 and EXOC4 were identified in both Y2H and Bio-ID based approaches indicating that STX19 may directly interact with them. SNAP23, ZWINT1, PRMT3, TBK1, KDM1A, TP53RK, STXBPs 1, 2, and 5, were previously identified as STX19 interactors using high throughput based approaches (Huttlin et al., 2015). From the list of STX19 interactors, I suggest that STX19 has a novel role in regulating cytoskeleton organisation, cell migration and cell polarity. SNAREs have previously been shown to be important players in establishing cell polarity as well as cell migration (Sharma et al., 2006, Low et al., 2006, Day et al., 2011, Veale et al., 2011)

5.3.2 The role of SNAREs in cell migration and cell polarity.

Based on our BioID data and RNAi studies it has become apparent that STX19 may be an important player in regulating cell migration and cell polarity. Cell migration and cell polarity are physiological processes that are required for tissue development, embryogenesis and immune response. Aberrant regulation of cell migration and/or polarity causes cancer and gross abnormal organ development including several neuronal, lung and kidney defects. SNARE such as STXs 3 and 4, VAMP 3 and 8 and SNAP 23 play critical role in cell migration by regulating the trafficking and delivery of cell adhesion molecules such as integrins (Veale et al., 2011, Riggs et al., 2012, Day et al., 2011).

SNAREs have also been shown to be key players in establishing and maintaining cell polarity (Reales et al., 2011, Galvez-Santisteban et al., 2012, Apodaca et al., 2012). STX4 is localised to basolateral membranes in MDCK cells and interfering with its function leads to delayed tight junction formation thus impairing the ability of MDCK cells to polarise. My data suggests that

STX19 may be a novel SNARE which functions on these pathways. Below is a summary of the functions of some of the potential interacting partners of STX19.

5.3.3 NDRG1

N-myc downstream regulated gene 1 protein, NDRG1, was identified in our Bio-ID data to be the third most enriched protein in the biotin-treated group only after STX19 and SNAP23 (83.8 fold) (Table 5-2). NDRG1, a 43-kDa protein, is a member of the NDGR family which consist of four members NDGRs 2-4 (Melotte et al., 2010). All family members have a conserved NDR domain and alpha/beta hydrolase fold (Melotte et al., 2010). NDGR1 is involved in the recycling of E-cadherin by acting as a Rab4 effector. The recruitment of NDGR1 onto recycling endosomes via phosphatidylinositol 4-phosphate is required for both transferrin and E-cadherin recycling (Kachhap et al., 2007). The role of NDGR1 in stabilising E-cadherin trafficking prevents epithelial-to-mesenchymal transition (EMT) which is required for cancer metastasis. Depletion of STX19 using RNAi leads to dramatic alteration of the cytoskeleton in HeLaM cells which is seen as potential hallmark of EMT. It will be important to repeat these experiments in a more physiological cell line such as CACO-2 cells.

5.3.4 ERBB2IP/LAP2/ERBIN

ERBB2IP was the fourth most enriched protein in the STX19 biotin-treated group (79.7 fold) (Table 5-2). ERBB2IP is part of the LAP family of proteins which also include SCRIB, DENSIN-180, LET-413 and LANO (Santoni et al., 2002). LAP proteins contain a 16 leucine rich repeats (LRR), two conserved LAP specific domain and 1-4 PDZ domains (Santoni et al., 2002). ERBB2IP contains one PDZ domain. SCRIB was 11 fold enriched in the biotin-treated samples (Table 5-2). The 16 LRR target ERBB2IP to the basolateral membranes. A study has also shown that cysteines 14 and 16 in this region are vital for ERBB2IP plasma membrane localisation (Izawa et al., 2008). ERBB2IP interacts with ERBB2 receptor via its PDZ domain which localises the latter (ERBB2 receptor) to the basolateral membranes of epithelial cells (Borg et al., 2000). Studies have shown that both ERBB2IP and SCRIB may interact with integrins (Favre et al., 2001, Byron et al., 2012). Moreover, ERBB2IP interacts with beta-catenin and DST (Favre et al., 2001, Hein et al., 2015). Thus

ERBB2IP and SCRIB together with the other members of the LAP family are required for maintaining cell shape and polarity (Bryant and Huwe, 2000). It will be interesting to define the role of STX19 in linking ERBB2IP and SCRIB in the regulation of cell polarity.

5.3.5 VANGL1 (Van Gogh-like protein 1)/STB2/KITENIN

VANGL1 was the fifth most enriched protein in our STX19 biotin-treated group (66 fold) (Table 5-2). VANGL1 shares about 73 % identity with VANGL2 (Katoh, 2002). VANGLs were first identified in *Drosophila* as Strabismus gene responsible for maintaining planar cell polarity (PCP) in *Drosophila* eye (Wolff and Rubin, 1998). VANGLs are membrane proteins that have four transmembrane domains and their N- and C-termini localised to the cytoplasm (Katoh, 2002). They harbour a coiled-coil domain, loop tail and PDZ protein binding motif and SYXV motif at the C-terminus which is required for interacting with dishevelled proteins (DSH) and binding to other PCP proteins. A point mutation at V239I abolishes VANGL1 interaction with DSH which is partly responsible for neural tube defects (Kibar et al., 2007). Epithelial cells in the lung, heart, kidney, intestine and other tissues need to be aligned properly along the planar axis orthogonal to the apical-basal axis (Hatakeyama et al., 2014). VANGLs by virtue of their extracellular and intracellular localisation act as scaffolding protein required for assembling PCP proteins to align epithelial cells in different tissues (Hatakeyama et al., 2014). To maintain planar cell polarity, core PCP proteins including Flamingo, Diego, Dishevelled, VANGLs, and Prickled are arranged along a specific pattern from the distal to the proximal end of the cells (Fanto and McNeill, 2004). Mutations in VANGLs and their associated PCP proteins can cause defects in the organisation of the lung, heart, kidney and neural tissue (Hatakeyama et al., 2014). VANGLs also play a role in cell migration. VANGL1 is localised at the leading edge of invasive breast cancer cells where it interacts with SCRIB and NOS1AP (Anastas et al., 2012). In MCF-7 cells SCRIB and VANGL1 colocalise at cell adherent junctions marked by beta-catenin (Anastas et al., 2012). Depletion of VANGL1 or SCRIB using RNAi reduces the invasive properties of MDA-MB-231 cells (Anastas et al., 2012). The study also showed that overexpression of VANGL1 is associated

with increased relapse in oestrogen-positive breast cancer patients (Anastas et al., 2012). Furthermore, increased expression of VANGL1 is associated with other cancers including gastric, oral, colon and glioma (Yoon et al., 2013, Ryu et al., 2010, Oh et al., 2016, Lee et al., 2015). It will be interesting to link the relationship between ERBB2IP, SCRIB, VANGL and STX19 potential complex formation in regulating cell migration and cell polarity.

ZDHHC5/zinc finger DHHC domain-containing protein 5

ZDHHC5 was the tenth most enriched protein in our STX19 biotin-treated group (39 fold) (Table 5-2). ZDHHC5 is a member of the 23 palmitoyl-acyltransferase family which are required for catalysing protein palmitoylation (Fukata et al., 2004). ZDHHC5 plays a role in maintaining cell polarity. ZDHHC5/8 colocalises with AnkyrinG and beta1-spectrin at the lateral membrane of MDCK cells (He et al., 2014). ZDHHC5 functions together with ZDHHC8 to regulate the palmitoylation of AnkyrinG (He et al., 2014). These components function together to drive lateral membrane assembly in MDCK cells (He et al., 2014). Identifying PATs required for STX19 palmitoylation, we performed both immunolocalisation and palmitate labelling coupled to click chemistry. Overexpressed ZDHHC5 in HeLaM cells colocalises with endogenous STX19 on the tubular recycling endosomes and the plasma membrane (Figure 4-12). However, ZDHHC5 does not palmitoylate STX19 (Figure 4-13). Presently, it is unclear if there is a relationship between ZDHHC5 and STX19. It is possible that STX19 plays a role in the trafficking of ZDHHC5.

5.3.6 ZW10-interacting protein 1/ZWINT

ZWINT was identified both in our Y2H screen and Bio-ID analysis (Table 5-1; Table 5-2). In the Y2H screen, ZWINT interacts with STX19 via 63-277 which harbours ZWINT coiled-coil domain (Table 5-1; Table 5-2). Previous studies have identified that ZWINT interacts with STXs 3, 9, 11 and 18 and SNAP29 (Hein et al., 2015, Huttlin et al., 2015, Hutchins et al., 2010). HZWINT is a 43 kDa protein, was first identified in a yeast two-hybrid screen to interact with ZW10 as its name implies human ZW10 interacting protein (Starr et al., 2000). ZWINT localises to kinetochores and plays a role in the correct functioning of centromeres (Starr et al., 2000). Mutation in ZWINT is characterised by a rare

genetic disorder called Robert syndrome (Musio et al., 2004). Affected individuals have retarded growth and symmetrical reduction of limbs (Musio et al., 2004). SIP30 (SNAP25 interacting protein of 30 kDa), shares 56% identity with ZWINT, was found to interact with SNAP25 and suggested to facilitate the trafficking of SNAP25 (Lee et al., 2002). The role of ZWINT in post-Golgi trafficking still remains obscure. ZW10 the main interacting partner of ZWINT has been identified to play a role in ER to Golgi trafficking (Hirose et al., 2004). It remains unclear why a nuclear-localised ZWINT1 directly interacts with STX19. Previous studies have shown that during cytokinesis there is a continual delivery of endocytic cargoes to the intercellular bridge via Rab11 recycling endosomes and MICAL-L1 tubular recycling endosomes (Hehnlly and Doxsey, 2014, Reinecke et al., 2014a). From my immunolocalisation studies, STX19 colocalises with MICAL-L1 on the tubular recycling endosomes (Figure 3-5). It could be possible that STX19 could also mediate the delivery of endocytic cargoes that are required for cytokinesis and by so doing directly interact with ZWINT to regulate kinetochore formation.

5.3.7 Spectraplakins

Our Y2H screen and Bio-ID analysis have identified two spectraplakins (DST and MACF1) to interact with STX19 (Table 5-1; Table 5-2). From the Y2H screen, DST interacts with STX19 via amino acids 3596-3708 (lies in the spectrin repeats) and 4193-4362 aa (lies in the coiled-coil domain), meanwhile, MACF1 interacts with STX19 via 3373-3509 aa (lies in the coiled-coil domain). DST was 7 fold enriched whereas MACF1 was 1.3 fold (Table 5-1; Table 5-3). Interestingly, MACF1 has been shown to interact with SNAP29 (Huttlin et al., 2015).

Spectraplakins are very large proteins >5,000 amino acids involve in cytoskeleton regulation (Roper et al., 2002, Brown, 2008). They include: MACF1, DST and Drosophila Short stop (Kakapo)(Roper et al., 2002). The spectraplakins family are found in metazoans and encode proteins that have both spectrin and plakin domains (Roper et al., 2002, Huelsmann and Brown, 2014). Spectraplakins have an N-terminal domain, plakin domain, plectin repeats, spectrin repeats and C-terminal domain (Figure 5-1) (Roper et al., 2002, Poliakova et al., 2014).

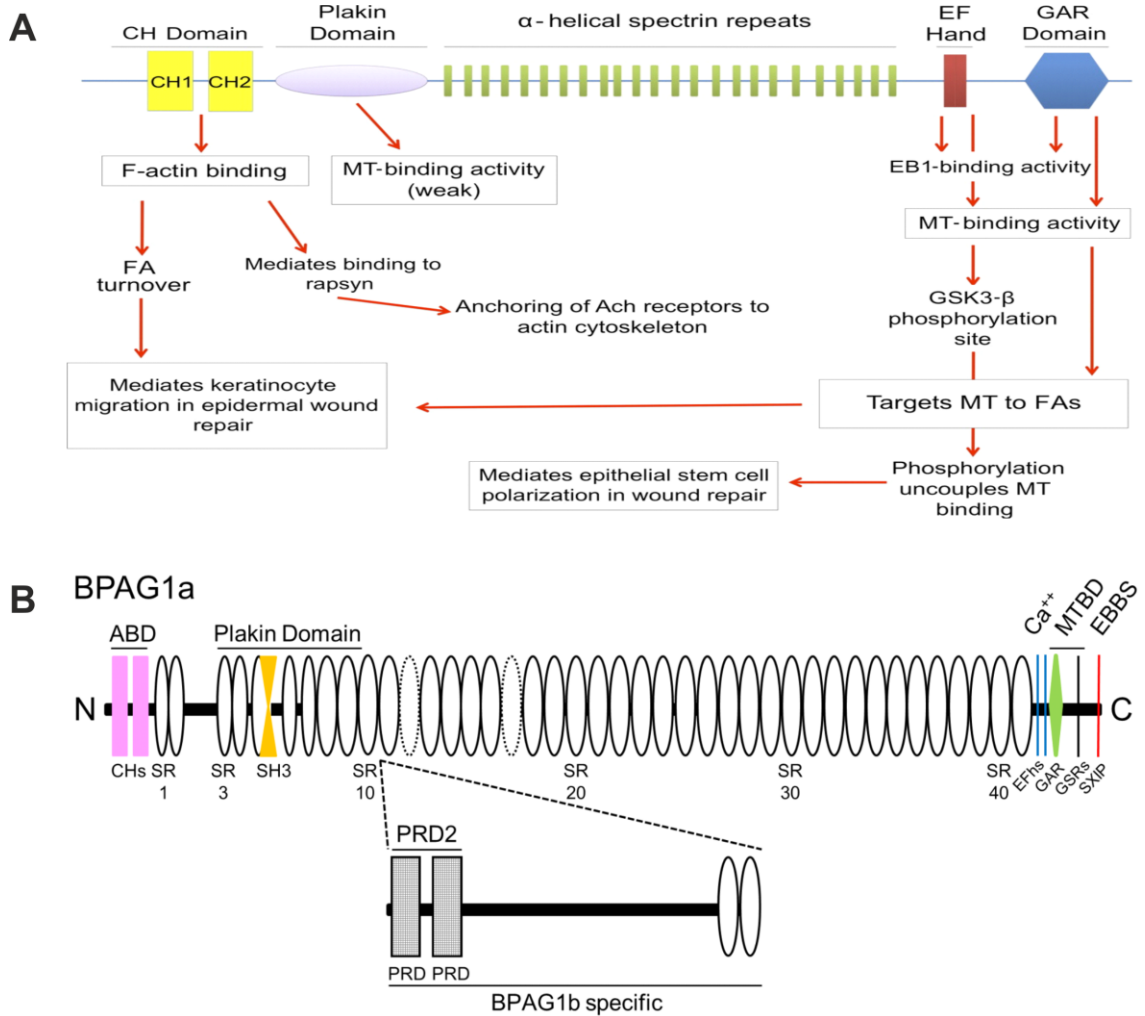


Figure 5-1 Cartoon of MACF1 and DST.

A) Diagrammatic representation of MACF1 showing its domains and their functions (Suozzi et al., 2012). **B)** Diagrammatic representation of DST showing its domains (Poliakova et al., 2014).

5.3.8 Microtubule actin cross linking factor 1/ actin cross linking factor 7 (MACF1/ACF7)

MACF1 was first partially cloned as actin cross linking factor 7 (Byers et al., 1995). Subsequently, the full-length version of the protein was cloned in several laboratories and given different names including macrophin to denote microfilament and actin filament cross linker protein related to plectin and dystrophin (Okuda et al., 1999); trabeculin-alpha (Leung et al., 1999); and

MACF denoting microtubule actin cross-linking factor (Leung et al., 1999). MACF1 exist in four isoforms 1, 2, 3 and 4 (Gong et al., 2001). It is structurally homologous to dystonin and dystrophin (Leung et al., 1999). MACF1 has been proposed to play an important role in cell migration, cell proliferation, focal adhesion turnover, protein trafficking and sorting by regulating actin and microtubules dynamics (Yucel and Oro, 2011, Wu et al., 2011, Legg, 2011, Kodama et al., 2003, Wu et al., 2008, Burgo et al., 2012, Kakinuma et al., 2004, Hu et al., 2015). During cell migration, MACF1 tethers microtubules to actin-rich cortical sites, which enables the cell to correctly coordinate its polarisation and movement (Kodama et al., 2003). MACF1 interaction with ELMO (engulfment and motility proteins), APC (adenomatous polyposis coli), and CLASPs (cytoplasmic linker-associated proteins) mediates integrin focal adhesion dynamics (Stehbens and Wittmann, 2012, Stroud et al., 2014, Ka et al., 2014). MACF1 via its complex interaction with GOLGA4, VARP, and RAB21 has been implicated in the sorting of VAMP7 vesicles from the Golgi to the cell periphery (Burgo et al., 2012). The MACF1 interaction with GOLGA4 has been shown to be important for the trafficking of GPI-anchored proteins from the Trans-Golgi Network to the cell periphery (Kakinuma et al., 2004). STX19 colocalises with GPI-anchored proteins (Refer to chapter three) and GOLGA4 was identified as a potential interacting partner of STX19 in our Y2H screen. It is possible that STX19 is required for the fusion of VAMP7 positive vesicles with the plasma membrane and that the interaction between STX19 and MACF1 and GOLGA4 may help tether these vesicles either to the cytoskeleton or plasma membrane.

5.3.9 Dystonin/DST/BPAG1

DST also called BPAG1 because it was first identified as an autoantigen of bullous pemphigoid (Minoshima et al., 1991). DST has four isoforms (BPAG1 a, b, e, and n) depending on whether they have spectrin repeats only, plectin repeats only or both repeats (Huelsmann and Brown, 2014). Isoform “a” and “b” are ubiquitously expressed, isoform “e” mostly found in epidermal tissues and isoform “n” is in neuronal tissues (Suozzi et al., 2012, Bouameur et al., 2014). These are further classified based on splicing such as BPAG1a1, a2, a3; BPAG1b1, b2, b3; and BPAG1n4 (Suozzi et al., 2012).

DST is proposed to have a wide range of functions including cell migration, adhesion, hemidesmosomes assembly, spreading, cargo transport, and Golgi integrity maintenance, cell polarity (Poliakova et al., 2014, Michael et al., 2014, Hamill et al., 2009, Koster et al., 2003). Defects in DST are associated with muscle disorders, skin diseases, autoimmune diseases, neurological diseases (Bouameur et al., 2014, Simpson et al., 2011, Sonnenberg and Liem, 2007, Edvardson et al., 2012).

Isolated keratinocytes from patients with homozygous mutant DST shows an increased cell spreading and migratory behaviour (Michael et al., 2014). These phenotypic behaviours recapitulate the knockdown of STX19 in HeLaM cells whereby I see an increased cell spreading and formation of several lamellipodia (Figure 3-8; Figure 3-13).

5.3.10 Future direction and experiments

My proteomic and Y2H studies have uncovered a novel and exciting link between STX19 and the machinery involved in regulating cell migration and cell polarity. We will first need to establish whether STX19 directly interacts with this machinery or is playing a role in coordinating and regulating the trafficking of this machinery. Approaches including immunolocalisation, GST pull downs and immunoprecipitation studies will help address this question. To fully explore the role of STX19 in cell polarity and migration we will need to develop tissue culture models for these processes. My preliminary studies indicate that STX19 is expressed in CACO-2 so it will be possible to investigate the role of STX19 in establishing cell polarity using RNAi. The use of in vitro scratch wound healing and Transwell migration assays could also be used to determine the role of STX19 in cell migration.

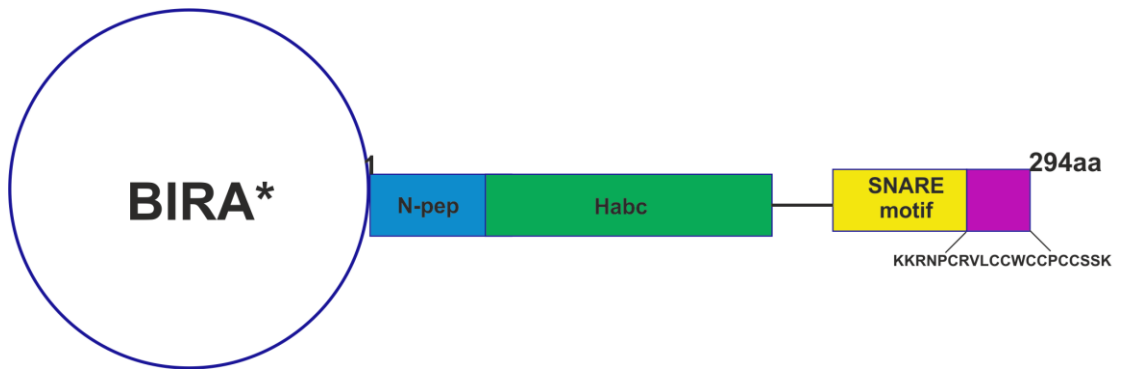


Figure 5-2 Cartoon of BirA*STX19.

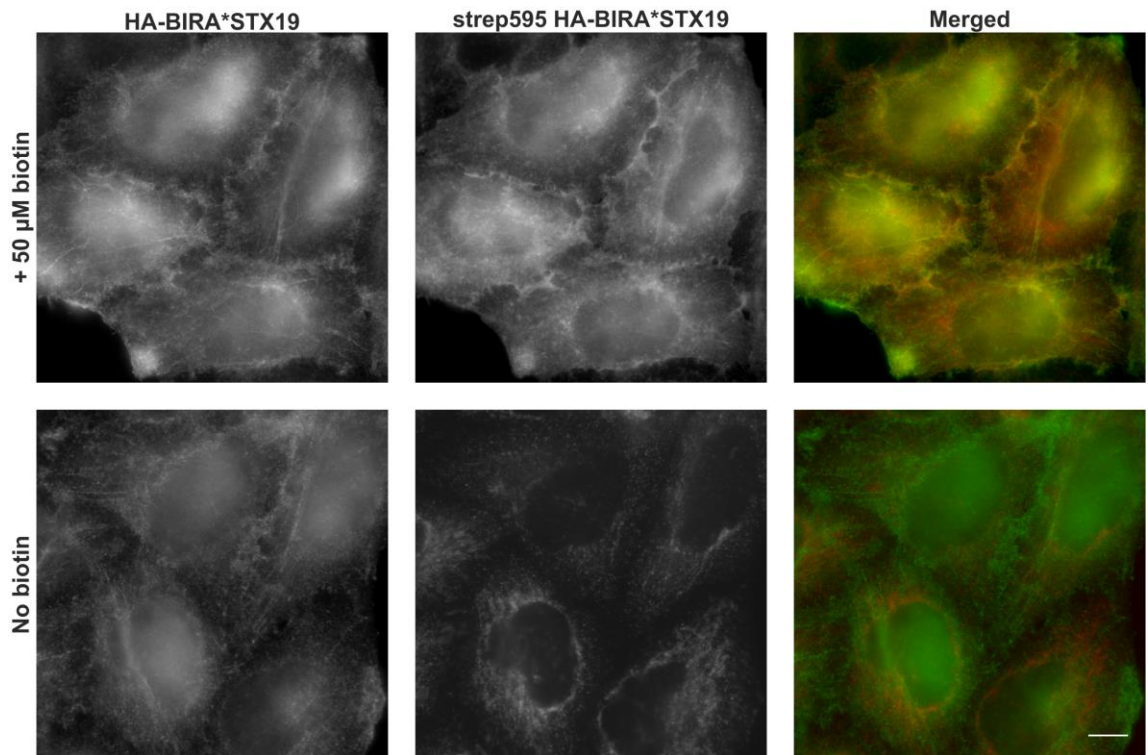


Figure 5-3 BirA tagged STX19 is localised to the PM and TRE.

BirA*STX19 clonal HeLaM cells were grown overnight on coverslips and then incubated with 50 μM of biotin for 24 h or without biotin. The cells were then fixed, washed and then stained with anti-HA followed by donkey anti-mouse Alexa 488 and streptavidin 595 nm. Images were obtained from wide field microscope. Scale bar = 10 μm.

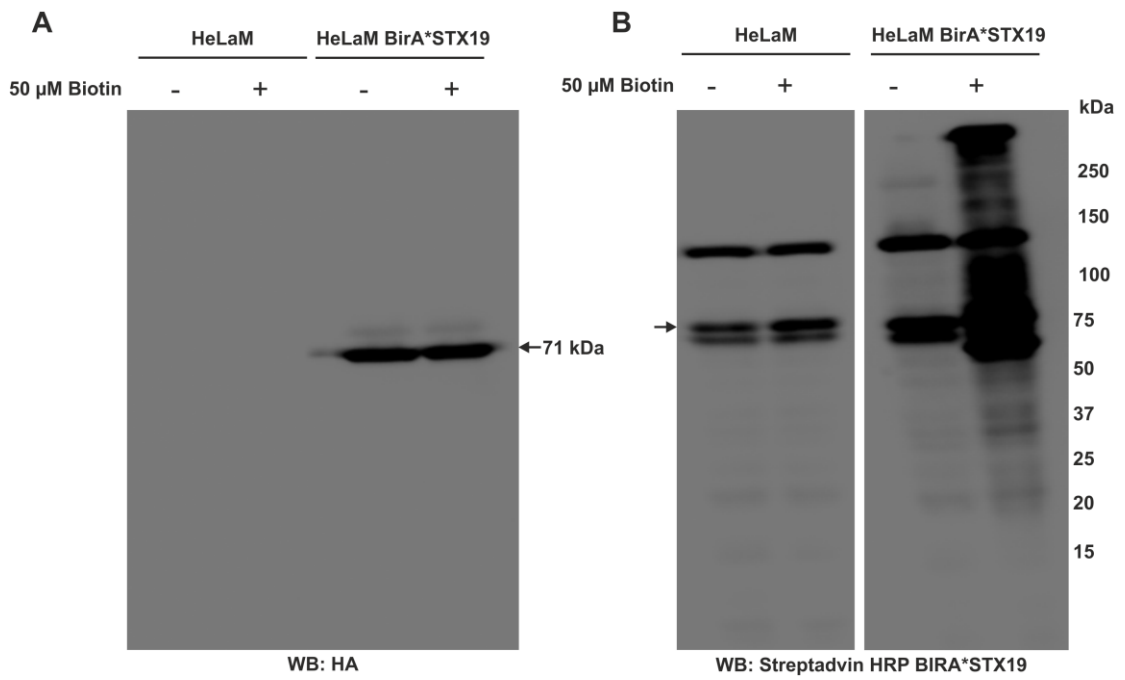


Figure 5-4 BirA*STX19 is capable of biotinylating proteins.

HeLaM cells and BirA*STX19 clonal HeLaM cells were grown overnight in 10 cm plates and incubated for 24 h without biotin (-) or with 50 μ M biotin (+). Whole cell lysates were made and then Western blot on nitrocellulose membranes. **A)** HeLaM cells and BirA*STX19 clonal HeLaM cells were incubated with anti-HA followed by goat anti-mouse HRP. **B)** HeLaM cells and BirA*STX19 clonal HeLaM cells were incubated with streptavidin HRP only.

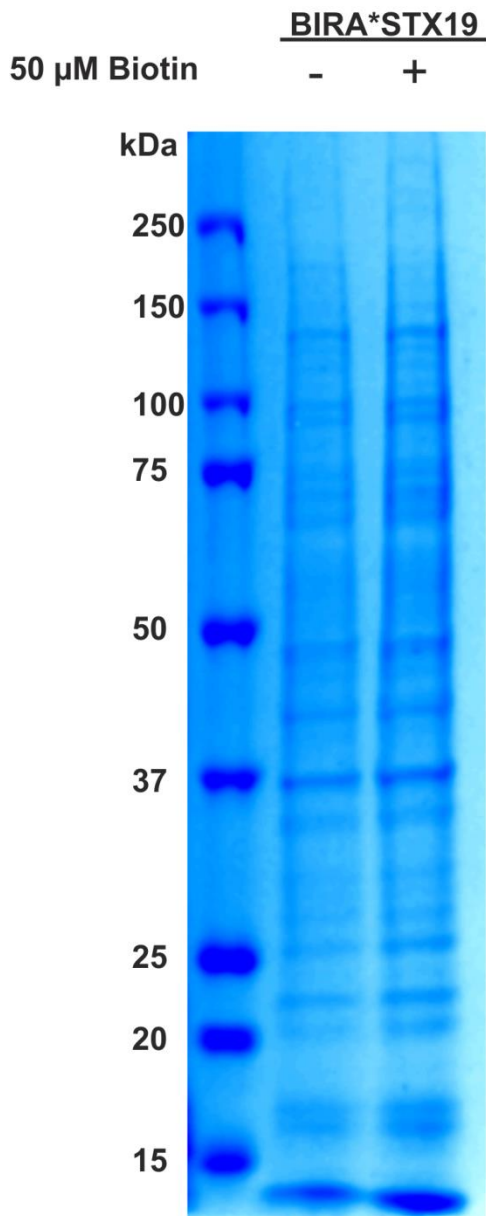


Figure 5-5 Coomassie staining of streptavidin enrich proteins.

BirA*STX19 cells were grown overnight in T175 flasks. The cells were collected, lysed with RIPA buffer and purified using streptavidin agarose beads. 50 mM of TCEP and 50 mM iodoacetamide (pH 8) was added to the beads to reduce and alkylate the cysteines. The gel was sliced, washed and trypsin digested. The samples were run on mass spectrometer and further analysis including peptide identification was performed using MaxQuant and Perseus (Cox and Mann, 2008).

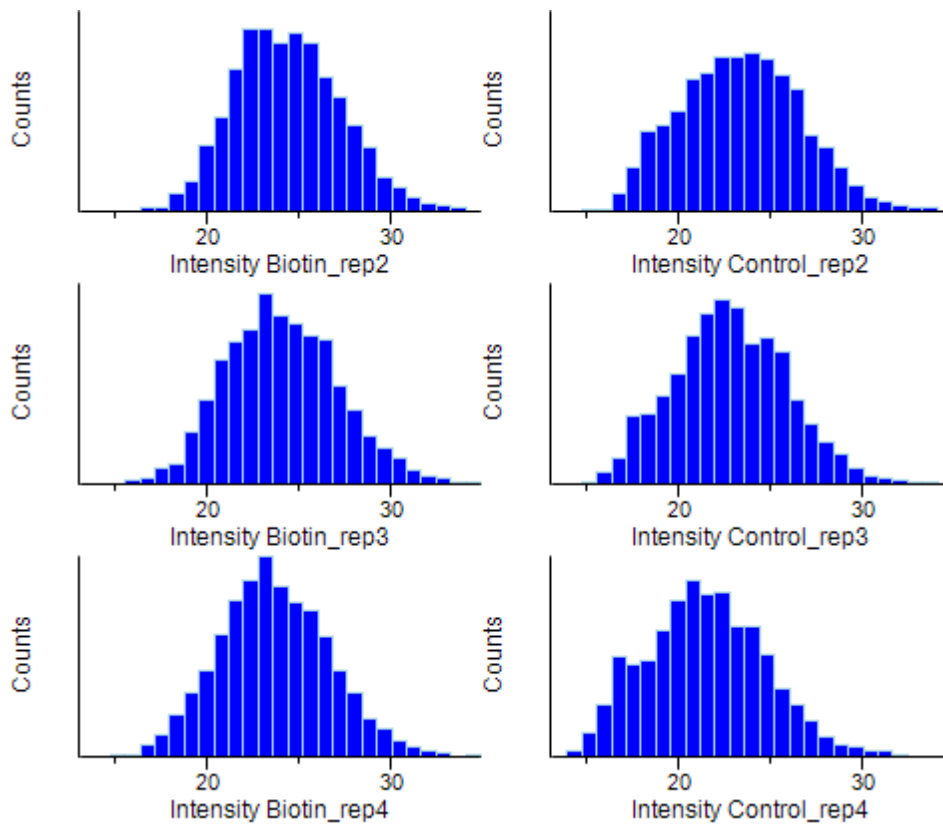


Figure 5-6 Biological repeats of BirA*STX19 follows a normal distribution curve.

A histogram plot showing the average protein enrichment levels (protein intensity) in both biotin-treated and control groups. The analysis was performed by Dr Mark Collins (Lecturer, The University of Sheffield, UK)

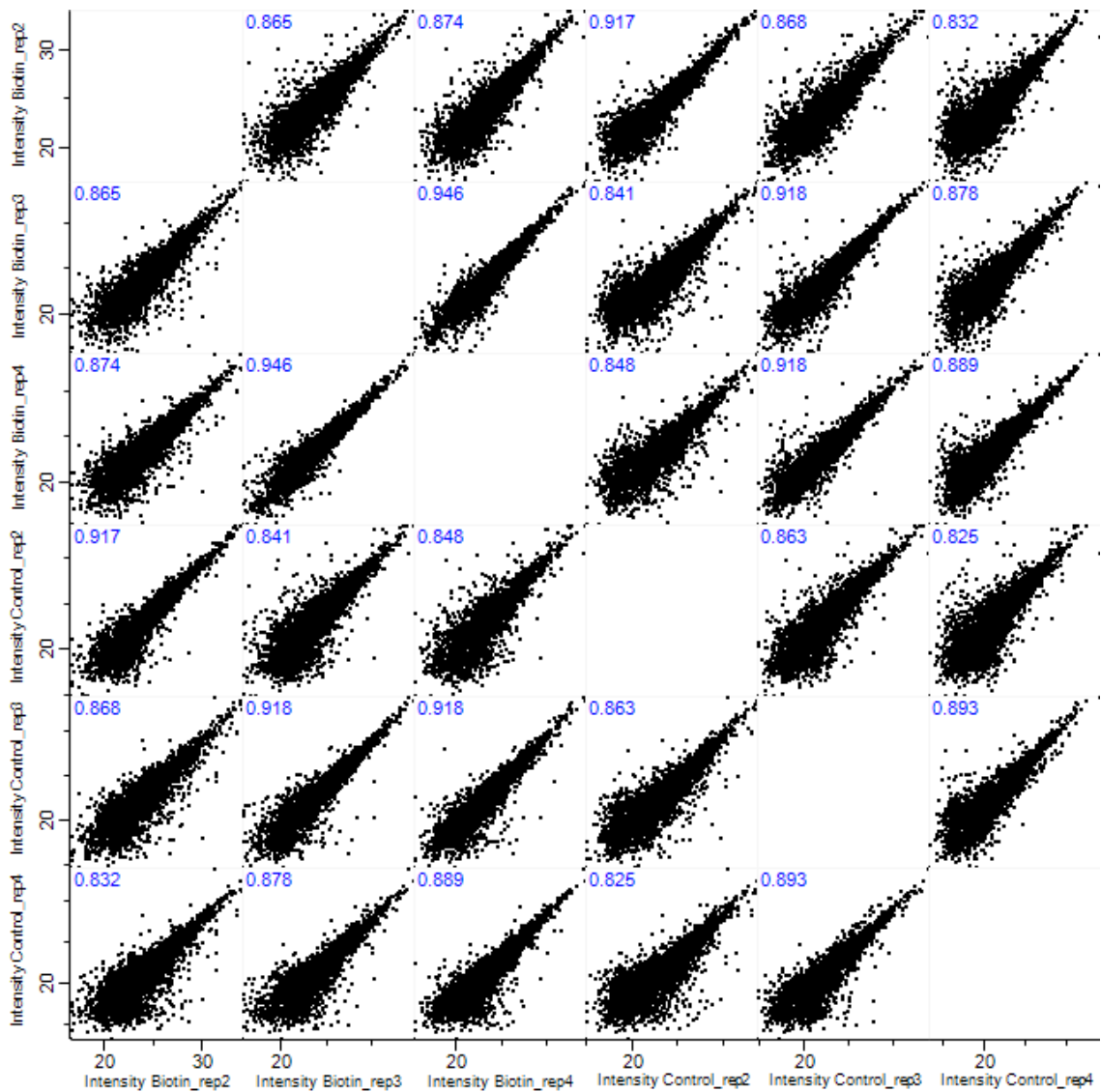


Figure 5-7 Biological repeats of BirA*STX19 correlates within and among groups.

A scatter plot showing the correlation within the individual biotin-treated and control groups. The plot also shows a correlation between the biotin-treated and control groups. The analysis was performed by Dr Mark Collins (Lecturer, The University of Sheffield, UK).

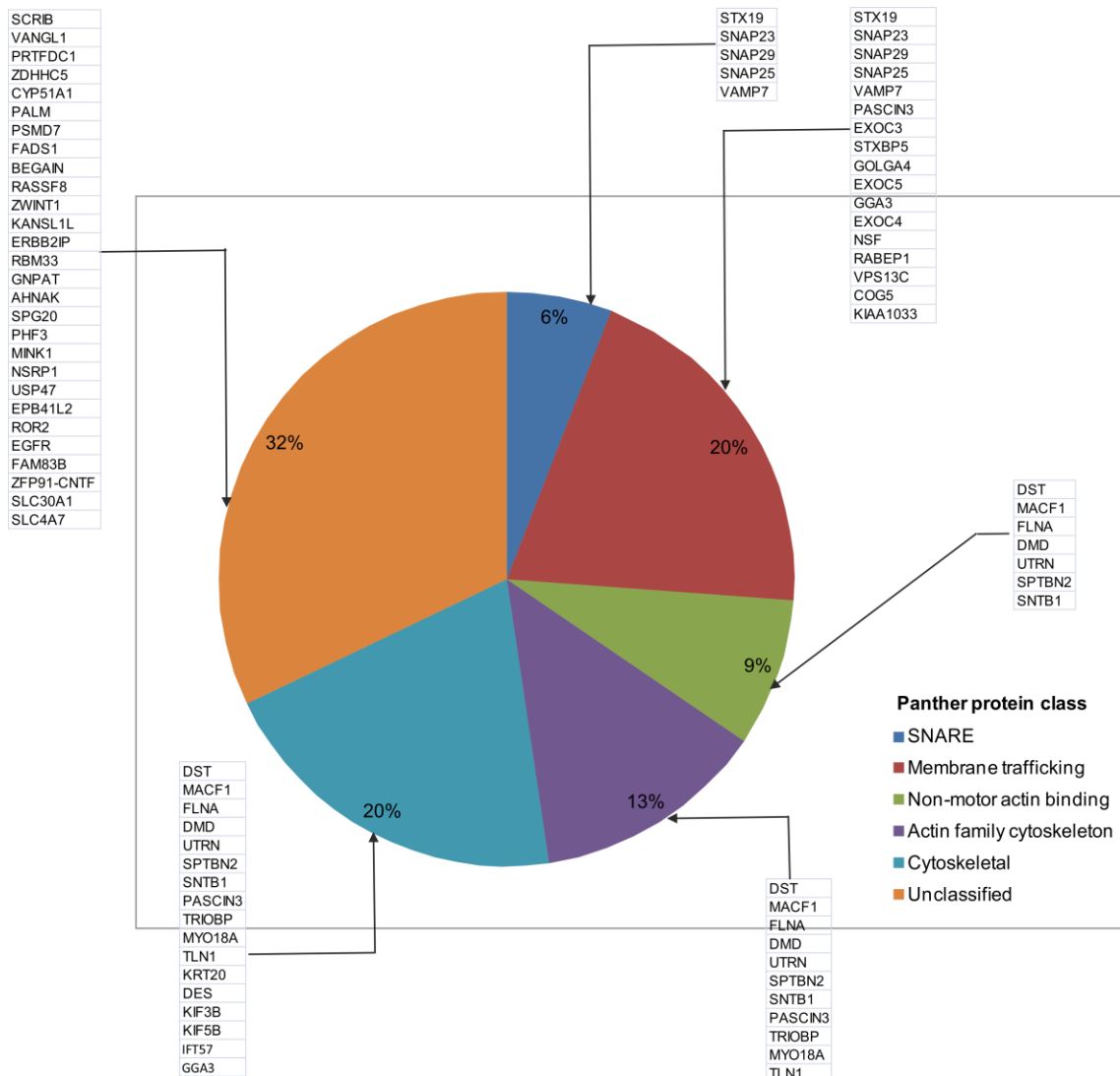


Figure 5-8 Protein classification using the Panther Gene ontology consortium.

81 proteins selected from both the Y2H screen list and the Bio-ID analysis were inputted into the Gene ontology consortium and the protein classes identified using the PANTHER protein class (Ashburner et al., 2000, Gene Ontology, 2015). Bonferroni correction was selected. Only class with P-values < 0.05 were selected. Further analysis was performed using Microsoft Excel 2007 and CorelDRAW X7. Data downloaded from GO ontology database released 2016-05-20.

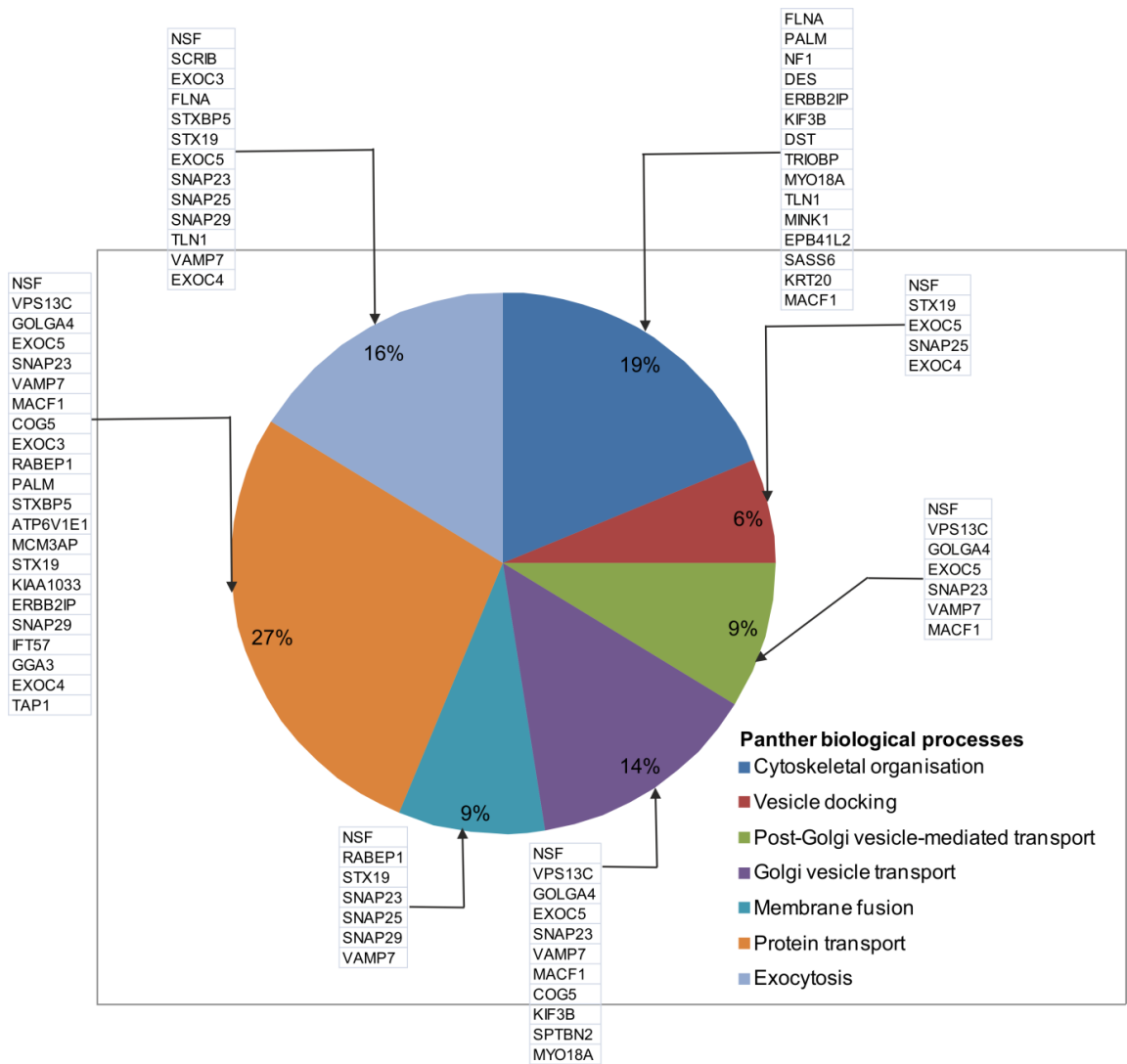


Figure 5-9 Protein biological processes using the Panther Gene ontology consortium.

81 proteins selected from both the Y2H screen list and the Bio-ID analysis were inputted into the Gene ontology consortium and the protein biological processes identified using the PANTHER Gene ontology consortium (Ashburner et al., 2000, Gene Ontology, 2015). Bonferroni correction was selected. Only class with P-values < 0.05 were selected. Further analysis was performed using Microsoft Excel 2007 and CoreIDRAW X7. Data downloaded from GO ontology database released 2016-05-20.

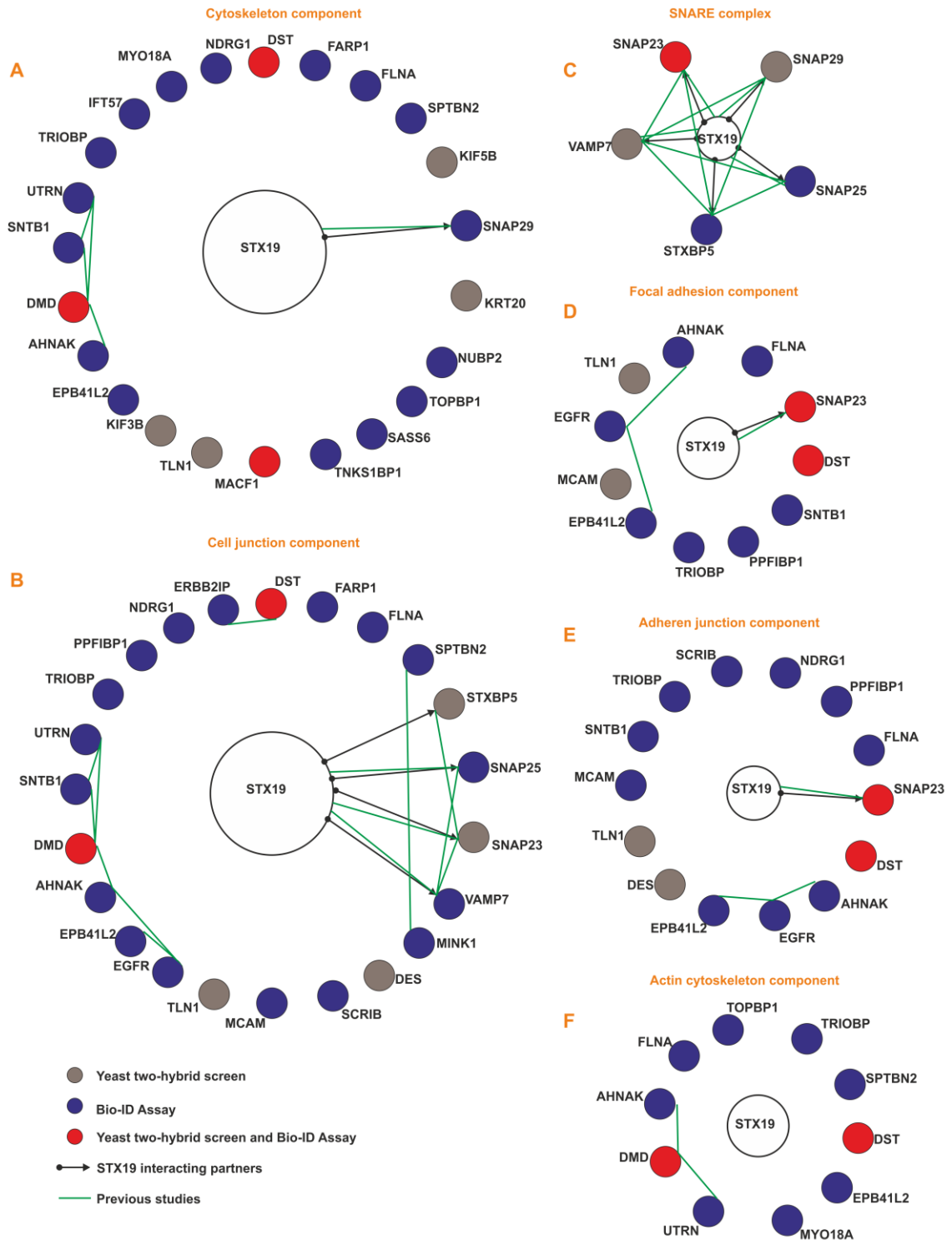


Figure 5-10 Protein cellular component using the Panther Gene ontology and STRING consortia.

81 proteins selected from both the Y2H screen list and the Bio-ID analysis were inputted into the Gene ontology and STRING consortia. The protein cellular components were identified using the PANTHER Gene ontology consortium (Ashburner et al., 2000, Gene Ontology, 2015). Bonferroni correction was selected. Only class with P-values < 0.05 were selected. **A)** Cytoskeleton

component **B**) Cell junction component **C**) SNARE complex component **D**) Focal adhesion component **E**) Adheren junction component **F**) Actin cytoskeleton component. Previously shown STX19 protein interaction partners were identified using the STRING consortium (Franceschini et al., 2013). Only interactions identified by experimental evidence were selected. Further analysis was performed using CoreIDRAW X7. Data downloaded from GO ontology database released 2016-05-20. Data downloaded from STRING database released 2016-07-01.

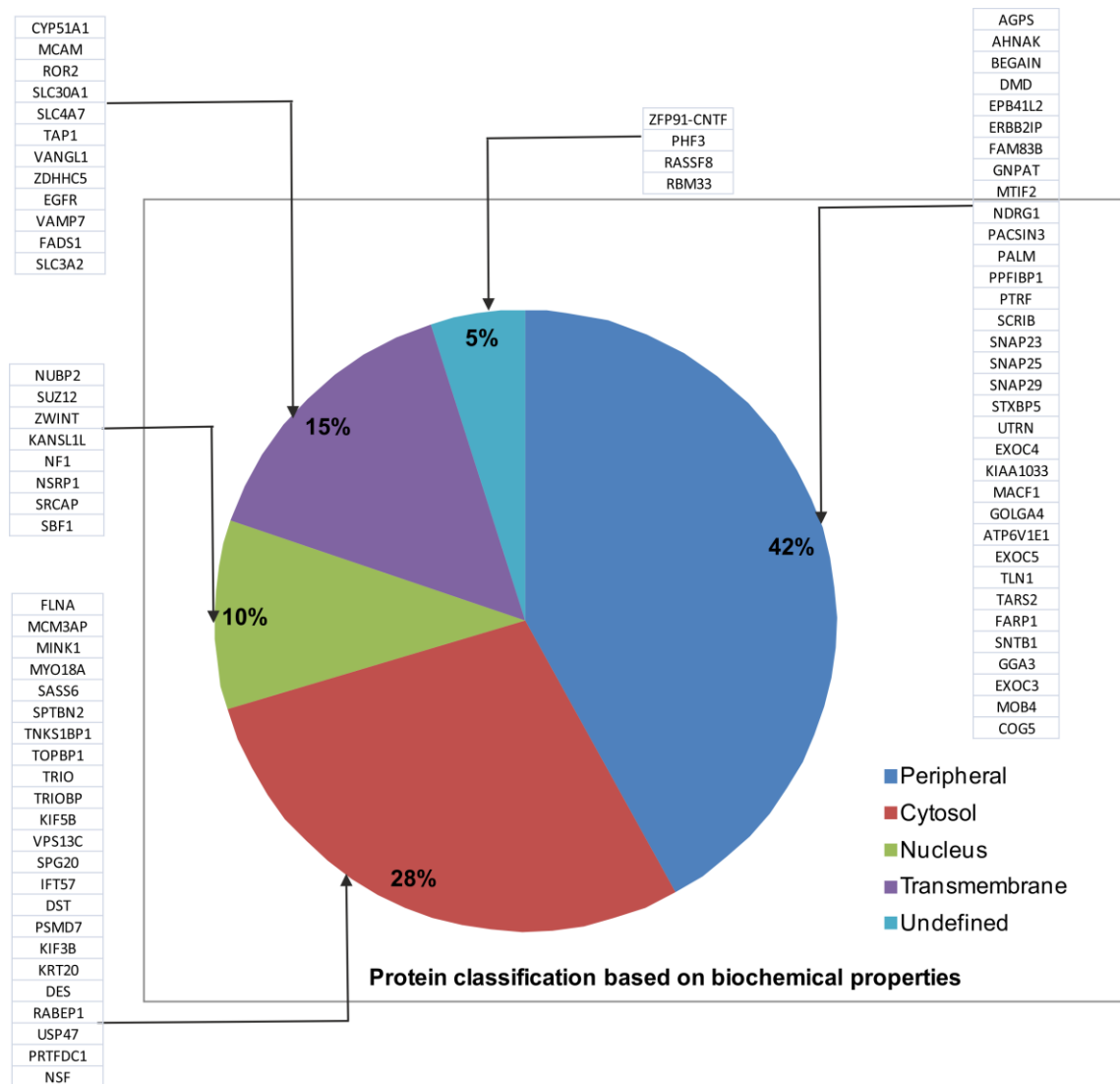


Figure 5-11 Protein classification based on biochemical properties.

The cellular localisation of the proteins was identified using UniProt consortium (UniProt, 2014). The proteins were grouped into those localised to either peripheral membranes or cytosol or nucleus or have a transmembrane domain.

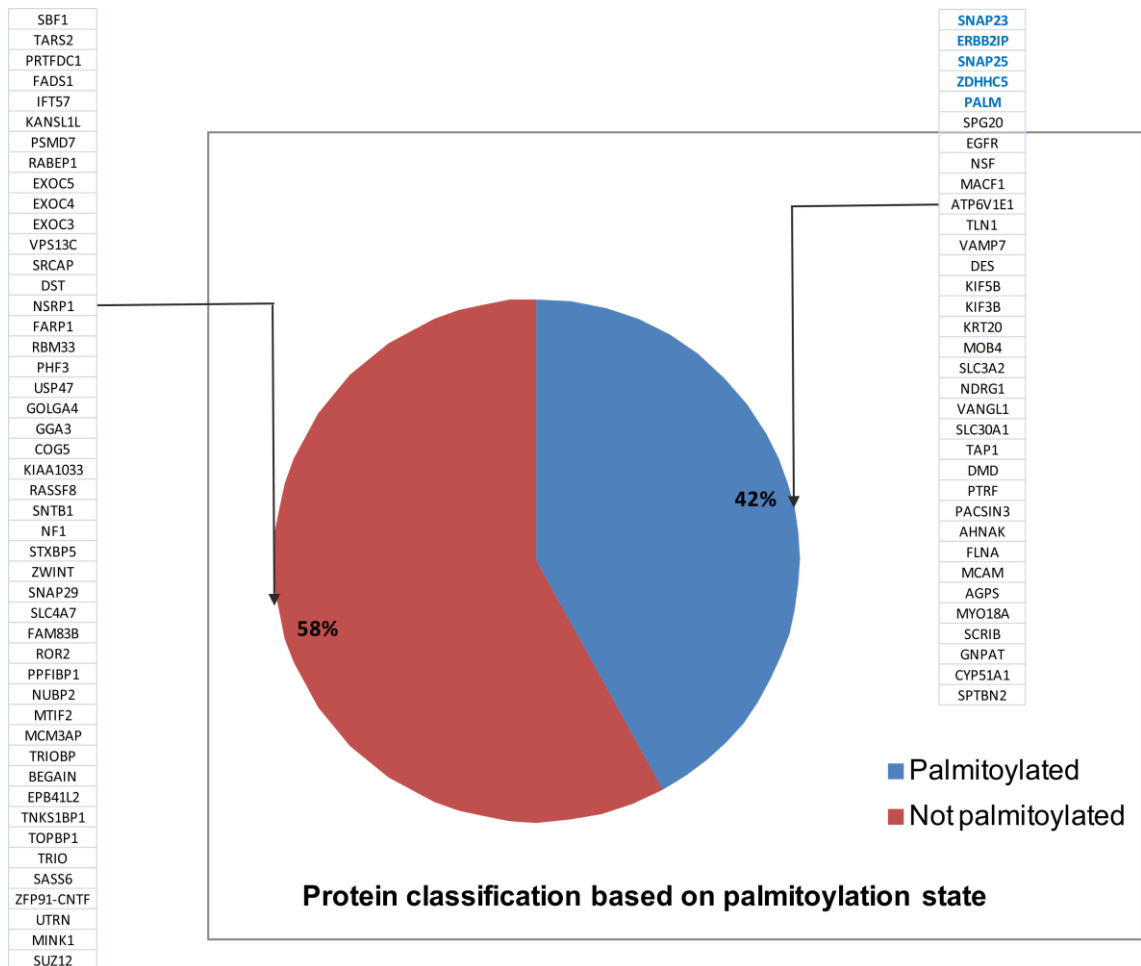


Figure 5-12 Protein classification based on palmitoylation state.

The proteins were grouped into whether they have been previously identified to be palmitoylated or not from a palmitoyl proteome analysis or specific target studies (that is studies that have actually characterised the palmitoylation state of that protein) using the SwissPalm database (Blanc et al., 2015). The bold highlighted are palmitoylated proteins identified both in specific target studies and palmitoyl proteome analysis.

Table 5-4 Protein classification based on biochemical properties and palmitoylation state.

Palmitoylation state based on palmitoyl-proteome or targeted studies. The bold highlighted are palmitoylated proteins identified both in specific target studies and palmitoyl proteome analysis.

Protein	Biochemical properties	Palmitoylation state	Protein	Biochemical properties	Palmitoylation state
SNAP23	peripheral	Yes	NF1	nucleus	No
NDRG1	peripheral	Yes	SPG20	cytosol	Yes
ERBB2IP	peripheral	Yes	EGFR	transmembrane	Yes
VANGL1	transmembrane	Yes	NSF	cytosol	Yes
SLC30A1	transmembrane	Yes	SBF1	nucleus	No
STXBP5	peripheral	No	DST	cytosol	No
SNAP25	peripheral	Yes	TARS2	peripheral	No
TAP1	transmembrane	Yes	PRTFDC1	cytosol	No
ZDHC5	transmembrane	Yes	FADS1	transmembrane	No
ZWINT	nucleus	No	NSRP1	nucleus	No
SNAP29	peripheral	No	FARP1	peripheral	No
SLC4A7	transmembrane	No	RBM33	undefined	No
FAM83B	peripheral	No	PHF3	undefined	No
ROR2	transmembrane	No	USP47	cytosol	No
PPFIBP1	peripheral	No	VAMP7	transmembrane	Yes
DMD	peripheral	Yes	MACF1	peripheral	Yes
NUBP2	nucleus	No	DES	cytosol	Yes
MTIF2	peripheral	No	GOLGA4	peripheral	No
PTRF	peripheral	Yes	IFT57	cytosol	No
MCM3AP	cytosol	No	GGA3	peripheral	No
TRIOBP	cytosol	No	COG5	peripheral	No
PACSIN3	peripheral	Yes	ATP6V1E1	peripheral	Yes
BEGAIN	peripheral	No	KIAA1033	peripheral	No
EPB41L2	peripheral	No	KIF5B	cytosol	Yes
TNKS1BP1	cytosol	No	KIF3B	cytosol	Yes
TOPBP1	cytosol	No	KRT20	cytosol	Yes
AHNAK	peripheral	Yes	KANSL1L	nucleus	No
FLNA	cytosol	Yes	PSMD7	cytosol	No
MCAM	transmembrane	Yes	RABEP1	cytosol	No
TRIO	cytosol	No	RASSF8	undefined	No
PALM	peripheral	Yes	EXOC5	peripheral	No
AGPS	peripheral	Yes	EXOC4	peripheral	No
MYO18A	cytosol	Yes	EXOC3	peripheral	No
SCRIB	peripheral	Yes	TLN1	peripheral	Yes
SASS6	cytosol	No	MOB4	peripheral	Yes
GNPAT	peripheral	Yes	VPS13C	cytosol	No
FP91-CNTF	undefined	No	SLC3A2	transmembrane	Yes
UTRN	peripheral	No	SNTB1	peripheral	No
CYP51A1	transmembrane	Yes	SRCAP	nucleus	No
SPTBN2	cytosol	Yes	SUZ12	nucleus	No
MINK1	cytosol	No			

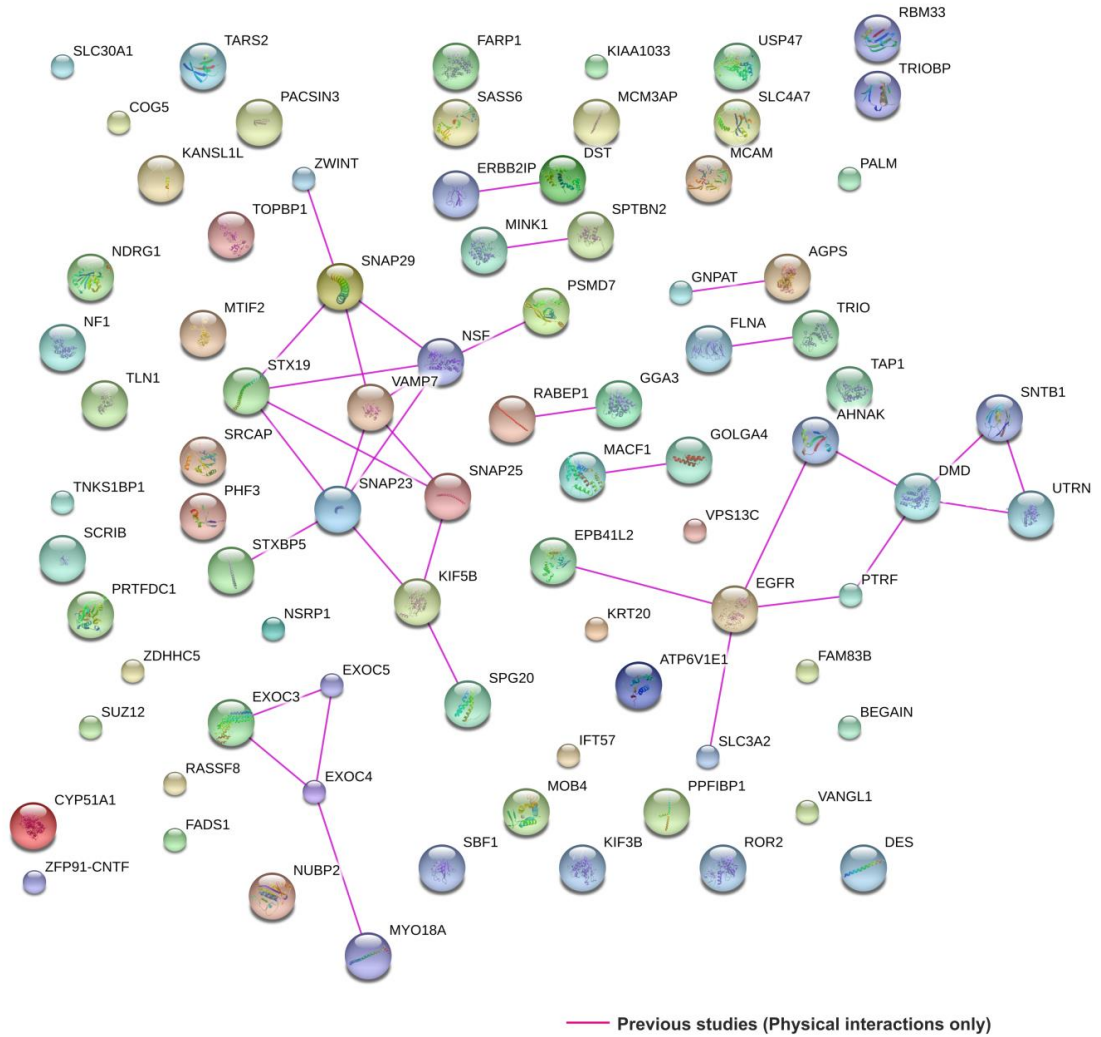


Figure 5-13 STRING consortium showing STX19 interacting partners.

81 proteins selected from both the Y2H screen list and the Bio-ID analysis were inputted into the STRING consortia. Previously shown STX19 protein interaction partners were identified using the STRING consortium (Franceschini et al., 2013). Only interactions identified by experimental evidence were selected. Data downloaded from STRING database released 2016-07-01.

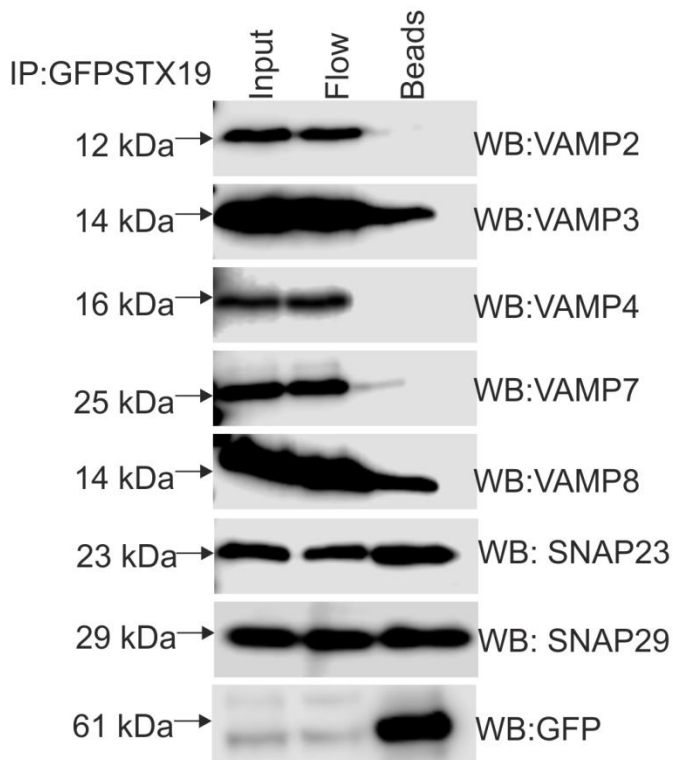


Figure 5-14 STX19 forms SNARE complexes with SNAPs (23, 29) and VAMPS (3, 8).

HeLaM cells were seeded overnight into 10 cm plates and then transfected with GFPSTX19. The cells were treated with 100 mM NEM for 30 minutes prior to collection. The cells were lysed and GFPSTX19 immuno-isolated. The samples were then blotted with the indicated antibodies followed by either rabbit or mouse HRP.

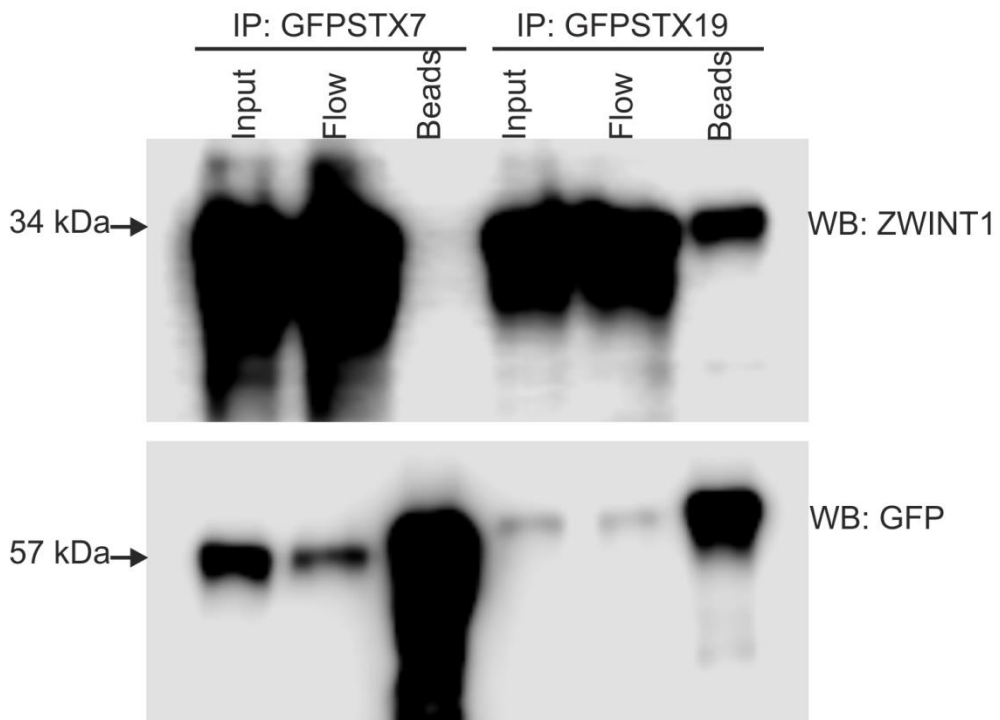


Figure 5-15 STX19 interacts with ZWINT1.

HeLaM cells were seeded overnight into 10 cm plates and then transfected with GFPSTX19. The cells were collected, lysed and GFP-STX19 immuno-isolated. The samples were then blotted with either ZWINT1 or anti-GFP followed by rabbit HRP.

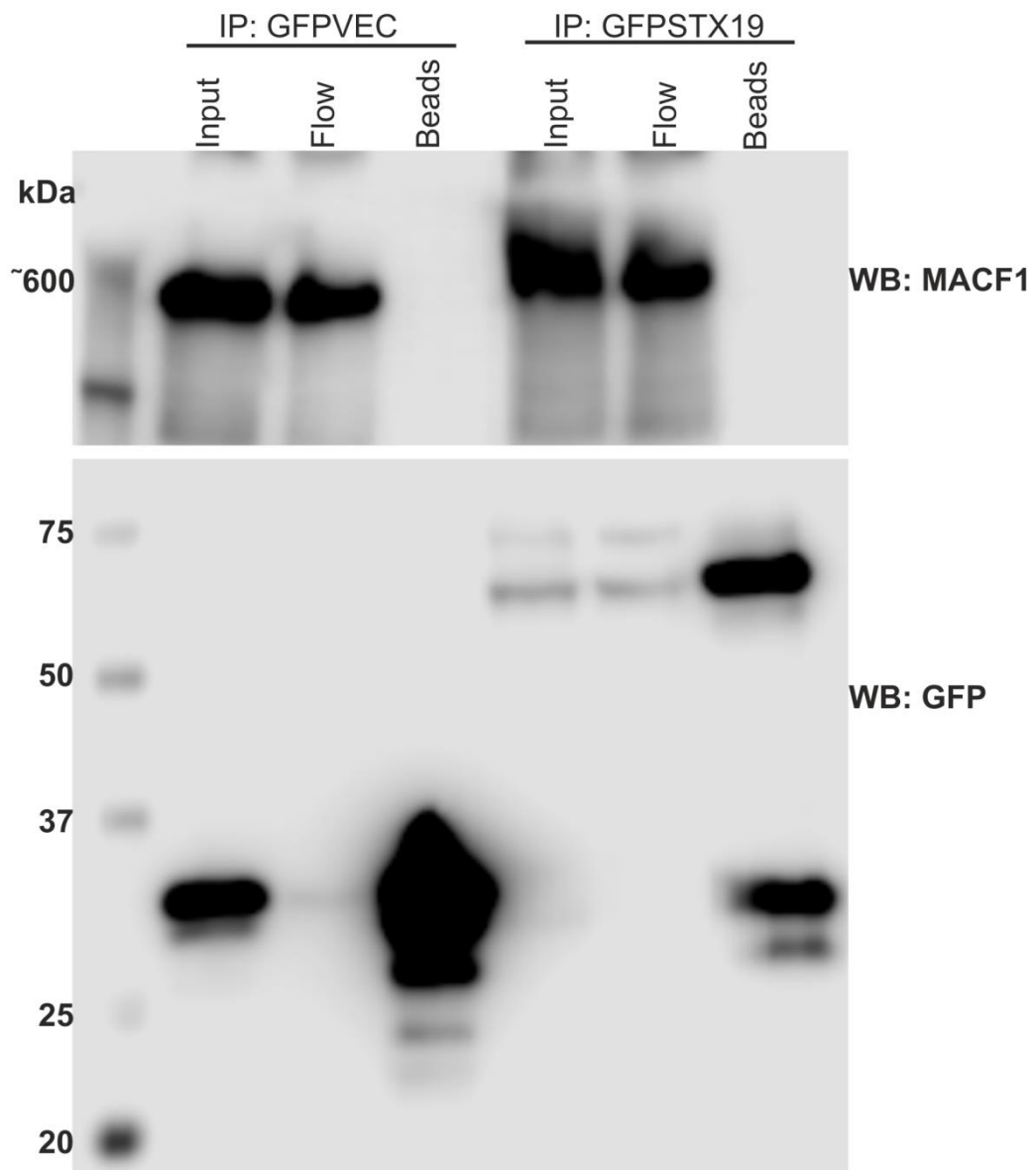


Figure 5-16 MACF1 does not co-immunoprecipitate with GFP-tagged STX19.

HeLaM cells were seeded overnight into 10 cm plates and then transfected with GFP only or GFPSTX19. The cells were collected, lysed and the GFPSTX19 immuno-isolated. The samples were then blotted with either MACF1 or anti-GFP followed by rabbit HRP.

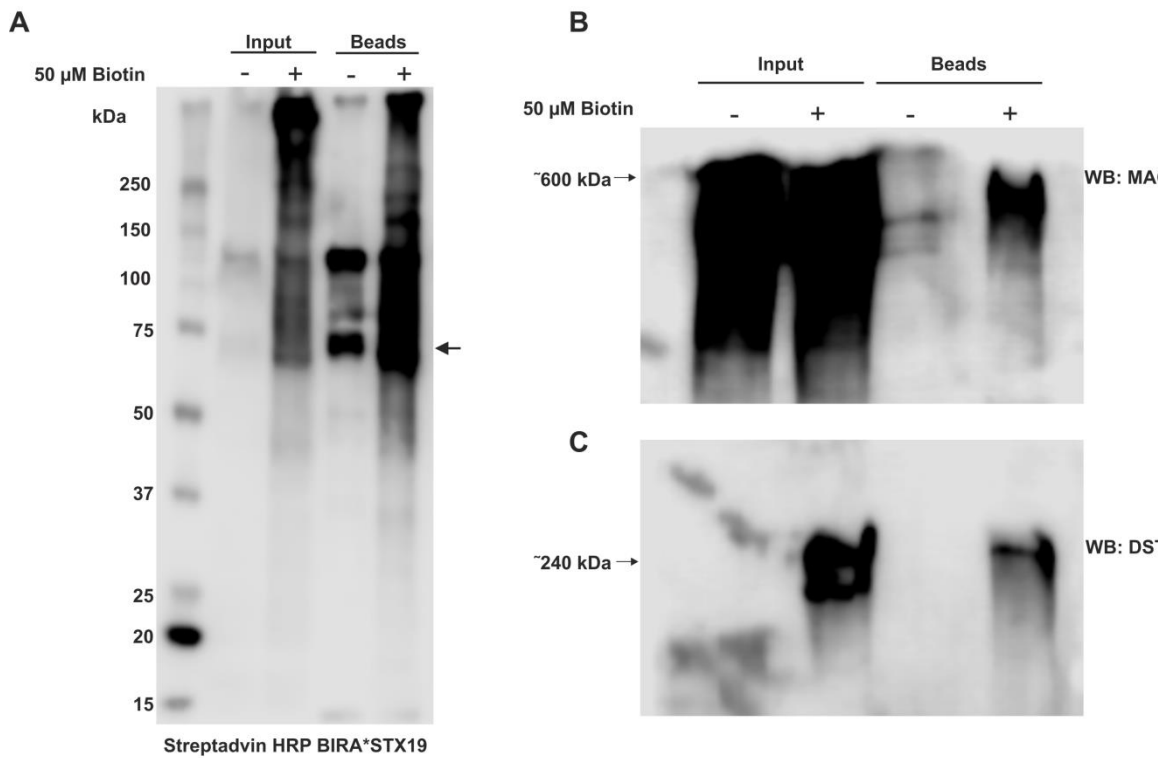


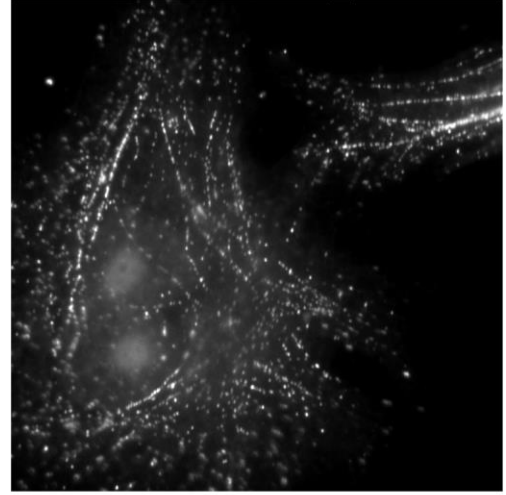
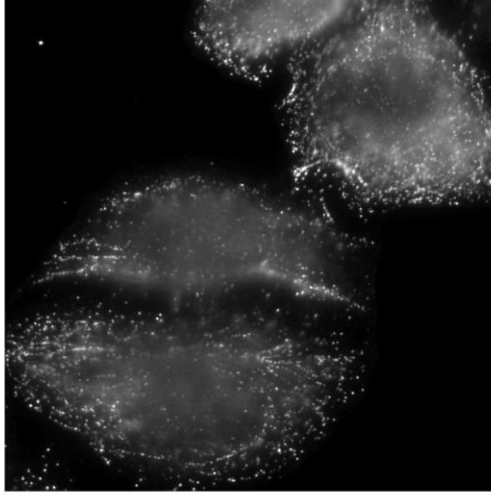
Figure 5-17 BirA*STX19 biotinylates MACF1 and DST.

BirA*STX19 cells were grown overnight in 10 cm plates and incubated for 24 h without biotin (-) or with 50 μ M biotin (+). The cells were collected, lysed and the biotinylated proteins purified with streptavidin agarose beads. **A)** The samples were blotted with streptavidin HRP or MACF1 or DST (**B and C**) followed by either rabbit HRP or goat anti-mouse HRP.

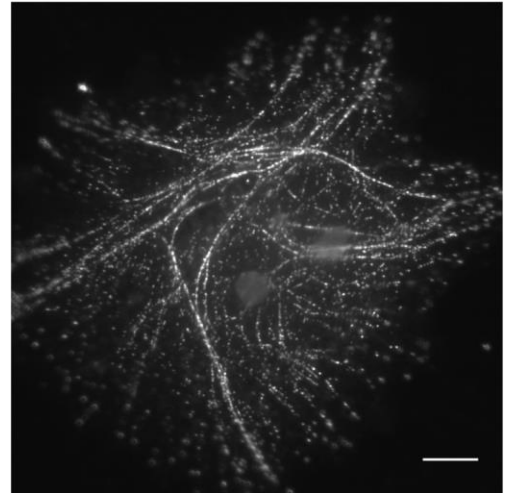
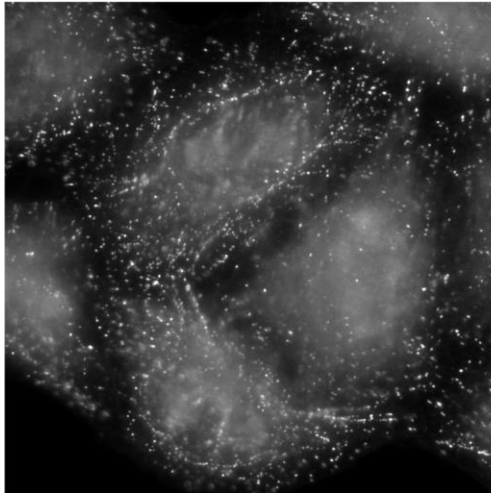
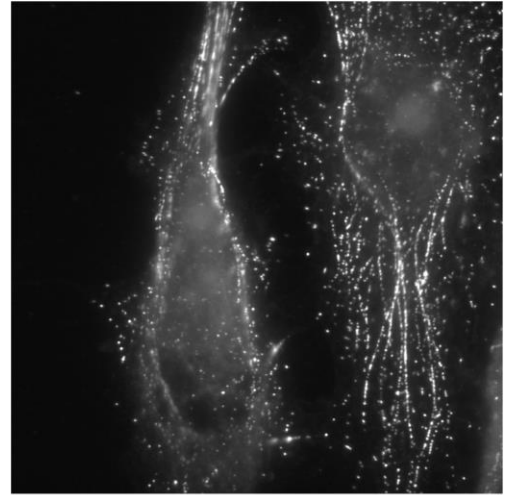
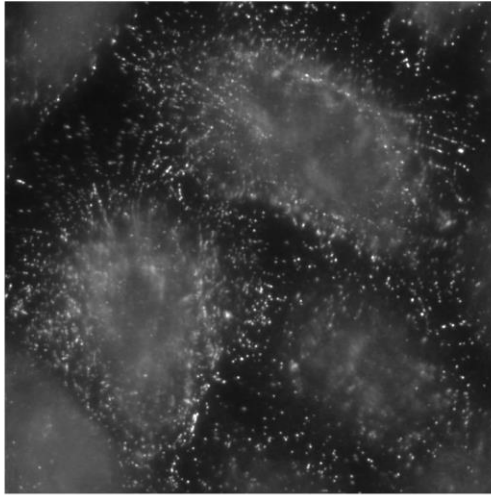
A

Mock

STX19 siRNA 10



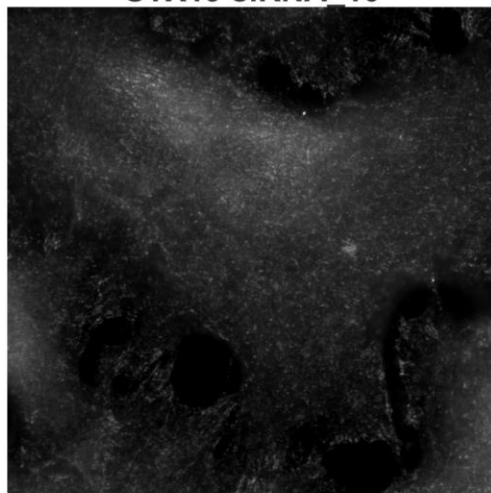
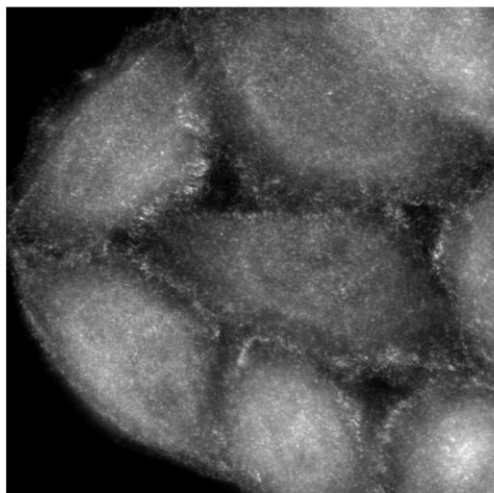
DST



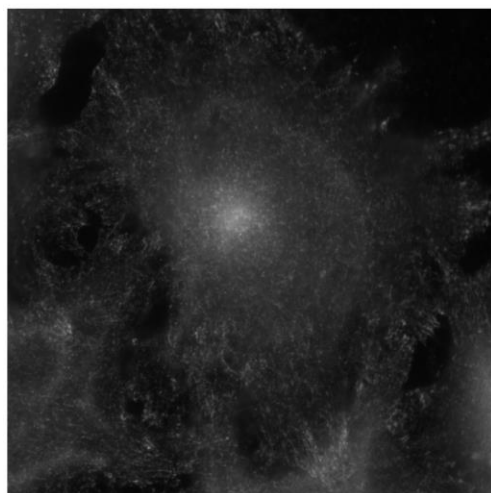
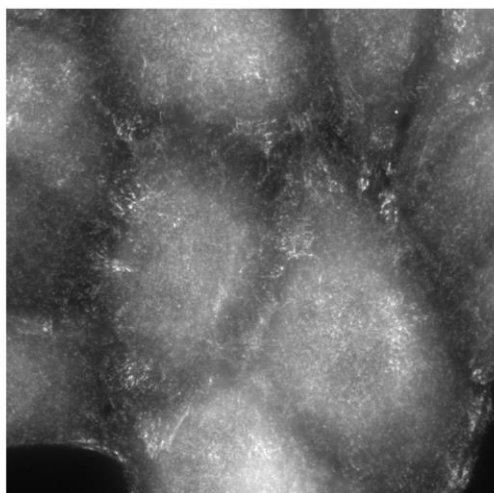
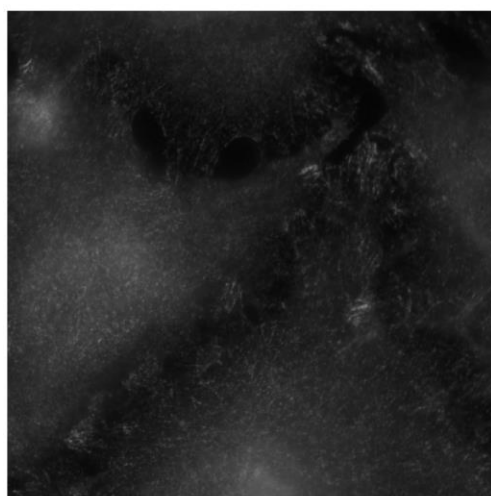
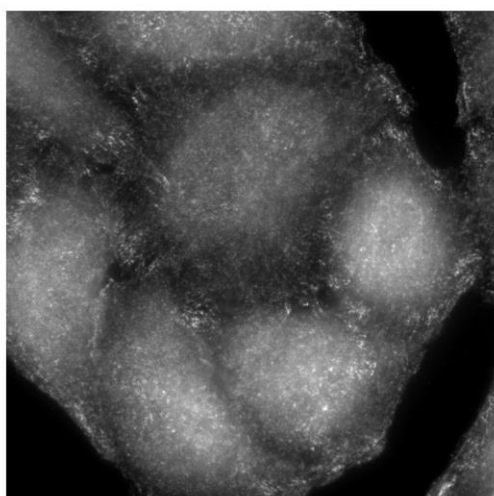
B

Mock

STX19 siRNA 10



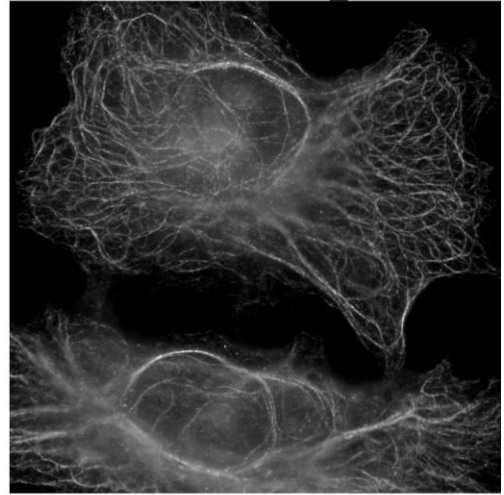
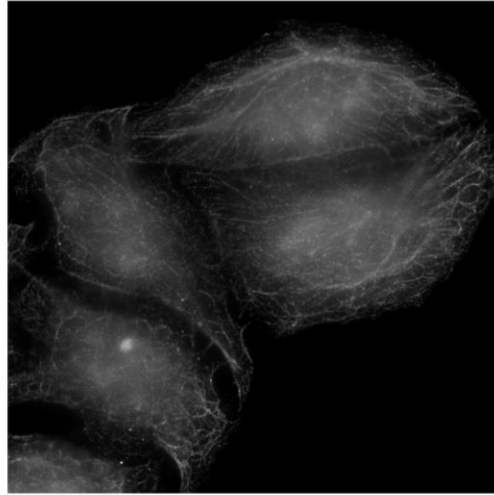
MACF1



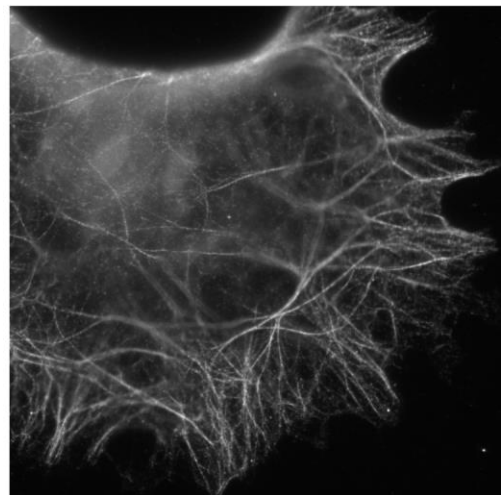
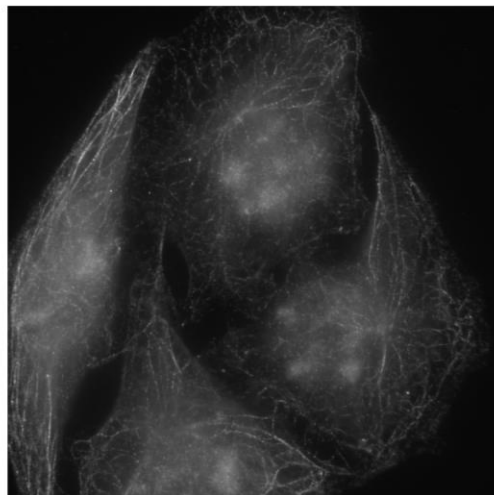
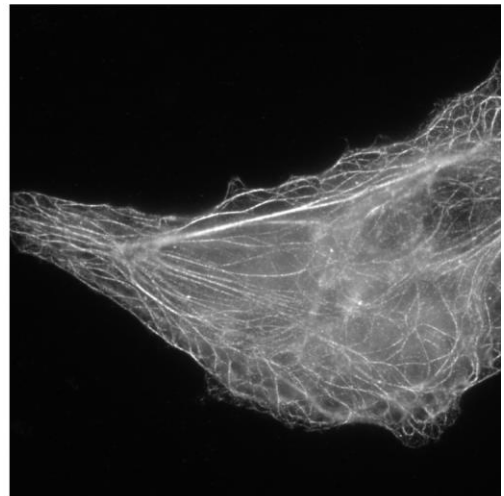
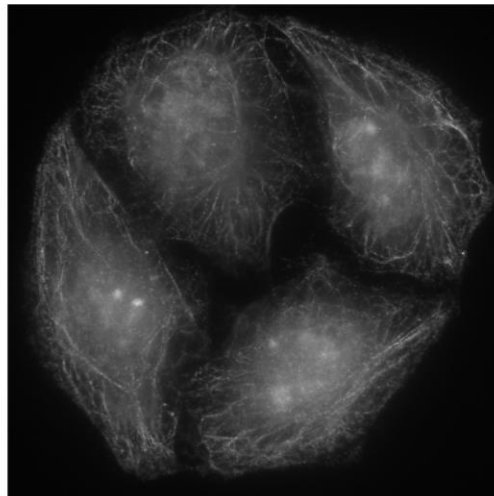
C

Mock

STX19 siRNA 10



KRT20



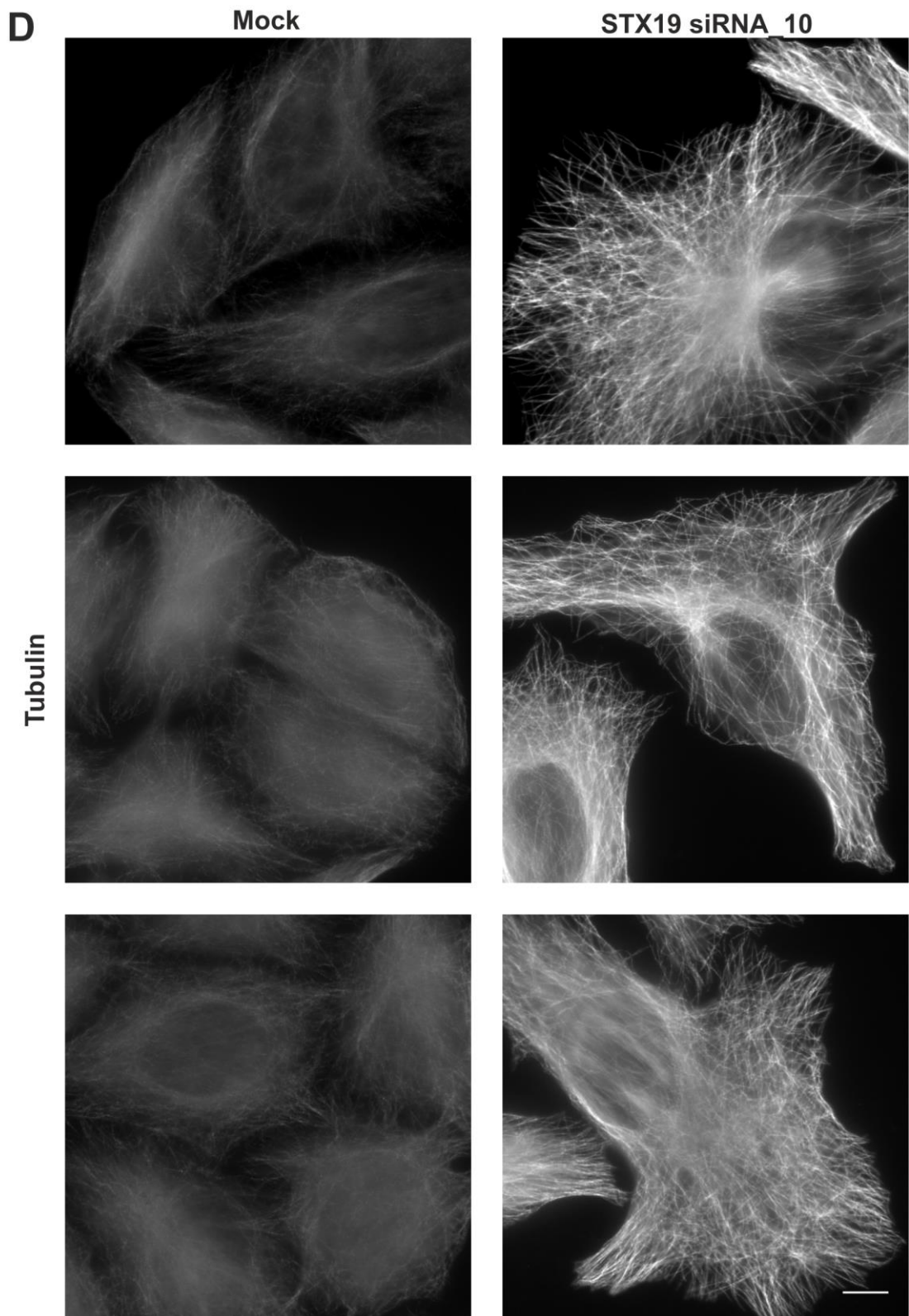


Figure 5-18 STX19 depletion affects the organisation of the cytoskeleton.

HeLaM cells were transfected with STX19 siRNA oligo_10 or mock transfected with lipofectamine RNAiMAX transfection reagent. The cells were fixed, washed, permeabilized with 0.1% saponin and stained with **(A)** DST **(B)** MACF1, **(C)** KRT20, or **(D)** tubulin followed by goat anti-rabbit Alexa 488 nm or

anti-rat 488 nm. Images were obtained from wide field microscope at x60 oil immersion. Scale bar = 10 μm .

6 Chapter Characterisation of SNAP29 membrane targeting

6.1 Introduction

SNAREs have different distribution patterns within the cell and this is determined by their interaction with other SNARE proteins, post-translation modifications and adaptor proteins (Watson and Pessin, 2001, Fukasawa et al., 2004, Fdez et al., 2010, Greaves and Chamberlain, 2011b). SNAP29 belongs to the Qbc_SNAREs subfamily which also includes SNAP23, SNAP25 and SNAP47 (Hong, 2005, Holt et al., 2006). Both SNAP23 and SNAP25 have a cysteine-rich region located within their flexible linker that is palmitoylated (Veit et al., 1996, Greaves et al., 2010, Steegmaier et al., 1998, Ravichandran et al., 1996). This modification allows them to associate with the plasma membrane. SNAP29 does not have this cysteine-rich region indicating that its membrane recruitment must be mediated by an alternate mechanism. SNAP29 has an N-terminal NPF motif which has been shown biochemically to interact with EHD1 (Rotem-Yehudar et al., 2001, Xu et al., 2004). However, it is unclear what role this motif plays in SNAP29s membrane targeting.

MICAL-L1 is a master regulator of endocytic recycling that recruits endocytic machinery such as EHD1, RAB8 and PASCIN2 on to tubular recycling endosomes (Sharma et al., 2009, Giridharan et al., 2013). My research has shown that a pool of SNAP29 is localised to tubular recycling endosomes (TREs), which are enriched with MICAL-L1, RAB8, PASCIN2 and EHD1. I have determined whether MICAL-L1 together with other endocytic machinery play a role in recruiting SNAP29 onto the tubular recycling endosomes. SNAP29 recruitment onto the TREs might regulate its function in both the endocytic and the biosynthetic pathway.

6.2 Chapter aims

The aim of this chapter is to determine how SNAP29 is recruited to TREs by investigating the role of MICAL-L1 and TRE machinery. To address this, I have:

1. Performed immunolocalisation studies in different cells to determine the intracellular distribution of SNAP29.
2. Developed truncation mutants in MICAL-L1 to determine which of the domains were important for SNAP29 membrane targeting.
3. Overexpressed other tubular recycling endosomal markers to determine their role in SNAP29 membrane recruitment.
4. Performed a GFPTRAP IP to determine whether there is a direct interaction between MICAL-L1 and SNAP29.
5. Depleted EHD1 with siRNA to determine its effect on SNAP29 membrane targeting.

6.3 Results

6.3.1 A pool of SNAP29, EHD1, MICAL-L1, PASCIN2 and RAB8 are localised to endocytic recycling tubules

Previous studies using HeLa cells have shown that EHD1, MICAL-L1, PASCIN2 and RAB8 are localised to endocytic recycling tubules (Sharma et al., 2009, Giridharan et al., 2013). To confirm these observations, I have stained HeLaM and RPE cells with antibodies against these markers. My studies confirm that these markers are localised to tubular recycling endosomes in both HeLaM and RPE cells, albeit with differences in the length of the observed tubules (**Figure 6-2**). In addition, I have also identified that a pool of SNAP29 is localised to the tubular recycling endosomes (**Figure 6-2**). In HeLaM cells SNAP29, EHD1 and PASCIN2 localised to short tubules with few long tubules; whereas MICAL-L1 and RAB8 localised to long tubular structures (**Figure 6-2**). To obtain higher resolution images of the TRE, super-resolution microscopy was performed. I observed that endogenous SNAP29, MICAL-L1, and RAB8 is found localised to microdomains on the tubular recycling endosomes, however, with the conventional wide field microscope these markers showed a continuous staining pattern (**Figure 6-3; Figure 6-2**). These studies suggest that SNAP29 is localised to microdomains on TRE.

6.3.2 A pool of SNAP29 colocalises with endogenous MICAL-L1 on tubular recycling endosomes

MICAL-L1 has been used as a marker for the tubular recycling endosomes (Sharma et al., 2009). To identify whether SNAP29 localises to the same compartment marked by MICAL-L1, colocalisation studies were performed. I observed that SNAP29 colocalises with MICAL-L1 on tubular recycling endosomes in HeLaM, A431, CACO-2, RPE and HTIFF cells indicating that this localisation is not cell type specific (Figure 6-4). The length in the tubular recycling endosomes varied between the different cell types. The longest TRE were observed in HeLaM cells and the shortest were found in A431, CACO-2, RPE and HTIFF cells (Figure 6-4). SNAP29 and MICAL-L1 were found to colocalise at the leading edge of CACO-2, RPE and HTIFF cells (Figure 6-4).

6.3.3 Overexpression of MICAL-L1 recruits SNAP29, EHD1, PASCIN2 and RAB8 on to tubular recycling endosomes

MICAL-L1 regulates the recruitment of EHD1 and RAB8 on to the TREs (Sharma et al., 2009, Giridharan et al., 2013, Rahajeng et al., 2012). To investigate whether MICAL-L1 is also required for the recruitment of SNAP29 onto the TREs, HeLaM cells were transfected with GFP-tagged MICAL-L1 and then stained for endogenous SNAP29, EHD1, PASCIN2 and RAB8. In non-transfected cells, only a small pool of SNAP29, EHD1, PASCIN2 and RAB8 are localised to TREs (**Figure 6-2**; Figure 6-5). However, when MICAL-L1 is overexpressed there was a dramatic increase in the tubular staining of SNAP29, EHD1, PASCIN2 and RAB8 (Figure 6-5). This data demonstrates that MICAL-L1 is involved in the recruitment of SNAP29, EHD1, PASCIN2 and RAB8 on to the tubules.

6.3.4 Overexpression of MICAL-L1 does not recruit SNAPs 23-47 or other SNAREs on to tubular recycling endosomes

SNAP29 is a member of the Qbc_SNARE family which consists of SNAPs 23, 25 and 47 (Figure 6-1). To investigate whether MICAL-L1 plays a role in recruiting these other SNAPs on to the TREs, HeLaM cells were transfected with GFP-tagged MICAL-L1 and then stained for endogenous SNAPs 23, 25, 29 and 47. As previously described, we observed endogenous SNAPs 23 and 25

to localise to the plasma membrane and SNAP 47 in the cytoplasm (Figure 6-6) (Veit et al., 1996, Ravichandran et al., 1996, Holt et al., 2006). SNAP29 was localised to the TRE (Figure 6-6). Overexpressed MICAL-L1 did not recruit SNAPs 23, 25 and 47 on to TRE (Figure 6-7). Occasionally in a small proportion of cells, SNAP23 staining was observed on TREs (Figure 6-7). However, the level of recruitment was far less than what was observed for SNAP29 (Figure 6-7). This suggests that MICAL-L1 specifically recruits only SNAP29 on to tubules and not the other members of the SNARE family.

6.3.5 Overexpression of PASCIN2, RAB11, RAB8 and EHD1 does not contribute to SNAP29 recruitment to tubular recycling endosomes

To determine if other TRE components are involved in recruiting SNAP29 to TRE we overexpressed mCherry PASCIN2, GFP RAB11, Strawberry RAB8 and MYC EHD1 in HeLaM cells and determined if SNAP29 localisation was altered. Overexpressed RAB8 and EHD1 are both localised to tubular recycling endosomes, whereas overexpressed PASCIN2 is associated to the plasma membrane and overexpressed RAB11 is localised to recycling endosomes (Sharma et al., 2009, Qualmann and Kelly, 2000, Sonnichsen et al., 2000). I observed that endogenous SNAP29 is lost from the TREs when either RAB8 or EHD1 is overexpressed (Figure 6-8). This result suggests that overexpressed RAB8 and EHD1 might compete with SNAP29 tubular recruitment. Endogenous SNAP29 was not recruited to Rab11 recycling endosomes when Rab11 was overexpressed neither did SNAP29 lose its tubular recycling endosomal localisation (Figure 6-8). Overexpressed PASCIN2 appears to recruit endogenous SNAP29 onto the PM (Figure 6-8; Figure 6-9). This result was very surprising. In order to gain further insight into overexpressed PASCIN2 function, HeLaM cells were transfected with mCherry PASCIN2 and then stained for endogenous SNAP29, STX19, EHD1, MICAL-L1, and RAB8. PASCIN2 did not recruit STX19, EHD1, RAB8 and MICAL-L1 onto the plasma membrane (Figure 6-9). The fact that overexpressed PASCIN2 recruits SNAP29 on to the plasma membrane instead of TRE indicates that it might compete with MICAL-L1 in the recruitment of SNAP29 to tubules. Overall my data suggests that MICAL-L1 is

the key factor in regulating the recruitment of SNAP29 onto TRE and that PASCIN2 may contribute to SNAP29 targeting to the plasma membrane.

6.3.6 Mapping MICAL-L1 domain required for SNAP29 recruitment onto tubular recycling endosomes

MICAL-L1 has two NPF motifs, two coiled-coil domain and a proline-rich region (Rahajeng et al., 2010). EHD1 binds MICAL-L1's NPF motif, MICAL-L1 coiled-coil domain recruits Rab8 and the proline-rich region binds PASCIN2 on to the TREs (Figure 6-10) (Rahajeng et al., 2010). When MICAL-L1 NPF motifs are changed to NAF, the EH-domain of EHD1 no longer binds to MICAL-L1 (Sharma et al., 2009). To gain insight into which of the domains is required in recruiting SNAP29 onto TREs, HeLaM cells were transfected with either MICAL-L1 NPF mutant or the coiled-coil domain of MICAL-L1 and stained for endogenous SNAP29, EHD1, PASCIN2, and RAB8.

As predicted the NPF mutant MICAL-L1 construct is still recruited to TRE. Interestingly, the tubular staining observed in these cells was far more dramatic than that seen with the wild-type construct (Figure 6-11). This suggests the mutant construct is more stably associated with the TRE. The NPF mutant construct recruits both SNAP29 and PASCIN2 efficiently to the TRE but was less efficient at recruiting EHD1 (Figure 6-11).

As previously shown the MICAL-L1 coiled-coil domain is still capable of being recruited to TRE (Sharma et al., 2009). The coiled-coil domain efficiently recruits Rab8 but not SNAP29 and PASCIN2 (

Figure 6-12). Thus, MICAL-L1 coiled-coil domain is not involved in SNAP29 recruitment onto the TREs. However, it should be noted that MICAL-L1 cannot associate with tubular recycling endosomes without its coiled-coil domain as it is this domain that it uses to associate with phosphatidic generated TREs (Sharma et al., 2009, Giridharan et al., 2013).

6.3.7 Developing a biochemical assay to investigate the role of MICAL-L1 in SNAP29 recruitment

My results so far show that MICAL-L1 regulates the recruitment of SNAP29 to TREs. However, it is unclear whether there is a direct interaction between these

proteins or other factors such as PACSIN2 or EHD1 are involved. Based on the fact that SNAP29 has an NPF motif we predict that EHD1 is most likely mediating this process. To investigate this, I have developed a co-immunoprecipitation assay. HEK cells were transfected with wild type GFPMICAL-L1, GFPMICAL-L1 NPF mutant, GFPMICAL-L1 coiled-coil domain and GFP and immuno-isolated using GFPTRAP beads. The Western blot analysis shows that each of the GFP-tagged proteins was effectively trapped onto the beads (Figure 6-13).

The samples were then blotted against EHD1, PASCIN2 and SNAP29. EHD1 co-IPs with wild type GFPMICAL-L1 but not GFPMICAL-L1 NPF mutant, GFPMICAL-L1 coiled-coil domain and GFP (Figure 6-13). This confirms previous studies that show that EHD1 binds to the NPF motif of MICAL-L1 (Giridharan et al., 2013, Sharma et al., 2009). As previously published, the binding of EHD1 to MICAL-L1 does not require the coiled-coil domain (Figure 6-13) (Sharma et al., 2009, Giridharan et al., 2013). PASCIN2 co-IPs with GFP MICAL-L1 and GFPMICAL-L1 NPF mutant but not with GFPMICAL-L1 coiled-coil domain and GFP (Figure 6-13). This also confirms previous studies that show that PASCIN2 interaction with MICAL-L1 does not involve MICAL-L1 NPF motif (Giridharan et al., 2013). Surprisingly, SNAP29 was absent from MICAL-L1 immunoprecipitations even though EHD1 was present (Figure 6-13). It is possible that the interaction between EHD1 and SNAP29 is weak or transient. At present it is difficult to draw any strong conclusion from this negative data.

6.3.8 Depletion of EHD1 impairs endogenous SNAP29 association with the tubular recycling endosomes

Previous studies have shown that the C-terminal EH domain of EHD1 directly binds to the NPF motif of SNAP29 (Xu et al., 2004). To directly determine if EHD1 is required for SNAP29 recruitment to TRE, I knocked down EHD1 using validated siRNA (Gokool et al., 2007) and performed Western blot and immunolocalisation studies. From the Western blot analysis, EHD1 was effectively reduced compared to mock cells (Figure 6-14). The efficiency of the EHD1 knock-down was about 76.46% (Figure 6-14). Surprisingly, we also saw a significant reduction in the levels of SNAP29 by immunoblotting suggesting

that the levels of SNAP29 may be co-regulated by EHD1. In the EHD1 depleted cells, the SNAP29 tubular localisation was reduced by 69.64%, which is statistically significant with $P = 0.0041$ (Figure 6-14). However, the interpretation of this data is complicated by the reduction in the levels of SNAP29. This result suggests that EHD1 is required for SNAP29 tubular localisation.

6.4 Discussion

6.4.1 Summary of results

My results show that endogenous SNAP29, EHD1, PASCIN2, MICAL-L1 and RAB8 localize to MICAL-L1 decorated tubular recycling endosomes. Endogenous SNAP29 colocalises with MICAL-L1 on the TRE in different cell types. Overexpression of MICAL-L1 recruits SNAP29 to TRE and this is specific as other Qbc-SNAREs are not altered by MICAL-L1 overexpression. Overexpression of EHD1, RAB8, PASCIN2 or RAB11 does not enhance the recruitment of SNAP29 to TRE. The recruitment of endogenous SNAP29 by MICAL-L1 on to TRE is unlikely to be direct but mediated by a complex interaction involving EHD1 and PASCIN2. Overexpressed PASCIN2 recruits SNAP29 to the plasma membrane but not onto the TRE. Altering EHD1 levels either by RNAi or overexpression impairs SNAP29 TRE recruitment.

6.4.2 SNAP29 recruitment onto membranes requires a network of interactions between MICAL-L1, EHD1 and PASCIN2

SNAP29, unlike SNAP23 and SNAP25, does not have a cysteine-rich domain for palmitoylation, so it is unclear how it associates with membranes (Steggmaier et al., 1998, Wong et al., 1999, Veit et al., 1996). It has been speculated that SNAP29 might interact with membranes via its interaction with syntaxins and/or other proteins like EHD1 (Rotem-Yehudar et al., 2001, Xu et al., 2004, Hohenstein and Roche, 2001). Recombinant SNAP29 is capable of binding EHD1 (Xu et al., 2004). This interaction involves SNAP29's NPF motif and the C-terminal Eps 15 Homology domain of EHD1 (An earlier study using yeast two-hybrid identified this interaction to rather involve the central coiled-coil domain of EHD1 (Rotem-Yehudar et al., 2001). In the same study, the authors identified PASCIN2 which has three NPF motifs to also interact with the EH

domain of EHD1 (Xu et al., 2004). Further analysis reveals that the interaction between EHD1 and SNAP29 and PASCIN2 are mutually exclusive (Xu et al., 2004).

More than a decade later, EHD1 and PASCIN2 were identified as direct interactors of MICAL-L1 using yeast two-hybrid and affinity capture mass spectrometry based approaches (Sharma et al., 2009, Linkermann et al., 2009). The EH domain of EHD1 interacts with MICAL-L1 NPF motif, whereas the SH3 domain of PASCIN2 associate with MICAL-L1 14 proline-rich domain (382-388 KPAPLPP and 476-482 RPAPRAP) (Figure 6-10) (Sharma et al., 2009, Linkermann et al., 2009, Giridharan et al., 2013).

My results show that endogenous SNAP29 together with EHD1, MICAL-L1, PASCIN2 and RAB8 are all localised to the TRE (**Figure 6-2**; Figure 6-3). Furthermore, endogenous SNAP29 colocalises with MICAL-L1 on the TRE (Figure 6-4). Interestingly, overexpression of MICAL-L1 causes SNAP29 to be recruited to the TREs (Figure 6-5). However, it is unclear how MICAL-L1 facilitates this. MICAL-L1 is a scaffolding protein which recruits many different endocytic accessory proteins (RAB8, EHD1 and PASCIN2) to TRE so it is possible that SNAP29 and MICAL-L1 do not directly interact with each other (Sharma et al., 2009, Giridharan et al., 2013). Based on the published literature it is most likely that MICAL-L1 is recruiting EHD1 onto TRE and EHD1 then binds SNAP29 via its NPF motif. Surprisingly, the NPF mutant of MICAL-L1 still recruits SNAP29 to TRE (Figure 6-11). This result was initially very confusing and went against our model. However, MICAL-L1 recruits proteins such as PASCIN2 which also contains NPF motifs so is capable of recruiting EHD1 (Giridharan et al., 2013). The NPF mutant of MICAL-L1 also recruited PASCIN2 on to the TRE confirming earlier studies that MICAL-L1 and PASCIN2 interaction involves MICAL-L1 proline-rich region and not MICAL-L1 NPF motif (Figure 6-10; Figure 6-11). There was occasionally very weak residual recruitment of EHD1 on to the TRE by NPF mutant of MICAL-L1, which was not as efficient as the wild-type MICAL-L1 (Figure 6-11). This residual weak recruitment of EHD1 could have been mediated by PASCIN2.

Because EHD1 was identified as a SNAP29 interacting partner (Rotem-Yehudar et al., 2001, Xu et al., 2004). I also investigated the role of EHD1 in the recruitment of SNAP29 onto the tubules using overexpression and siRNA approach. Overexpression of EHD1 does not increase the recruitment of SNAP29 on to TRE but results in the loss of SNAP29 (Figure 6-8). This observation suggests EHD1 and SNAP29 are competing with each for their recruitment onto MICAL-L1 decorated tubules. In support of the role of EHD1 having a role in the recruitment of SNAP29 onto TRE, depletion of EHD1 using siRNA also reduces SNAP29 localisation on TRE (Figure 6-14). At present, it is unclear why the levels of SNAP29 are reduced when EHD1 is depleted. It is possible that the loss of SNAP29 from TRE leads to its degradation.

6.4.3 Predicted model of SNAP29 membrane recruitment

I propose that MICAL-L1 recruits SNAP29 to membranes via a network of interactions involving EHD1 and PACSIN2 (Figure 6-15). Under normal conditions MICAL-L1 recruits EHD1 directly via its NPF motif. However, when this motif is disrupted EHD1 is still recruited onto TRE via PACSIN2 which also contains an NPF motif (Figure 6-15). This will facilitate SNAP29 recruitment onto the TREs even in the absence of MICAL-L1's NPF motif. To confirm this model, a mutant version of MICAL-L1 must be generated which is unable to directly bind EHD1 or PACSIN2. It might be possible that MICAL-L1 still recruits SNAP29 via some yet to be identified MICAL-L1 and SNAP29 common interacting partners.

6.4.4 A pool of SNAP29 has a role in cell migration

The localisation of SNAP29 in mammalian cell lines has been poorly defined. I have characterised SNAP29 distribution in HeLaM, A431, CACO-2, RPE and HTIFF cells. From my immunolocalisation studies, SNAP29 was distributed mainly in the cytoplasm but there was a pool of SNAP29 that was localised to tubular recycling endosomes (Figure 6-2; Figure 6-4). Further analysis of SNAP29 distribution patterns in these cells shows that SNAP29 colocalises with MICAL-L1 on the TREs (Figure 6-4). In actively migratory cells (CACO-2, RPE, and HTIFF) which have well formed lamellipodia, SNAP29 colocalises with MICAL-L1 on endosomal structures at the leading edge of cells (Figure 6-4).

During cell migration, focal adhesions at the leading edge of cells are actively turned over (Hood and Cheresh, 2002). Thus, the proper recycling of integrins to these adhesive structures is vital. My data suggests that the pool of SNAP29 localised to TRE at leading edge of cells facilitate the recycling of materials that are required for the formation of adhesion structures. In support of this hypothesis it has been shown that fibroblasts derived from patients deficient in SNAP29 (CEDNIK syndrome) showed defects in cell migration and an accumulation integrin beta one, TF-R, Rab11 and EEA1 vesicles (Sprecher et al., 2005, Rapaport et al., 2010). Depletion of MICAL-L1, EHD1, RAB8 or PASCIN2 cause defects in cell migration and adhesion similar to that observed in CEDNIK fibroblasts (Jovic et al., 2007, Sharma et al., 2009, Reinecke et al., 2014b, Xie et al., 2015, Cousin et al., 2008). Taken together my localisation and targeting studies help explain why loss of SNAP29 causes defects in integrin recycling.

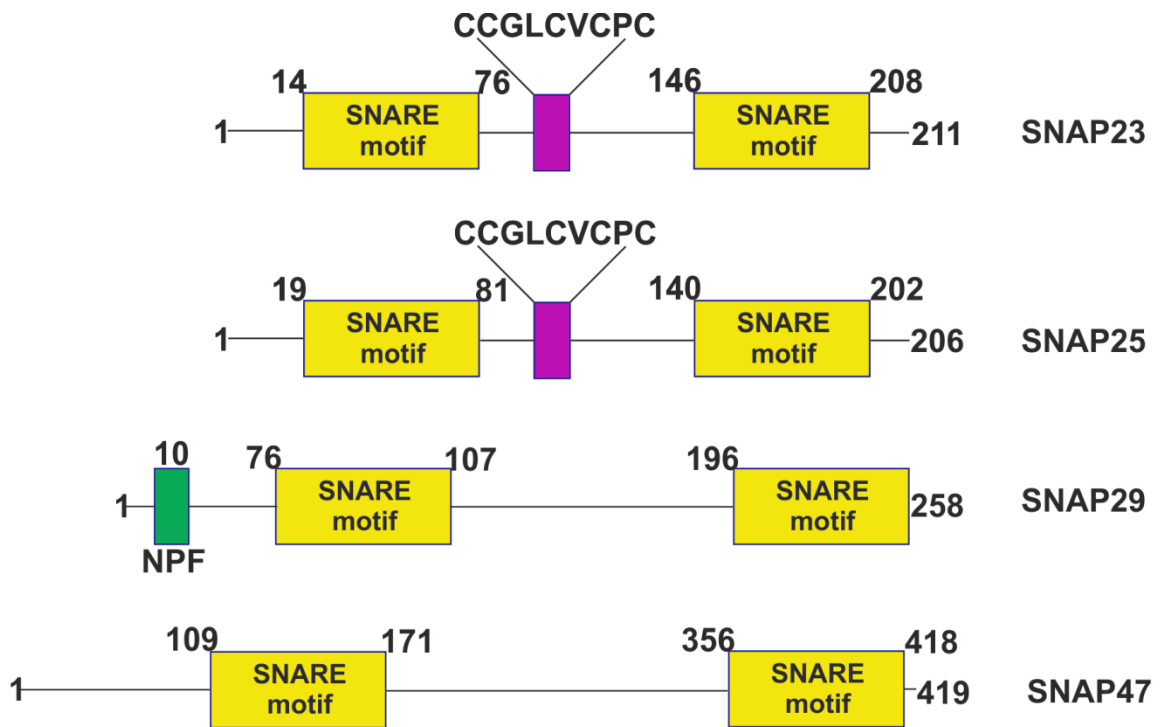


Figure 6-1 Cartoon of SNAPs 23, 25, 29 and 47.

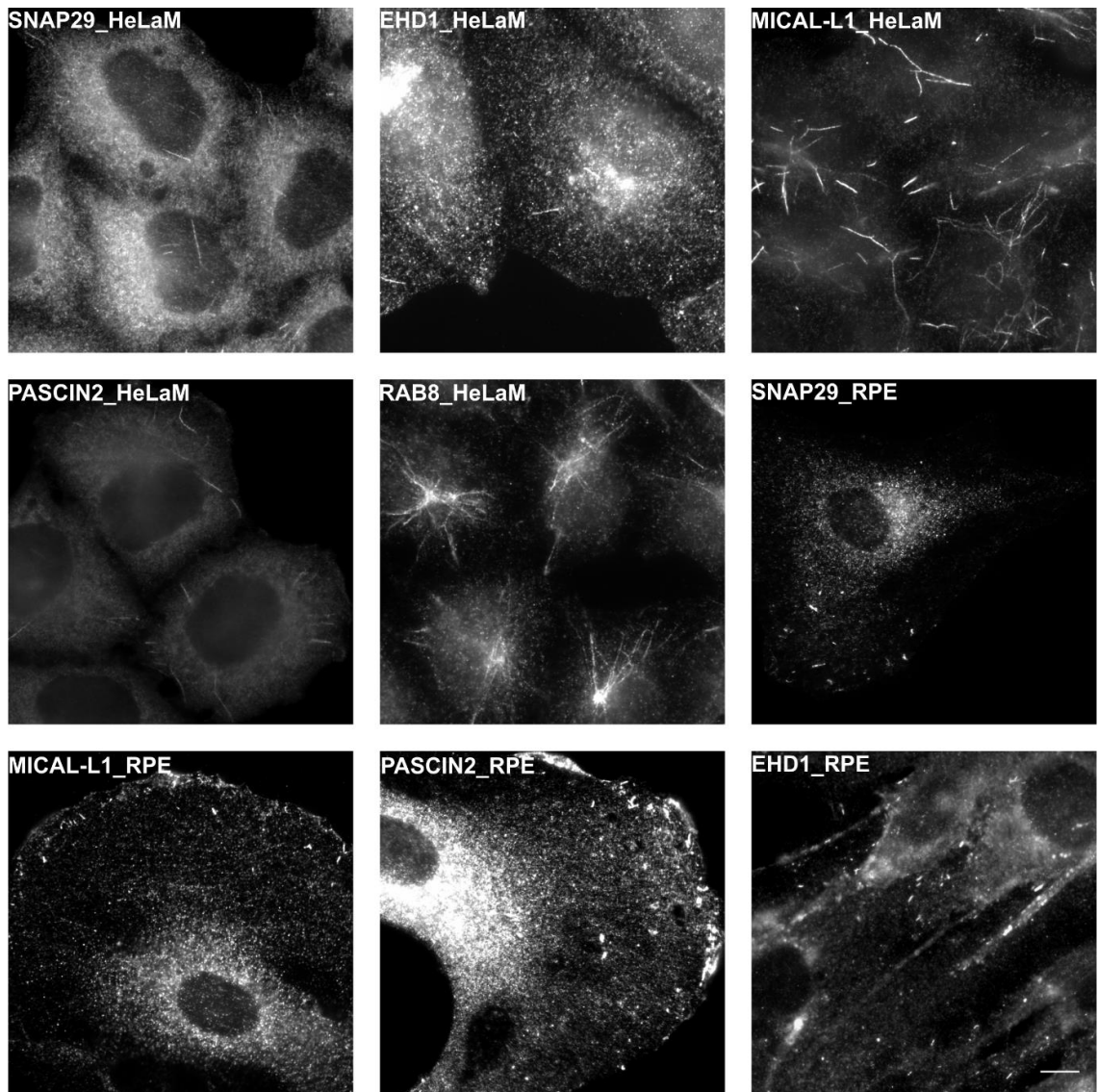


Figure 6-2 Localisation of tubular recycling endosomal markers in both polarised and non-polarised cells.

HeLaM and RPE cells were grown on coverslips. The cells were fixed, washed, permeabilized with 0.1% saponin and stained with anti-SNAP29, anti-EHD1, anti-MICAL-L1 anti-PASCIN2 and anti-RAB8 and followed by donkey anti-rabbit 488 nm or goat anti-mouse Alexa 594 nm. Images were obtained from wide field microscope at x60 oil immersion. Scale bar = 10 μ m.

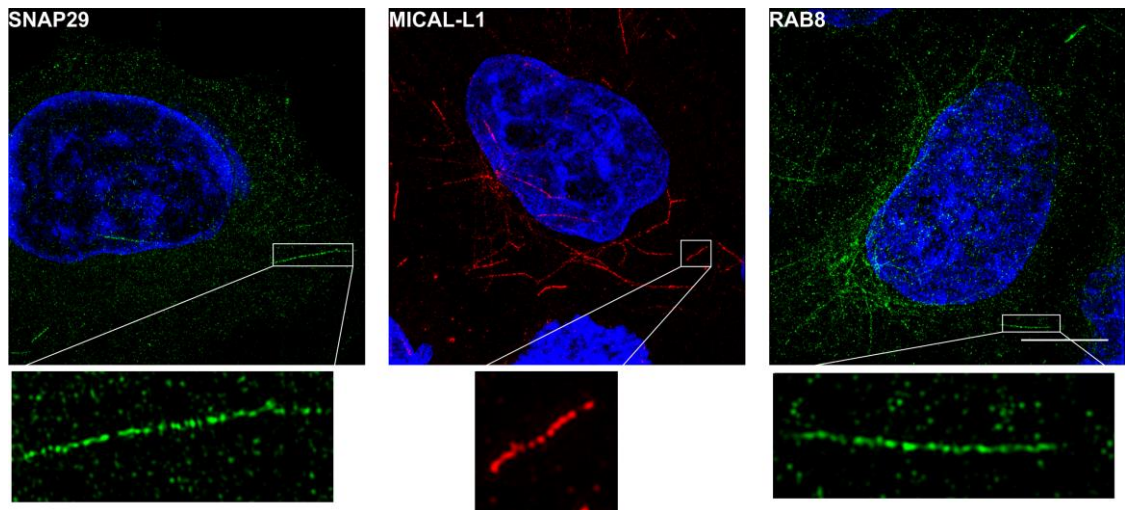


Figure 6-3 SIM images of tubular recycling endosomal markers.

HeLaM cells were grown on coverslips. The cells were fixed, washed, permeabilized with 0.1% saponin and stained with anti-SNAP29, anti-MICAL-L1, and anti-RAB8 and followed by donkey anti-rabbit 488 nm or goat anti-mouse Alexa 594 nm. Images were obtained from DeltaVision Optical Microscopy Experimental (OMX) Three-Dimensional Structured Illumination Microscopy. Scale bar = 2 μ m

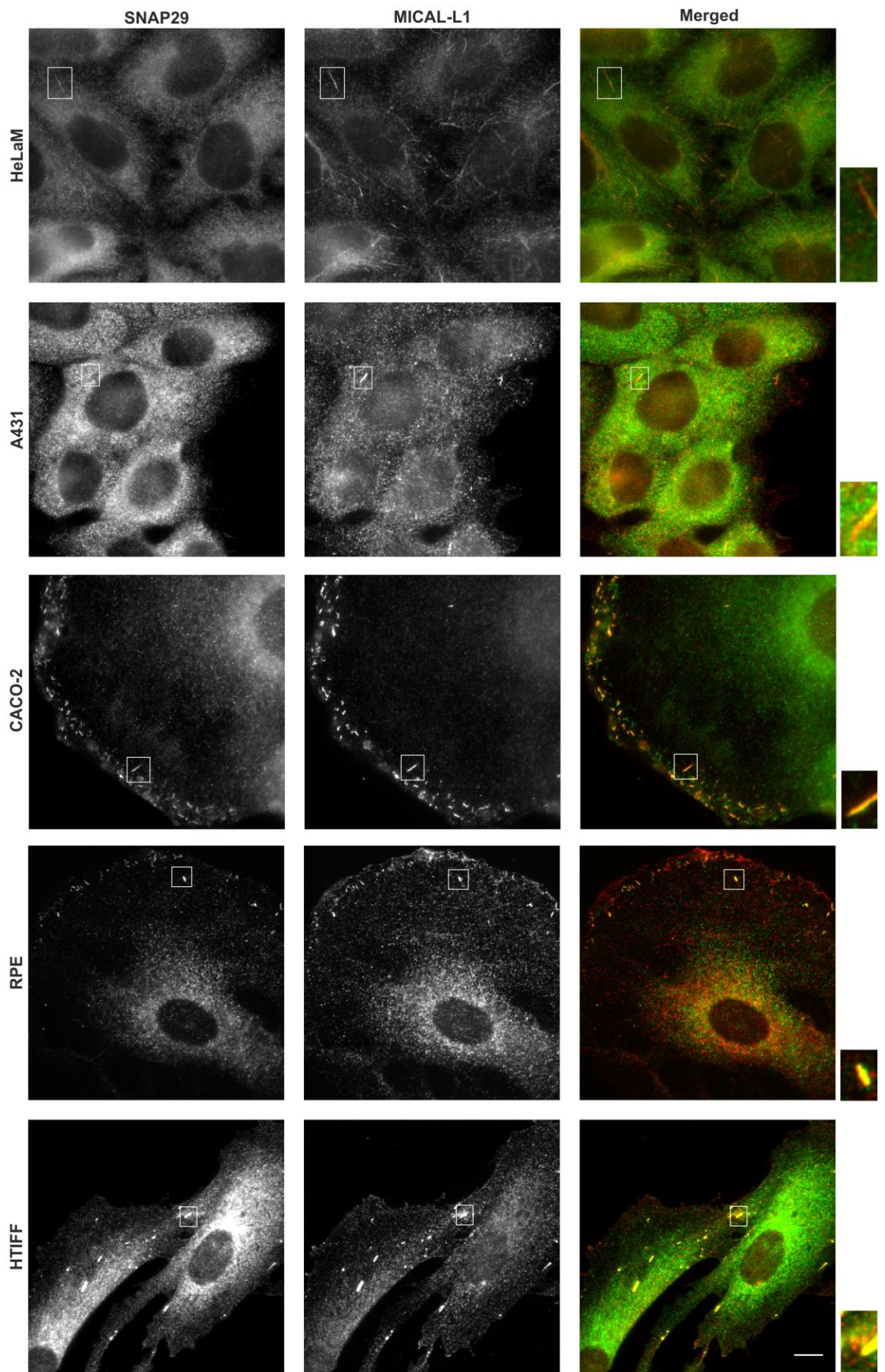


Figure 6-4 SNAP29 colocalises with MICAL-L1 in both polarised and non-polarised cells.

Different cells types were grown on coverslips. The cells were fixed, washed, permeabilized with 0.1% saponin and stained with both anti-SNAP29 and anti-MICAL-L1 followed by donkey anti-rabbit 488 nm and goat anti-mouse Alexa 594 nm. Images were obtained from wide field microscope at x60 oil immersion. Scale bar = 10 μ m.

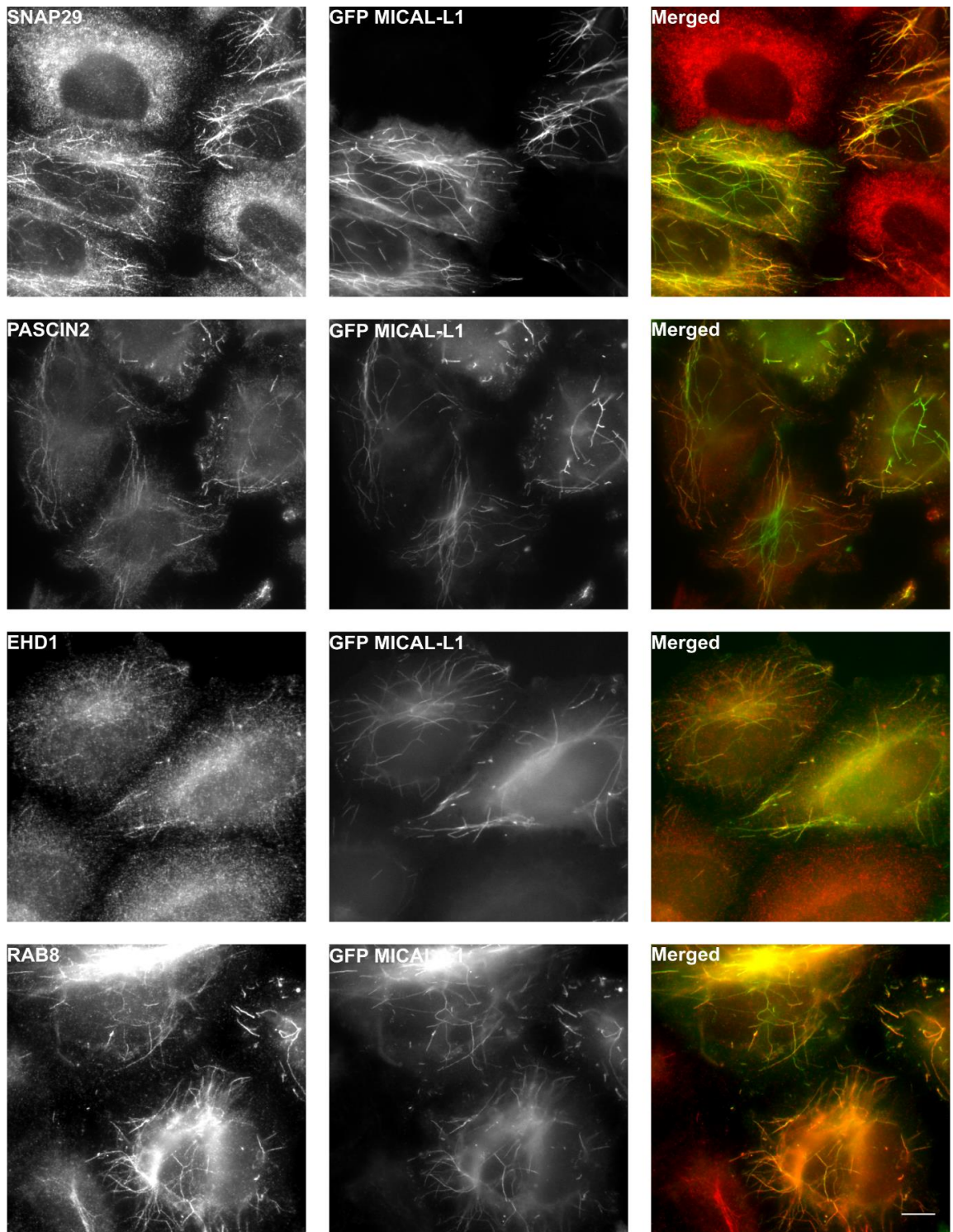


Figure 6-5 Overexpression of MICAL-L1 recruits tubular recycling endosomal markers.

HeLaM cells were grown overnight on coverslips and then transfected with GFP MICAL-L1. 24 h post transfection, the cells were fixed, washed, permeabilized with 0.1% saponin and stained with anti-SNAP29, anti-PASCIN2, anti-EHD1, and anti-RAB8 followed by goat anti-rabbit 594 nm. Images were obtained from

wide field microscope at x60 oil immersion. Scale bar = 10 μ m.

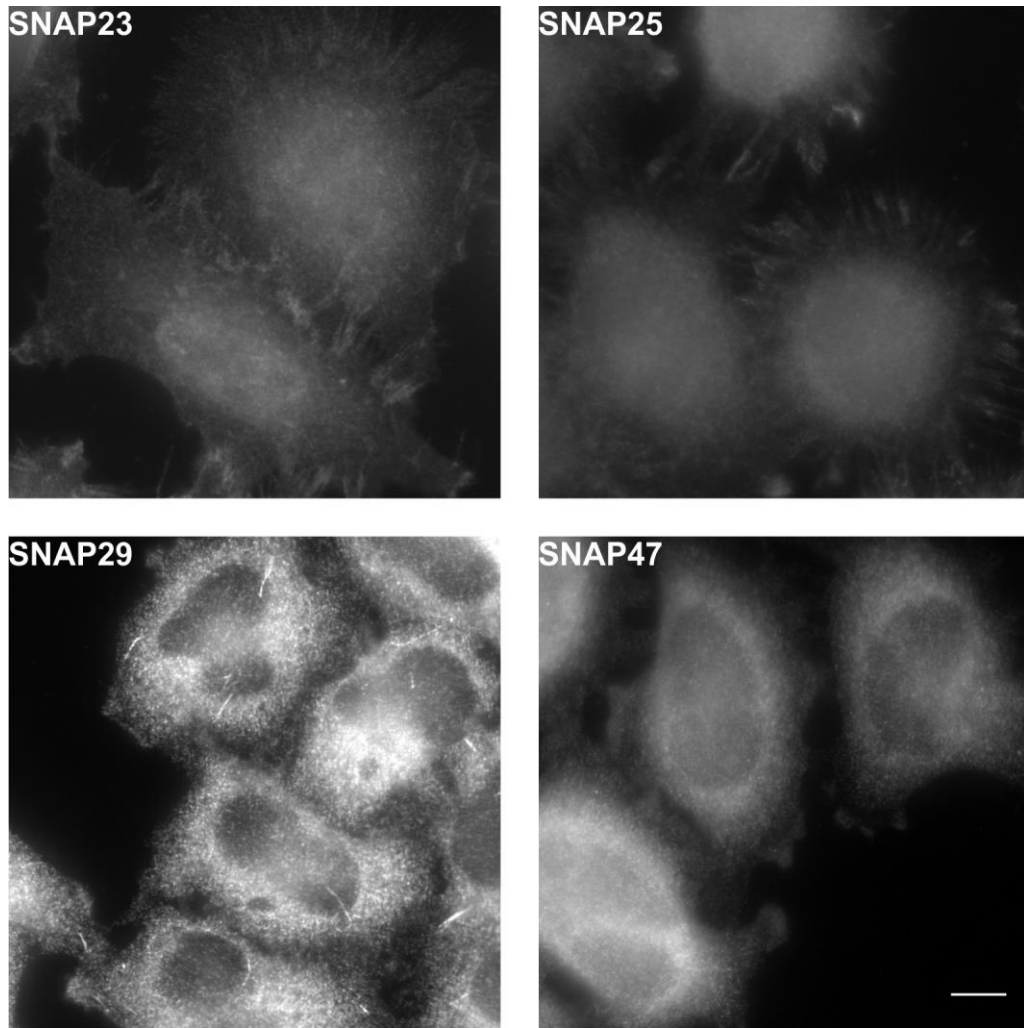


Figure 6-6 Localisation of endogenous SNAPs 23, 25, 29 and 47.

HeLaM were grown on coverslips. The cells were fixed, washed, permeabilized with 0.1% saponin and stained with anti-SNAP23, anti-SNAP25, anti-SNAP29 and anti-SNAP47 and followed by either goat anti-rabbit 594 nm or goat anti-mouse 594 nm. Images were obtained from wide field microscope at x60 oil immersion. Scale bar = 10 μ m.

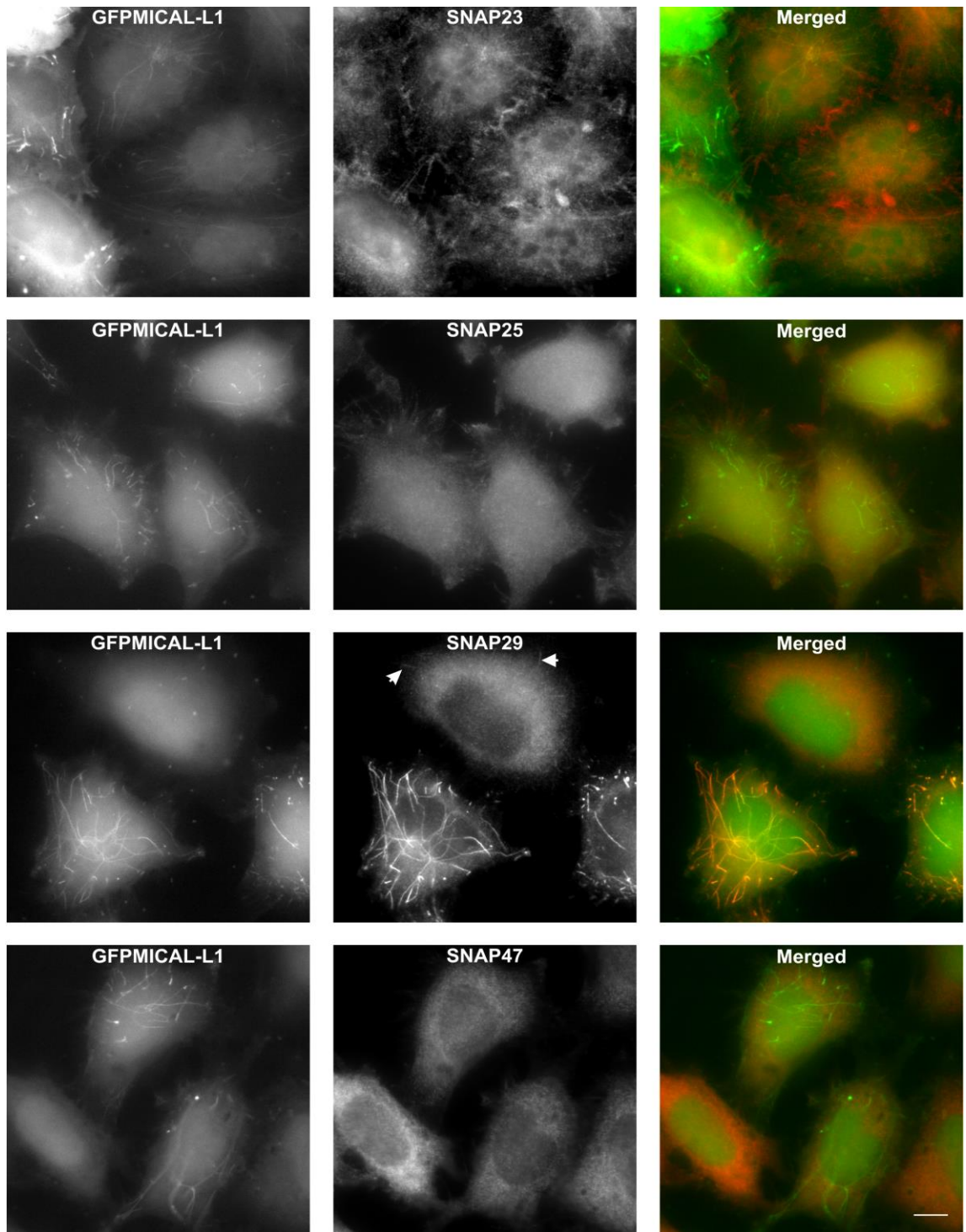


Figure 6-7 Overexpression of MICAL-L1 does not recruit other SNAPs onto tubular recycling endosomes.

HeLaM cells were grown overnight on coverslips and then transfected with GFP MICAL-L1. 24 h post transfection, the cells were fixed, washed, permeabilized with 0.1% saponin and stained with anti-SNAP23, anti-SNAP25, anti-SNAP29, and anti-SNAP47 followed by either goat anti-rabbit 594 nm or goat-anti mouse 594 nm. Images were obtained from wide field microscope at x60 oil immersion.

Arrow points endogenous SNAP29 tubular localisation. Scale bar = 10 μ m.

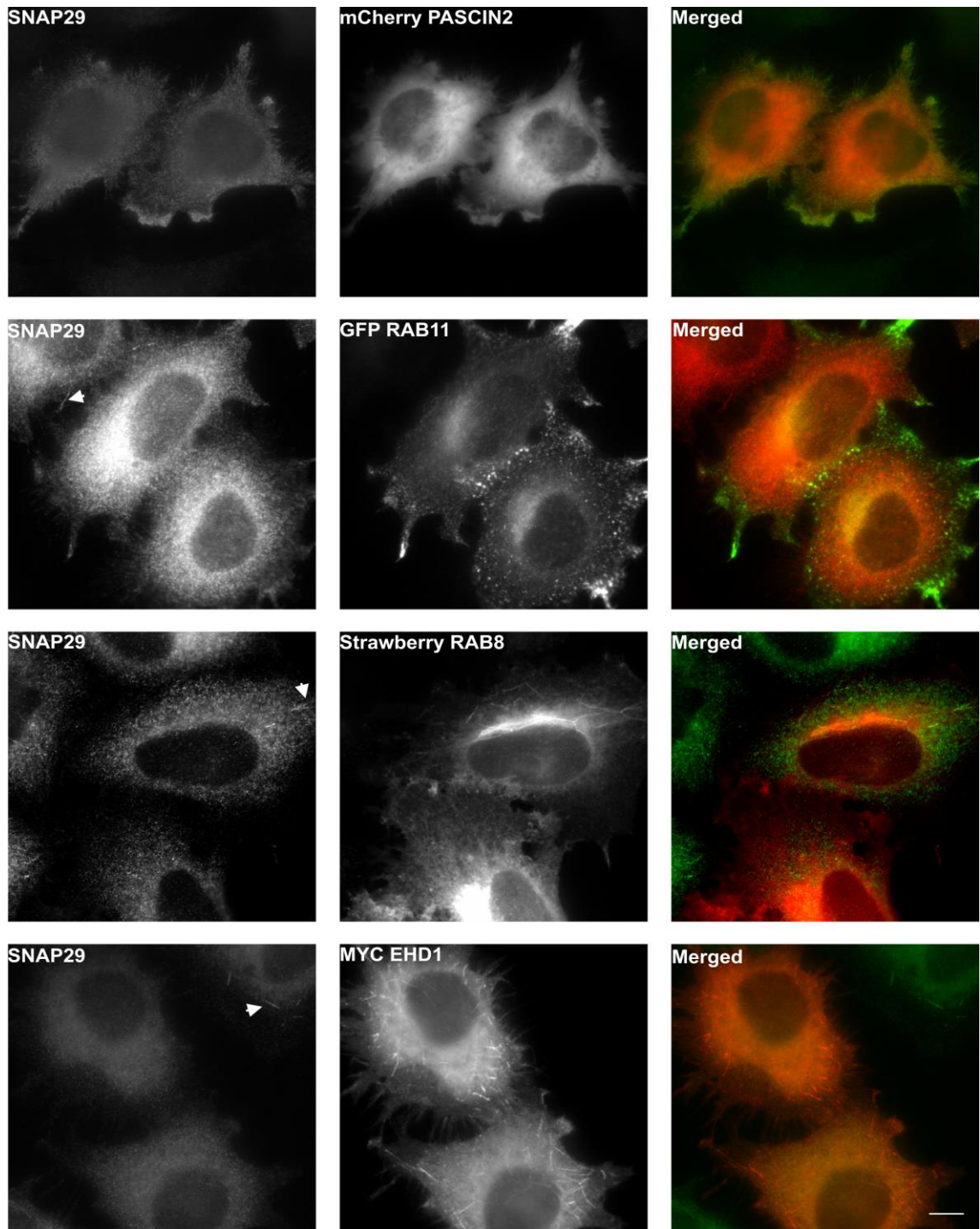


Figure 6-8 Overexpression of Rab8, Rab11, PACSIN2 and EHD1 does not increase the recruitment of SNAP29 on to the TREs.

HeLaM cells were grown overnight on coverslips and then transfected with mCherry PASCIN2, GFP RAB11, Strawberry RAB8 and MYC EHD1. 24 h post transfection, the cells were fixed, washed, permeabilized with 0.1% saponin and stained with anti-SNAP29, followed by either goat anti-rabbit 594 nm or donkey anti-rabbit 488 nm. Images were obtained from wide field microscope at x60 oil immersion. Arrow points endogenous SNAP29 tubular localisation. Scale bar =

10 μm .

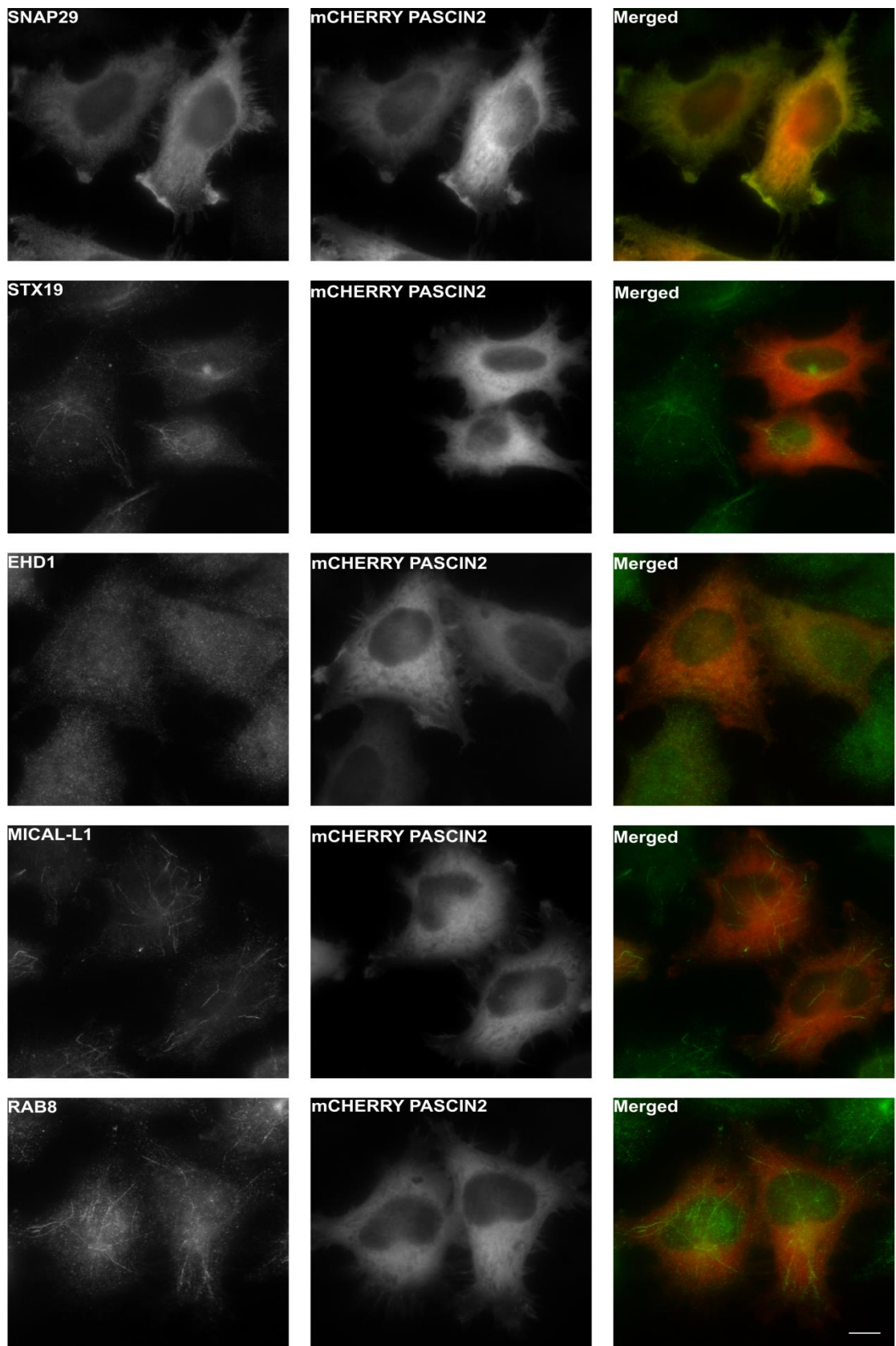


Figure 6-9 Overexpression of PASCIN2 recruits SNAP29 on to the plasma membrane.

Overexpression of PASCIN2 recruits SNAP29 on to the plasma membrane. HeLaM cells were grown overnight on coverslips and then transfected with mCherry PASCIN2. 24 h post transfection, the cells were fixed, washed, permeabilized with 0.1% saponin and stained with anti-SNAP29, anti-STX19, anti-EHD1, anti-MICAL-L1 and anti-RAB8 and followed by either donkey anti-rabbit 488 nm or donkey anti-mouse Alexa 488 nm. Images were obtained from wide field microscope at x60 oil immersion. Scale bar = 10 μ m.

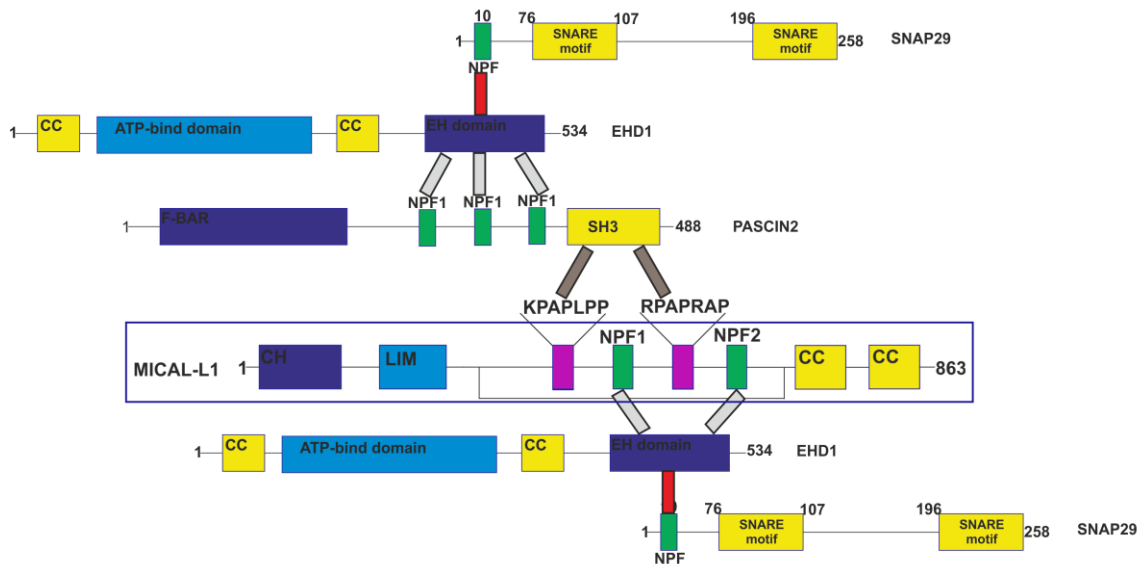


Figure 6-10 Cartoon showing the interaction between MICAL-L1 and other tubular recycling endosomal markers.

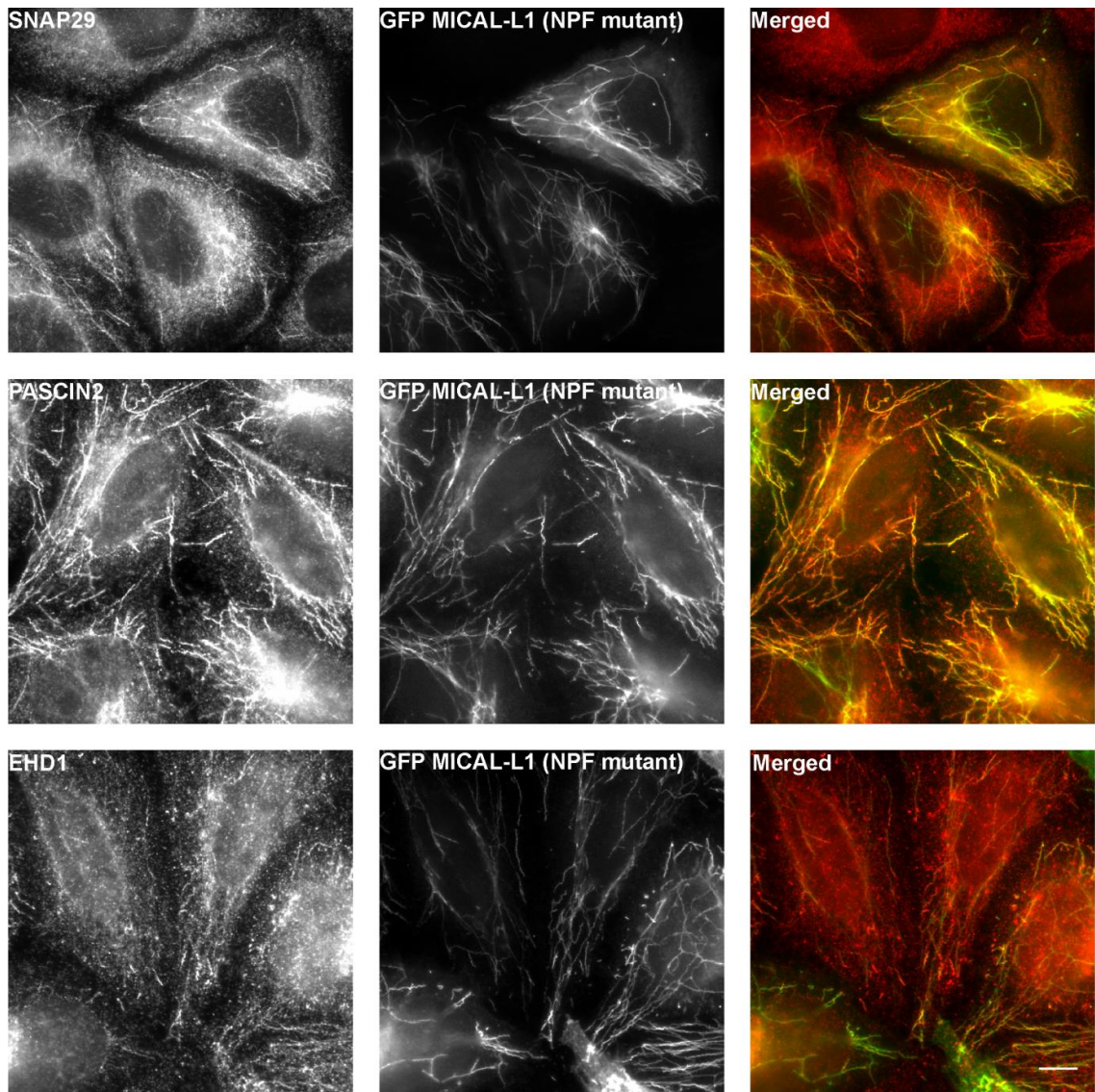


Figure 6-11 SNAP29 recruitment onto the tubular recycling endosomes does not require MICAL-L1 NPF-motif.

HeLaM cells were grown overnight on coverslips and then transfected with GFP MICAL-L1 NPF mutant. 24 h post transfection, the cells were fixed, washed, permeabilized with 0.1% saponin and stained with anti-SNAP29, anti-PASCIN2, and anti-EHD1 followed by goat anti-rabbit 594 nm. Images were obtained from wide field microscope at x60 oil immersion. Scale bar = 10 μ m.

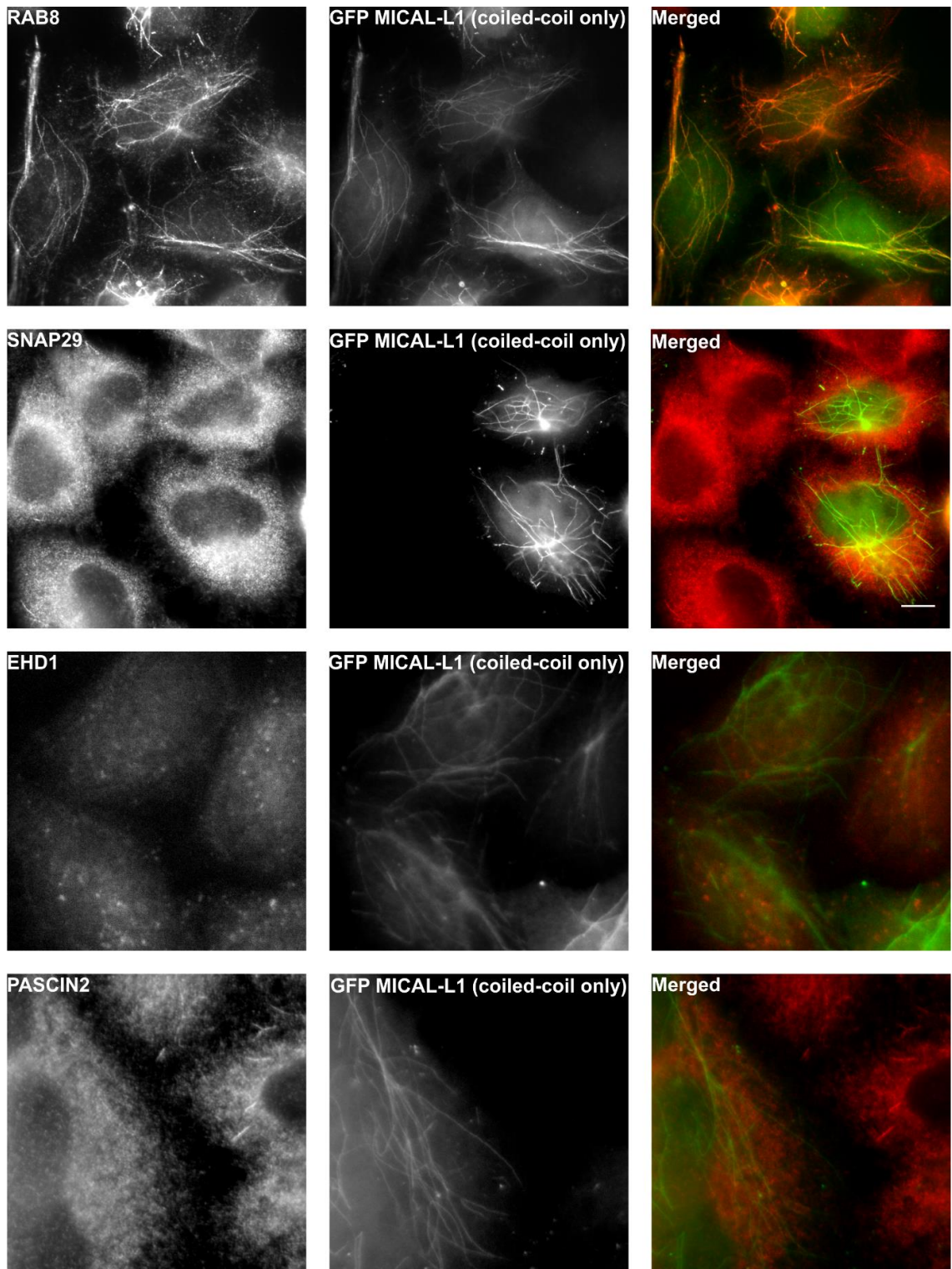


Figure 6-12 Overexpression of MICAL-L1 coiled-coil domain only does not recruit SNAP29 and PASCIN2 onto tubular recycling endosomes.

HeLaM cells were grown overnight on coverslips and then transfected with GFP MICAL-L1 coiled-coil domain only. 24 h post transfection, the cells were fixed, washed, permeabilized with 0.1% saponin and stained with anti-RAB8, anti-

SNAP29, and anti-PASCIN2 followed by either goat anti-rabbit 594 nm. Images were obtained from wide field microscope at x60 oil immersion. Scale bar = 10 μ m.

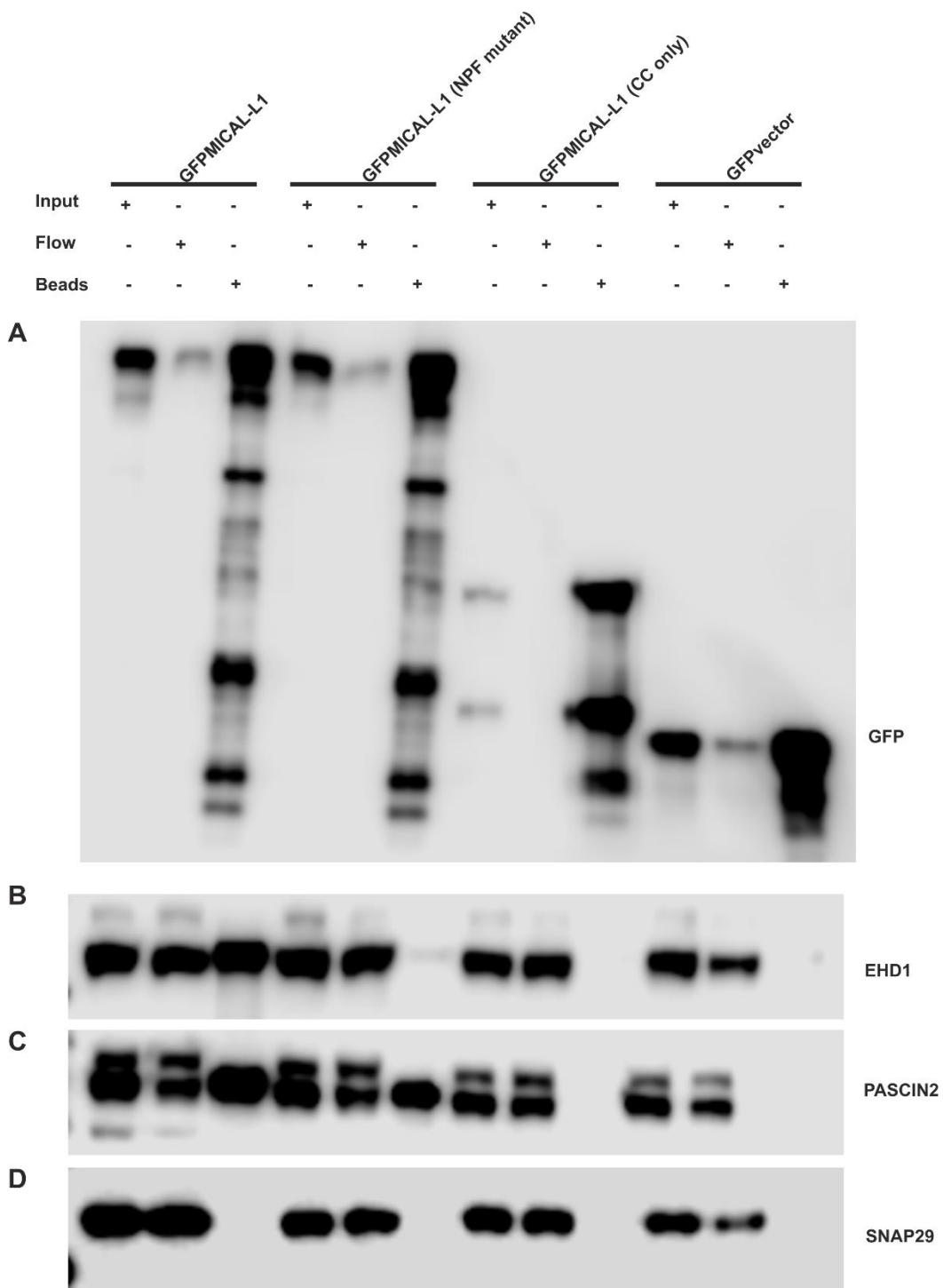


Figure 6-13 SNAP29 does not co-immunoprecipitate with MICAL-L1.

HEK293T cells were seeded overnight into 10 cm plates and then transfected with GFPMICAL-L1, GFPMICAL-L1 NPF mutant, GFPMICAL-L1 coiled-coil domain only and GFP vector only. 48 h post transfection, the cells were collected, lysed with 0.5% Triton x-100 [(TBS (50 mM Tris-HCl (pH 7.4) and 150 mM NaCl), protease inhibitor] and trapped onto GFP beads. The purified samples were blotted with **A**) Anti-GFP **B**) Anti-EHD1 **C**) Anti-PASCIN2 **D**) Anti-

SNAP29 followed by rabbit HRP. Western blots were detected using LI-COR Image Studio Digits Ver 4.0.

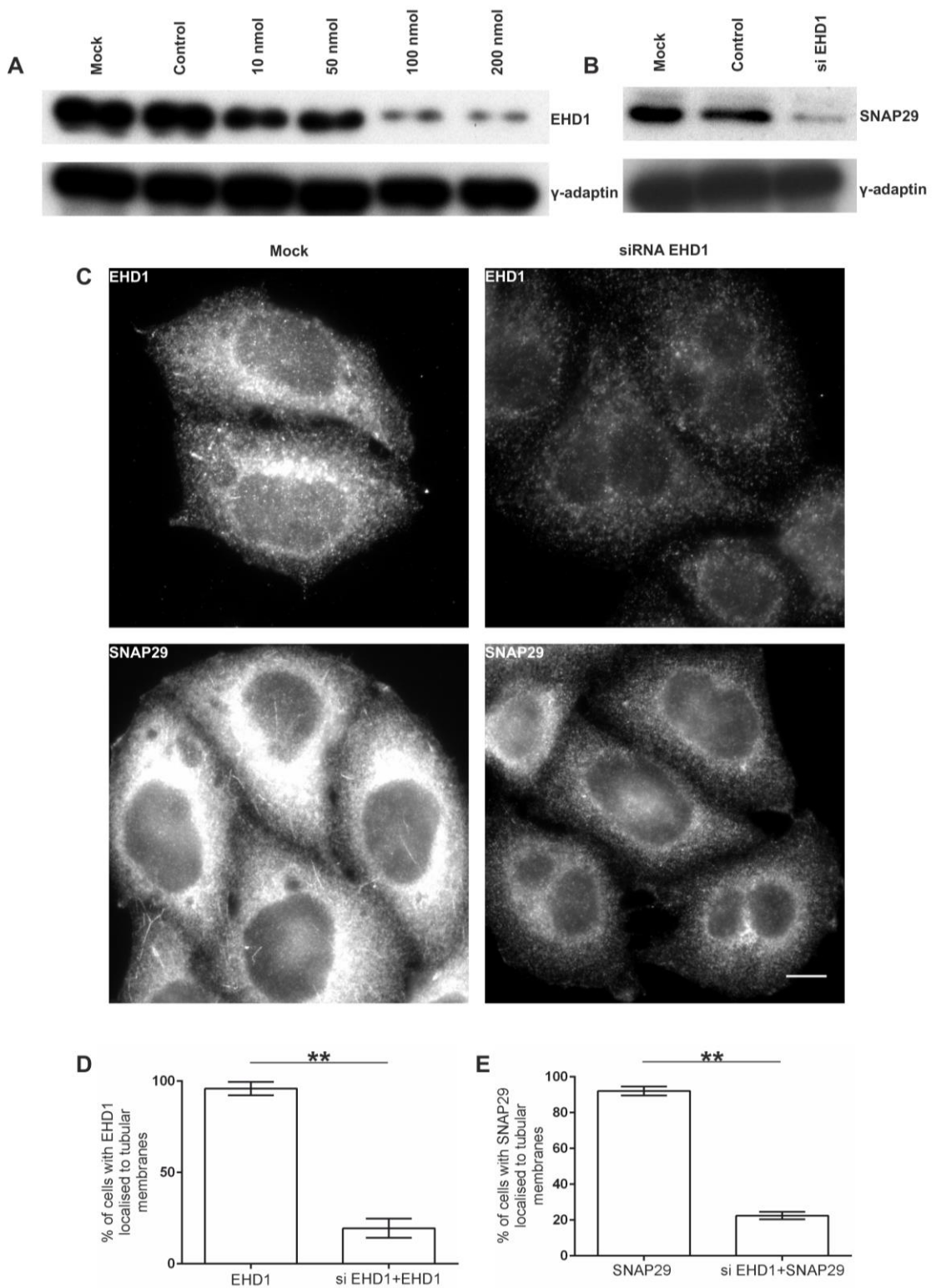


Figure 6-14 Knockdown of EHD1 impairs SNAP29 tubular membrane localisation.

HeLaM cells were seeded into six-well plates overnight and then transfected with or without 100 nM siRNA EHD1 for 72 h. **A and B**) Whole cell lysate of mock, siRNA EHD1 transfected (10, 50, 100, 200 nM) or untransfected cells were blotted with either **A**) EHD1 or **B**) SNAP29 followed by rabbit HRP. Anti-

gamma adaptin monoclonal antibody was used as a loading control. **C, D and E)** 72 h post transfection some cells were plated onto cover slip for another 24 h. The cells were fixed with 4% PFA, permeabilized with 0.2% triton (containing 5% FBS). They were stained with either anti-SNAP29 or anti-EHD1 primary antibody and then counterstained with donkey anti-rabbit Alexa Fluor 488 nm secondary antibody. **C)** Images were obtained from wide field microscope at x60 oil immersion. **D and E)** Approximately 300 cells were counted and the percentage of cells showing tubular EHD1 and SNAP29 membrane localisation quantified (** = $P < 0.01$). Error bar indicates means \pm SEM from three independent experiments.

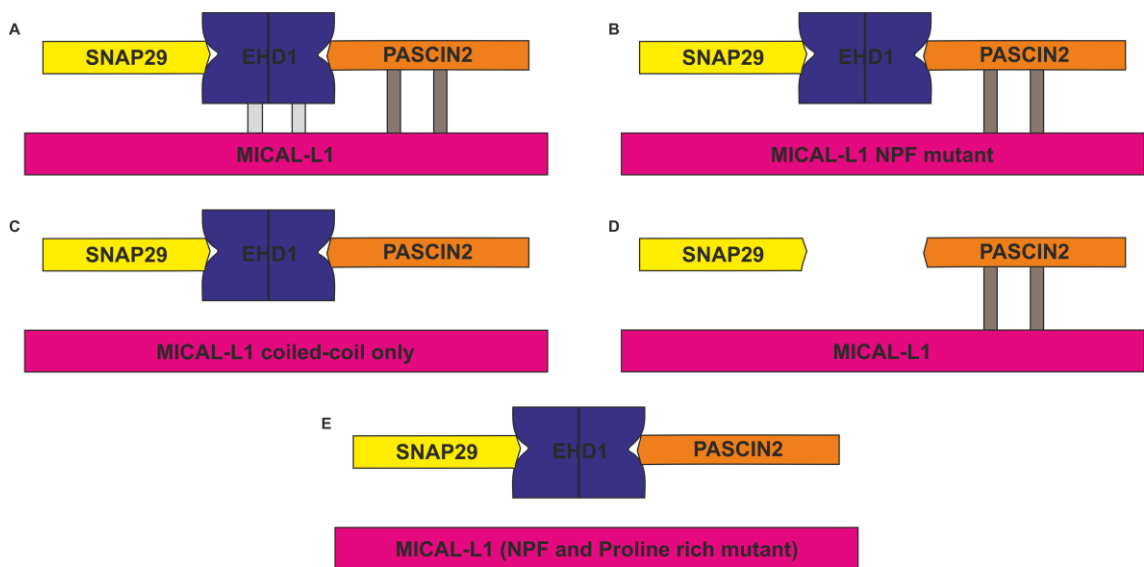


Figure 6-15 Proposed model for the recruitment of SNAP29 on to tubular recycling endosomes.

A) MICAL-L1 recruits SNAP29 onto TRE directly via EHD1. **B)** MICAL-L1 NPF mutant recruits SNAP29 onto the TRE indirectly via EHD1-PASCIN2 interaction **C)** MICAL-L1 coiled-coil domain fails to recruit SNAP29 onto the TRE in the absence of both EHD1 and PASCIN2 binding site. **D)** SNAP29 recruitment onto TRE reduced in the absence of EHD1 **E)** MICAL-L1 NPF and proline mutants might not recruit SNAP29 on to the TRE (Not yet tested).

7 Chapter Discussion and future studies

7.1 Introduction

The aim of my thesis was to elucidate the role of STX19 and SNAP29 in post-Golgi trafficking. To address this: I have examined the cellular distribution pattern of STX19 and SNAP29; dissected how they are targeted to membranes and identified their interacting partners. I have also examined the function of STX19 using RNAi. My data indicates that a pool of SNAP29 and STX19 are localised to TRE where they play an important role in endocytic recycling. However, many questions remain. How is STX19 trafficked to TRE? Is STX19 required for the formation of TRE? Does STX19 function only at the cell surface and what other pathways does STX19 function on?

7.2 A pool of STX19 and SNAP29 is localised to tubular recycling endosomes

STX19 is predominantly localised to TRE and the Golgi region in most cells types we have examined. In CACO-2 cells there is also a significant plasma membrane pool of STX19. Overexpression and RNAi studies confirm STX19's localisation pattern. The pool of STX19 on TRE colocalises with MICAL-L1, RAB8 and internalised GPI-anchored proteins such as CD55 and CD59. Endogenous SNAP29 was also found to colocalise with MICAL-L1 and RAB8 on this tubular recycling endosomal compartment. MICAL-L1 and RAB8 have been studied extensively by the Caplan group and have been shown to be involved in the recycling of several cargo proteins including integrins, TfR, and GPI-anchored proteins (Sharma et al., 2009, Cai et al., 2012, Giridharan et al., 2013, Rahajeng et al., 2012). Similar results were also obtained when STX19 and SNAP29 (unpublished observations from the Peden group) were depleted using RNAi.

At present, it is unclear what role the endosomal pool of STX19 and SNAP29 have in endocytic recycling. Are SNAP29 and STX19 directly involved in the

formation of the TRE or are they involved in the fusion of TRE with the cell surface or the Golgi? (Gordon et al., 2010, Breusegem and Seaman, 2014) In the RNAi studies we see an accumulation of endocytosed material within the cell suggesting that recycling to the cell surface has been perturbed.

A recent super-resolution microscopy study examining the morphology of the TRE compartment showed that TfR positive vesicles were in some instances bridged by endogenous VAMP3/cellubrevin (Xie et al., 2015). VAMP3, STX19 and SNAP29 can form SNARE complexes (Gordon et al., 2010). Thus STX19 and SNAP29 could be required for either the fusion of endocytic vesicles with TRE or be involved in tethering vesicles with the TRE compartment. Future studies will require using two colour SIM and immuno-EM to dissect whether STX19 and SNAP29 are playing a role in forming “bridges” during the transport of cargoes along the tubular recycling endosomes.

7.3 How is STX19 is sorted to TRE?

A pool of STX19 is localised to tubular recycling endosomes. However, it remains unclear how STX19 reaches this compartment. We propose that STX19 is palmitoylated at the Golgi and is then trafficked to the plasma membrane where it is endocytosed and delivered to TRE. However, it is possible that STX19 is directly delivered to TRE from the Golgi.

7.3.1 How is STX19 endocytosed?

My data and Kang et al., 2008 studies have shown that STX19 is palmitoylated and that this palmitoylation is necessary and sufficient for targeting STX19 to the plasma membrane and TRE. Recombinant STX19 colocalises with HRAS, CDC42 and CAG which have been shown to be palmitoylated (Misaki et al., 2010, Kang et al., 2008). Palmitoylation has been shown to allow proteins to associate with lipid rafts/ lipid microdomains (Resh, 2006a, Lingwood and Simons, 2010). Lipid rafts are membrane microdomains are enriched in cholesterol and sphingolipids (Simons and Toomre, 2000, Pike, 2006). These microdomains have also been shown to play an important role in non-clathrin mediated endocytosis (Le Roy and Wrana, 2005, Pelkmans and Helenius, 2002). Thus it is possible that STX19 is endocytosed via non-clathrin mediated

endocytosis and delivered to TRE. However, attempts to colocalise STX19 with lipid microdomains markers such as MYO1C have been unsuccessful. However, we have not looked at caveolin. STX19 segregation into lipid rafts microdomains could be tested by treating cells with methyl-beta-cyclodextrin (a cholesterol sequestering drug known to disrupt lipid rafts) (Ilangumaran and Hoessli, 1998). In the future, it will be important to determine if STX19 is internalised via clathrin or non-clathrin mediated endocytosis.

7.3.2 Is STX19 trafficking between the cell surface, TRE and Golgi?

My STX19 immunolocalisation studies have detected a pool of STX19 at the Golgi region. It is unclear whether this pool represents newly synthesised STX19 on route to the plasma membrane or a stable pool. It has been shown that STX19 is required for endosome to Golgi retrieval so it is possible that the Golgi localised pool of STX19 may be involved in this process. Our Y2H screen and Bio-ID analysis have identified three putative STX19 interacting partners that may be involved in sorting STX19 (GGA3, KIAA1033 and VPS13C). GGA3 was found in our Y2H assay. In the Y2H assay GGA3, was found to interact with STX19 via its VHS and the GAT domains (41-170aa). GGA3 is a member of the GGA family of clathrin adaptor protein which also include GGA1 and GGA3 (Bonifacino, 2004). The VHS domain of GGA proteins binds DXXLL sorting motifs found in proteins such as the CI-MPR and CD-MPR. The GAT domain binds ARF (Bonifacino, 2004). GGA proteins are involved in protein sorting at the TGN have been shown to label tubulovesicular carriers that move along microtubules (Ghosh and Kornfeld, 2004, Bonifacino, 2004, Puertollano et al., 2003). At present it is unclear whether this a physiological interaction as STX19 does not have a classical DXXLL motif. KIAA1033 was found in both our Y2H screen and Bio-ID analysis (enriched by 1.4 fold). KIAA1033 is part of the five-member WASH complex involved in nucleating actin filament formation at the endosomes (Seaman et al., 2013). The WASH-VPSs 26, 29 and 35 retromer complex has been shown to be required for endosome to Golgi and endosome to plasma membrane trafficking (Seaman et al., 2013, Mukadam and Seaman, 2015). VPS13C was only identified in the Bio-ID analysis and is enriched by 9 fold. VPS13C is a member of the VPS

family which also include VPS13 A, B and D (Kolehmainen et al., 2003, Velayos-Baeza et al., 2004). VPS13 have a role in maintaining Golgi integrity, protein sorting and formation of Golgi-derived tubules (Kolehmainen et al., 2003, Seifert et al., 2011). Further studies will be required to validate these putative interacting partners.

As STX19 does not have a transmembrane domain it has made it impossible to use standard antibody-based feeding approaches to study its trafficking. In the future we plan to use a photoactivable GFPSTX19 to follow its trafficking. We can then photoactive GFPSTX19 at the Golgi or different cellular compartments and then follow its trafficking in relation to different markers such as MICAL-L1 or putative interacting partners.

7.4 SNAP29 is recruited to TRE by MICAL-L1

A pool of SNAP29 is localised to tubular recycling endosomes that colocalise with MICAL-L1. Previous studies have identified MICAL-L1 as a key player in the recruitment of other proteins including RAB8, EHD1 and PACSIN2 onto the tubular recycling endosomes (Sharma et al., 2009, Giridharan et al., 2013). Overexpression of MICAL-L1 dramatically increased SNAP29 localisation to the tubular recycling endosome. SNAP29 is the only SNARE protein that has an NPF motif. EHD1, a C-terminal EH-domain containing protein, has been shown to directly interact with SNAP29's NPF motif (Rotem-Yehudar et al., 2001, Xu et al., 2004). We predicted that MICAL-L1 indirectly recruits SNAP29 to membranes via EHD1. In order to confirm this hypothesis, we mutated MICAL-L1 NPF motif so that it no longer binds EHD1. Surprisingly, overexpression of this mutant still recruited SNAP29 onto membranes. Thus we hypothesised PACSIN2 may be recruiting SNAP29 via EHD1. We have been unable to directly examine the role of SNAP29's NPF motif in its membrane recruitment as both overexpressed wild-type and NPF mutant SNAP29 are not targeted to membranes. At the moment, we are unable to explain why overexpressed SNAP29 is not correctly targeted membrane.

SNAP29 membrane attachment has also been shown to be mediated by interactions with syntaxins (4, 6 and 7) (Hohenstein and Roche, 2001). My

studies show that depletion of STX19 impairs SNAP29, MICAL-L1 and RAB8 recruitment to membranes suggesting that STX19 is required for their recruitment onto membranes. STX19 forms a SNARE complex with SNAP29 (Gordon et al., 2010) supporting its role in SNAP29 recruitment. However, overexpression of MICAL-L1 causes STX19 to be lost from TRE suggesting that STX19 only plays a minor role in this process.

7.5 STX19 may have a role in epithelial cell polarity

STX19 is predominantly expressed in mucosal epithelial cells in both rodents and humans. My preliminary localisation studies suggest that STX19 is localised to the basolateral membrane in CACO-2 cells. However, its function in polarised cells is still to be addressed. From our Bio-ID and Y2H screen data, we have identified proteins including NDRG1, ERBB2IP, VANGL1, SCRIB, DMD, DES, MACF1, DST, MYO18A, and STXBP2 (MUNC18-2) which have all been implicated in establishing and maintaining cell polarity. The data suggests that STX19 may have a role in the fusion of material with the plasma membrane which is required for establishing apical/basolateral polarity. To test this we will perform colocalisation studies in CACO-2 cells with markers of cell polarity such as ZO-1, beta-catenin or E-cadherin. We could also determine STX19's role in establishing cell polarity by measuring transepithelial electrical resistance in CACO2 cells depleted for STX19. Furthermore, we will need to determine how STX19 depletion affect the delivery of apical and basolateral markers such as dipeptidyl peptidase IV, GLUT5, sodium hydrogen exchanger (NHE3), aminopeptidase-N, GPI-anchored proteins to the apical or basolateral membrane. Interestingly, depletion of STX19 in HeLaM cells (epithelial-like clone of HeLa cells) causes a dramatic change in cytoskeletal organisation similar to that observed in epithelial to mesenchymal transition (EMT) (Mellman and Nelson, 2008). It will be interesting to determine if STX19 depletion affects the motility of epithelial cells.

7.6 STX19 may function in several post-Golgi pathways.

I have generated several annotated networks for STX19 and its potential interactors from both the yeast two-hybrid screen and Bio-ID analysis. From

these annotated maps it is clear that STX19 has novel links to the cytoskeleton and machinery involved in cell polarity and cell migration. I have summarised below some potential pathways that STX19 might function on.

7.6.1 STX19-MACF1-GOLGA4-Exocyst complex may regulate the trafficking of GPI-anchored proteins

STX19 might form a complex with MACF1, GOLGA4 and the exocyst complex to aid the trafficking of GPI-linked anchored proteins. A previous study has shown that GOLGA4 interacts with MACF1 to aid the trafficking of GPI-linked VSVG (VSVG3-GL-YFP) from the trans-Golgi network to the cell periphery (Kakinuma et al., 2004). EXOC1 was identified to interact with MACF1 and GOLGA4 in a previous yeast two-hybrid screen (Camargo et al., 2007) and affinity capture mass spectrometry (Huttlin et al., 2015). My Y2H screen and Bio-ID analysis have identified three members of the exocyst complex including EXOCs 3-5 and GOLGA4 as STX19 potential interacting partners. My immunolocalisation studies show that internalised GPI-anchored proteins (CD55 and CD59) colocalise with STX19 on the tubular recycling endosomes. My data suggests that STX19 might serve as a unique syntaxin to mediate the fusion of vesicles containing GPI-anchored proteins to the cell surface. In addition, the exocyst complex might provide the docking site (Boyd et al., 2004) to fuse the GPI-linked anchored proteins to the plasma membrane.

7.6.2 ERBB2IP-STX19-DST-MYO18A-Exocyst complex may regulate integrin-mediated cell migration.

ERBB2IP, DST, MYO18A were all identified to be a STX19 potential interacting partner. Previously DST was shown to interact with both ERBB2IP and MYO18A (Hein et al., 2015, Hopkinson and Jones, 2000). ERBB2IP, DST and MYO18A regulate integrin trafficking (Byron et al., 2012, Michael et al., 2014, Litjens et al., 2003). Thus it is possible that ERBB2IP, DST and MYO18A may regulate STX19 function and modulate integrin trafficking with the exocyst complex serving as the docking site. In fact, knockdown of STX19 results in the accumulation of internalised integrins. STX19 also directly interacts with MACF1 which is a close homologue of DST. MACF1 is RAB21 effector protein that has

also been shown to be required for integrin recycling. Thus it is possible that in different cell types STX19 will interact with either MACF1 or DST.

7.6.3 STX19-ZWINT complex may be required for tethering vesicles during mitosis

ZWINT is a multifunctional protein that aids the correct tethering of microtubules to kinetochores during cell division or onto the ER (Schmitt, 2010, Kops et al., 2005). Previously, it was shown that ZW10 (ZWINT interacting protein) is a part of a multisubunit complex involved in tethering Golgi -derived vesicles (Hirose et al., 2004, Arasaki et al., 2006). Using affinity capture mass spectrometry analysis ZWINT was found to interact with SNAP29 (Hutchins et al., 2010). We have also identified ZWINT as a direct interactor of STX19 (found in both Y2H screen, Bio-ID and STX19-IP). MICAL-L1 tubular recycling endosomes have been shown to be required for cytokinesis (Reinecke et al., 2014a). I propose that ZW10 and ZWINT1 may be involved in tethering STX19 positive TRE during mitosis. It may also be possible that ZW10 and ZWINT1 are also required for docking STX19 positive endosomes with the kinetochore. There is increasing evidence that endosomal vesicles play some role in chromosome separation (Capalbo et al., 2011)

At present all of these models are very speculative and will need a significant amount of work to determine if they are correct. However, they provide a framework for working hypothesis to be generated and tested.

References

- ABOU-ZEID, N., PANDJAITAN, R., SENGMANIVONG, L., DAVID, V., LE PAVEC, G., SALAMERO, J. & ZAHRAOUI, A. 2011. MICAL-like1 mediates epidermal growth factor receptor endocytosis. *Mol Biol Cell*, 22, 3431-41.
- ABRAMI, L., LEPPLA, S. H. & VAN DER GOOT, F. G. 2006. Receptor palmitoylation and ubiquitination regulate anthrax toxin endocytosis. *J Cell Biol*, 172, 309-20.
- ACCONCIA, F., SIGISMUND, S. & POLO, S. 2009. Ubiquitin in trafficking: the network at work. *Exp Cell Res*, 315, 1610-8.
- AKIMZHANOV, A. M. & BOEHNING, D. 2015. Rapid and transient palmitoylation of the tyrosine kinase Lck mediates Fas signaling. *Proc Natl Acad Sci U S A*.
- ALBERTS, B., JOHNSON, A., LEWIS, J., MORGAN, D., RAFF, M., ROBERTS, K. & WALTER, P. 2015. Molecular Biology of the Cell, Sixth Edition. *Molecular Biology of the Cell, Sixth Edition*, 1-1342.
- ANASTAS, J. N., BIECHELE, T. L., ROBITAILLE, M., MUSTER, J., ALLISON, K. H., ANGERS, S. & MOON, R. T. 2012. A protein complex of SCRIB, NOS1AP and VANGL1 regulates cell polarity and migration, and is associated with breast cancer progression. *Oncogene*, 31, 3696-708.
- APODACA, G., GALLO, L. I. & BRYANT, D. M. 2012. Role of membrane traffic in the generation of epithelial cell asymmetry. *Nat Cell Biol*, 14, 1235-43.
- ARASAKI, K., TANIGUCHI, M., TANI, K. & TAGAYA, M. 2006. RINT-1 regulates the localization and entry of ZW10 to the syntaxin 18 complex. *Mol Biol Cell*, 17, 2780-8.
- ARMSTRONG, J., THOMPSON, N., SQUIRE, J. H., SMITH, J., HAYES, B. & SOLARI, R. 1996. Identification of a novel member of the Rab8 family from the rat basophilic leukaemia cell line, RBL.2H3. *Journal of Cell Science*, 109, 1265-1274.
- ASHBURNER, M., BALL, C. A., BLAKE, J. A., BOTSTEIN, D., BUTLER, H., CHERRY, J. M., DAVIS, A. P., DOLINSKI, K., DWIGHT, S. S., EPPIG, J. T., HARRIS, M. A., HILL, D. P., ISSEL-TARVER, L., KASARSKIS, A., LEWIS, S., MATESE, J. C., RICHARDSON, J. E., RINGWALD, M., RUBIN, G. M. & SHERLOCK, G. 2000. Gene ontology: tool for the unification of biology. The Gene Ontology Consortium. *Nat Genet*, 25, 25-9.
- BAKER, R. W. & HUGHSON, F. M. 2016. Chaperoning SNARE assembly and disassembly. *Nat Rev Mol Cell Biol*.
- BALCH, W. E., DUNPHY, W. G., BRAELL, W. A. & ROTHMAN, J. E. 1984. Reconstitution of the transport of protein between successive compartments of the Golgi measured by the coupled incorporation of N-acetylglucosamine. *Cell*, 39, 405-16.
- BENNETT, M. K., CALAKOS, N. & SCHELLER, R. H. 1992. Syntaxin: a synaptic protein implicated in docking of synaptic vesicles at presynaptic active zones. *Science*, 257, 255-9.
- BETHANI, I., LANG, T., GEUMANN, U., SIEBER, J. J., JAHN, R. & RIZZOLI, S. O. 2007. The specificity of SNARE pairing in biological membranes is mediated by both proof-reading and spatial segregation. *EMBO J*, 26, 3981-92.
- BILLCLIFF, P. G., NOAKES, C. J., MEHTA, Z. B., YAN, G. H., MAK, L., WOSCHOLSKI, R. & LOWE, M. 2016. OCRL1 engages with the F-BAR protein pacsin 2 to promote biogenesis of membrane-trafficking intermediates. *Molecular Biology of the Cell*, 27, 90-107.
- BITSIKAS, V., CORREA, I. R. & NICHOLS, B. J. 2014. Clathrin-independent pathways do not contribute significantly to endocytic flux. *Elife*, 3.
- BLANC, M., DAVID, F., ABRAMI, L., MIGLIOZZI, D., ARMAND, F., BURGI, J. & VAN DER GOOT, F. G. 2015. SwissPalm: Protein Palmitoylation database. *F1000Res*, 4, 261.
- BOCK, J. B., MATERN, H. T., PEDEN, A. A. & SCHELLER, R. H. 2001. A genomic perspective on membrane compartment organization. *Nature*, 409, 839-41.

- BONIFACINO, J. S. 2004. The GGA proteins: adaptors on the move. *Nat Rev Mol Cell Biol*, 5, 23-32.
- BONIFACINO, J. S. 2014. Vesicular transport earns a Nobel. *Trends Cell Biol*, 24, 3-5.
- BONIFACINO, J. S. & GLICK, B. S. 2004. The mechanisms of vesicle budding and fusion. *Cell*, 116, 153-66.
- BORG, J. P., MARCHETTO, S., LE BIVIC, A., OLLENDORFF, V., JAULIN-BASTARD, F., SAITO, H., FOURNIER, E., ADELAIDE, J., MARGOLIS, B. & BIRNBAUM, D. 2000. ERBIN: a basolateral PDZ protein that interacts with the mammalian ERBB2/HER2 receptor. *Nat Cell Biol*, 2, 407-14.
- BOUAMEUR, J. E., FAVRE, B. & BORRADORI, L. 2014. Plakins, a versatile family of cytolinkers: roles in skin integrity and in human diseases. *J Invest Dermatol*, 134, 885-94.
- BOYD, C., HUGHES, T., PYPAERT, M. & NOVICK, P. 2004. Vesicles carry most exocyst subunits to exocytic sites marked by the remaining two subunits, Sec3p and Exo70p. *J Cell Biol*, 167, 889-901.
- BRAVO-CORDERO, J. J., MARRERO-DIAZ, R., MEGIAS, D., GENIS, L., GARCIA-GRANDE, A., GARCIA, M. A., ARROYO, A. G. & MONTOYA, M. C. 2007. MT1-MMP proinvasive activity is regulated by a novel Rab8-dependent exocytic pathway. *Embo Journal*, 26, 1499-1510.
- BREUSEGEM, S. Y. & SEAMAN, M. N. 2014. Genome-wide RNAi screen reveals a role for multipass membrane proteins in endosome-to-golgi retrieval. *Cell Rep*, 9, 1931-45.
- BRIDGEWATER, R. E., NORMAN, J. C. & CASWELL, P. T. 2012. Integrin trafficking at a glance. *J Cell Sci*, 125, 3695-701.
- BROWN, D. & ORCI, L. 1986. The "coat" of kidney intercalated cell tubulovesicles does not contain clathrin. *Am J Physiol*, 250, C605-8.
- BROWN, N. H. 2008. Spectraplakins: the cytoskeleton's Swiss army knife. *Cell*, 135, 16-8.
- BRUNGER, A. T. 2005. Structure and function of SNARE and SNARE-interacting proteins. *Q Rev Biophys*, 38, 1-47.
- BRYANT, D. M. & MOSTOV, K. E. 2008. From cells to organs: building polarized tissue. *Nat Rev Mol Cell Biol*, 9, 887-901.
- BRYANT, P. J. & HUWE, A. 2000. LAP proteins: what's up with epithelia? *Nat Cell Biol*, 2, E141-3.
- BURGO, A., PROUX-GILLARDEAUX, V., SOTIRAKIS, E., BUN, P., CASANO, A., VERRAES, A., LIEM, R. K., FORMSTECHE, E., COPPEY-MOISAN, M. & GALLI, T. 2012. A molecular network for the transport of the TI-VAMP/VAMP7 vesicles from cell center to periphery. *Dev Cell*, 23, 166-80.
- BURGOYNE, J. R., OVIOSU, O. & EATON, P. 2013a. The PEG-switch assay: A fast semi-quantitative method to determine protein reversible cysteine oxidation. *Journal of Pharmacological and Toxicological Methods*, 68, 297-301.
- BURGOYNE, J. R., OVIOSU, O. & EATON, P. 2013b. The PEG-switch assay: a fast semi-quantitative method to determine protein reversible cysteine oxidation. *J Pharmacol Toxicol Methods*, 68, 297-301.
- BYERS, T. J., BEGGS, A. H., MCNALLY, E. M. & KUNKEL, L. M. 1995. Novel actin crosslinker superfamily member identified by a two step degenerate PCR procedure. *FEBS Lett*, 368, 500-4.
- BYRON, A., HUMPHRIES, J. D., CRAIG, S. E., KNIGHT, D. & HUMPHRIES, M. J. 2012. Proteomic analysis of alpha4beta1 integrin adhesion complexes reveals alpha-subunit-dependent protein recruitment. *Proteomics*, 12, 2107-14.
- CAI, B., CAPLAN, S. & NASLAVSKY, N. 2012. cPLA2alpha and EHD1 interact and regulate the vesiculation of cholesterol-rich, GPI-anchored, protein-containing endosomes. *Mol Biol Cell*, 23, 1874-88.

- CAMARGO, L. M., COLLURA, V., RAIN, J. C., MIZUGUCHI, K., HERMJAKOB, H., KERRIEN, S., BONNERT, T. P., WHITING, P. J. & BRANDON, N. J. 2007. Disrupted in Schizophrenia 1 Interactome: evidence for the close connectivity of risk genes and a potential synaptic basis for schizophrenia. *Mol Psychiatry*, 12, 74-86.
- CAPALBO, L., D'AVINO, P. P., ARCHAMBAULT, V. & GLOVER, D. M. 2011. Rab5 GTPase controls chromosome alignment through Lamin disassembly and relocation of the NuMA-like protein Mud to the poles during mitosis. *Proc Natl Acad Sci U S A*, 108, 17343-8.
- CAPLAN, S., NASLAVSKY, N., HARTNELL, L. M., LODGE, R., POLISHCHUK, R. S., DONALDSON, J. G. & BONIFACINO, J. S. 2002. A tubular EHD1-containing compartment involved in the recycling of major histocompatibility complex class I molecules to the plasma membrane. *EMBO J*, 21, 2557-67.
- CARO, L. G. & PALADE, G. E. 1964. Protein Synthesis, Storage, and Discharge in the Pancreatic Exocrine Cell. An Autoradiographic Study. *J Cell Biol*, 20, 473-95.
- CHAMBERLAIN, L. H., LEMONIDIS, K., SANCHEZ-PEREZ, M., WERNO, M. W., GORLEKU, O. A. & GREAVES, J. 2013. Palmitoylation and the trafficking of peripheral membrane proteins. *Biochem Soc Trans*, 41, 62-6.
- CHAVRIER, P., VINGRON, M., SANDER, C., SIMONS, K. & ZERIAL, M. 1990. Molecular-Cloning of Ypt1/Sec4-Related Cdnas from an Epithelial-Cell Line. *Molecular and Cellular Biology*, 10, 6578-6585.
- CHEN, Z. J. & SUN, L. J. 2009. Nonproteolytic functions of ubiquitin in cell signaling. *Mol Cell*, 33, 275-86.
- CHUNG, H. S., WANG, S. B., VENKATRAMAN, V., MURRAY, C. I. & VAN EYK, J. E. 2013. Cysteine oxidative posttranslational modifications: emerging regulation in the cardiovascular system. *Circ Res*, 112, 382-92.
- CIECHANOVER, A., ELIAS, S., HELLER, H. & HERSHKO, A. 1982. "Covalent affinity" purification of ubiquitin-activating enzyme. *J Biol Chem*, 257, 2537-42.
- CIECHANOVER, A., HELLER, H., ELIAS, S., HAAS, A. L. & HERSHKO, A. 1980. ATP-dependent conjugation of reticulocyte proteins with the polypeptide required for protein degradation. *Proc Natl Acad Sci U S A*, 77, 1365-8.
- CIECHANOVER, A., HELLER, H., KATZ-ETZION, R. & HERSHKO, A. 1981. Activation of the heat-stable polypeptide of the ATP-dependent proteolytic system. *Proc Natl Acad Sci U S A*, 78, 761-5.
- COLEMAN, R. A., RAO, P., FOGELSONG, R. J. & BARDES, E. S. 1992. 2-Bromopalmitoyl-CoA and 2-bromopalmitate: promiscuous inhibitors of membrane-bound enzymes. *Biochim Biophys Acta*, 1125, 203-9.
- COLICELLI, J. 2004. Human RAS superfamily proteins and related GTPases. *Sci STKE*, 2004, RE13.
- CONIBEAR, E. & DAVIS, N. G. 2010. Palmitoylation and depalmitoylation dynamics at a glance. *J Cell Sci*, 123, 4007-10.
- COUSIN, H., DESIMONE, D. W. & ALFANDARI, D. 2008. PACSIN2 regulates cell adhesion during gastrulation in *Xenopus laevis*. *Dev Biol*, 319, 86-99.
- COX, J. & MANN, M. 2008. MaxQuant enables high peptide identification rates, individualized p.p.b.-range mass accuracies and proteome-wide protein quantification. *Nat Biotechnol*, 26, 1367-72.
- CROSS, G. A. 1987. Eukaryotic protein modification and membrane attachment via phosphatidylinositol. *Cell*, 48, 179-81.
- CURRAN, J., MAKARA, M. A., LITTLE, S. C., MUSA, H., LIU, B., WU, X., POLINA, I., ALECUSAN, J. S., WRIGHT, P., LI, J., BILLMAN, G. E., BOYDEN, P. A., GYORKE, S., BAND, H., HUND, T. J. & MOHLER, P. J. 2014. EHD3-dependent endosome pathway regulates cardiac membrane excitability and physiology. *Circ Res*, 115, 68-78.

- DAVDA, D., EL AZZOUNY, M. A., TOM, C. T., HERNANDEZ, J. L., MAJMUDAR, J. D., KENNEDY, R. T. & MARTIN, B. R. 2013. Profiling targets of the irreversible palmitoylation inhibitor 2-bromopalmitate. *ACS Chem Biol*, 8, 1912-7.
- DAWSON, J. C., LEGG, J. A. & MACHESKY, L. M. 2006. Bar domain proteins: a role in tubulation, scission and actin assembly in clathrin-mediated endocytosis. *Trends Cell Biol*, 16, 493-8.
- DAY, P., RIGGS, K. A., HASAN, N., CORBIN, D., HUMPHREY, D. & HU, C. 2011. Syntaxins 3 and 4 mediate vesicular trafficking of alpha5beta1 and alpha3beta1 integrins and cancer cell migration. *Int J Oncol*, 39, 863-71.
- DE BIE, P. & CIECHANOVER, A. 2011. Ubiquitination of E3 ligases: self-regulation of the ubiquitin system via proteolytic and non-proteolytic mechanisms. *Cell Death Differ*, 18, 1393-402.
- DE DUVE, C., PRESSMAN, B. C., GIANETTO, R., WATTIAUX, R. & APPELMANS, F. 1955. Tissue fractionation studies. 6. Intracellular distribution patterns of enzymes in rat-liver tissue. *Biochem J*, 60, 604-17.
- DE DUVE, C. & WATTIAUX, R. 1966. Functions of lysosomes. *Annu Rev Physiol*, 28, 435-92.
- DESHAIES, R. J. & JOAZEIRO, C. A. 2009. RING domain E3 ubiquitin ligases. *Annu Rev Biochem*, 78, 399-434.
- DESOUZA, S., FU, J., STATES, B. A. & ZIFF, E. B. 2002. Differential palmitoylation directs the AMPA receptor-binding protein ABP to spines or to intracellular clusters. *J Neurosci*, 22, 3493-503.
- DIECKMANN, N. M. G., HACKMANN, Y., ARICO, M. & GRIFFITHS, G. M. 2015. Munc18-2 is required for Syntaxin 11 Localization on the Plasma Membrane in Cytotoxic T-Lymphocytes. *Traffic*, 16, 1330-1341.
- DIETRICH, L. E., BOEDDINGHAUS, C., LAGRASSA, T. J. & UNGERMANN, C. 2003. Control of eukaryotic membrane fusion by N-terminal domains of SNARE proteins. *Biochim Biophys Acta*, 1641, 111-9.
- DINKEL, H., VAN ROEY, K., MICHAEL, S., KUMAR, M., UYAR, B., ALTENBERG, B., MILCHEVSKAYA, V., SCHNEIDER, M., KUHN, H., BEHRENDT, A., DAHL, S. L., DAMERELL, V., DIEBEL, S., KALMAN, S., KLEIN, S., KNUDSEN, A. C., MADER, C., MERRILL, S., STAUDT, A., THIEL, V., WELTI, L., DAVEY, N. E., DIELLA, F. & GIBSON, T. J. 2016. ELM 2016-data update and new functionality of the eukaryotic linear motif resource. *Nucleic Acids Research*, 44, D294-D300.
- DOHERTY, G. J. & MCMAHON, H. T. 2009. Mechanisms of endocytosis. *Annu Rev Biochem*, 78, 857-902.
- DOWNWARD, J. 2003. Targeting RAS signalling pathways in cancer therapy. *Nat Rev Cancer*, 3, 11-22.
- DULUBOVA, I., SUGITA, S., HILL, S., HOSAKA, M., FERNANDEZ, I., SUDHOF, T. C. & RIZO, J. 1999. A conformational switch in syntaxin during exocytosis: role of munc18. *EMBO J*, 18, 4372-82.
- DUNCAN, J. R. & KORNFELD, S. 1988. Intracellular movement of two mannose 6-phosphate receptors: return to the Golgi apparatus. *J Cell Biol*, 106, 617-28.
- DUNPHY, J. T. & LINDER, M. E. 1998. Signalling functions of protein palmitoylation. *Biochim Biophys Acta*, 1436, 245-61.
- EDVARDSON, S., CINNAMON, Y., JALAS, C., SHAAG, A., MAAYAN, C., AXELROD, F. B. & ELPELEG, O. 2012. Hereditary sensory autonomic neuropathy caused by a mutation in dystonin. *Ann Neurol*, 71, 569-72.
- FAIRBANK, M., HUANG, K., EL-HUSSEINI, A. & NABI, I. R. 2012. RING finger palmitoylation of the endoplasmic reticulum Gp78 E3 ubiquitin ligase. *FEBS Lett*, 586, 2488-93.
- FANTO, M. & MCNEILL, H. 2004. Planar polarity from flies to vertebrates. *J Cell Sci*, 117, 527-33.

- FASSHAUER, D., SUTTON, R. B., BRUNGER, A. T. & JAHN, R. 1998. Conserved structural features of the synaptic fusion complex: SNARE proteins reclassified as Q- and R-SNAREs. *Proc Natl Acad Sci U S A*, 95, 15781-6.
- FAVRE, B., FONTAO, L., KOSTER, J., SHAFATAIAN, R., JAUNIN, F., SAURAT, J. H., SONNENBERG, A. & BORRADORI, L. 2001. The hemidesmosomal protein bullous pemphigoid antigen 1 and the integrin beta 4 subunit bind to ERBIN. Molecular cloning of multiple alternative splice variants of ERBIN and analysis of their tissue expression. *J Biol Chem*, 276, 32427-36.
- FDEZ, E., MARTINEZ-SALVADOR, M., BEARD, M., WOODMAN, P. & HILFIKER, S. 2010. Transmembrane-domain determinants for SNARE-mediated membrane fusion. *J Cell Sci*, 123, 2473-80.
- FEDOROV, Y., ANDERSON, E. M., BIRMINGHAM, A., REYNOLDS, A., KARPILOW, J., ROBINSON, K., LEAKE, D., MARSHALL, W. S. & KHVOROVA, A. 2006. Off-target effects by siRNA can induce toxic phenotype. *RNA*, 12, 1188-96.
- FELDMANN, A., WINTERSTEIN, C., WHITE, R., TROTTER, J. & KRAMER-ALBERS, E. M. 2009. Comprehensive analysis of expression, subcellular localization, and cognate pairing of SNARE proteins in oligodendrocytes. *J Neurosci Res*, 87, 1760-72.
- FERNANDEZ-SUAREZ, M., CHEN, T. S. & TING, A. Y. 2008. Protein-protein interaction detection in vitro and in cells by proximity biotinylation. *J Am Chem Soc*, 130, 9251-3.
- FIELDS, S. & SONG, O. 1989. A novel genetic system to detect protein-protein interactions. *Nature*, 340, 245-6.
- FILIPPINI, F., ROSSI, V., GALLI, T., BUDILLON, A., D'URSO, M. & D'ESPOSITO, M. 2001. Longins: a new evolutionary conserved VAMP family sharing a novel SNARE domain. *Trends Biochem Sci*, 26, 407-9.
- FIRAT-KARALAR, E. N., RAUNIYAR, N., YATES, J. R., 3RD & STEARNS, T. 2014. Proximity interactions among centrosome components identify regulators of centriole duplication. *Curr Biol*, 24, 664-70.
- FRANCESCHINI, A., SZKLARCZYK, D., FRANKILD, S., KUHN, M., SIMONOVIC, M., ROTH, A., LIN, J., MINGUEZ, P., BORK, P., VON MERING, C. & JENSEN, L. J. 2013. STRING v9.1: protein-protein interaction networks, with increased coverage and integration. *Nucleic Acids Res*, 41, D808-15.
- FUKASAWA, M., VARLAMOV, O., ENG, W. S., SOLLNER, T. H. & ROTHMAN, J. E. 2004. Localization and activity of the SNARE Ykt6 determined by its regulatory domain and palmitoylation. *Proc Natl Acad Sci U S A*, 101, 4815-20.
- FUKATA, M., FUKATA, Y., ADESNIK, H., NICOLL, R. A. & BREDDT, D. S. 2004. Identification of PSD-95 palmitoylating enzymes. *Neuron*, 44, 987-96.
- GALVEZ-SANTISTEBAN, M., RODRIGUEZ-FRATICELLI, A. E., BRYANT, D. M., VERGARAJAUREGUI, S., YASUDA, T., BANON-RODRIGUEZ, I., BERNASCONI, I., DATTA, A., SPIVAK, N., YOUNG, K., SLIM, C. L., BRAKEMAN, P. R., FUKUDA, M., MOSTOV, K. E. & MARTIN-BELMONTE, F. 2012. Synaptotagmin-like proteins control the formation of a single apical membrane domain in epithelial cells. *Nat Cell Biol*, 14, 838-49.
- GALVEZ, T., GILLERON, J., ZERIAL, M. & O'SULLIVAN, G. A. 2012. SnapShot: Mammalian Rab proteins in endocytic trafficking. *Cell*, 151, 234-234 e2.
- GEIGER, B., SPATZ, J. P. & BERSHADSKY, A. D. 2009. Environmental sensing through focal adhesions. *Nat Rev Mol Cell Biol*, 10, 21-33.
- GENE ONTOLOGY, C. 2015. Gene Ontology Consortium: going forward. *Nucleic Acids Res*, 43, D1049-56.
- GEORGE, M., RAINEY, M. A., NARAMURA, M., FOSTER, K. W., HOLZAPFEL, M. S., WILLOUGHBY, L. L., YING, G., GOSWAMI, R. M., GURUMURTHY, C. B., BAND, V., SATCHELL, S. C. & BAND, H. 2011. Renal thrombotic microangiopathy in mice with combined deletion of endocytic recycling regulators EHD3 and EHD4. *PLoS One*, 6, e17838.

- GHOSH, P., DAHMS, N. M. & KORNFELD, S. 2003. Mannose 6-phosphate receptors: new twists in the tale. *Nat Rev Mol Cell Biol*, 4, 202-12.
- GHOSH, P. & KORNFELD, S. 2004. The GGA proteins: key players in protein sorting at the trans-Golgi network. *Eur J Cell Biol*, 83, 257-62.
- GIRIDHARAN, S. S., CAI, B., VITALE, N., NASLAVSKY, N. & CAPLAN, S. 2013. Cooperation of MICAL-L1, syndapin2, and phosphatidic acid in tubular recycling endosome biogenesis. *Mol Biol Cell*, 24, 1776-90, S1-15.
- GIRIDHARAN, S. S., ROHN, J. L., NASLAVSKY, N. & CAPLAN, S. 2012. Differential regulation of actin microfilaments by human MICAL proteins. *J Cell Sci*, 125, 614-24.
- GLICKMAN, M. H. & CIECHANOVER, A. 2002. The ubiquitin-proteasome proteolytic pathway: destruction for the sake of construction. *Physiol Rev*, 82, 373-428.
- GOKOOL, S., TATTERSALL, D. & SEAMAN, M. N. 2007. EHD1 interacts with retromer to stabilize SNX1 tubules and facilitate endosome-to-Golgi retrieval. *Traffic*, 8, 1873-86.
- GOLDENRING, J. R. 2015. Recycling endosomes. *Curr Opin Cell Biol*, 35, 117-122.
- GOLDSTEIN, G., SCHEID, M., HAMMERLING, U., SCHLESINGER, D. H., NIALL, H. D. & BOYSE, E. A. 1975. Isolation of a polypeptide that has lymphocyte-differentiating properties and is probably represented universally in living cells. *Proc Natl Acad Sci U S A*, 72, 11-5.
- GONG, T. W., BESIRLI, C. G. & LOMAX, M. I. 2001. MACF1 gene structure: a hybrid of plectin and dystrophin. *Mamm Genome*, 12, 852-61.
- GONZALEZ, L. C., JR., WEIS, W. I. & SCHELLER, R. H. 2001. A novel snare N-terminal domain revealed by the crystal structure of Sec22b. *J Biol Chem*, 276, 24203-11.
- GONZALO, S. & LINDER, M. E. 1998. SNAP-25 palmitoylation and plasma membrane targeting require a functional secretory pathway. *Mol Biol Cell*, 9, 585-97.
- GOODWIN, J. S., DRAKE, K. R., ROGERS, C., WRIGHT, L., LIPPINCOTT-SCHWARTZ, J., PHILIPS, M. R. & KENWORTHY, A. K. 2005. Depalmitoylated Ras traffics to and from the Golgi complex via a nonvesicular pathway. *J Cell Biol*, 170, 261-72.
- GORDON, D. E., BOND, L. M., SAHLENDER, D. A. & PEDEN, A. A. 2010. A targeted siRNA screen to identify SNAREs required for constitutive secretion in mammalian cells. *Traffic*, 11, 1191-204.
- GORDON, D. E., MIRZA, M., SAHLENDER, D. A., JAKOVLESKA, J. & PEDEN, A. A. 2009. Coiled-coil interactions are required for post-Golgi R-SNARE trafficking. *EMBO Rep*, 10, 851-6.
- GORLEKU, O. A., BARNS, A. M., PRESCOTT, G. R., GREAVES, J. & CHAMBERLAIN, L. H. 2011. Endoplasmic reticulum localization of DHHC palmitoyltransferases mediated by lysine-based sorting signals. *J Biol Chem*, 286, 39573-84.
- GOVERNMENT, U. 2015. *Basic Local Alignment Search Tool* [Online]. Available: http://blast.ncbi.nlm.nih.gov/blast/Blast.cgi?PROGRAM=blastp&PAGE_TYPE=BlastSearch&LINK_LOC=blasthome [Accessed 24th August 2015].
- GRAHAM, S. C., WARTOSCH, L., GRAY, S. R., SCOURFIELD, E. J., DEANE, J. E., LUZIO, J. P. & OWEN, D. J. 2013. Structural basis of Vps33A recruitment to the human HOPS complex by Vps16. *Proc Natl Acad Sci U S A*, 110, 13345-50.
- GRANT, B. D. & CAPLAN, S. 2008. Mechanisms of EHD/RME-1 protein function in endocytic transport. *Traffic*, 9, 2043-52.
- GRANT, B. D. & DONALDSON, J. G. 2009. Pathways and mechanisms of endocytic recycling. *Nat Rev Mol Cell Biol*, 10, 597-608.
- GREAVES, J. & CHAMBERLAIN, L. H. 2011a. DHHC palmitoyl transferases: substrate interactions and (patho)physiology. *Trends Biochem Sci*, 36, 245-53.
- GREAVES, J. & CHAMBERLAIN, L. H. 2011b. Differential palmitoylation regulates intracellular patterning of SNAP25. *J Cell Sci*, 124, 1351-60.

- GREAVES, J., GORLEKU, O. A., SALAUN, C. & CHAMBERLAIN, L. H. 2010. Palmitoylation of the SNAP25 protein family: specificity and regulation by DHHC palmitoyl transferases. *J Biol Chem*, 285, 24629-38.
- GREAVES, J., PRESCOTT, G. R., FUKATA, Y., FUKATA, M., SALAUN, C. & CHAMBERLAIN, L. H. 2009. The hydrophobic cysteine-rich domain of SNAP25 couples with downstream residues to mediate membrane interactions and recognition by DHHC palmitoyl transferases. *Mol Biol Cell*, 20, 1845-54.
- GREAVES, J., SALAUN, C., FUKATA, Y., FUKATA, M. & CHAMBERLAIN, L. H. 2008. Palmitoylation and membrane interactions of the neuroprotective chaperone cysteine-string protein. *J Biol Chem*, 283, 25014-26.
- GRIGORIEV, I., YU, K. L., MARTINEZ-SANCHEZ, E., SERRA-MARQUES, A., SMAL, I., MEIJERING, E., DEMMERS, J., PERANEN, J., PASTERKAMP, R. J., VAN DER SLUIJS, P., HOOGENRAAD, C. C. & AKHMANOVA, A. 2011. Rab6, Rab8, and MICAL3 cooperate in controlling docking and fusion of exocytotic carriers. *Curr Biol*, 21, 967-74.
- GUILHERME, A., SORIANO, N. A., BOSE, S., HOLIK, J., BOSE, A., POMERLEAU, D. P., FURCINITTI, P., LESZYK, J., CORVERA, S. & CZECH, M. P. 2004. EHD2 and the novel EH domain binding protein EHBP1 couple endocytosis to the actin cytoskeleton. *J Biol Chem*, 279, 10593-605.
- GUO, B., LIANG, Q., LI, L., HU, Z., WU, F., ZHANG, P., MA, Y., ZHAO, B., KOVACS, A. L., ZHANG, Z., FENG, D., CHEN, S. & ZHANG, H. 2014. O-GlcNAc-modification of SNAP-29 regulates autophagosome maturation. *Nat Cell Biol*.
- GUO, Z., HOU, X., GOODY, R. S. & ITZEN, A. 2013. Intermediates in the guanine nucleotide exchange reaction of Rab8 protein catalyzed by guanine nucleotide exchange factors Rabin8 and GRAB. *J Biol Chem*, 288, 32466-74.
- GURKAN, C., LAPP, H., ALORY, C., SU, A. I., HOGENESCH, J. B. & BALCH, W. E. 2005. Large-scale profiling of Rab GTPase trafficking networks: the membrome. *Mol Biol Cell*, 16, 3847-64.
- HAAS, A. L., WARMS, J. V., HERSHKO, A. & ROSE, I. A. 1982. Ubiquitin-activating enzyme. Mechanism and role in protein-ubiquitin conjugation. *J Biol Chem*, 257, 2543-8.
- HAGLUND, K., SIGISMUND, S., POLO, S., SZYMKIEWICZ, I., DI FIORE, P. P. & DIKIC, I. 2003. Multiple monoubiquitination of RTKs is sufficient for their endocytosis and degradation. *Nat Cell Biol*, 5, 461-6.
- HALIMANI, M., PATTU, V., MARSHALL, M. R., CHANG, H. F., MATTI, U., JUNG, M., BECHERER, U., KRAUSE, E., HOTH, M., SCHWARZ, E. C. & RETTIG, J. 2014. Syntaxin11 serves as a t-SNARE for the fusion of lytic granules in human cytotoxic T lymphocytes. *Eur J Immunol*, 44, 573-84.
- HAMILL, K. J., HOPKINSON, S. B., DEBIASE, P. & JONES, J. C. 2009. BPAG1e maintains keratinocyte polarity through beta4 integrin-mediated modulation of Rac1 and cofilin activities. *Mol Biol Cell*, 20, 2954-62.
- HAN, G. A., MALINTAN, N. T., SAW, N. M., LI, L., HAN, L., MEUNIER, F. A., COLLINS, B. M. & SUGITA, S. 2011. Munc18-1 domain-1 controls vesicle docking and secretion by interacting with syntaxin-1 and chaperoning it to the plasma membrane. *Mol Biol Cell*, 22, 4134-49.
- HANCOCK, J. F. 2003. Ras proteins: different signals from different locations. *Nat Rev Mol Cell Biol*, 4, 373-84.
- HANCOCK, J. F., CADWALLADER, K., PATERSON, H. & MARSHALL, C. J. 1991. A CAAX or a CAAL motif and a second signal are sufficient for plasma membrane targeting of ras proteins. *EMBO J*, 10, 4033-9.
- HANCOCK, J. F., PATERSON, H. & MARSHALL, C. J. 1990. A polybasic domain or palmitoylation is required in addition to the CAAX motif to localize p21ras to the plasma membrane. *Cell*, 63, 133-9.

- HAO, Y. H., FOUNTAIN, M. D., JR., FON TACER, K., XIA, F., BI, W., KANG, S. L., PATEL, A., ROSENFELD, J. A., LE CAIGNEC, C., ISIDOR, B., KRANTZ, I. D., NOON, S. E., PFOTENHAUER, J. P., MORGAN, T. M., MORAN, R., PEDERSEN, R. C., SAENZ, M. S., SCHAAF, C. P. & POTTS, P. R. 2015. USP7 Acts as a Molecular Rheostat to Promote WASH-Dependent Endosomal Protein Recycling and Is Mutated in a Human Neurodevelopmental Disorder. *Mol Cell*.
- HATAKEYAMA, J., WALD, J. H., PRINTSEV, I., HO, H. Y. & CARRAWAY, K. L., 3RD 2014. Vangl1 and Vangl2: planar cell polarity components with a developing role in cancer. *Endocr Relat Cancer*, 21, R345-56.
- HATSUZAWA, K., HIROSE, H., TANI, K., YAMAMOTO, A., SCHELLER, R. H. & TAGAYA, M. 2000. Syntaxin 18, a SNAP receptor that functions in the endoplasmic reticulum, intermediate compartment, and cis-Golgi vesicle trafficking. *J Biol Chem*, 275, 13713-20.
- HATTULA, K., FURUHJELM, J., ARFFMAN, A. & PERANEN, J. 2002. A Rab8-specific GDP/GTP exchange factor is involved in actin remodeling and polarized membrane transport. *Mol Biol Cell*, 13, 3268-80.
- HATTULA, K., FURUHJELM, J., TIKKANEN, J., TANHUANPAA, K., LAAKKONEN, P. & PERANEN, J. 2006. Characterization of the Rab8-specific membrane traffic route linked to protrusion formation. *Journal of Cell Science*, 119, 4866-4877.
- HE, M., ABDI, K. M. & BENNETT, V. 2014. Ankyrin-G palmitoylation and beta1-spectrin binding to phosphoinositide lipids drive lateral membrane assembly. *J Cell Biol*, 206, 273-88.
- HE, Y. & LINDER, M. E. 2009. Differential palmitoylation of the endosomal SNAREs syntaxin 7 and syntaxin 8. *J Lipid Res*, 50, 398-404.
- HEHNLY, H. & DOXSEY, S. 2014. Rab11 endosomes contribute to mitotic spindle organization and orientation. *Dev Cell*, 28, 497-507.
- HEIN, M. Y., HUBNER, N. C., POSER, I., COX, J., NAGARAJ, N., TOYODA, Y., GAK, I. A., WEISSWANGE, I., MANSFELD, J., BUCHHOLZ, F., HYMAN, A. A. & MANN, M. 2015. A human interactome in three quantitative dimensions organized by stoichiometries and abundances. *Cell*, 163, 712-23.
- HELLEWELL, A. L., FORESTI, O., GOVER, N., PORTER, M. Y. & HEWITT, E. W. 2014. Analysis of familial hemophagocytic lymphohistiocytosis type 4 (FHL-4) mutant proteins reveals that S-acylation is required for the function of syntaxin 11 in natural killer cells. *PLoS One*, 9, e98900.
- HERSHKO, A. 1983. Ubiquitin: roles in protein modification and breakdown. *Cell*, 34, 11-2.
- HERSHKO, A. & CIECHANOVER, A. 1992. The ubiquitin system for protein degradation. *Annu Rev Biochem*, 61, 761-807.
- HERSHKO, A., CIECHANOVER, A. & ROSE, I. A. 1979. Resolution of the ATP-dependent proteolytic system from reticulocytes: a component that interacts with ATP. *Proc Natl Acad Sci U S A*, 76, 3107-10.
- HERSHKO, A., HELLER, H., ELIAS, S. & CIECHANOVER, A. 1983. Components of ubiquitin-protein ligase system. Resolution, affinity purification, and role in protein breakdown. *J Biol Chem*, 258, 8206-14.
- HESKETH, G. G., PEREZ-DORADO, I., JACKSON, L. P., WARTOSCH, L., SCHAFER, I. B., GRAY, S. R., MCCOY, A. J., ZELDIN, O. B., GARMAN, E. F., HARBOUR, M. E., EVANS, P. R., SEAMAN, M. N., LUZIO, J. P. & OWEN, D. J. 2014. VARP is recruited on to endosomes by direct interaction with retromer, where together they function in export to the cell surface. *Dev Cell*, 29, 591-606.
- HICKE, L. & RIEZMAN, H. 1996. Ubiquitination of a yeast plasma membrane receptor signals its ligand-stimulated endocytosis. *Cell*, 84, 277-87.
- HIROSE, H., ARASAKI, K., DOHMAE, N., TAKIO, K., HATSUZAWA, K., NAGAHAMA, M., TANI, K., YAMAMOTO, A., TOHYAMA, M. & TAGAYA, M. 2004. Implication of ZW10 in

- membrane trafficking between the endoplasmic reticulum and Golgi. *EMBO J*, 23, 1267-78.
- HOFMANN, K. & BARON, M. D. 2015. *BoxShade* [Online]. Available: http://www.ch.embnet.org/software/BOX_form.html [Accessed 24th August 2015].
- HOHENSTEIN, A. C. & ROCHE, P. A. 2001. SNAP-29 is a promiscuous syntaxin-binding SNARE. *Biochem Biophys Res Commun*, 285, 167-71.
- HOLT, M., VAROQUEAUX, F., WIEDERHOLD, K., TAKAMORI, S., URLAUB, H., FASSHAUER, D. & JAHN, R. 2006. Identification of SNAP-47, a novel Qbc-SNARE with ubiquitous expression. *J Biol Chem*, 281, 17076-83.
- HONG, W. 2005. SNAREs and traffic. *Biochim Biophys Acta*, 1744, 120-44.
- HONG, W. & LEV, S. 2014. Tethering the assembly of SNARE complexes. *Trends Cell Biol*, 24, 35-43.
- HOOD, J. D. & CHERESH, D. A. 2002. Role of integrins in cell invasion and migration. *Nat Rev Cancer*, 2, 91-100.
- HOPKINSON, S. B. & JONES, J. C. 2000. The N terminus of the transmembrane protein BP180 interacts with the N-terminal domain of BP230, thereby mediating keratin cytoskeleton anchorage to the cell surface at the site of the hemidesmosome. *Mol Biol Cell*, 11, 277-86.
- HORNEMANN, T. 2014. Palmitoylation and depalmitoylation defects. *J Inherit Metab Dis*.
- HOU, X. M., HAGEMANN, N., SCHOEBEL, S., BLANKENFELDT, W., GOODY, R. S., ERDMANN, K. S. & ITZEN, A. 2011. A structural basis for Lowe syndrome caused by mutations in the Rab-binding domain of OCRL1. *Embo Journal*, 30, 1659-1670.
- HOWIE, J., REILLY, L., FRASER, N. J., VLACHAKI WALKER, J. M., WYPIJEWSKI, K. J., ASHFORD, M. L., CALAGHAN, S. C., MCCLAFFERTY, H., TIAN, L., SHIPSTON, M. J., BOGUSLAVSKYI, A., SHATTOCK, M. J. & FULLER, W. 2014a. Substrate recognition by the cell surface palmitoyl transferase DHH5. *Proc Natl Acad Sci U S A*, 111, 17534-9.
- HOWIE, J., REILLY, L., FRASER, N. J., WALKER, J. M. V., WYPIJEWSKI, K. J., ASHFORD, M. L. J., CALAGHAN, S. C., MCCLAFFERTY, H., TIAN, L. J., SHIPSTON, M. J., BOGUSLAVSKYI, A., SHATTOCK, M. J. & FULLER, W. 2014b. Substrate recognition by the cell surface palmitoyl transferase DHH5. *Proceedings of the National Academy of Sciences of the United States of America*, 111, 17534-17539.
- HSU, V. W. & PREKERIS, R. 2010. Transport at the recycling endosome. *Curr Opin Cell Biol*, 22, 528-34.
- HU, L., SU, P., LI, R., YAN, K., CHEN, Z., SHANG, P. & QIAN, A. 2015. Knockdown of microtubule actin crosslinking factor 1 inhibits cell proliferation in MC3T3-E1 osteoblastic cells. *BMB Rep*.
- HU, S. H., CHRISTIE, M. P., SAEZ, N. J., LATHAM, C. F., JARROTT, R., LUA, L. H., COLLINS, B. M. & MARTIN, J. L. 2011. Possible roles for Munc18-1 domain 3a and Syntaxin1 N-peptide and C-terminal anchor in SNARE complex formation. *Proc Natl Acad Sci U S A*, 108, 1040-5.
- HUANG, F., KIRKPATRICK, D., JIANG, X., GYGI, S. & SORKIN, A. 2006. Differential regulation of EGF receptor internalization and degradation by multiubiquitination within the kinase domain. *Mol Cell*, 21, 737-48.
- HUANG, H., JEDYNAK, B. M. & BADER, J. S. 2007. Where have all the interactions gone? Estimating the coverage of two-hybrid protein interaction maps. *PLoS Comput Biol*, 3, e214.
- HUANG, K., SANDERS, S., SINGARAJA, R., ORBAN, P., CIJSOUW, T., ARSTIKAITIS, P., YANAI, A., HAYDEN, M. R. & EL-HUSSEINI, A. 2009. Neuronal palmitoyl acyl transferases exhibit distinct substrate specificity. *FASEB J*, 23, 2605-15.
- HUELSMANN, S. & BROWN, N. H. 2014. Spectraplakins. *Curr Biol*, 24, R307-8.

- HUMPHRIES, J. D., WANG, P., STREULI, C., GEIGER, B., HUMPHRIES, M. J. & BALLESTREM, C. 2007. Vinculin controls focal adhesion formation by direct interactions with talin and actin. *J Cell Biol*, 179, 1043-57.
- HUNTER, T. 2007. The age of crosstalk: phosphorylation, ubiquitination, and beyond. *Mol Cell*, 28, 730-8.
- HUOTARI, J. & HELENIUS, A. 2011. Endosome maturation. *EMBO J*, 30, 3481-500.
- HUTAGALUNG, A. H. & NOVICK, P. J. 2011. Role of Rab GTPases in membrane traffic and cell physiology. *Physiol Rev*, 91, 119-49.
- HUTCHINS, J. R., TOYODA, Y., HEGEMANN, B., POSER, I., HERICHE, J. K., SYKORA, M. M., AUGSBURG, M., HUDECZ, O., BUSCHHORN, B. A., BULKESCHER, J., CONRAD, C., COMARTIN, D., SCHLEIFFER, A., SAROV, M., POZNIAKOVSKY, A., SLABICKI, M. M., SCHLOISSNIG, S., STEINMACHER, I., LEUSCHNER, M., SSKOR, A., LAWOW, S., PELLETIER, L., STARK, H., NASMYTH, K., ELLENBERG, J., DURBIN, R., BUCHHOLZ, F., MECHTLER, K., HYMAN, A. A. & PETERS, J. M. 2010. Systematic analysis of human protein complexes identifies chromosome segregation proteins. *Science*, 328, 593-9.
- HUTTLIN, E. L., TING, L., BRUCKNER, R. J., GEBREAB, F., GYGI, M. P., SZPYT, J., TAM, S., ZARRAGA, G., COLBY, G., BALTIER, K., DONG, R., GUARANI, V., VAITES, L. P., ORDUREAU, A., RAD, R., ERICKSON, B. K., WUHR, M., CHICK, J., ZHAI, B., KOLIPPAKKAM, D., MINTSERIS, J., OBAR, R. A., HARRIS, T., ARTAVANIS-TSAKONAS, S., SOWA, M. E., DE CAMILLI, P., PAULO, J. A., HARPER, J. W. & GYGI, S. P. 2015. The BioPlex Network: A Systematic Exploration of the Human Interactome. *Cell*, 162, 425-440.
- HYNES, R. O. 2002. Integrins: bidirectional, allosteric signaling machines. *Cell*, 110, 673-87.
- IKEDA, F. & DIKIC, I. 2008. Atypical ubiquitin chains: new molecular signals. 'Protein Modifications: Beyond the Usual Suspects' review series. *EMBO Rep*, 9, 536-42.
- ILANGUMARAN, S. & HOESSLI, D. C. 1998. Effects of cholesterol depletion by cyclodextrin on the sphingolipid microdomains of the plasma membrane. *Biochem J*, 335 (Pt 2), 433-40.
- ITAKURA, E., KISHI-ITAKURA, C. & MIZUSHIMA, N. 2012. The hairpin-type tail-anchored SNARE syntaxin 17 targets to autophagosomes for fusion with endosomes/lysosomes. *Cell*, 151, 1256-69.
- IZAWA, I., NISHIZAWA, M., HAYASHI, Y. & INAGAKI, M. 2008. Palmitoylation of ERBIN is required for its plasma membrane localization. *Genes Cells*, 13, 691-701.
- JACKSON, A. L. & LINSLEY, P. S. 2010. Recognizing and avoiding siRNA off-target effects for target identification and therapeutic application. *Nat Rev Drug Discov*, 9, 57-67.
- JAHN, R. & FASSHAUER, D. 2012. Molecular machines governing exocytosis of synaptic vesicles. *Nature*, 490, 201-7.
- JAHN, R. & SCHELLER, R. H. 2006. SNAREs--engines for membrane fusion. *Nat Rev Mol Cell Biol*, 7, 631-43.
- JOVIC, M., NASLAVSKY, N., RAPAPORT, D., HOROWITZ, M. & CAPLAN, S. 2007. EHD1 regulates beta 1 integrin endosomal transport: effects on focal adhesions, cell spreading and migration. *Journal of Cell Science*, 120, 802-814.
- JUNG, J. J., INAMDAR, S. M., TIWARI, A. & CHOUDHURY, A. 2012. Regulation of intracellular membrane trafficking and cell dynamics by syntaxin-6. *Biosci Rep*, 32, 383-91.
- KA, M., JUNG, E. M., MUELLER, U. & KIM, W. Y. 2014. MACF1 regulates the migration of pyramidal neurons via microtubule dynamics and GSK-3 signaling. *Dev Biol*, 395, 4-18.
- KACHHAP, S. K., FAITH, D., QIAN, D. Z., SHABBEER, S., GALLOWAY, N. L., PILI, R., DENMEADE, S. R., DEMARZO, A. M. & CARDUCCI, M. A. 2007. The N-Myc down regulated Gene1 (NDRG1) Is a Rab4a effector involved in vesicular recycling of E-cadherin. *PLoS One*, 2, e844.

- KAKINUMA, T., ICHIKAWA, H., TSUKADA, Y., NAKAMURA, T. & TOH, B. H. 2004. Interaction between p230 and MACF1 is associated with transport of a glycosyl phosphatidyl inositol-anchored protein from the Golgi to the cell periphery. *Exp Cell Res*, 298, 388-98.
- KANG, J., BAI, Z., ZEGAREK, M. H., GRANT, B. D. & LEE, J. 2011. Essential roles of snap-29 in *C. elegans*. *Dev Biol*, 355, 77-88.
- KANG, R., WAN, J., ARSTIKAITIS, P., TAKAHASHI, H., HUANG, K., BAILEY, A. O., THOMPSON, J. X., ROTH, A. F., DRISDEL, R. C., MASTRO, R., GREEN, W. N., YATES, J. R., 3RD, DAVIS, N. G. & EL-HUSSEINI, A. 2008. Neural palmitoyl-proteomics reveals dynamic synaptic palmitoylation. *Nature*, 456, 904-9.
- KATOH, M. 2002. Molecular cloning and characterization of Strabismus 2 (STB2). *Int J Oncol*, 20, 993-8.
- KATUNUMA, N. 1973. Enzyme degradation and its regulation by group-specific proteases in various organs of rats. *Curr Top Cell Regul*, 7, 175-203.
- KATUNUMA, N., KATSUNUMA, T., KOMINAMI, E., SUZUKI, K. & HAMAGUCHI, Y. 1973. Regulation of intracellular enzyme levels by group specific proteases in various organs. *Adv Enzyme Regul*, 11, 37-51.
- KHAN, A. R. & MENETREY, J. 2013. Structural Biology of Arf and Rab GTPases' Effector Recruitment and Specificity. *Structure*, 21, 1284-1297.
- KIBAR, Z., TORBAN, E., MCDEARMID, J. R., REYNOLDS, A., BERGHOUT, J., MATHIEU, M., KIRILLOVA, I., DE MARCO, P., MERELLO, E., HAYES, J. M., WALLINGFORD, J. B., DRAPEAU, P., CAPRA, V. & GROS, P. 2007. Mutations in VANGL1 associated with neural-tube defects. *N Engl J Med*, 356, 1432-7.
- KILLIAN, J. A. & VON HEIJNE, G. 2000. How proteins adapt to a membrane-water interface. *Trends Biochem Sci*, 25, 429-34.
- KIRKPATRICK, D. S., DENISON, C. & GYGI, S. P. 2005. Weighing in on ubiquitin: the expanding role of mass-spectrometry-based proteomics. *Nat Cell Biol*, 7, 750-7.
- KLOEPPER, T. H., KIENLE, C. N. & FASSHAUER, D. 2007. An elaborate classification of SNARE proteins sheds light on the conservation of the eukaryotic endomembrane system. *Mol Biol Cell*, 18, 3463-71.
- KLOEPPER, T. H., KIENLE, C. N. & FASSHAUER, D. 2008. SNAREing the basis of multicellularity: consequences of protein family expansion during evolution. *Mol Biol Evol*, 25, 2055-68.
- KNODLER, A., FENG, S. S., ZHANG, J., ZHANG, X. Y., DAS, A., PERANEN, J. & GUO, W. 2010. Coordination of Rab8 and Rab11 in primary ciliogenesis. *Proceedings of the National Academy of Sciences of the United States of America*, 107, 6346-6351.
- KODAMA, A., KARAKESISOGLOU, I., WONG, E., VAEZI, A. & FUCHS, E. 2003. ACF7: an essential integrator of microtubule dynamics. *Cell*, 115, 343-54.
- KOLEHMAINEN, J., BLACK, G. C., SAARINEN, A., CHANDLER, K., CLAYTON-SMITH, J., TRASKELIN, A. L., PERVEEN, R., KIVITIE-KALLIO, S., NORIO, R., WARBURG, M., FRYNS, J. P., DE LA CHAPELLE, A. & LEHESJOKI, A. E. 2003. Cohen syndrome is caused by mutations in a novel gene, COH1, encoding a transmembrane protein with a presumed role in vesicle-mediated sorting and intracellular protein transport. *Am J Hum Genet*, 72, 1359-69.
- KOLLING, R. & HOLLENBERG, C. P. 1994. The ABC-transporter Ste6 accumulates in the plasma membrane in a ubiquitinated form in endocytosis mutants. *EMBO J*, 13, 3261-71.
- KOMANDER, D. 2009. The emerging complexity of protein ubiquitination. *Biochem Soc Trans*, 37, 937-53.
- KONG, C., LANGE, J. J., SAMOVSKI, D., SU, X., LIU, J., SUNDARESAN, S. & STAHL, P. D. 2013. Ubiquitination and degradation of the hominoid-specific oncoprotein TBC1D3 is regulated by protein palmitoylation. *Biochem Biophys Res Commun*, 434, 388-93.

- KOPS, G. J., KIM, Y., WEAVER, B. A., MAO, Y., MCLEOD, I., YATES, J. R., 3RD, TAGAYA, M. & CLEVELAND, D. W. 2005. ZW10 links mitotic checkpoint signaling to the structural kinetochore. *J Cell Biol*, 169, 49-60.
- KOSTER, J., GEERTS, D., FAVRE, B., BORRADORI, L. & SONNENBERG, A. 2003. Analysis of the interactions between BP180, BP230, plectin and the integrin alpha6beta4 important for hemidesmosome assembly. *J Cell Sci*, 116, 387-99.
- KRAYNOV, V. S., CHAMBERLAIN, C., BOKOCH, G. M., SCHWARTZ, M. A., SLABAUGH, S. & HAHN, K. M. 2000. Localized Rac activation dynamics visualized in living cells. *Science*, 290, 333-7.
- KUMMEL, D., HEINEMANN, U. & VEIT, M. 2006. Unique self-palmitoylation activity of the transport protein particle component Bet3: a mechanism required for protein stability. *Proc Natl Acad Sci U S A*, 103, 12701-6.
- KUMMEL, D. & UNGERMANN, C. 2014. Principles of membrane tethering and fusion in endosome and lysosome biogenesis. *Curr Opin Cell Biol*, 29, 61-6.
- KUPERSHMIDT, I., SU, Q. J., GREWAL, A., SUNDARESH, S., HALPERIN, I., FLYNN, J., SHEKAR, M., WANG, H., PARK, J., CUI, W., WALL, G. D., WISOTZKEY, R., ALAG, S., AKHTARI, S. & RONAGHI, M. 2010. Ontology-based meta-analysis of global collections of high-throughput public data. *PLoS One*, 5.
- KWEON, D. H., KIM, C. S. & SHIN, Y. K. 2003a. Insertion of the membrane-proximal region of the neuronal SNARE coiled coil into the membrane. *J Biol Chem*, 278, 12367-73.
- KWEON, D. H., KIM, C. S. & SHIN, Y. K. 2003b. Regulation of neuronal SNARE assembly by the membrane. *Nat Struct Biol*, 10, 440-7.
- LAKKARAJU, A. K., ABRAMI, L., LEMMIN, T., BLASKOVIC, S., KUNZ, B., KIHARA, A., DAL PERARO, M. & VAN DER GOOT, F. G. 2012. Palmitoylated calnexin is a key component of the ribosome-translocon complex. *EMBO J*, 31, 1823-35.
- LE ROY, C. & WRANA, J. L. 2005. Clathrin- and non-clathrin-mediated endocytic regulation of cell signalling. *Nat Rev Mol Cell Biol*, 6, 112-26.
- LECKER, S. H., GOLDBERG, A. L. & MITCH, W. E. 2006. Protein degradation by the ubiquitin-proteasome pathway in normal and disease states. *J Am Soc Nephrol*, 17, 1807-19.
- LEE, D. H. & GOLDBERG, A. L. 1998. Proteasome inhibitors: valuable new tools for cell biologists. *Trends Cell Biol*, 8, 397-403.
- LEE, H. K., SAFIEDDINE, S., PETRALIA, R. S. & WENTHOLD, R. J. 2002. Identification of a novel SNAP25 interacting protein (SIP30). *J Neurochem*, 81, 1338-47.
- LEE, K. H., AHN, E. J., OH, S. J., KIM, O., JOO, Y. E., BAE, J. A., YOON, S., RYU, H. H., JUNG, S., KIM, K. K., LEE, J. H. & MOON, K. S. 2015. KITENIN promotes glioma invasiveness and progression, associated with the induction of EMT and stemness markers. *Oncotarget*, 6, 3240-53.
- LEE, M. T., MISHRA, A. & LAMBRIGHT, D. G. 2009. Structural mechanisms for regulation of membrane traffic by rab GTPases. *Traffic*, 10, 1377-89.
- LEGG, K. 2011. Cell migration: Regulating the (missing) link. *Nat Rev Mol Cell Biol*, 12, 207.
- LEMONIDIS, K., WERNO, M. W., GREAVES, J., DIEZ-ARDANUY, C., SANCHEZ-PEREZ, M. C., SALAUN, C., THOMSON, D. M. & CHAMBERLAIN, L. H. 2015. The zDHC family of S-acyltransferases. *Biochem Soc Trans*, 43, 217-21.
- LEUNG, C. L., SUN, D., ZHENG, M., KNOWLES, D. R. & LIEM, R. K. 1999. Microtubule actin cross-linking factor (MACF): a hybrid of dystonin and dystrophin that can interact with the actin and microtubule cytoskeletons. *J Cell Biol*, 147, 1275-86.
- LI, Y., ROY, B. D., WANG, W., ZHANG, L., ZHANG, L., SAMPSON, S. B., YANG, Y. & LIN, D. T. 2012. Identification of two functionally distinct endosomal recycling pathways for dopamine D(2) receptor. *J Neurosci*, 32, 7178-90.

- LIN, S. X., GRANT, B., HIRSH, D. & MAXFIELD, F. R. 2001. Rme-1 regulates the distribution and function of the endocytic recycling compartment in mammalian cells. *Nature Cell Biology*, 3, 567-572.
- LINDER, M. E. & DESCHENES, R. J. 2007. Palmitoylation: policing protein stability and traffic. *Nat Rev Mol Cell Biol*, 8, 74-84.
- LINGWOOD, D. & SIMONS, K. 2010. Lipid rafts as a membrane-organizing principle. *Science*, 327, 46-50.
- LINKERMANN, A., GELHAUS, C., LETTAU, M., QIAN, J., KABELITZ, D. & JANSSEN, O. 2009. Identification of interaction partners for individual SH3 domains of Fas ligand associated members of the PCH protein family in T lymphocytes. *Biochim Biophys Acta*, 1794, 168-76.
- LITJENS, S. H., KOSTER, J., KUIKMAN, I., VAN WILPE, S., DE PEREDA, J. M. & SONNENBERG, A. 2003. Specificity of binding of the plectin actin-binding domain to beta4 integrin. *Mol Biol Cell*, 14, 4039-50.
- LONGATTI, A. & TOOZE, S. A. 2012. Recycling endosomes contribute to autophagosome formation. *Autophagy*, 8, 1682-1683.
- LOW, S. H., VASANJI, A., NANDURI, J., HE, M., SHARMA, N., KOO, M., DRAZBA, J. & WEIMBS, T. 2006. Syntaxins 3 and 4 are concentrated in separate clusters on the plasma membrane before the establishment of cell polarity. *Mol Biol Cell*, 17, 977-89.
- LU, D., SUN, H. Q., WANG, H., BARYLKO, B., FUKATA, Y., FUKATA, M., ALBANESI, J. P. & YIN, H. L. 2012. Phosphatidylinositol 4-kinase IIalpha is palmitoylated by Golgi-localized palmitoyltransferases in cholesterol-dependent manner. *J Biol Chem*, 287, 21856-65.
- LUZIO, J. P., PRYOR, P. R. & BRIGHT, N. A. 2007. Lysosomes: fusion and function. *Nat Rev Mol Cell Biol*, 8, 622-32.
- MACGURN, J. A., HSU, P. C. & EMR, S. D. 2012. Ubiquitin and membrane protein turnover: from cradle to grave. *Annu Rev Biochem*, 81, 231-59.
- MALSAM, J., KREYE, S. & SOLLNER, T. H. 2008. Membrane fusion: SNAREs and regulation. *Cell Mol Life Sci*, 65, 2814-32.
- MARTIN, B. R. & CRAVATT, B. F. 2009. Large-scale profiling of protein palmitoylation in mammalian cells. *Nat Methods*, 6, 135-8.
- MATSUDA, T. & CEPKO, C. L. 2007. Controlled expression of transgenes introduced by in vivo electroporation. *Proc Natl Acad Sci U S A*, 104, 1027-32.
- MAXFIELD, F. R. & MCGRAW, T. E. 2004. Endocytic recycling. *Nat Rev Mol Cell Biol*, 5, 121-32.
- MCCORMICK, P. J., DUMARESQ-DOIRON, K., PLUVIOSE, A. S., PICHETTE, V., TOSATO, G. & LEFRANCOIS, S. 2008. Palmitoylation Controls Recycling in Lysosomal Sorting and Trafficking. *Traffic*, 9, 1984-1997.
- MELLMAN, I. & NELSON, W. J. 2008. Coordinated protein sorting, targeting and distribution in polarized cells. *Nat Rev Mol Cell Biol*, 9, 833-45.
- MELOTTE, V., QU, X., ONGENAERT, M., VAN CRIEKINGE, W., DE BRUINE, A. P., BALDWIN, H. S. & VAN ENGELAND, M. 2010. The N-myc downstream regulated gene (NDRG) family: diverse functions, multiple applications. *FASEB J*, 24, 4153-66.
- MERITHEW, E., HATHERLY, S., DUMAS, J. J., LAWE, D. C., HELLER-HARRISON, R. & LAMBRIGHT, D. G. 2001. Structural plasticity of an invariant hydrophobic triad in the switch regions of Rab GTPases is a determinant of effector recognition. *Journal of Biological Chemistry*, 276, 13982-13988.
- MICHAEL, M., BEGUM, R., FONG, K., POURREYRON, C., SOUTH, A. P., MCGRATH, J. A. & PARSONS, M. 2014. BPAG1-e restricts keratinocyte migration through control of adhesion stability. *J Invest Dermatol*, 134, 773-82.
- MIINEA, C. P., SANO, H., KANE, S., SANO, E., FUKUDA, M., PERANEN, J., LANE, W. S. & LIENHARD, G. E. 2005. AS160, the Akt substrate regulating GLUT4 translocation, has a functional Rab GTPase-activating protein domain. *Biochemical Journal*, 391, 87-93.

- MILDE, S. & COLEMAN, M. P. 2014. Identification of palmitoyltransferase and thioesterase enzymes that control the subcellular localization of axon survival factor nicotinamide mononucleotide adenylyltransferase 2 (NMNAT2). *J Biol Chem*, 289, 32858-70.
- MINOSHIMA, S., AMAGAI, M., KUDOH, J., FUKUYAMA, R., HASHIMOTO, T., NISHIKAWA, T. & SHIMIZU, N. 1991. Localization of the human gene for 230-kDal bullous pemphigoid autoantigen (BPAG1) to chromosome 6pter----q15. *Cytogenet Cell Genet*, 57, 30-2.
- MISAKI, R., MORIMATSU, M., UEMURA, T., WAGURI, S., MIYOSHI, E., TANIGUCHI, N., MATSUDA, M. & TAGUCHI, T. 2010. Palmitoylated Ras proteins traffic through recycling endosomes to the plasma membrane during exocytosis. *J Cell Biol*, 191, 23-9.
- MISURA, K. M., SCHELLER, R. H. & WEIS, W. I. 2000. Three-dimensional structure of the neuronal-Sec1-syntaxin 1a complex. *Nature*, 404, 355-62.
- MITCHELL, D. A., VASUDEVAN, A., LINDER, M. E. & DESCHENES, R. J. 2006. Protein palmitoylation by a family of DHHC protein S-acyltransferases. *J Lipid Res*, 47, 1118-27.
- MORRISWOOD, B., HAVLICEK, K., DEMMEL, L., YAVUZ, S., SEALEY-CARDONA, M., VIDILASERIS, K., ANRATHER, D., KOSTAN, J., DJINOVIC-CARUGO, K., ROUX, K. J. & WARREN, G. 2013. Novel bilobe components in *Trypanosoma brucei* identified using proximity-dependent biotinylation. *Eukaryot Cell*, 12, 356-67.
- MUKADAM, A. S. & SEAMAN, M. N. 2015. Retromer-mediated endosomal protein sorting: The role of unstructured domains. *FEBS Lett*, 589, 2620-6.
- MUNRO, S. & NICHOLS, B. J. 1999. The GRIP domain - a novel Golgi-targeting domain found in several coiled-coil proteins. *Curr Biol*, 9, 377-80.
- MUSIO, A., MARIANI, T., MONTAGNA, C., ZAMBRONI, D., ASCOLI, C., RIED, T. & VEZZONI, P. 2004. Recapitulation of the Roberts syndrome cellular phenotype by inhibition of INCENP, ZWINT-1 and ZW10 genes. *Gene*, 331, 33-40.
- MYUNG, J., KIM, K. B. & CREWS, C. M. 2001. The ubiquitin-proteasome pathway and proteasome inhibitors. *Med Res Rev*, 21, 245-73.
- NADOLSKI, M. J. & LINDER, M. E. 2007. Protein lipidation. *FEBS J*, 274, 5202-10.
- NAKAMURA, N., RABOUILLE, C., WATSON, R., NILSSON, T., HUI, N., SLUSAREWICZ, P., KREIS, T. E. & WARREN, G. 1995. Characterization of a cis-Golgi matrix protein, GM130. *J Cell Biol*, 131, 1715-26.
- NALBANT, P., HODGSON, L., KRAYNOV, V., TOUTCHKINE, A. & HAHN, K. M. 2004. Activation of endogenous Cdc42 visualized in living cells. *Science*, 305, 1615-9.
- NASLAVSKY, N. & CAPLAN, S. 2011. EHD proteins: key conductors of endocytic transport. *Trends Cell Biol*, 21, 122-31.
- NASLAVSKY, N., MCKENZIE, J., ALTAN-BONNET, N., SHEFF, D. & CAPLAN, S. 2009. EHD3 regulates early-endosome-to-Golgi transport and preserves Golgi morphology. *J Cell Sci*, 122, 389-400.
- NASLAVSKY, N., RAHAJENG, J., SHARMA, M., JOVIC, M. & CAPLAN, S. 2006. Interactions between EHD proteins and Rab11-FIP2: a role for EHD3 in early endosomal transport. *Mol Biol Cell*, 17, 163-77.
- NIJMAN, S. M., LUNA-VARGAS, M. P., VELDS, A., BRUMMELKAMP, T. R., DIRAC, A. M., SIXMA, T. K. & BERNARDS, R. 2005. A genomic and functional inventory of deubiquitinating enzymes. *Cell*, 123, 773-86.
- OH, H. H., PARK, K. J., KIM, N., PARK, S. Y., PARK, Y. L., OAK, C. Y., MYUNG, D. S., CHO, S. B., LEE, W. S., KIM, K. K. & JOO, Y. E. 2016. Impact of KITENIN on tumor angiogenesis and lymphangiogenesis in colorectal cancer. *Oncol Rep*, 35, 253-60.
- OHNO, Y., KIHARA, A., SANO, T. & IGARASHI, Y. 2006. Intracellular localization and tissue-specific distribution of human and yeast DHHC cysteine-rich domain-containing proteins. *Biochim Biophys Acta*, 1761, 474-83.
- OKUDA, T., MATSUDA, S., NAKATSUGAWA, S., ICHIGOTANI, Y., IWAHASHI, N., TAKAHASHI, M., ISHIGAKI, T. & HAMAGUCHI, M. 1999. Molecular cloning of macrophin, a human

- homologue of *Drosophila kakapo* with a close structural similarity to plectin and dystrophin. *Biochem Biophys Res Commun*, 264, 568-74.
- OO, H. Z., SENTANI, K., SAKAMOTO, N., ANAMI, K., NAITO, Y., URAOKA, N., OSHIMA, T., YANAGIHARA, K., OUE, N. & YASUI, W. 2014. Overexpression of ZDHHC14 promotes migration and invasion of scirrhus type gastric cancer. *Oncol Rep*, 32, 403-10.
- PALADE, G. 1975. Intracellular aspects of the process of protein synthesis. *Science*, 189, 347-58.
- PARLATI, F., MCNEW, J. A., FUKUDA, R., MILLER, R., SOLLNER, T. H. & ROTHMAN, J. E. 2000. Topological restriction of SNARE-dependent membrane fusion. *Nature*, 407, 194-8.
- PARLATI, F., VARLAMOV, O., PAZ, K., MCNEW, J. A., HURTADO, D., SOLLNER, T. H. & ROTHMAN, J. E. 2002. Distinct SNARE complexes mediating membrane fusion in Golgi transport based on combinatorial specificity. *Proc Natl Acad Sci U S A*, 99, 5424-9.
- PATEL, V. J., THALASSINOS, K., SLADE, S. E., CONNOLLY, J. B., CROMBIE, A., MURRELL, J. C. & SCRIVENS, J. H. 2009. A comparison of labeling and label-free mass spectrometry-based proteomics approaches. *J Proteome Res*, 8, 3752-9.
- PEARSE, B. M. 1976. Clathrin: a unique protein associated with intracellular transfer of membrane by coated vesicles. *Proc Natl Acad Sci U S A*, 73, 1255-9.
- PEDEN, A. A., PARK, G. Y. & SCHELLER, R. H. 2001. The Di-leucine motif of vesicle-associated membrane protein 4 is required for its localization and AP-1 binding. *J Biol Chem*, 276, 49183-7.
- PELKMANS, L. & HELENIUS, A. 2002. Endocytosis via caveolae. *Traffic*, 3, 311-20.
- PERANEN, J. 2011. Rab8 GTPase as a regulator of cell shape. *Cytoskeleton (Hoboken)*, 68, 527-39.
- PERCHERANCIER, Y., PLANCHENAU, T., VALENZUELA-FERNANDEZ, A., VIRELIZIER, J. L., ARENZANA-SEISDEDOS, F. & BACHELERIE, F. 2001. Palmitoylation-dependent control of degradation, life span, and membrane expression of the CCR5 receptor. *J Biol Chem*, 276, 31936-44.
- PEREIRA-LEAL, J. B. & SEABRA, M. C. 2000. The mammalian Rab family of small GTPases: Definition of family and subfamily sequence motifs suggests a mechanism for functional specificity in the Ras superfamily. *Journal of Molecular Biology*, 301, 1077-1087.
- PICKART, C. M. & ROSE, I. A. 1985. Ubiquitin carboxyl-terminal hydrolase acts on ubiquitin carboxyl-terminal amides. *J Biol Chem*, 260, 7903-10.
- PIKE, L. J. 2006. Rafts defined: a report on the Keystone Symposium on Lipid Rafts and Cell Function. *J Lipid Res*, 47, 1597-8.
- PIPER, R. C. & LUZIO, J. P. 2004. CUPpling calcium to lysosomal biogenesis. *Trends Cell Biol*, 14, 471-3.
- POLIAKOVA, K., ADEBOLA, A., LEUNG, C. L., FAVRE, B., LIEM, R. K., SCHEPENS, I. & BORRADORI, L. 2014. BPAG1a and b associate with EB1 and EB3 and modulate vesicular transport, Golgi apparatus structure, and cell migration in C2.7 myoblasts. *PLoS One*, 9, e107535.
- PORTER, K. R., CLAUDE, A. & FULLAM, E. F. 1945. A Study of Tissue Culture Cells by Electron Microscopy : Methods and Preliminary Observations. *J Exp Med*, 81, 233-46.
- POWELKA, A. M., SUN, J., LI, J., GAO, M., SHAW, L. M., SONNENBERG, A. & HSU, V. W. 2004. Stimulation-dependent recycling of integrin beta1 regulated by ARF6 and Rab11. *Traffic*, 5, 20-36.
- PREKERIS, R., KLUMPERMAN, J. & SCHELLER, R. H. 2000. Syntaxin 11 is an atypical SNARE abundant in the immune system. *Eur J Cell Biol*, 79, 771-80.
- PRESCOTT, G. R., GORLEKU, O. A., GREAVES, J. & CHAMBERLAIN, L. H. 2009. Palmitoylation of the synaptic vesicle fusion machinery. *J Neurochem*, 110, 1135-49.

- PROTOCOLS, C. S. H. 2006. *PEI reagent* [Online]. Cold Spring Harbor Protocols. Available: http://cshprotocols.cshlp.org/content/2006/1/pdb.rec10471.full?text_only=true [Accessed 11th January 2014].
- PRYOR, P. R., JACKSON, L., GRAY, S. R., EDELING, M. A., THOMPSON, A., SANDERSON, C. M., EVANS, P. R., OWEN, D. J. & LUZIO, J. P. 2008. Molecular basis for the sorting of the SNARE VAMP7 into endocytic clathrin-coated vesicles by the ArfGAP Hrb. *Cell*, 134, 817-27.
- PUERTOLLANO, R., VAN DER WEL, N. N., GREENE, L. E., EISENBERG, E., PETERS, P. J. & BONIFACINO, J. S. 2003. Morphology and dynamics of clathrin/GGA1-coated carriers budding from the trans-Golgi network. *Mol Biol Cell*, 14, 1545-57.
- PULIDO, I. R., JAHN, R. & GERKE, V. 2011. VAMP3 is associated with endothelial weibel-palade bodies and participates in their Ca(2+)-dependent exocytosis. *Biochim Biophys Acta*, 1813, 1038-44.
- PUTILINA, T., WONG, P. & GENTLEMAN, S. 1999. The DHHC domain: a new highly conserved cysteine-rich motif. *Mol Cell Biochem*, 195, 219-26.
- QIU, S., ADEMA, C. M. & LANE, T. 2005. A computational study of off-target effects of RNA interference. *Nucleic Acids Res*, 33, 1834-47.
- QUALMANN, B. & KELLY, R. B. 2000. Syndapin isoforms participate in receptor-mediated endocytosis and actin organization. *J Cell Biol*, 148, 1047-62.
- QUAN, A. & ROBINSON, P. J. 2013. Syndapin - a membrane remodelling and endocytic F-BAR protein. *Febs Journal*, 280, 5198-5212.
- RAHAJENG, J., GIRIDHARAN, S. S., CAI, B., NASLAVSKY, N. & CAPLAN, S. 2010. Important relationships between Rab and MICAL proteins in endocytic trafficking. *World J Biol Chem*, 1, 254-64.
- RAHAJENG, J., GIRIDHARAN, S. S., CAI, B., NASLAVSKY, N. & CAPLAN, S. 2012. MICAL-L1 is a tubular endosomal membrane hub that connects Rab35 and Arf6 with Rab8a. *Traffic*, 13, 82-93.
- RAINEY, M. A., GEORGE, M., YING, G., AKAKURA, R., BURGESS, D. J., SIEFKER, E., BARGAR, T., DOGLIO, L., CRAWFORD, S. E., TODD, G. L., GOVINDARAJAN, V., HESS, R. A., BAND, V., NARAMURA, M. & BAND, H. 2010. The endocytic recycling regulator EHD1 is essential for spermatogenesis and male fertility in mice. *BMC Dev Biol*, 10, 37.
- RAPAPORT, D., LUGASSY, Y., SPRECHER, E. & HOROWITZ, M. 2010. Loss of SNAP29 impairs endocytic recycling and cell motility. *PLoS One*, 5, e9759.
- RATHORE, S. S., BEND, E. G., YU, H., HAMMARLUND, M., JORGENSEN, E. M. & SHEN, J. 2010. Syntaxin N-terminal peptide motif is an initiation factor for the assembly of the SNARE-Sec1/Munc18 membrane fusion complex. *Proc Natl Acad Sci U S A*, 107, 22399-406.
- RAVICHANDRAN, V., CHAWLA, A. & ROCHE, P. A. 1996. Identification of a novel syntaxin- and synaptobrevin/VAMP-binding protein, SNAP-23, expressed in non-neuronal tissues. *J Biol Chem*, 271, 13300-3.
- REALES, E., SHARMA, N., LOW, S. H., FOLSCH, H. & WEIMBS, T. 2011. Basolateral sorting of syntaxin 4 is dependent on its N-terminal domain and the AP1B clathrin adaptor, and required for the epithelial cell polarity. *PLoS One*, 6, e21181.
- REINECKE, J. B., KATAFIASZ, D., NASLAVSKY, N. & CAPLAN, S. 2014a. Novel Functions for the Endocytic Regulatory Proteins MICAL-L1 AND EHD1 in Mitosis. *Traffic*.
- REINECKE, J. B., KATAFIASZ, D., NASLAVSKY, N. & CAPLAN, S. 2014b. Regulation of Src trafficking and activation by the endocytic regulatory proteins MICAL-L1 and EHD1. *J Cell Sci*, 127, 1684-98.
- REN, M., XU, G., ZENG, J., DE LEMOS-CHIARANDINI, C., ADESNIK, M. & SABATINI, D. D. 1998. Hydrolysis of GTP on rab11 is required for the direct delivery of transferrin from the pericentriolar recycling compartment to the cell surface but not from sorting endosomes. *Proc Natl Acad Sci U S A*, 95, 6187-92.

- RESH, M. D. 1999. Fatty acylation of proteins: new insights into membrane targeting of myristoylated and palmitoylated proteins. *Biochim Biophys Acta*, 1451, 1-16.
- RESH, M. D. 2006a. Palmitoylation of ligands, receptors, and intracellular signaling molecules. *Sci STKE*, 2006, re14.
- RESH, M. D. 2006b. Use of analogs and inhibitors to study the functional significance of protein palmitoylation. *Methods*, 40, 191-7.
- REYES-TURCU, F. E., VENTII, K. H. & WILKINSON, K. D. 2009. Regulation and cellular roles of ubiquitin-specific deubiquitinating enzymes. *Annu Rev Biochem*, 78, 363-97.
- RIGGS, K. A., HASAN, N., HUMPHREY, D., RALEIGH, C., NEVITT, C., CORBIN, D. & HU, C. 2012. Regulation of integrin endocytic recycling and chemotactic cell migration by syntaxin 6 and VAMP3 interaction. *J Cell Sci*, 125, 3827-39.
- ROLAND, J. T., BRYANT, D. M., DATTA, A., ITZEN, A., MOSTOV, K. E. & GOLDENRING, J. R. 2011. Rab GTPase-Myo5B complexes control membrane recycling and epithelial polarization. *Proceedings of the National Academy of Sciences of the United States of America*, 108, 2789-2794.
- ROPER, K., GREGORY, S. L. & BROWN, N. H. 2002. The 'spectraplakins': cytoskeletal giants with characteristics of both spectrin and plakin families. *J Cell Sci*, 115, 4215-25.
- ROSE, I. A. & WARMS, J. V. 1983. An enzyme with ubiquitin carboxy-terminal esterase activity from reticulocytes. *Biochemistry*, 22, 4234-7.
- ROSSI, V., BANFIELD, D. K., VACCA, M., DIETRICH, L. E., UNGERMANN, C., D'ESPOSITO, M., GALLI, T. & FILIPPINI, F. 2004. Longins and their longin domains: regulated SNAREs and multifunctional SNARE regulators. *Trends Biochem Sci*, 29, 682-8.
- ROTEM-YEHUDAR, R., GALPERIN, E. & HOROWITZ, M. 2001. Association of insulin-like growth factor 1 receptor with EHD1 and SNAP29. *J Biol Chem*, 276, 33054-60.
- ROTHBAUER, U., ZOLGHADR, K., MUYLDERMANS, S., SCHEPERS, A., CARDOSO, M. C. & LEONHARDT, H. 2008. A versatile nanotrapp for biochemical and functional studies with fluorescent fusion proteins. *Mol Cell Proteomics*, 7, 282-9.
- ROTHMAN, J. E. 1994. Mechanisms of intracellular protein transport. *Nature*, 372, 55-63.
- ROUX, K. J., KIM, D. I., RAIDA, M. & BURKE, B. 2012. A promiscuous biotin ligase fusion protein identifies proximal and interacting proteins in mammalian cells. *J Cell Biol*, 196, 801-10.
- RYAN, S. D., BHANOT, K., FERRIER, A., DE REPENTIGNY, Y., CHU, A., BLAIS, A. & KOTHARY, R. 2012. Microtubule stability, Golgi organization, and transport flux require dystonin-a2-MAP1B interaction. *J Cell Biol*, 196, 727-42.
- RYU, H. S., PARK, Y. L., PARK, S. J., LEE, J. H., CHO, S. B., LEE, W. S., CHUNG, I. J., KIM, K. K., LEE, K. H., KWEON, S. S. & JOO, Y. E. 2010. KITENIN is associated with tumor progression in human gastric cancer. *Anticancer Res*, 30, 3479-86.
- SADOK, A. & MARSHALL, C. J. 2014. Rho GTPases: masters of cell migration. *Small GTPases*, 5, e29710.
- SALAUN, C., GREAVES, J. & CHAMBERLAIN, L. H. 2010. The intracellular dynamic of protein palmitoylation. *J Cell Biol*, 191, 1229-38.
- SANTONI, M. J., PONTAROTTI, P., BIRNBAUM, D. & BORG, J. P. 2002. The LAP family: a phylogenetic point of view. *Trends Genet*, 18, 494-7.
- SCALES, S. J., CHEN, Y. A., YOO, B. Y., PATEL, S. M., DOUNG, Y. C. & SCHELLER, R. H. 2000. SNAREs contribute to the specificity of membrane fusion. *Neuron*, 26, 457-64.
- SCALES, S. J., YOO, B. Y. & SCHELLER, R. H. 2001. The ionic layer is required for efficient dissociation of the SNARE complex by alpha-SNAP and NSF. *Proc Natl Acad Sci U S A*, 98, 14262-7.
- SCHAFFER, I. B., HESKETH, G. G., BRIGHT, N. A., GRAY, S. R., PRYOR, P. R., EVANS, P. R., LUZIO, J. P. & OWEN, D. J. 2012. The binding of Varp to VAMP7 traps VAMP7 in a closed, fusogenically inactive conformation. *Nat Struct Mol Biol*, 19, 1300-9.
- SCHEKMAN, R. & NOVICK, P. 2004. 23 genes, 23 years later. *Cell*, 116, S13-5, 1 p following S19.

- SCHMICK, M., VARTAK, N., PAPKE, B., KOVACEVIC, M., TRUXIUS, D. C., ROSSMANNEK, L. & BASTIAENS, P. I. 2014. KRas localizes to the plasma membrane by spatial cycles of solubilization, trapping and vesicular transport. *Cell*, 157, 459-71.
- SCHMITT, H. D. 2010. Dsl1p/Zw10: common mechanisms behind tethering vesicles and microtubules. *Trends Cell Biol*, 20, 257-68.
- SCOTT, C. C. & GRUENBERG, J. 2011. Ion flux and the function of endosomes and lysosomes: pH is just the start: the flux of ions across endosomal membranes influences endosome function not only through regulation of the luminal pH. *Bioessays*, 33, 103-10.
- SCOTT, C. C., VACCA, F. & GRUENBERG, J. 2014. Endosome maturation, transport and functions. *Semin Cell Dev Biol*, 31, 2-10.
- SEAMAN, M. N., GAUTREAU, A. & BILLADEAU, D. D. 2013. Retromer-mediated endosomal protein sorting: all WASHed up! *Trends Cell Biol*, 23, 522-8.
- SEIFERT, W., KUHNISCH, J., MARITZEN, T., HORN, D., HAUCKE, V. & HENNIES, H. C. 2011. Cohen syndrome-associated protein, COH1, is a novel, giant Golgi matrix protein required for Golgi integrity. *J Biol Chem*, 286, 37665-75.
- SENJU, Y., ITOH, Y., TAKANO, K., HAMADA, S. & SUETSUGU, S. 2011. Essential role of PACSIN2/syndapin-II in caveolae membrane sculpting. *J Cell Sci*, 124, 2032-40.
- SEONG, J., LU, S., OUYANG, M., HUANG, H., ZHANG, J., FRAME, M. C. & WANG, Y. 2009. Visualization of Src activity at different compartments of the plasma membrane by FRET imaging. *Chem Biol*, 16, 48-57.
- SHAHINIAN, S. & SILVIUS, J. R. 1995. Doubly-lipid-modified protein sequence motifs exhibit long-lived anchorage to lipid bilayer membranes. *Biochemistry*, 34, 3813-22.
- SHARMA, M., GIRIDHARAN, S. S., RAHAJENG, J., CAPLAN, S. & NASLAVSKY, N. 2010. MICAL-L1: An unusual Rab effector that links EHD1 to tubular recycling endosomes. *Commun Integr Biol*, 3, 181-3.
- SHARMA, M., GIRIDHARAN, S. S., RAHAJENG, J., NASLAVSKY, N. & CAPLAN, S. 2009. MICAL-L1 links EHD1 to tubular recycling endosomes and regulates receptor recycling. *Mol Biol Cell*, 20, 5181-94.
- SHARMA, M., NASLAVSKY, N. & CAPLAN, S. 2008. A role for EHD4 in the regulation of early endosomal transport. *Traffic*, 9, 995-1018.
- SHARMA, N., LOW, S. H., MISRA, S., PALLAVI, B. & WEIMBS, T. 2006. Apical targeting of syntaxin 3 is essential for epithelial cell polarity. *J Cell Biol*, 173, 937-48.
- SHENOY, S. K., MCDONALD, P. H., KOHOUT, T. A. & LEFKOWITZ, R. J. 2001. Regulation of receptor fate by ubiquitination of activated beta 2-adrenergic receptor and beta-arrestin. *Science*, 294, 1307-13.
- SHI, Y., LIU, X., SUN, Y., WU, D., QIU, A., CHENG, H., WU, C. & WANG, X. 2015. Decreased expression and prognostic role of EHD2 in human breast carcinoma: correlation with E-cadherin. *J Mol Histol*, 46, 221-31.
- SHIMA, T., NADA, S. & OKADA, M. 2003. Transmembrane phosphoprotein Cbp senses cell adhesion signaling mediated by Src family kinase in lipid rafts. *Proc Natl Acad Sci U S A*, 100, 14897-902.
- SIMONS, K. & TOOMRE, D. 2000. Lipid rafts and signal transduction. *Nat Rev Mol Cell Biol*, 1, 31-9.
- SIMPSON, C. L., PATEL, D. M. & GREEN, K. J. 2011. Deconstructing the skin: cytoarchitectural determinants of epidermal morphogenesis. *Nat Rev Mol Cell Biol*, 12, 565-80.
- SIMPSON, J. C., JOGGERST, B., LAKETA, V., VERISSIMO, F., CETIN, C., ERFLE, H., BEXIGA, M. G., SINGAN, V. R., HERICHE, J. K., NEUMANN, B., MATEOS, A., BLAKE, J., BECHTEL, S., BENES, V., WIEMANN, S., ELLENBERG, J. & PEPPERKOK, R. 2012. Genome-wide RNAi screening identifies human proteins with a regulatory function in the early secretory pathway. *Nat Cell Biol*, 14, 764-74.

- SOLLNER, T., WHITEHEART, S. W., BRUNNER, M., ERDJUMENT-BROMAGE, H., GEROMANOS, S., TEMPST, P. & ROTHMAN, J. E. 1993. SNAP receptors implicated in vesicle targeting and fusion. *Nature*, 362, 318-24.
- SONNENBERG, A. & LIEM, R. K. 2007. Plakins in development and disease. *Exp Cell Res*, 313, 2189-203.
- SONNICHSEN, B., DE RENZIS, S., NIELSEN, E., RIETDORF, J. & ZERIAL, M. 2000. Distinct membrane domains on endosomes in the recycling pathway visualized by multicolor imaging of Rab4, Rab5, and Rab11. *J Cell Biol*, 149, 901-14.
- SORKIN, A. & VON ZASTROW, M. 2009. Endocytosis and signalling: intertwining molecular networks. *Nat Rev Mol Cell Biol*, 10, 609-22.
- SPRECHER, E., ISHIDA-YAMAMOTO, A., MIZRAHI-KOREN, M., RAPAPORT, D., GOLDSHER, D., INDELMAN, M., TOPAZ, O., CHEFETZ, I., KEREN, H., O'BRIEN T, J., BERCOVICH, D., SHALEV, S., GEIGER, D., BERGMAN, R., HOROWITZ, M. & MANDEL, H. 2005. A mutation in SNAP29, coding for a SNARE protein involved in intracellular trafficking, causes a novel neurocutaneous syndrome characterized by cerebral dysgenesis, neuropathy, ichthyosis, and palmoplantar keratoderma. *Am J Hum Genet*, 77, 242-51.
- STARR, D. A., SAFFERY, R., LI, Z., SIMPSON, A. E., CHOO, K. H., YEN, T. J. & GOLDBERG, M. L. 2000. HZwint-1, a novel human kinetochore component that interacts with HZW10. *J Cell Sci*, 113 (Pt 11), 1939-50.
- STEEGMAIER, M., YANG, B., YOO, J. S., HUANG, B., SHEN, M., YU, S., LUO, Y. & SCHELLER, R. H. 1998. Three novel proteins of the syntaxin/SNAP-25 family. *J Biol Chem*, 273, 34171-9.
- STEBENS, S. & WITTMANN, T. 2012. Targeting and transport: how microtubules control focal adhesion dynamics. *J Cell Biol*, 198, 481-9.
- STEINBERG, F., GALLON, M., WINFIELD, M., THOMAS, E. C., BELL, A. J., HEESOM, K. J., TAVARE, J. M. & CULLEN, P. J. 2013. A global analysis of SNX27-retromer assembly and cargo specificity reveals a function in glucose and metal ion transport. *Nat Cell Biol*, 15, 461-71.
- STEINMAN, R. M., MELLMAN, I. S., MULLER, W. A. & COHN, Z. A. 1983. Endocytosis and the recycling of plasma membrane. *J Cell Biol*, 96, 1-27.
- STENMARK, H. 2009. Rab GTPases as coordinators of vesicle traffic. *Nat Rev Mol Cell Biol*, 10, 513-25.
- STROUD, M. J., NAZGIEWICZ, A., MCKENZIE, E. A., WANG, Y., KAMMERER, R. A. & BALLESTREM, C. 2014. GAS2-like proteins mediate communication between microtubules and actin through interactions with end-binding proteins. *J Cell Sci*, 127, 2672-82.
- SUDHOF, T. C. & ROTHMAN, J. E. 2009. Membrane fusion: grappling with SNARE and SM proteins. *Science*, 323, 474-7.
- SUOZZI, K. C., WU, X. & FUCHS, E. 2012. Spectraplakins: master orchestrators of cytoskeletal dynamics. *J Cell Biol*, 197, 465-75.
- SURESH, B., LEE, J., HONG, S. H., KIM, K. S. & RAMAKRISHNA, S. 2015. The role of deubiquitinating enzymes in spermatogenesis. *Cell Mol Life Sci*.
- SUTTON, R. B., FASSHAUER, D., JAHN, R. & BRUNGER, A. T. 1998. Crystal structure of a SNARE complex involved in synaptic exocytosis at 2.4 Å resolution. *Nature*, 395, 347-53.
- TAGUCHI, T. 2013. Emerging roles of recycling endosomes. *Journal of Biochemistry*, 153, 505-510.
- TAKATS, S., NAGY, P., VARGA, A., PIRCS, K., KARPATI, M., VARGA, K., KOVACS, A. L., HEGEDUS, K. & JUHASZ, G. 2013. Autophagosomal Syntaxin17-dependent lysosomal degradation maintains neuronal function in *Drosophila*. *J Cell Biol*, 201, 531-9.
- TASAKI, T. & KWON, Y. T. 2007. The mammalian N-end rule pathway: new insights into its components and physiological roles. *Trends in Biochemical Sciences*, 32, 520-528.
- THROWER, J. S., HOFFMAN, L., RECHSTEINER, M. & PICKART, C. M. 2000. Recognition of the polyubiquitin proteolytic signal. *EMBO J*, 19, 94-102.

- TOCHIO, H., TSUI, M. M., BANFIELD, D. K. & ZHANG, M. 2001. An autoinhibitory mechanism for nonsyntaxin SNARE proteins revealed by the structure of Ykt6p. *Science*, 293, 698-702.
- TOMATIS, V. M., TRENCHI, A., GOMEZ, G. A. & DANIOTTI, J. L. 2010. Acyl-protein thioesterase 2 catalyzes the deacylation of peripheral membrane-associated GAP-43. *PLoS One*, 5, e15045.
- TRIMBLE, W. S., COWAN, D. M. & SCHELLER, R. H. 1988. VAMP-1: a synaptic vesicle-associated integral membrane protein. *Proc Natl Acad Sci U S A*, 85, 4538-42.
- TSUTSUMI, R., FUKATA, Y., NORITAKE, J., IWANAGA, T., PEREZ, F. & FUKATA, M. 2009. Identification of G protein alpha subunit-palmitoylating enzyme. *Mol Cell Biol*, 29, 435-47.
- UNGAR, D. & HUGHSON, F. M. 2003. SNARE protein structure and function. *Annu Rev Cell Dev Biol*, 19, 493-517.
- UNIPROT, C. 2014. Activities at the Universal Protein Resource (UniProt). *Nucleic Acids Res*, 42, D191-8.
- UY, R. & WOLD, F. 1977. Posttranslational covalent modification of proteins. *Science*, 198, 890-6.
- VALDEZ-TAUBAS, J. & PELHAM, H. 2005. Swf1-dependent palmitoylation of the SNARE Tlg1 prevents its ubiquitination and degradation. *EMBO J*, 24, 2524-32.
- VALDEZ, A. C., CABANIOLS, J. P., BROWN, M. J. & ROCHE, P. A. 1999. Syntaxin 11 is associated with SNAP-23 on late endosomes and the trans-Golgi network. *J Cell Sci*, 112 (Pt 6), 845-54.
- VARSHAVSKY, A. 2011. The N-end rule pathway and regulation by proteolysis. *Protein Sci*, 20, 1298-345.
- VEALE, K. J., OFFENHAUSER, C., LEI, N., STANLEY, A. C., STOW, J. L. & MURRAY, R. Z. 2011. VAMP3 regulates podosome organisation in macrophages and together with Stx4/SNAP23 mediates adhesion, cell spreading and persistent migration. *Exp Cell Res*, 317, 1817-29.
- VEIT, M. 2000. Palmitoylation of the 25-kDa synaptosomal protein (SNAP-25) in vitro occurs in the absence of an enzyme, but is stimulated by binding to syntaxin. *Biochem J*, 345 Pt 1, 145-51.
- VEIT, M., SOLLNER, T. H. & ROTHMAN, J. E. 1996. Multiple palmitoylation of synaptotagmin and the t-SNARE SNAP-25. *FEBS Lett*, 385, 119-23.
- VELAYOS-BAEZA, A., VETTORI, A., COPLEY, R. R., DOBSON-STONE, C. & MONACO, A. P. 2004. Analysis of the human VPS13 gene family. *Genomics*, 84, 536-49.
- VOLCHUK, A., RAVAZZOLA, M., PERRELET, A., ENG, W. S., DI LIBERTO, M., VARLAMOV, O., FUKASAWA, M., ENGEL, T., SOLLNER, T. H., ROTHMAN, J. E. & ORCI, L. 2004. Countercurrent distribution of two distinct SNARE complexes mediating transport within the Golgi stack. *Mol Biol Cell*, 15, 1506-18.
- WALSH, C. T., GARNEAU-TSODIKOVA, S. & GATTO, G. J., JR. 2005. Protein posttranslational modifications: the chemistry of proteome diversifications. *Angew Chem Int Ed Engl*, 44, 7342-72.
- WANDINGER-NESS, A. & ZERIAL, M. 2014. Rab proteins and the compartmentalization of the endosomal system. *Cold Spring Harb Perspect Biol*, 6, a022616.
- WANG, Q., NAVARRO, M. V., PENG, G., MOLINELLI, E., GOH, S. L., JUDSON, B. L., RAJASHANKAR, K. R. & SONDERMANN, H. 2009. Molecular mechanism of membrane constriction and tubulation mediated by the F-BAR protein Pacsin/Syndapin. *Proc Natl Acad Sci U S A*, 106, 12700-5.
- WANG, Y., FOO, L. Y., GUO, K., GAN, B. Q., ZENG, Q., HONG, W. & TANG, B. L. 2006. Syntaxin 9 is enriched in skin hair follicle epithelium and interacts with the epidermal growth factor receptor. *Traffic*, 7, 216-26.

- WATSON, R. T. & PESSIN, J. E. 2000. Functional cooperation of two independent targeting domains in syntaxin 6 is required for its efficient localization in the trans-golgi network of 3T3L1 adipocytes. *J Biol Chem*, 275, 1261-8.
- WATSON, R. T. & PESSIN, J. E. 2001. Transmembrane domain length determines intracellular membrane compartment localization of syntaxins 3, 4, and 5. *Am J Physiol Cell Physiol*, 281, C215-23.
- WESSEL, D. & FLUGGE, U. I. 1984. A method for the quantitative recovery of protein in dilute solution in the presence of detergents and lipids. *Anal Biochem*, 138, 141-3.
- WILKINSON, K. D. 1997. Regulation of ubiquitin-dependent processes by deubiquitinating enzymes. *FASEB J*, 11, 1245-56.
- WILKINSON, K. D., URBAN, M. K. & HAAS, A. L. 1980. Ubiquitin is the ATP-dependent proteolysis factor I of rabbit reticulocytes. *J Biol Chem*, 255, 7529-32.
- WILSON, A. L., ERDMAN, R. A., CASTELLANO, F. & MALTESE, W. A. 1998. Prenylation of Rab8 GTPase by type I and type II geranylgeranyl transferases. *Biochemical Journal*, 333, 497-504.
- WOLD, F. 1981. In vivo chemical modification of proteins (post-translational modification). *Annu Rev Biochem*, 50, 783-814.
- WOLFF, T. & RUBIN, G. M. 1998. Strabismus, a novel gene that regulates tissue polarity and cell fate decisions in Drosophila. *Development*, 125, 1149-59.
- WONG, S. H., XU, Y., ZHANG, T., GRIFFITHS, G., LOWE, S. L., SUBRAMANIAM, V. N., SEOW, K. T. & HONG, W. 1999. GS32, a novel Golgi SNARE of 32 kDa, interacts preferentially with syntaxin 6. *Mol Biol Cell*, 10, 119-34.
- WOOLFREY, K. M., SANDERSON, J. L. & DELL'ACQUA, M. L. 2015. The Palmitoyl Acyltransferase DHHC2 Regulates Recycling Endosome Exocytosis and Synaptic Potentiation through Palmitoylation of AKAP79/150. *J Neurosci*, 35, 442-56.
- WU, X., KODAMA, A. & FUCHS, E. 2008. ACF7 regulates cytoskeletal-focal adhesion dynamics and migration and has ATPase activity. *Cell*, 135, 137-48.
- WU, X., SHEN, Q. T., ORISTIAN, D. S., LU, C. P., ZHENG, Q., WANG, H. W. & FUCHS, E. 2011. Skin stem cells orchestrate directional migration by regulating microtubule-ACF7 connections through GSK3beta. *Cell*, 144, 341-52.
- XIE, S., BAHL, K., REINECKE, J. B., HAMMOND, G. R., NASLAVSKY, N. & CAPLAN, S. 2015. The endocytic recycling compartment maintains cargo segregation acquired upon exit from the sorting endosome. *Mol Biol Cell*.
- XU, Y., MARTIN, S., JAMES, D. E. & HONG, W. 2002. GS15 forms a SNARE complex with syntaxin 5, GS28, and Ykt6 and is implicated in traffic in the early cisternae of the Golgi apparatus. *Mol Biol Cell*, 13, 3493-507.
- XU, Y., SHI, H., WEI, S., WONG, S. H. & HONG, W. 2004. Mutually exclusive interactions of EHD1 with GS32 and syndapin II. *Mol Membr Biol*, 21, 269-77.
- YAMAMOTO, Y., CHOCHI, Y., MATSUYAMA, H., EGUCHI, S., KAWAUCHI, S., FURUYA, T., OGA, A., KANG, J. J., NAITO, K. & SASAKI, K. 2007. Gain of 5p15.33 is associated with progression of bladder cancer. *Oncology*, 72, 132-8.
- YANG, B., GONZALEZ, L., JR., PREKERIS, R., STEEGMAIER, M., ADVANI, R. J. & SCHELLER, R. H. 1999. SNARE interactions are not selective. Implications for membrane fusion specificity. *J Biol Chem*, 274, 5649-53.
- YAP, M. C., KOSTIUK, M. A., MARTIN, D. D. O., PERINPANAYAGAM, M. A., HAK, P. G., SIDDAM, A., MAJJIGAPU, J. R., RAJAIAH, G., KELLER, B. O., PRESCHER, J. A., WU, P., BERTOZZI, C. R., FALCK, J. R. & BERTHIAUME, L. G. 2010. Rapid and selective detection of fatty acylated proteins using omega-alkynyl-fatty acids and click chemistry. *Journal of Lipid Research*, 51, 1566-1580.
- YESTE-VELASCO, M., LINDER, M. E. & LU, Y. J. 2015. Protein S-Palmitoylation and Cancer. *Biochim Biophys Acta*.

- YOON, T. M., KIM, S. A., LEE, J. K., PARK, Y. L., KIM, G. Y., JOO, Y. E., LEE, J. H., KIM, K. K. & LIM, S. C. 2013. Expression of KITENIN and its association with tumor progression in oral squamous cell carcinoma. *Auris Nasus Larynx*, 40, 222-6.
- YOSHIMURA, S., GERONDOPOULOS, A., LINFORD, A., RIGDEN, D. J. & BARR, F. A. 2010. Family-wide characterization of the DENN domain Rab GDP-GTP exchange factors. *J Cell Biol*, 191, 367-81.
- YUCEL, G. & ORO, A. E. 2011. Cell migration: GSK3beta steers the cytoskeleton's tip. *Cell*, 144, 319-21.
- ZAGURY, D., UHR, J. W., JAMIESON, J. D. & PALADE, G. E. 1970. Immunoglobulin synthesis and secretion. II. Radioautographic studies of sites of addition of carbohydrate moieties and intracellular transport. *J Cell Biol*, 46, 52-63.
- ZEIDMAN, R., JACKSON, C. S. & MAGEE, A. I. 2009. Protein acyl thioesterases (Review). *Mol Membr Biol*, 26, 32-41.
- ZHANG, F. L. & CASEY, P. J. 1996. Protein prenylation: molecular mechanisms and functional consequences. *Annu Rev Biochem*, 65, 241-69.
- ZHEN, Y. & STENMARK, H. 2015. Cellular functions of Rab GTPases at a glance. *J Cell Sci*, 128, 3171-6.
- ZHOU, Q., TOIVOLA, D. M., FENG, N., GREENBERG, H. B., FRANKE, W. W. & OMARY, M. B. 2003. Keratin 20 helps maintain intermediate filament organization in intestinal epithelia. *Mol Biol Cell*, 14, 2959-71.